Experimental Determination of Heat Transfer Coefficient for Water-Lithium Bromide Mixture

by

Hussain Abdulla Al-Bazroon

A Thesis Presented to the

FACULTY OF THE COLLEGE OF GRADUATE STUDIES

KING FAHD UNIVERSITY OF PETROLEUM & MINERALS

DHAHRAN, SAUDI ARABIA

In Partial Fulfillment of the
Requirements for the Degree of

MASTER OF SCIENCE

In

MECHANICAL ENGINEERING

January, 1992

Order Number 1354082

Experimental determination of heat transfer coefficient for water-lithium bromide mixture

Al-Bazroon, Hussain Abdulla, M.S.

King Fahd University of Petroleum and Minerals (Saudi Arabia), 1992

U·M·I
300 N. Zeeb Rd.
Ann Arbor, MI 48106

EXPERIMENTAL DETERMINATION OF HEAT TRANSFER COEFFICIENT FOR WATER-LITHIUM BROMIDE MIXTURE

BY

HUSSAIN ABDULLA AL-BAZROON

A Thesis Presented to the

FACULTY OF THE COLLEGE OF GRADUATE STUDIES

KING FAHD UNIVERSITY OF PETROLEUM & MINERALS

DHAHRAN, SAUDI ARABIA

In Partial Fulfillment of the
Requirements for the Degree of

MASTER OF SCIENCE

In

MECHANICAL ENGINEERING

JANUARY 1992

KING FAHD UNIVERSITY OF PETROLEUM AND MINERALS
DHAHRAN 31261, SAUDI ARABIA

COLLEGE OF GRADUATE STUDIES

This thesis, written by **HUSSAIN ABDULLA AL-BAZROON** under the direction of his Thesis Advisor and approved by his Thesis Committee, has been presented to and accepted by the Dean of the College of Graduate Studies, in partial fulfillment of the requirements for degree of **MASTER OF SCIENCE IN MECHANICAL ENGINEERING.**

Thesis Committee

Thesis Advisor(Dr. A.F.M.Abdul Ali)

Member (Dr. S.M.Zubair)

Member (Dr. A.Z.Sahin)

15/1/92

Department Chairman

Dean, College of Graduate Studies

Date: 19.1.92

DEDICATION

This Thesis is dedicated to my dear Mother and Father, my brothers Abdulla and Ali, my Wife and my beloved Children Ail, Hassan and Sukaina.

ACKNOWLEDGMENT

Glory and greatness be to *All Mighty ALLAH, Subhanahu Wa Taallah*, who by his Grace has made this work possible.

To my dear beloved Mother and Father whom have taught me all what I know and through their wisdom and many sacrifices had the foresight to quid and encourage me in every aspect of my life.

Acknowledgment is due to King Fahd University of Petroleum and Minerals and Saudi ARAMCO for support of this research.

I wish to express my appreciation to Dr. A.F.M. Ali who served as my major advisor and the other committee members Dr. S.M.Zubair and Dr. A.Z.Sahin. I also wish to thank the supervisors of both the mechanical and the chemical engineering, Mr. Barrie R.Rose and John Chapman whom have assisted me. I further would like to thank the library staff in both Saudi ARAMCO and KFUPM.

TABLE OF CONTENTS

CHAPTER 4

LIST OF TABLES

LIST OF FIGURES

ABSTRACT

A heat transfer apparatus was fabricated to predict the heat transfer coefficient of lithium bromide-water solutions during forced convection and low quality boiling at different concentrations. The apparatus was connected to a computer system that collects the required heat transfer data such as surface and fluid temperatures.

The data were analyzed and several plots were generated for temperature, heat transfer coefficient and vapor quality distributions. Two correlations were obtained, one for forced convection and another for saturated boiling. They correlated the experimental data within ± 12% . The convection correlation was compared with Dittus-Boelter equation and it was found that they differ with only 7%.

الخلاصة

في هذا البحث تم تصميم جهاز نقل حراري لقياس معامل الانتقال الحراري لمادة الليثيوم بروميد المذاب في الماء وذلك في حالة الحمل الحراري والغليان للسوائل المندفعة في الأنابيب .

وقد وصل هذا الجهاز الى حاسوب يعمل على جمع وتبويب المعلومات المطلوبه مثل حرارة سطح انبوب الأختبار وحرارة السائل المندفع بداخله .

وبعد جمع المعلومات وتحليلها عملت الكثير من الرسومات لتوزيع الحراره ومعامل الأنتقال الحراري ونسبة المادة المتبخره في داخل انبوب الأختبار . ثم استنتجت علاقتي تبادل لمعامل الأنتقال الحراري احدهما في حالة الحمل الحراري والاخرى في حالة الغليان المندفع وهاتين العلاقتين قادرتان على تمثيل المعلومات المخبريه بنسبة ١٢ ٪ وقد تم مقارنه علاقة الحمل الحراري مع علاقة ديتوس – بولتر حيث وجدان نسبة الاختلاف بينهما هي ٧ ٪ فقط .

CHAPTER I

INTRODUCTION

Lithium Bromide water mixture is a well known binary solution used in industrial absorption heat pumps. It has several advantages over the famous binary solution ammonia water mixture. Among these advantages are the higher coefficient of performance and the design simplicity of its refrigeration system . In recent years lithium bromide refrigeration units are widely used due to the ingenuous mechanical arrangements of the equipment pieces, their reliability and high fabrication quality. To maximize the coefficient of performance of these units, accurate prediction of heat transfer characteristics in the different locations of the unit is required. To find out the heat transfer coefficient in a single-phase , forced-convection heat transfer flow, the physical properties of the fluid and certain dimensions are used with a suitable equation , whether it is analytical or empirical. However, in two phase flow, the situation is absolutely different since the coefficient of heat transfer is not only a function of the fluid properties and the geometry characteristic dimension but many parameters are required to

to describe a specific fluid in a unique flow. Some of these parameters are pipe geometry, flow direction, surface tension, pressure and flow rates of each phase. Besides that, many flow patterns are usually involved in a single flow that must be identified and described by a certain model. Unfortunately, it is not only impossible to describe the flow patterns like slug flows and annular flow with the same model it is also difficult to adopt a different model to each flow because of the lack of information about the transition zone between different patterns. For the above reasons, analytical formulation of two phase flow is not possible and cannot be described by the known fundamental equations. Therefore, the best way to describe a two phase flow is to conduct an experiment, and to correlate its data by an equation whose form and parameters depend on the pattern of the flow. For example, in subcooled boiling, coefficient of heat transfer can be described by an equation similar to that of a single phase forced convection flow that can be expressed as,

$$Nu = C1\ Re^{C2}\ Pr^{C3}$$

where,

C1,C2 and C3 are constants found from the data

The resulting correlation can be used to predict heat transfer data for another problem conducted under similar situation as that of the experiment.

While there is considerable published information on two

phase forced convection flow, very little has been known on forced convection of binary mixtures because it is more complicated than that of two phase flow and its field is largely unexplored. Besides the random character of the flow and the parameters that govern the configuration of each pattern, the saturation temperature and the properties of the mixture keep changing due to the starvation of the more volatile component as heat is added that changes the concentration of mixture and therefore its properties. Although various models of correlations have been suggested to describe the different regimes of binary mixture boiling heat transfer, these correlations cannot be applied as general equations even for the same fluid that was used in collecting the data because of the misunderstanding of the different parameters involved in boiling while collecting and correlating the data. Besides that some correlations cannot describe even their data better than ± 30 % error. Therefore the user of these correlations should be very careful when applying them in their problems. To determine the heat transfer coefficient of lithium bromide water mixture, a boiling apparatus was fabricated.
In this apparatus, the binary mixture flow inside a vertical tube which is heated at a constant heat flux. Sixty thermocouples were used to measure both the tube surface temperature and the fluid mean temperature. Data acquisition system was used to collect temperature and flow rate data while other data were calculated manually.

The advantage of this apparatus is that it reads the mean temperature at each section of the boiling tube giving an accurate information about the heat transfer inside the tube. This criteria was not available in most of the equipment used for collecting previous data in the literature where average values of the fluid mean temperatures were used.

The other eight chapters in this study are described briefly as follows:

Chapter II is the objective of this investigation and chapter III is a literature review which is a general study of binary mixtures heat transfer and two phase flow since it is the main aim for understanding forced convection and boiling of binary mixtures.

Chapter IV is a general study about lithium bromide solution which includes first, the thermal and physical properties, of lithium bromide solutions at different temperatures and solution concentrations. These properties are needed for the various calculations involved in data reduction section. Second, it includes the procedure followed when preparing a specific concentration solution and precautions that should be followed when working with these solutions. Also this section gives some information about the medical hazards of the solutions. Third, general information about absorption heat pumps where lithium bromide is used, and the characteristics of the ideal working fluid with evaluations of

lithium bromide as a working fluid.

Chapter V includes the theories that will be used in analyzing the experimental data and the procedures used in calculation .

Chapter VI includes the specification and the design of the different components of the apparatus, the procedure used in fabrication and sample calculations to justify the assumptions used in design.

Chapter VII describes the various instruments used in the experiment such as the data acquisition unit and the ultrasonic flow meter.

Chapter VIII consists of the data collected from the experiment and the data reduction . Various plots for temperature, heat transfer coefficient and vapor quality at different locations of the test section are included with the suggested correlations for both convection and boiling. Also it includes the errors analysis and the source of errors .

Chapter IX is the conclusion and recommendations .

CHAPTER II

OBJECTIVE

Lithium bromide-water refrigeration system is a simple absorption system that operates with higher coefficient of performance than ammonia-water refrigeration system. To increase the coefficient of performance of this system , accurate prediction of heat transfer characteristic of its binary mixture is required. Since the available theory and the experimental data in binary mixture do not allow a general correlation that can be used for any binary mixture , an experimental heat transfer investigation for lithium bromide-water mixture should be done.

To accomplish this task , number of objectives are required which can be summarized as follow.

1. Fabricate a heat transfer boiling apparatus which will be utilized to collect data in convection, subcooled and saturated boiling of lithium bromide-water mixtures. A diagram that describes this apparatus is shown in figure 2.1.

2. Collect the required data that will include the surface and the fluid mean temperatures, the heat added to the test section , the flow rate and the inlet and outlet pressures.
3. Analyze the collected data within the available theories and correlate the experimental heat transfer coefficients in both convection and saturated boiling.

The convection data may be correlated as ,

$$Nu = C\ Re^{m}\ Pr^{n}\ f$$

Where Nu,Re and Pr are Nusselt , Reynolds and Prandtl numbers respectively . The function f accounts for the concentration effect on heat transfer coefficient whereas c,m and n are constants determined experimentally.

The boiling data can be correlated as,

$$\frac{h_B}{h_c} = C1\ Bo + C2 \left[\frac{1}{Xtt}\right]^{C2}$$

Where h_B and h_c are the heat transfer coefficients for boiling and convection respectively and Xtt is the Lockhart Martinlli parameter which will be define in chapter 5.

4. Testing the correlations by calculating their

All the above objectives make sequential tasks that lead to the main goal which is experimental determination of heat transfer coefficient for lithium bromide- water mixture at different concentrations.

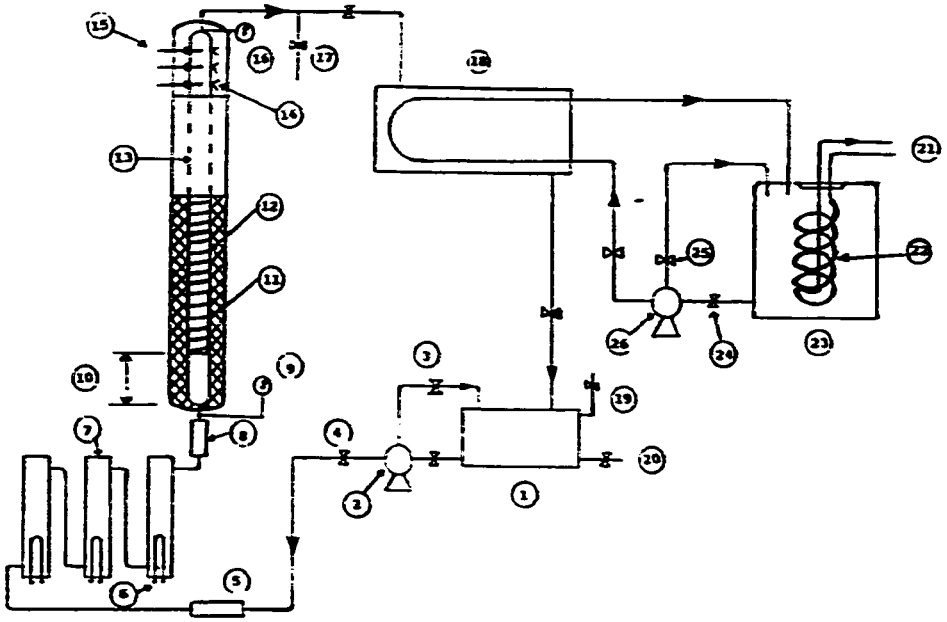

Figure 2.1 Schematic representation of the experiment apparatus

Item No.	description
1	liquid reservoir
2	lithium bromide-water solution
3	feedback
4	flow rate control valve
5	turbine flow meter
6	electric heater
7	preheater
8	eye glass
9	inlet pressure gauge
10	25 cm unheated length
11	ceramic insulator
12	electric heater
13	tube test section
14	surface temperature thermocouple
15	fluid mean temperature thermocouple
16	exit pressure gauge
17	evacuation valve
18	heat exchanger
19	filling valve
20	drainage valve
21	cooling unit lines
22	evaporator
23	water reservoir
24	main valve
25	feedback valve
26	water pump

CHAPTER III

LITERATURE REVIEW

The discussion that follows is included here to complement information about binary systems and two phase flow which may help in understanding the problem under investigation . A summary of each study is given and we will refer to discussion while analyzing the experimental data .

3.1 SURFACE BOILING

In a form of nucleate boiling here a subcooled liquid boils as it gets in contact with a hot surface, the vapor bubbles condense on the cold liquid without any net vapor generation . Mosciki and Broder [28] were the first to investigate this phenomena. Wooda found that the coefficients of heat transfer were four times those predicted for nonboiling condition due to the local boiling at the surface and condensation of the vapor in the cold liquid .

Gilmour [29] proposed the following correlation for nucleate boiling:

$$St \quad Pr^{0.6} \left(\frac{\Gamma_L \sigma}{P^2}\right)^{0.425} = \frac{\phi}{Re^{0.3}} \qquad (3.1)$$

Where:

ϕ = Proportionately constant = 0.001 for copper tube.

Γ_L , Γ_v = Density for liquid and vapor phase

P = Boiling pressure

σ = Surface tension of liquid and

$$G = \frac{m}{A}\,\frac{\Gamma_L}{\Gamma_v}\,,\quad St = \frac{h}{C_p G}\,,\quad Re = \frac{DG}{\mu}\,,\quad Pr = \frac{Cp\ \mu}{k}$$

Where:

G = Mass flux , kg/sm^2

m = Vapor Rate , kg/s

A = Surface Area, m^2

Cp = Liquid specific heat , kj/kg k

μ = Liquid viscosity , Pa s

h = Film coefficient of heat transfer , W/m^2 k

k = Liquid conductivity , W /m k

D = Tube diameter , m

In this correlation he introduced a new dimensionless group ($\Gamma_L \sigma / P^2$) which accounts for pressure and the surface

tension. Also he introduced a proportionality constant that includes the effect of the material and type of the boiling in the tube. Experimental data for methanol and benzene were used to find the exponents. This data sets ranged between Re=120 -5 x 10^5 . Results showed that heat transfer coefficients obtained from experiments using stainless steel or chromium tubes are about 43% lower than those obtained from copper or steel surfaces.

Bergles and Rohsenow [28] distinguished three regions in forced convection surface boiling. At -low wall superheat the heat transfer is governed by forced convection and the related correlations can be successfully used to predict the heat transfer. At moderate wall superheat both forced convection and surface boiling govern the heat transfer. At high superheat the effect of force convection dissappear and the heat transfer is governed by the fully developed surface boiling. In the third region the surface boiling must be based on actual forced convection boiling data and not on saturated pool boiling data.

3.2 Boiling Mechanism

The accepted nucleation theory suggests that vapor bubbles are formed at small cavities on the heating surface (See Figure 3.1)[27]. For a bubble to grow, a net heat

transfer through the thermal layer surrounding the bubble must be maintained.

3.3 Forced Convection Boiling

In a fully developed subcooled liquid flow within a uniformally heated tube, both the mean and surface temperatures increase linearly until they reach to the point where the fluid mean temperature becomes equal to the saturation temperature while the surface temperature maintains a certain amount of superheat , (See Figure 3.2). This point is called the onset of nucleat boiling where stable vapor bubbles are generated. Nine definitions exist for the onset of boiling. The location of the onset in each definition is shown in figure 3.2 and there appears to be a significant disagreement between these definitions [30].

The following expression can be derived for the degree of subcooling ΔT_{SUB} at which boiling begins by assuming the onset criteria of $T_{cov} = T_{boiling}$,

$$\Delta T_{SUB} = \frac{q''}{h_c} - \frac{q''}{h_B} \qquad (3.2)$$

Where:

q" = Heat Flux Density

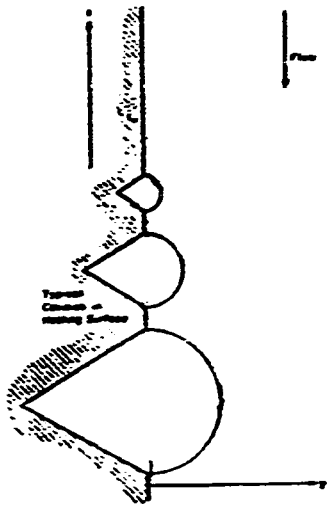

Figure 3.1 Initiation of bubble growth in forced-convection surface boiling [27].

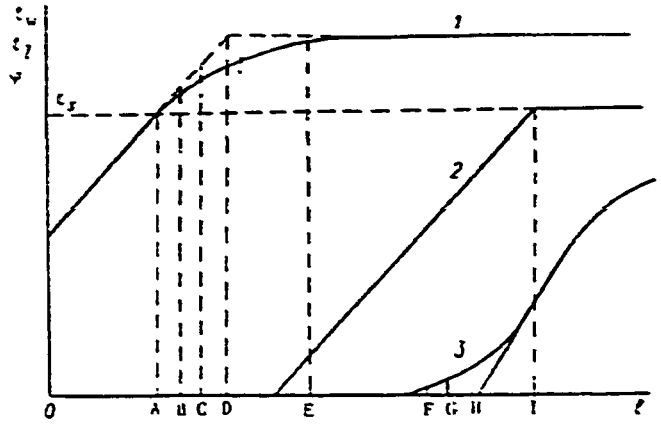

Figure 3.2 Variation of void fraction and wall and surface temperature [30].

h_c , h_B = Heat transfer coefficient for convection and boiling respectively.

h_c and h_B can be found from the following equation:

$$Nu = 0.021\ R_e^{0.8}\ Pr^{0.43} \left[\frac{Pr_m}{Pr_s} \right]^{.25}$$

$$h_B = \frac{3.4(10^{-5}P)^{0.18}\ q^{2/3}}{1-0.045\ (10^{-5}\ P)}$$

where,

P= system pressure , Pa

Pr_s , Pr_m = Prandtl number calculated at surface and fluid mean temperatures respectively

3.4 Critical Heat Flux (CHF) of Subcooled Flow Boiling

Critical heat flux of subcooled flow boiling has great similarities to the pool boiling CHF in both mechanism and behavior . For predicting the critical heat flux for low quality flow boiling , various models have been considered in analytical and experimental studies. Those models can be classified into five groups [31].

1 - Liquid layer superheat Limit Model (1965) Tong et. al

Assumes that CHF occurs when the liquid layer adjacent to the wall has a critical super heat caused by the overlaying bubbly layer resistance to transport the enthalpy to the cooled liquid.

2 - Boundry layer separation model: Kutateladze and Leont'eu (1968-1975)

In this model, it is assumed that CHF is caused by flow stagnation out to the injection of vapor from the wall.

3 - Liquid Flow Blockage Model: (Bergel'son, Smogaleu 1980-1981)

It assumes that CHF occurs when flow normal to the wall is blocked due to the flow of vapor.

4 - Vapor Removal Limit and Bubble Crowding Model (Hebel et 1981-1985)

This model assumes that CHF is caused due to the limitation in vapor removal by the axial flow.

5 - Liquid Sublayer Dryout Model (Lee and Mudawar 1988):

It assumes that CHF occurs due to the dryout of a thin liquid sublayer underneath the vapor layer adjacent

to the wall.

Phenomena Associated with Subcooled Boiling CHF

1 - Thin vapor layer exists near the wall.
2 - Surface temperature fluctuations in the uniformly heated tubes precedes the CHF.
3 - No change in the bulk flow pattern at CHF.
4 - CHF is effected by the wall thickness.

3.5 Nucleate Boiling in Binary Mixtures

Nucleate boiling in a binary mixture differs significantly from that in pure fluid with identical physical properties. Due to a change in bubble growth rate caused by species diffusion resistance or due to difference in the superheat required to initiate the bubbles in aqueous system caused by a change in wetting characteristics for organic solvents at low concentration. In binary mixture, the nucleate boiling heat transfer coefficient and the bubble departure diameter are lower than that for a pure fluid with identical physical properties while the critical heat flux is greater [25,26].

R. A. Shock (1976)[25] showed that an addition of small amounts of solutes to pure solvents increases the wall superheat significantly for the given heat fluxes. The reduction in heat transfer coefficient is due to local depletion in the low boiling component at the liquid vapor interface. This causes the local saturation temperature to be greater than that in the bulk fluid which reduces the bubble growth rates and so are heat transfer coefficients.

Van Stralen [25] found that the maximum reduction in bubble growth rate, departure diameter and maximum critical heat flux increase occurs at the maximum mole fraction difference between the vapor mole fraction in equilibrium with liquid and the bulk liquid phase mole fraction of the component which has lower boiling point in the pure state.

3.6 Studies Concerning Lithium Bromide Solutions

In order to understand the absorption process inside the absorber vessel of an absorption machine, many studies were conducted recently on absorption process of low pressure water vapor into a film or lithium bromide water film.

One of these studies is the study of Nobusi Kawae and his colleagues (1989) [33] who studied numerically the absorption of low pressure water vapor into a laminar lithium

bromide water film flowing down a constant temperature vertical flat plate. The assumptions are made to numerically solve this problem , these are :

1 - Laminar and fuly developed solution film.

2 - Shear force exerted on at the vapor-solution interface is negligible.

3 - Constant pressure.

The results obtained from the study are the following:

1 - The maximum absorption mass transfer over a certain distance depends on a certain inlet film thickness.

2 - Total absorption mass transfer rate with variable properties is lower than that with constant properties.

3 - Total absorption mass transfer rate increases with the system pressure, inlet concentration and Lewis number increase.

Patil and his colleagues [36] experimentally studied aqueous lithium halides as single and double-salt solutions in absorption heat pumps. The experiment was conducted at the condenser and absorber temperatures of 70°C, while the generator and evaporator were at 100°C and 45°C,

respectively. The flow ratio was in the range between 10 to 60. The solutions which were studied were prepared from LiBr, liCl, LiI, liBr/LiCl and LiI/LiCl. The double salt solutions were prepared with 1:1 weight ratio . The coefficients of performance (COP) for the different salt were plotted against the flow ratio (FR). They show that the COP decreases with the increase in the flow ratio (FR) for all salts(See Figure 3.3).

Horoshi and his colleagues [24] studied experimentally forced convective boiling for nonazeotropic, binary mixtures for R22 and R114 inside a horizontal tube. These mixtures have great potentials as working fluids in vapor compression heat pump systems due to their high performance. The result of the study can be summarized as follows:

1 - Surface and bulk temperature were plotted against the tube sections. From the plots it is seen that surface temperature increases almost linearly with the tube sections , while the mixture temperature increase depends on the concentration.

2 - The quality of the mixture increases almost linearly from 0.2 to 1.0.

3 - Boiling heat transfer coefficients were correlated to

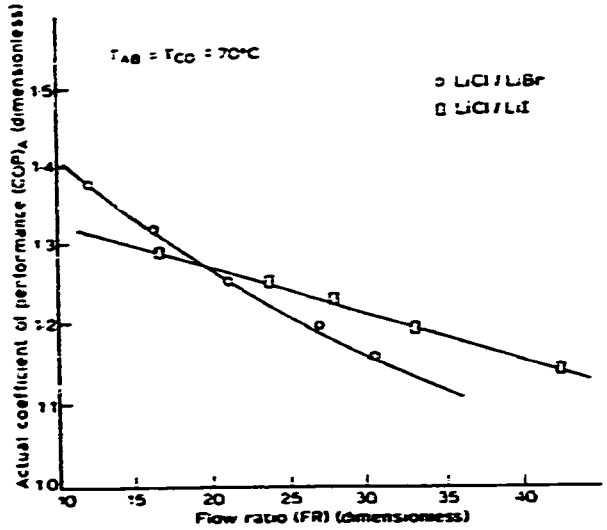

Figure 3.3 (a) Coefficientof perfrmance againest flow ratio for lithium halides [36].

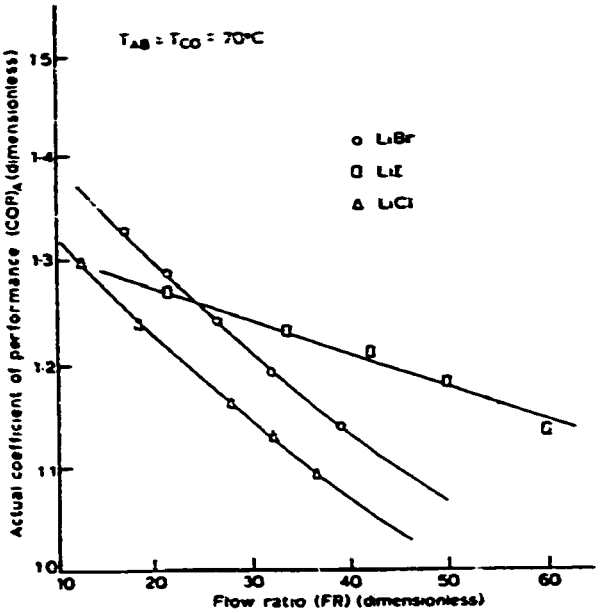

Figure 3.3 (b) Coefficint of performance againest flow ratio [36].

the liquid forced convection heat transfer coefficient as:

$$h/h_{con} = C_1 B_o + C_2 \left(\frac{1}{X_t}\right)^{C3} \qquad (3.3)$$

Where

B_o = Boiling number = $q/G(h_v - h_l)$

X_t = Lockhart - Martinelli Parameter [17]

$$= \left(\frac{\mu_l}{\mu_v}\right)^{0.1} \left(\frac{\Gamma_v}{\Gamma_L}\right)^{0.5} \left(\frac{1 - X}{X}\right)^{0.9}$$

and $$h_{con} = 0.023 \frac{k_L}{d_i} \left(\frac{G(1-X)d_i}{\mu_L}\right)^{0.8} Pr_L^{0.4}$$

C_1, C_2, and C_3, functions of mole fractions of R114 found from the experimental data.

Equation (3.3) correlates the experimental data within ± 30%.

Kriji Murata and Kenichi Hashizume [23] experimentally studied binary mixtures in forced convection boiling of R11 and R114 in a horizontal tube. They found that heat transfer coefficient of binary mixtures decreases in the boiling domain because of an increase in the local boiling due to the starvation of the more volatile component in the liquid near the growing bubbles . In correlating their data they split

the correlation into two terms. One accounts for forced convection h_{FC} and the other accounts for nucleate boiling h_{NB}. Also they related nucleate boiling coefficient to the pool boiling coefficient by a parameter Y which is affected only by the change of the fluid properties. The correlation predicts the data within ± 15%, this relation is given by

$$h = h_{PB}\ Y + h_L\ F = \frac{h_{PB}}{[1+A(MG-ML)]}\ Y + h_L\ F \qquad (3.4)$$

Where

h_{PB} = Pool boiling heat transfer coefficient , W/m^2k

h_L = Forced convection heat transfer coefficient for single phase , w/m^2k

Y = Factor accounts for suppression by the flow.

F = Factor accounts for liquid velocity increase due to the presence of vapor.

MG, ML = Mole fraction of vapor and liquid phase.

CHAPTER IV

LITHIUM BROMIDE AND ITS USAGE

4.1 GENERAL CHEMICAL INFORMATION

Lithium bromide is a white crystalline deliquescent solid which is produced by the reaction of either lithium carbonate or lithium hydroxide monohydrate with hydrobromic acid .The product of the reaction is a solution which can be evaporated and cooled to give crystallized lithium bromide that depends on the final temperature .

Lithium bromide solutions have unusual low vapor pressures . Concentrated solutions can dissolve large quantites of polar organic substances such as cellulose . Some of its properties are listed in table 4.1 .

4.2 PREPARATION OF A SPECIFIC CONCENTRATION SOLUTION

Due to the hygroscopic character of lithium bromide , preparation of its solutions by weighing both solvent and solute cannot be conducted [34]. Instead , a solution whose

Melting point [a]	823°K; 550°C
Heat of fusion, ΔH_m [a]	4.22 kcal mole^{-1}
Boiling point [a]	1555°K; 1282°C
Heat of vaporization, ΔH_{vap} [a]	27.0 kcal mole^{-1}
Heat capacity, C_p^s [b]	12.4 cal mole^{-1} deg^{-1}
Entropy, $S°$ (298°K) [a]	16.0 cal mole^{-1} deg^{-1}
Heat of formation, ΔH_f^s (298°K) [b]	−83.72 kcal mole^{-1}
Free energy of formation, ΔF_f^s (298°K) [a]	−80.993 kcal mole^{-1}
Lattice energy, U [c]	−189.9 kcal mole^{-1}
Density [d]	3.463 g cm^{-3} at 25°C
Solubility, aqueous [e,f]	0°C, 56.7 wt.% LiBr
	30°C, 61.6 wt.% LiBr
	100°C, 69.6 wt.% LiBr
Formula weight	86.85 awu
Crystal structure [g]	Sodium-chloride structure

Table 4.1.Properties of Lithium Bromide

concentration was determined by titration method should be used to give other concentrations .

One of the best methods for determining the concentration of lithium bromide is by measuring its density. The following procedures descibe this method [34].

1- Heate the lithium bromide salt , to get rid of absorbed material , to it add a known quantity of conductivity grade water to prepare what is called the initial solution. Then its concentration is estimated by determinig the difference in the weight .

2- Different concentration solutions can be prepared from the initial solution by adding different amount of conductivity grade water .

3- Concentration of each solution can be found from the value of its experimental density by substitution in the follwowing expression [34],

$$\Gamma=(0.997055)*10^{3} +(0.00726) X \qquad (4.1)$$

where,

Γ = solution density in Kg/m3

X = weight concentration percentage

4.2.1 The Initial Solution Volume Required to Prepare a Certain Amount of Another Concentration Solution

Let V_2 is the volume in liter of lithium bromide solution whose weight concentration and density are X_2 and Γ_2 respectively. This amount is to be prepared out of an initial solution whose concentration and density are X_1 and Γ_1 respectivily . To find the required volume V_1 in liter of the initial solution , we proceed as follows:

Since the mass of lithium bromide in the final solution will be taken from the intial solution ,the mass of lithium bromide in the final solution M_{LiBr2} will be equal to that of the the initial solution M_{LiBr1} .

Expressing the mass of lithium bromide in terms of the volume , concentration and density of the solutions , we get

$$\Gamma_2 * X_2 * V_2 = \Gamma_1 * X_1 * V_1$$

If we subtitute equation (4.1) in the above equation for both densities we get the following expression

$$V_1=(A + B X_2) X_2 V_2 /((A + B X_1) X_1) \qquad (4.2)$$

where

A=997 , B=7.26

Note that this expression is used for solution temperature of 25 °C approximately , otherwise the constants A and B should be changed [34,40]. Some worked out examples are given inb Appendix B.

2.3 CORROSION AND CORROSION INHIBITORS -

To prevent corrosion of the various component of the system ,corrosion inhibitors should be added to the lithium bromide solution . The solution should contain sufficient amount of a nitrate and a triazole compoiund selected from benzotriazole and tolyltriazole .The nitrate concentration is in the range between 0.005 to 0.1 % by weight and the prefered concentration is in 0.01 to 0.05 % by weight . The other compound which is the triazole has a very low solubility in lithium bromide solutions hence, the concentration of the triazole compound is in the range of 0.001 to 0.12 % by weight[10] .

A study was performed on an absorption system constructed from carbon steel, oxygen-free copper (ASTM 102)

and cupronickel alloy (ASTM 703). The system was subjected to nine corrosion tests at 160 °C in vacuum for 200 hours . A 0.2 by weight of lithium hydroxide was added to 22 % by weight lithium bromide solution and then mixed with an aqueous solution containing lithium nitrate and benzotriazole separately prepared. The amount of corrosion in each test at that time is shown in table 4.2 . In the same table, there is a test result obtained from using an absorbing solution containing an organic inhibitor lithium chromate . This inhibitor is the one used in building #16 chiller system at KFUPM. Using lithium chromate causes sharp and deep pitting . The amount of corrosion for the chromate inhibitor is fluctuating, thus an average of ten tests pieces were employed. On the other hand , using the organic inhibitor leaves a uniform black film after the test and it reduces corrosion rate remarkably .

2.4 HEAT PUMP

A heat pump is a device that extracts heat from low temperature source and gives off this heat at higher temperature level where it can be used as shown in Fig. 4.1. Similar to that is the refrigeration system but it's usage is to extract heat from low temperature source only [11,12].

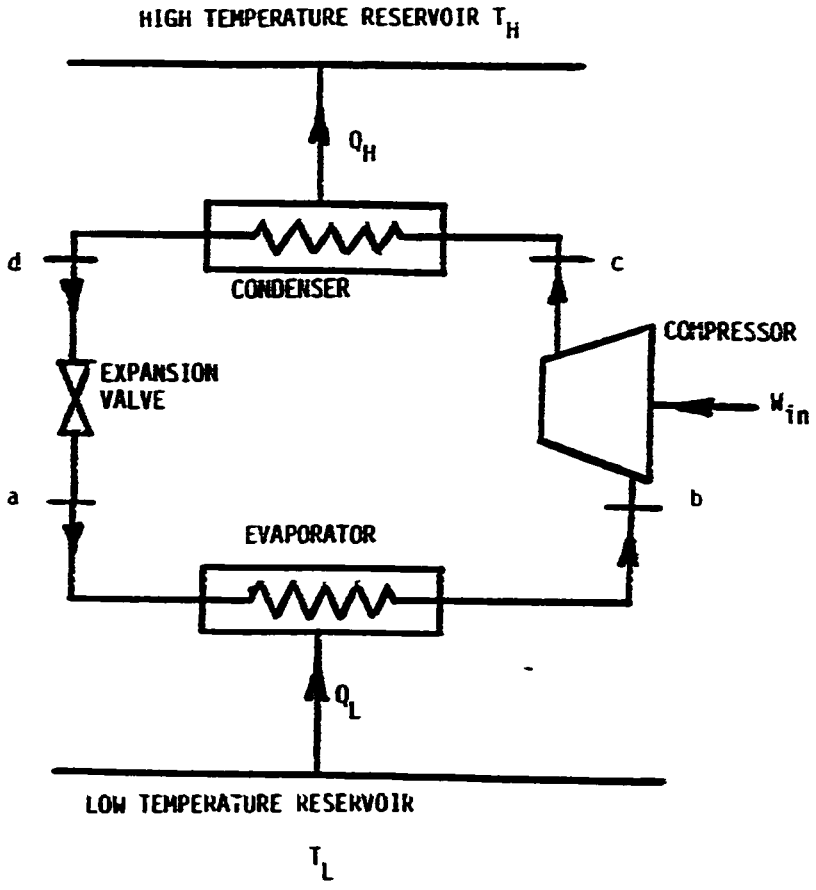

Figure 4.1.Schematic Representation of Heat Pump [11]

	Lithium nitrate concentration (wt. %)	Benzotriazole concentration (wt. %)	Corrosion (mg/dm²)		
			Carbon steel	Copper	Cupronickel
Example 1	0.035	0.005	320	45	40
Example 2	"	0.01	280	23	15
Example 3	"	0.05	250	20	12
Example 4	"	0.1	252	20	13
Example 5	0.003	0.05	350	18	10
Example 6	0.01	"	310	19	11
Example 7	0.05	"	340	50	18
Example 8	0.1	"	360	80	19
Example 9	0.15	"	430	130	23
Conventional Example	Lithium chromate (0.3 wt. %)		500	300	180

Table 4.2.Corrosion Inhibitors Tests for Different Materials in Lithium bromide Solutions.

4.4.1 Energy Used in Heat Pumps

Although the production of heat at high temperature level is maintained mostly by the consumption of primary energy like fossil or nuclear fuels and solar energy, heat pump does not require a source of primary energy because it upgrades the heat only . In addition to the low and high temperature sources which the heat pump utilizes, a third auxiliary energy source is needed for the heat pump to deliver the required heat . This drive source may be a mechanical or thermal energy .

4.4.2 Mechanically Driven Heat Pump

It uses high grade energy to drive the heat pump . One example of this is the vapor-compression heat pumps which requires mechanical work to compress the working fluid . This work is usually provided by compressors which are driven by electric motors as refrigerators or air conditioners found in residential applications .

4.4.3 Thermally Driven Heat Pumps

In the recent years, considerable interest is focused

towards the thermally driven heat pumps because of the following features .

1- It does not have compressors.

2- There is no vibration or noise .

3- It has high primary energy efficiency .

4- It has long life expectancy due to the absence of moving components .

5- It can be fired directly .

6- The cost of maintenance is relatively low.

4.4.4 Absorption Heat Pumps

The absorption heat pump is thermally driven heat pump where a fluid called tha absorbent is used to absorb the refrigerant coming from the evaporator forming what is called a binary mixture [13].

4.4.5 Binary Mixture

It is a mixture of two completely miscible substances. Binary mixtures can be classified as azeotropic and non azeotropic mixtures . Azeotropic mixtures are mixtures that have critical compositions where the composition of vapor is the same as that for liquid in such way there is no change of compositions upon evaporation .

4.4.6 Requirements to be Pulfilled by the Working Fluids

To use a specific working fluid in a heat pump, it has to meet some of the following requirements.

4.4.6.1 Substances Thermal Properties

It is desirable to have the following thermal properties [11].

1- Low melting temperature to avoid freezing of the substance or mixture .
2- The boiling point of the working substance should coincide with the working temperature of the process.
3- Boiling point of the solvent should be much higher than the working substance to get rid of the rectification process for separating the mixture . Usually a rectifier is not needed when the boiling temperature difference between the two substances is above 200 °C .
4- The enthalpy of evaporation should be large because the larger enhtalpy , the more heat per unit of vapor mass produced in the generator can be transfered. Large enthalpy can be obtained if the process temperature is far below the critical temperature .

5- Thermal conductivity and thermal capacity should be large .

6- Viscosity is desired to be low .

4.4.6.2 Mixture Thermal Properties

1- Complete solubility of the refrigerant and the absorbent over a large range of concentrations .

2- The chilling point should be beyond the working temperature when a solid is used as a solute .

3- The absorption enthalpy must be large enough to accelerate the mixing and absorption process.

4.4.6.3 Working Substance Molecular Structures

The working substance is prefered to be with small polar molecules and the solvent with large molecules containing polar groups. This is because polar groups within the solvent molecules increase the boiling point of the solvent and enhance the interaction with the polar molecules of the working substance, hence increasing the solubility and the mixing enthalpy .

4.4.6.4 Further Properties

Some additional properties that are desirable to be

fulfilled by the working fluid are the following [11,13,36].

1- Both the solvent and the working fluid must contain chemically stable molecules and are not allowed to decompose .

2- Both the solvent and the working fluid should not react with each other and form a new stable product which can not be separated into its original molecules .

3- They should not be poisonous and if ever they are, they should not be used in homes. -

4- They should not be corrosive , although inhibitors can be used to reduce corrosion of the system .

5- They should not be flamable .

6- The mixture should deviate negatively from Raoult's law [36] to reduce the mass flow rate in the secondary circuit for a given mass flow rate in the primary circuit. For aqueous salt solution which obeys Raoult's law the vapor pressure is given by the expression,

$$P = \theta P_{salt} + (1 - \theta) P_{water} \qquad (4.3)$$

where,

P = solution vapor pressure

P_{salt} = salt vapor pressure ≈ 0

P_{water} = water vapor pressure

θ= mole fraction of salt

Figure 4.2 shows negative deviation of the vapor pressure from Raoult's law for lithium halides at 100 °C .

For a solution that have negative deviation from Raoult's law , vapor pressure are lower than those which obey the law for a given mole fraction of water . Therefore for a given vapor pressure the mole fraction is higher than that calculated from Raoult's law which means lower volume flow rate of the solution in the secondary circuit for a given water flow rate in the primary circuit [36].

4.4.6.5 Some suitable mixtures

Before 1983 there were more than 70 binary mixtures and only a few of them were favorable and studied in detail . The studies were included all the aspects discussed earlier in the preceeding sections .The following mixtures were studied in detail [11].

1- Ammonia-water

2- R22-E181

3- Methylamine-water

4- Water-lithium bromide

5- Methanol- lithium bromide

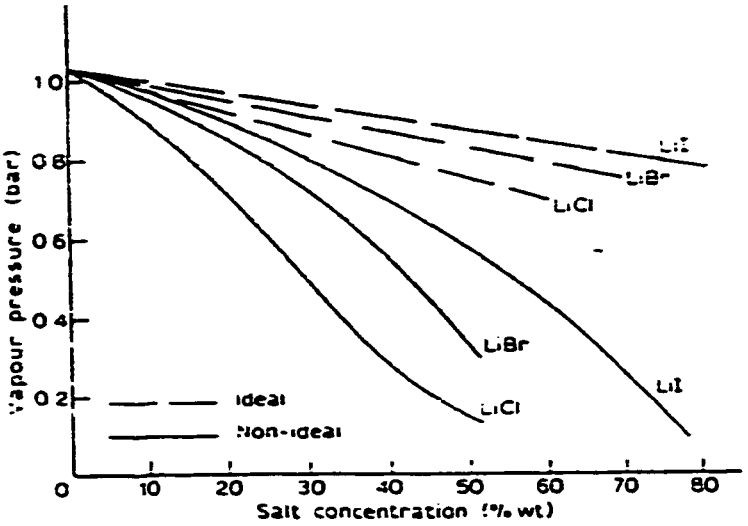

Figure 4.2.Negative Deviations from Raoult's Law of Lithium Halides Solution Vapor Pressure at 100°C [36].

6- Ammonia-lithium nitrate

7- Ammonia-sodiumthiocyanide

8- Methanol-Dimethylformamide

9- Methanol-E181

10-Methanol-water

11-R22-dimethylformamide

Only two of these are well known in industry . These are ammonia-water and water-lithium bromide .

i. Ammonia Water Mixture

Ammonia is a poisonous substance and only 50 ppm are allowed in the environment. It is used mostly in industrial areas. Because the difference between the boiling points of the two components in this mixture is only 133.6 °k in atmospheric pressure, rectification is needed. Thermal properties of the mixture is known up to pressure of 2500 MPa. Ammonia exhibits a high enthalpy of evaporation but it requires high pressure .

ii. Water Lithium Bromide Mixture

Water lithium bromide mixture is one of the important mixtures used in absorption system . Although it meets most of the requirements discussed earlier in the previous sections , major disadvantages of this mixture limit its

usage in industry . Some of the advantages and disadvantages of this mixture is discussed in the following [11]:

1- Because of the large difference between the boiling temperatures of each component (100 °C for water and 1282 °C for lithium bromide)in this mixture , rectification is not needed in heat pumps using this mixture .

2- Lithium bromide water solution achieves higher performance than ammonia water combination.

3- Water has moderate vapor pressure which does not require expensive thick walled equipment and piping.

4- Water is a safe working fluid and has high latent heat of evaporization .

5-Water is the most important polar solvent and has the highest dielectric constant of all the known liquids . Therefore, it has high ability to solubilise ionic salt and produces electrolyte solutions .

6- Alkali metal such as lithium bromide are more soluble in water than any salt .

7- Molecular interactions in lithium bromide water solutions are more favorable because the ions reduce the vapor pressure which decrease the tendency of water molecules to separate from the solution .

8- Crystallization of lithium bromide is one of the major disadvantages of this solution at low temperatures . From the concentration temperature diagram , we deduce that 60 % lithium bromide solution will crystallize at 15.6 °C which mean that tube plugage will occur on secondary circuit if the heat pump is operated at this temperature .

9- Due to the high water melting temperature , the evaporator temperature can not go below 0 °C otherwise refrigerant will freeze inside the evaporator which limits the usage of lithium bromide in freezer units. Also when the environment temperature approaches the freezing point of water, the viscosity of the aquaeous solutions increases rapidly with the risk of frost formation in the condenser .

10- Cooling by water is needed for the absorber and condenser .

11- Because of the corrosivity of lithium bromide solution especially at high temperatures, expensive materials are required for design in addition to the use of corrosion inhibitors .

4.4.6.6 Solutions to overcome lithium bromide crystalization

As mentioned above , crystallization is one othe major disadvantages of utilizing lithium bromide water mixture . In order to overcome this problem , some investigators attempted to add additives to the solution: Marcress [34,36] found that the addition of a second salt to the lithium bromide solution improves its solubility . Angelika and Keller [35] found that addition of ammonia to lithium bromide water system shifts the crystalization line to higher temperature and decreases the vapor pressure of ammonia .

4.4.6.7 Addition of lithium chloride to lithium bromide mixture

Addition of lithium chloride to lithium bromide solution reduces the amount of lithium bromide required which also decreases the corrosion rate and the medical hazards of the solution . In addition to that, the solubility range increases thus reducing the risk of crystallization . Although lithium chloride-lithium bromide mixture has

slightly higher viscosity than lithium bromide mixture , its viscosity is acceptable at the lowest temperature of the secondary circuit [36].

4.4.7 Coefficient of Performance

The coefficient of performance of heat pump is defined as the ratio of useful output to the required input . The performance of an absorption pump depends mainly on the evaporator, condenser, absorber, generator temperatures (T_{EV} ,T_{CO} ,T_{AB} ,T_{GE} respectively) and the flow ratio FR which is defined as the ratio of mass flow rate of the mixture M_{AB} from the absorber to that of water M_W from the evaporator .

$$FR= M_{AB}/M_W =X_{GE} /(X_{GE} -X_{AB}) \qquad (4.4)$$

where,

X_{GE} ,X_{AB} = weight concentrations for the generator and absorber mixtures respectively

The coefficient of performance (COP)$_A$ of an absorption heat pump operating in the heating mode is defined as

$$(COP)_A = \frac{\text{total heat delivered from condenser and absorber}}{\text{heat input to the generator}} \qquad (4.5)$$

4.4.8 Simplified Absorption Unit

Lithium bromide water absorption refrigeration units are widely used in commercial and residential refrigeration for food preservation and industrial process requirements [32]. The success of these units is due to their reliability and their high fabrication quality .

Figure 4.3 show a simplified diagram of lithium bromide water refrigeration unit. To minimize the pressure drop due to flow, similar pressure components are placed together . Therefore, both condenser and generator are placed in one vessel and the evaporator and absorber are placed in another. Mounting the condenser-generator vessel over the evaporator-absorber vessel make the condensate water flow by gravity to the evaporator.

In this unit the fluid to be cooled gives its heat by boiling low pressure water in the evaporator . The vapor flow by natural convection to the absorber where concentrated lithium bromide absorbs the coming vapor while the heat of absorbtion is carried out by cooling water .The diluted

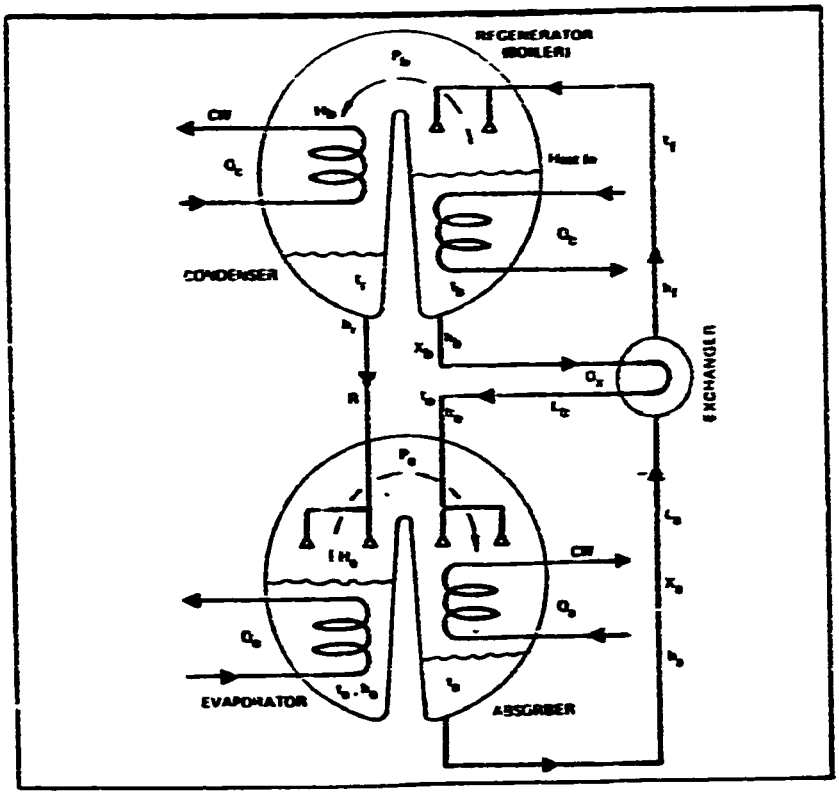

Figure 4.3. Simplified Flow Diagram for Lithium Bromide Absorption Unit [32].

mixture is pumped into the generator where it is heated by steam ,hot water or direct firing . Due to the significant difference in boiling point between water and lithium bromide in the mixture , water evaporates and moves to the condenser where it loses heat .The condensates (water) then is throttled just before it reaches the evaporator where it is boiled and the cycle starts again. The concentrated solution which was lifted from the generator moves by gravity to the absorber where it absorbs the vapor coming from the evaporator .

4.5 LITHIUM BROMIDE HANDLING PRECAUTIONS

When working with lithium bromide , avoid touching its solutions or inhaling its vapor . Careless handling of lithium bromide can cause severe problems. Some of these are [39] :

1- Implicated in the development of a plastic anemia .
2- Lithium ion has CNS (central nervous system) toxicity
3- Causes dizziness and prostration .
4- Can cause kidney damage , anorexia , nausea , apathy, coma and death .
5- Solution in water is very caustic .
6- Produces depression , emaciation and in severe cases,

psychosis and mental deterioration .

7- Bromide rashes , espsecially on the face and resembling ACNE and furunculosis often occur when bromide inhalation .

8- When strongly heated , it emits highly toxic fumes .

2.6 THERMODYNAMIC PROPERTIES OF LITHIUME BROMIDE WATER SOLUTIONS

In 1976 ASHRAE TC 8.3 started a project to review the properties of lithium bromide solution. Data were collected from the major manufacturers of lithium bromide equipment in the United States . In 1977 the result of the project was presented to ASHRAE TC 8.3 with a recommendation to use the Carrier Duhrtng chart and enthalpy concentration diagram because it gives good representation of the properties over a wide range .Summary of tables and charts is followed [14].

4.6.1 Duhrtng Chart

It based on the Duhrtng's rule [14] which assumes that the relation between the boiling point of a solution and its solvent is linear at the same pressure as can be seen figure A4.4 and table A4.3 in appendix A . Different data were

collected from various sources and straight line interpolation were used for calculating the constants . For concentration below 45 % , the maximum deviation was 0.8 °F at 37.5 % and the average deviation is 0.3 °F . For concentration above 45 % , the average deviation increases from 2.0 °F at 50 % to 7.0 °F at 68.8 % . The maximum deviation was 8.5 °F . This shows that high concentration values in this chart are in error and the greater deviation is near crystallization .

4.6.2 Carrier Data

Table A4.4, A4.5 and A4.6 include data taken prior to 1955 . The vapor pressure reading were converted to dew point temperature and compared to both Pennington equation and Duhring equation and found that the fit of the data to both equations was good .Table A4.7 compares the deviations between the data and the calculated values .

Pennington equation

$$\text{Log } P = A + B/T + C/T^2 \qquad (4.6)$$

where,

P=vapor pressure

A,B and C =constants

T = solution temperature

Duhring equatioin

$$T=A\ T_R + B \qquad (4.7)$$

where,

T_R=refregerant temperature

T=solution temperature

A and B =constants

4.6.3 Vapor Pressure Data of Greeley

Table A4.8 shows vapor pressure data taken in 1959 which covers the range of solvent temperature from 75 to 130 °F at concentration range from 58 to 64 % . The vapor pressure data were converted to dew point temperature . The maximum deviation was 0.7 °F and the average deviation was 0.2 °F at 57.96 % and 0.6 at 64.4 % .

4.6.4 Vapor Pressure Data Taken by the Dew Point Method

More than 250 data point were obtained to check the full range of the Duhring chart [14].The result of this test shown in figure A4.5 were very good . The average deviation was 0.2 °F in the first run and 0.5 in the second run . Sixteen of

the 250 points deviated from 1.0 to 1.2 °F due to experimental error. For more details see [14], page 415 .

4.6.5 The Differential Heat of dilution at 77 °F

This chart helps to check the accuracy of the Duhring chart at 77 °F . It represents the change of enthalpy of water before and after being added to the solution. Duhring lines give a poor fit beyond 60 % for differential heat of dilution as can be seen in figure A4.6 .

4.6.6 Enthalpy Concentration Diagram

Constructing the enthalpy concentration diagram depended upon experimental data available in figure A4.7 and table A4.9. The data in the chart can be calculated indirectly from the Duhring plot of figure A4.4 and the data of table A4.3 with the help of the steam table (see [14] , page 417 for calculation detail) .

4.7 PHYSICAL PROPERTIES

The only source available for the physical properties of

lithium bromide water solutions is the report of Kansai University in Japan where it gives only the results of the experiments . Data for the physical properties are listed in tables A4.10 to A4.13 . The specific heat of the solutions can be calculated using the following equation [43].

$$C_p = A + B\,T + C\,T^2 \qquad (4.8)$$

where,

$$A=1.098 - 1.529*10^{-2}\,X + 6.22*10^{-5}\,X^2$$

$$B=-3.651*10^{-3} + 4.204*10^{-5}\,X$$

$$C=3.576*10A^{-5} - 4.238*10^{-7}\,X$$

CHAPTER V

THEORY AND CALCULATION PROCEDURE

5.1 THERMODYNAMIC REVIEW

The first law of themodynamic is essential for calculating the vapor quality distribution along the test section since only the inlet condition and the heat added to each section along the test section tube are known.

5.1.1 First Law of Thermodynamics

The first law of thermodynamics for closed system with negligible potential and kinetic energy can be expressed in differential form as follows [12]:

$$dU = dQ + dW \qquad (5.1)$$

where,

dU= the change in internal energy

dq= the heat added to the system

dW= the work done by the system

Steady State Flow Process (SSSF)

It is a convenint form of the first law as applied to the steady operation of devices such as compressors and condensers where the fluid enters the device and exits at a diffferent end state.

Certain assumptions are implied when using this form. These asumptions are the following .

1-The control volume is stationary with respect to the coordinate frame .
2- Mass does not vary with time in the control volume .
3- Work and heat rate which cross the control surface remain constant .
4- Potential and kinetic energy are negligible .
5- The mass flux dose not vary with time .

With the above assumptions and further noting that flow work is negligible, the first law of thermodynamics for a control volume with one inlet and one outlet can be written as:

$$q_{CV} + m H_I = m H_E + W_{CV} \qquad (5.2)$$

where,

q_{CV}= heat added to the system

H_I, H_E = enthalpies at inlet and outlet conditions respectively

W_{CV} =work done by the system

m =mass flow rate

5.1.2 Continuity Equation

For a system with one inlet and one outlet , under the same asumptions as SSSF , the continuity equation can be expressed as

$$m_i = m_e = m$$

5.2 CONVECTION HEAT TRANSFER

i.Energy Balance for Flow Inside a Tube

Applying energy balance to flow inside a tube subjected to uniform heating , the following equation can be used,

$$dq_{con} = m\, C_p\, dT_m \qquad (5.3)$$

For the entire tube, equation (5.3) is,

where,
$$q_{con} = \dot{m}\, C_p\, (T_{mo} - T_{mi}) \qquad (5.4)$$

q_{con}= heat added or withdrawn from the tube

C_p= specific heat

T_{mi}, T_{mo}= inlet and exit fluid mean temperature

Rearranging equation (5.3) in terms of heat flow and the wetted perimeter, the fluid temperature variation is obtained.

$$\frac{dT_m}{dz} = \frac{q'' P}{\dot{m} C_p} = \frac{P}{\dot{m} C_p} h (T_s - T_m) \qquad (5.5)$$

where,

P= surface perimeter = πD

h= heat transfer coefficient

T_s= surface temperature

q''=Heat flux

Equation (5.5) can be integrated from z=0 to any z ,

$$T_m(z) = T_{mi} + \frac{\pi D\, q''}{\dot{m} C_p} z \qquad (5.6)$$

ii. Turbulent Flow Inside a Circular Tube

A steady and constant property but a turbulent flow inside a circular tube, where Reynolds number Re≥ 2300 can be represented by the following set of equations:

1. Momentum Equation

$$\frac{1}{r}\frac{d}{dr}\left[(\nu + \epsilon_m)\ \frac{\bar{du}}{dr}\right] = \frac{1}{\rho}\ \frac{\bar{dp}}{dx} \qquad (5.7)$$

where,

ν = molecular viscosity

ϵ_m = eddy viscosity

$\bar{u}$ = time averaged velosity

$\bar{P}$ = time averaged pressure

2. Energy equation

$$\frac{1}{r}\frac{\delta}{\delta r}\left[\ r\ (\omega+\epsilon_H)\ \frac{\bar{\delta T}}{\delta r}\right] = \bar{u}\ \frac{\bar{dT}_m}{dx} \qquad (5.8)$$

where,

$\bar{T}_m$= time averaged temperature

ω = molecular diffusivity

ϵ_H = eddy diffusivity

3. Mass equation

$$\frac{\delta\bar{u}}{\delta x} = 0 \qquad (5.9)$$

i.e. $\bar{u}$ = constant

To solve equation 5.7 to 5.9 , the following have to be assumed.

a. Axial conduction is negligible , $\frac{\delta t^2}{\delta x^2} \approx 0$

b. Radial velocity is zero , $v_r=0$

c. ϵ_H/ν can be neglected in the sublayer relative to molecular conduction for Pr≈1.0

A closed form solution is available for Prandtl number Pr≈1.0 however for Pr > 1 the assumption #3 is not valid any more and a simple closed form is not possible. Instead, numerical solutions are required. Fortunately, many empirical equations have been proposed to fit the experimental data over a wide range of Prandtl number. For constant heat flux in tube Sleicher and Rouse [18] sugested the emperical equation,

$$Nu=5+.015\ Re^a\ Pr^b$$

where,

$$a=.88-.24/(4+Pr) \qquad (5.10)$$

$$b=.333+.5\ EXP(-.6\ Pr) \quad \text{for}$$

$$.1< Pr< 10^4 \quad \text{and} \quad 10^4 < Re < 10^6$$

Other correlations which are in good agreement with the above correlation are,

a. Dittus and Boelter equation for heating liquids:

$$Nu = 0.0265 \ Re^{0.8} \ Pr^{0.4} \qquad (5.11)$$

b. Colburn equation for heating or cooling in tubes:

$$Nu = 0.023 \ Re^{0.8} \ Pr^{1/3} \qquad (5.12)$$

c. Seider and Tate equation for heating or cooling in tube:

$$Nu = 0.027 \ Re^{0.8} \ Pr^{1/3} \ \left(\frac{\mu}{\mu_s}\right)^{0.14} \qquad (5.13)$$

where,

μ, μ_s = viscosity at fluid mean temperature and surface temperature respectively

In the case of binary mixtures, such as LiBr water solution, it is expected that a suitable correlation to fit the data should include the effect of concentration variation. The correlation thus is of the form

$$Nu = C_1 \ Re^{C2} \ Pr^{C3} \ f(\mu^*) \qquad (5.14)$$

where,

C_1, C2, C3 = constants

$\mu^* = \mu_{LiBr} / \mu_{water}$

Nu, Re, Pr = Nusselt , Reynolds and Prandtl numbers respectively

For turbulent flows, common values of C3 is 0.4 for

heating fluids, and C2 is 0.8. Considering these values of C2 and C3 and combining C1 in the function f, equation (5.14) can be expressed as,

$$\frac{Nu}{Re^{.8}\ Pr^{.4}} = f(\mu) \qquad (5.15)$$

5.2.1 Temperature and Heat Transfer Coefficient Distribution

When the temperature profile is fully developed, or in other words the profile is invariant with x , the situation can be expressed as ,

$$\frac{\delta}{\delta x}\left[\frac{Ts - T}{Ts - Tm}\right] = 0 \qquad (5.16)$$

where,

Ts, Tm are the surface and the fluid mean temperatures respectively

For a constant heat flux , the convection equation can be written as ,

$$q'' = h(Ts-Tm) = \text{constant}$$

If h is constant , then

$$(Ts-Tm) = \text{constant}$$

which leads to

$$dT_s/dx = dT_m/dx$$

i.e.

$$dT_s/dx = dT_m/dx = \text{constant} \qquad (5.17)$$

Equation 5.12 suggests that both surface and mean fluid temperatures increase linearly and are parallel to each other for thermally fully developed flow.

When the flow is not thermally fully developed, the thermal conductance varies along the length of the tube, in which case the expression (Ts-Tm)=constant is not valid any more. To find the temperature distribution for the entry length region, equation (5.8) should be solved, but in this case the right side of the equation is not constant . Solution for this equation was obtained for circular tube with constant heat flux by Hallman and Seigel [18]. Their solution covered Pr number ranging from gases to 100. The solution of this equation shows that the profiles of the surface temperature is parabolic in shape until it becomes parallel to the mean fluid temperature, which increases linearly from the point where heat addition starts. The region where the surface temperature profile becomes parallel to the mean fluid temperature is called thermally fully developed region . Also it shows that heat transfer coefficient decreases exponentially until it approaches a constant value which coresponds to the value for the fully developed flow.

5.2.2 Heat Transfer Coefficient Calculation Procedure

The procedure used to correlate the convection heat transfer coefficient data can be discribed as follow.

1. Calculate heat transfer coefficient h_c using the equation,

$$h_c = \frac{q}{A_s\ (T_s - T_m)} \qquad (5.13)$$

where,

q= heat added to each section , W

A_s= tube surface area ,m^2

T_s ,T_m = surface and fluid mean temperature respectively, °C

The electrical heat input to the tube is,

$$q = E\ \ I\ \ \cos\ \ \theta \qquad (5.14)$$

where,

E =electric voltage drop across the heater

I = input current to the heater

cos θ = power factor =1.0

2. Calculate Renold's , Prandtl and Nusselt Numbers for the fully developed region using ,

$$Re = \frac{V\ D\ \Gamma}{\mu} \quad ; \quad Pr = \frac{\mu\ Cp}{k} \quad ; \quad Nu = \frac{h\ D}{k}$$

where

μ = dynamic viscosity N. S / m²

Cp= specific heat at constant pressure J/kg k

k= thermal conductivity W / m k

D= tube diameter m

Γ=density of LiBr solution Kg / m^3

V= velocity = m / Γ A = Q / A

Q= volumetric flow rate m^3/s

A= tube cross section m²

3. Plot (Nu/Re.8 Pr.4) versus (μ_{LiBr}/ μ_{water}) and fit the data with an equation using the least square methods .

Note that all the required physical properties for LiBr were punched in the computer and fitted with equation using the least square method to be used by the computer in the calculation.

5.3 TWO PHASE FLOW HEAT TRANSFER

Two-phase flow phenomena is completely different from single-phase flow which can be described by Navier-Stokes equations for Laminar flow and statistical averaging the Renolds equations and others for turbulent flow . In two phase-flow, it is impossible to describe the flow patterns for bubbly and annular flow using the same model. Even if two separate models are used to describe the two flow, the transition zone between the two is difficult to describe. In addition to that in two phase flow the vapor expands due to pressure drop along the pipe which may lead to a modification of the flow structure and causing the change from one flow regime to other (for example, transition from bubbly flow to slug flow). Also the flow pattern is dependent upon the pipe geometry [17].

Many parameters govern the configuration of two phase flow. Some of these are flow rates, pressure, wall heat flux, densities, vicosities, surface tension, pipe characteristic and geometry, flow direction and the inlet of the tube. Because of the lack of a general model that describes the different regimes of boiling, experimental correlations are used for heat transfer calculations. When finding these correlations, many assumptions are imposed to get rid of several parameters that influences the flow.

Therefore, the use of these correlations is limited to problems that resemble the experimental situation and cannot be used generally [17,19,21].

5.3.1 Two Phase Flow Pattern in a Vertical Pipe

Seven patterns can be distinguished in two phase flow in a vertical pipe, as shown in Figure 5.1 . They are as follows

1. **Bubbly Flow**

   It can be recognized by its configuration at low velocity in which bubbles are spherical in shape when their diameters are about one millimeter. Beyond that the shape become variable. Roumy (1969) distinguished two patterns in bubbly flow, independent bubbles where there is no interaction between bubbles, and packed bubbles where bubbles are crowded together [17,21].

2 - **Slug Flow**

   It is composed of gas plugs. Gas plug is usually blunt while its end is flat with bubbly wake. While the pattern changes its configuration to annular flow it is called churn flow [20, 22].

3 - Dispersed Annular Flow

It is categorized by central gas core with liquid droplets flowing at higher speed than the liquid film surrounding the gas core and adhering to the pipe wall. The liquid droplets move randomly from the gas core to the film surface and vice versa. When these droplets gather into clouds moving within the central core, the flow is called Wispy Annular Flow [17].

4 - Mist Flow

When the film is vaporized the droplets will make up what is called a mist flow. Near the entrance, the wall temperature is below that necessary for vapor bubble formation, and the flow remain as a single phase where heat transfer depends on the flow properties [17].

5.3.2 Heat Transfer in a vertical Heated Tube

Consider an uniformly heated vertical tube with subcooled liquid fed at its base (see figure 5.2). Near the entrance ,the wall temperature is below that necessary for vapor bubble formation and the flow remain single phase where heat transfer depends on flow properties . At some point along the tube, the condition of the wall

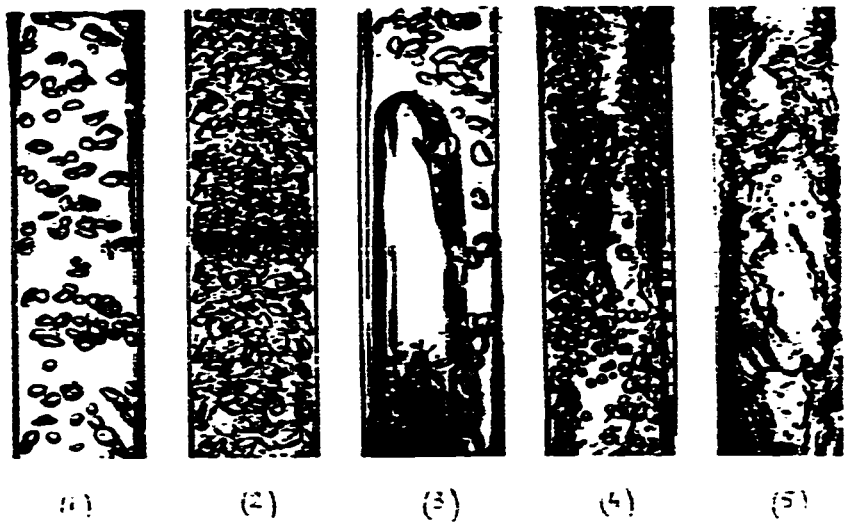

Figure 5.1. Air Water Flow Patterns in a Vertical Tube [17] (1)Independ bubbles (2) Packed bubbles (3) Slug flow (4) Churn flow (5) Annular flow [17].

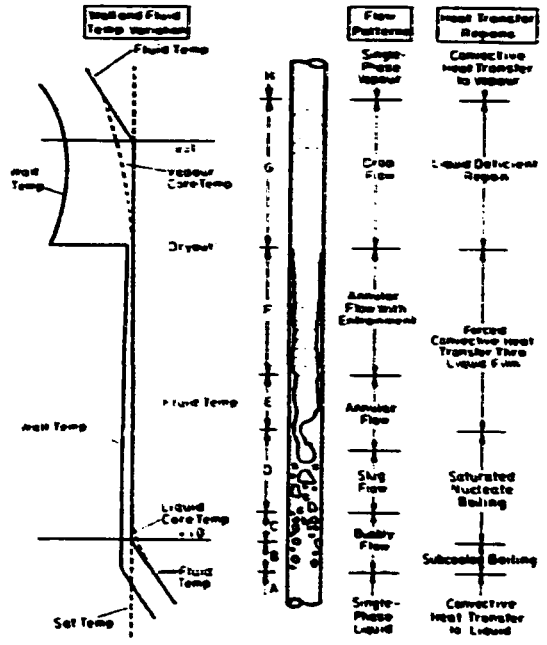

Figure 5.2 Regions of heat transfer in convective boiling [17].

allows the formation of vapor bubbles which grow and then disappear into the subcooled liquid (Region B). At that point the heat transfer mechanism is known as subcooled boiling. In subcooled boiling, the wall temperature remains constant a few degrees above saturation temperature while the mean temperature increases to saturation. The increase of surface temperature above the saturated temperatures is called the degree of superheat ΔT_{SAT} and the difference between the mean and the saturation temperature is known as the degree of subcooling ΔT_{SUB}. When the mean temperature reaches the saturation, the boiling is called saturated nucleate boiling which is characterized by the thermodynamic mass quality x which gives the fraction of vapor in the flows.

$$x_Z = \frac{H(Z) - H_L}{H_{LG}} \qquad (5.15)$$

Where:

$H(Z)$ = Fluid enthalpy at a distance Z

H_{FG} , H_L = Enthalpy of evaporization and liquid phase enthalpy respectively.

As the quality increases the fundamental changes in the mechanism of heat transfer take place and the boiling process is replaced by evaporation. In transition to

evaporation, the flow pattern changes from slug to annular boiling where heat transfer occurs by forced convection from the wall to the vapor core as the thermal conductivity of the film prevents superheating the liquid in contact to the wall. Since nucleation is completely suppressed the process is no longer called boiling but is called two phase forced convection Dryout is the region where complete evaporation of the liquid film occurs. It is charactreized by the raise in the wall temperature. The region between dryout and saturated vapor is called the liquid defficient region [17].

5.3.3 Variation of heat transfer coefficient with quality

Figure 5.3 shows the heat transfer coefficient versus the mass quality for the vertical tube with low heat flux where we see that in the single phase convection region heat transfer coefficient is approximately constant and it is only slightly effected by the temperature. In subcooled nucleate boiling the heat transfer coefficient increased linearly up to a point where x=0, at which the saturated nucleate boiling starts.

In the saturated region heat transfer coefficient

remains constant for a while then it increases linearly, because of the reducing thickness of the liquid film, upto the dryout region. Next a sudden decrease in the heat transfer coefficient corresponding to the forced convection steam flow occurs in the liquid defficient region while it increases linearly as the vapor velocity increases and the degree of superheat decreases. In the single phase vapor region where X=1, heat transfer coefficient levels out to that of single phase vapor [17] .

5.3.4 Sub-cooled Boiling

5.3.4.1 Single phase liquid heat transfer

In this region heat transfer coefficient relations are well established for both laminar and turbulent flow [18,19]. In turbulent flow Dittus-Boelter equation is satisfactory.

$$h\,D\,/k_L = 0.0265\,(\,V\,\Gamma\,D/\mu_L\,)^{0.8}\,(C_p\,\mu/k)_L^{\,0.4} \qquad (5.16)$$

For $Z / D > 50$ and $Re > 10{,}000$

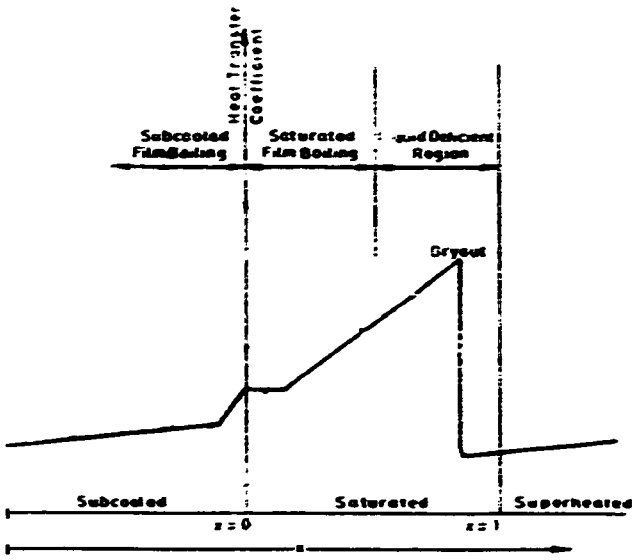

Figure 5.3 Variation of heat transfer coefficient with vapor quality [17].

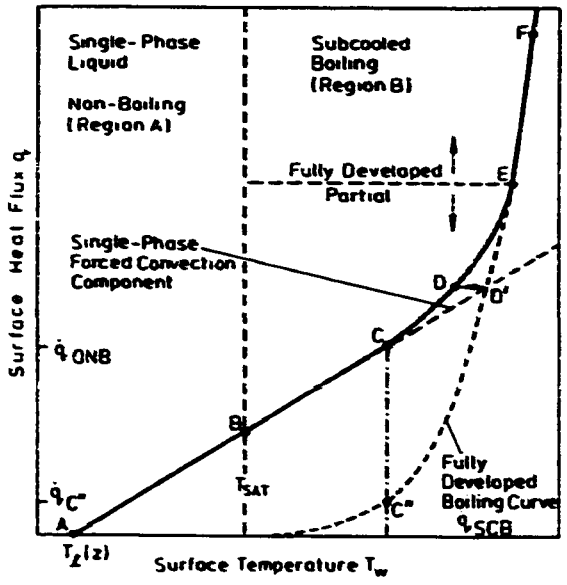

Figure 5.4. Subcooled boiling curve [17].

5.3.4.2 Onset of Subcooled Nucleate Boiling

Figure 5.4 is a surface heat flux versus surface temperature for boiling inside tube. The figure shows that as the heat flux increases, surface temperature increases along the line ABCD' until the first bubble nucleation starts. Since nucleation requires higher superheat , the surface temperature drops from D' to D. Further increase in the heat flux follows the line DEF. The onset of nucleate boiling can be roughly determined by the intersection of the line $\bar{A}D'$ and curve C"EF. Bergles and Rohsensow (1964) obtained an equation for wall superheat required for the onset of subcooled boiling for water only [17].

$$(T_S - T_{SAT})_{ONB} = 0.556 \left[\frac{q''}{1082\ P^{1.156}}\right]^{0.463P^{0.0234}} \qquad (5.17)$$

Where,

q" = surface heat flux W/m^2

P = pressure in bar.

NOTE: For a given heat flux q", nucleation will not start if wall superheat is less than that given by the above equation.

Frost and Dzakowic (1967) found an equation that cover all liquids [17]:

$$(T_S - T_{SAT})_{ONB} = 0.556 \left[\frac{8\ \sigma\ q''\ T^{SAT}}{K_L\ \Gamma_g\ \triangle H_{fg}}\right]^{0.5}\ Pr_L \qquad (5.18)$$

To find $(T_S - T_{SAT})$ and q'' for the onset, the above equation should be solved simultaneously with heat transfer equation:

$$q'' = h_{LO}(T_S - T_L(Z)) = h_{LO}\ (T_S - T_{SAT})_{ONB} + (T_{SAT} - T_L(Z)) \qquad (5.19)$$

where,

h_{LO}=heat transfer coefficient assuming the total flow to be liquid

$T_L(Z)$= liquid phase temperature at distance Z

5.3.4.3 Fully developed subcooled boiling

When single phase heat transfer coefficient reduces to zero, the flow becomes fully-developed and the whole surface is covered by bubbles. In fully developed boiling, velocity and subcooling have no effect on the surface temperature which is a function of surface heat flux and system pressure. Surface condition has little effect on forced convection boiling compared to that of pool boiling [21,22]. A suitable form of correlation that represent the data for subcooled boiling is the one suggested by Rohsennow (1952)[17].

$$\left[\frac{C_{pL}\,\Delta T_{SAT}}{\Delta H_{fg}}\right] = C_{sf}\left[\frac{q}{\mu_L\,\Delta H_{fg}}\left[\frac{\sigma}{g\,(\Gamma_L - \Gamma_g)}\right]^{\frac{1}{2}}\right]^{0.33} Pr_L^{1.7} \qquad (5.20)$$

where,

σ=surface tension N/m

C_{sf} = constant found from the experimental data.

g= gravity acceleration m/s²

ΔT_{SAT} and h calculated from this equation is not markedly different from those calculated using pool boiling correlations [17]. Hence, pool boiling data can be used to represent fully developed subcooled boiling.

5.3.4.4 Partial boiling

Rohsenow (1952) proposed the superposition of single phase forced convection and subcooled boiling since they occur simultaneously in this region [21].

$$q'' = q''_{LO} + q''_{SUB} \qquad (5.21)$$

Where,

$q''_{LO} = h_{LO} (T_S - T_L(Z))$ and

q''_{SUB} is calculated using equation 5.18

5.3.4.5 Void fraction and pressure drop in subcooled boling

Void fraction α is defined as the ratio of local vapor volume to the total local flow volume.

$$\alpha = \frac{V_g}{V_{TOTAL}} = \frac{V_g}{V_g + V_L} \qquad (5.22)$$

For low subcooling, void is effected by the bulk fluid and the void fraction usually remains low which can be neglected. For high subcooling just after the onset of nucleation, voidage is reflected by the surface condition [17,21,22,37]. A simple method to find out the point of net vapor generation which can be assumed to be at point B in figure 5.4 was proposed by Shah and Zuber (1974)[17].

For Pe < 70,000

$$\Delta T_{SUB}(Z)_B = T_{SAT} - T_L(Z)_B = 0.0022 \left(\frac{\dot{q} D}{K_L}\right)$$

For pe > 70,000

$$\Delta T_{SAT(Z)_B} = 153.8 \left[\frac{\dot{q}}{m\, C_{pL}} \right] \qquad (5.23)$$

where,

Pe = Peclet number defined by,

$$Pe = \left[\frac{m\, D\, C_{pL}}{K_L} \right]$$

5.3.6 SATURATED BOILING

5.3.6.1- Saturated Nucleate Boiling

In this region where nucleation starts, heat transfer mechanism is the same as that in subcool boiling and the heat transfer process is independent of mass quality x and mass velocity m since the bulk temperature is constant and hence the heat transfer coefficient [17,19].

5.3.6.2 Two Phase Forced Convection Region

In this region, heat is transferred by conduction or convection through the liquid film and vapor is generated at the liquid-vapor interface. Heat transfer coefficient is usually very high and its correlations

usually are in the form [23,24]:

$$\frac{h_{TP}}{h_L} = fn\left(\frac{1}{X_{tt}}\right) \qquad (5.24)$$

where:

h_L = single phase heat transfer coefficient for liquid.

h_{TP} = Two phase heat transfer coefficient.

X_{tt} = Lockhart Martinelli Parameter defined as,

$$X_{tt} = \left(\frac{1-x}{x}\right)^{.9} \left(\frac{\Gamma g}{\Gamma f}\right)^{.5} \left(\frac{\mu f}{\mu g}\right)^{.1}$$

Usually these correlations have high mean error (± 30%).

Chen (1966)[17,23] proposed one of the best correlations which covers both saturated nucleate and forced convection boiling region. He assumed that the contributions of both mechanisms are additive.

$$h_{TP} = h_{NCB} + h_C$$

where,

$$h_C = 0.023 \left[\frac{G(1-X)D}{\mu_L}\right]^{.8} \left[\frac{\mu C_p}{k}\right]^{.4} \left[\frac{k_l}{d}\right] F \qquad (5.25)$$

$$F = C_1 / X_{tt}^{C2}$$

C_1 and C_2 are constants

G= mass velocity (flux)

5.4 BINARY SOLUTION HEAT TRANSFER

Some of the definitions which may help in understanding the heat transfer of binary solution are given below [17,41].

5.4.1 Definitions

1- Molar concentration C_i of a component i is given by

$$C_i=\Gamma_i/M_i$$

where,

Γ_i = density of component i , Kg/m^3

M_i = Molecular weight of component i

2- Mole fraction in liquid ML_i or vapor yi is given by,

ML_i(or MG_i)$=C_i/C$ where

$$C=\text{total molar concentration}=\sum_{i=1}^{n} C_i$$

3- Partial pressure P_A for component A is the pressure that will be exerted by component A if it was alone in a volume

proportional to its concentration in the mixture

$$P_A = MG_A \, P \qquad (5.26)$$

5.4.2 Bubble growth in a binary system

Bubble growth in a binary liquid is not limited only by the rate at which heat diffuses to the liquid surface interface but also by the depletion of the more volatile component near the bubble interface. For the bubbles to grow, diffusion of the more volatile component to the depletion region must occur.

5.4.3 Forced convection boiling

1- Saturated Nucleate Boiling

Chen correlation can be used to correlate the data for heat transfer coefficients with little modification to account for the concentration:

$$h = h_{NCB} + h_C \qquad (5.27)$$

Where:

$$1/h_{NCB} = \left[\frac{(1-x)}{Y \, h_A} + \frac{x}{Y \, h_B} \right] (1 + \tau \, |MG - ML|)$$

ML = mole fraction of the more volatile component B in the liquid phase.

MG = Mole fraction of the vapor phase.

h_A, h_B = Nucleate pool boiling coefficient for pure component of A and B.

h_C = convective heat transfer coefficient as given in equation (5.25) using the mixture physical properties or as a pure component.

S = suppression factor

τ = constant

The lack of the more volatile component leave a more viscous non-volatile liquid shell around each bubble. Consequently, more time is needed to drain the film between the colliding bubbles which may effect the convective term h_C.

5.4.4 Critical Heat Flux in Forced Convection Boiling (CHF)

Critical heat flux (CHF) in forced convection boiling CHF increases with both velocity and subcooling and the maximum of the CHF occurs usualy at the maximum of|MG-ML| [17,31]. The critical heat flux $q_{cr,M}$ can be expressed as:

$$q_{cr,M} = q_{cr,I} + q_{cr,E} = q_{cr,I}\,(1 + \tau) \qquad (5.28)$$

where,

$q_{cr,I}$=The ideal value of CHF for the two pure components A and B at the same pressure , velocity and subcooling in the mixture .

$q_{cr,E}$= Additional heat flux to account for the mass transfer effects.

$$q_{cr,I}=[\ q_{cr,A}(1-ML)+ q_{cr,B}\ ML\ ]$$

$$\tau=f(|MG-ML|,(GD/\mu_l)_A,[T_{sat,B}/(T_{sat,M}-T_{sat,B})])$$

5.5 VAPOR QUALITY x

To calculate the vapor quality , enthalpies of the liquid LiBr mixture , and that of the vapor must be known at each section of the boiling tube, in addition to the location where the quality, x=0 . For the enthalpy calculations , the equations listed in appendex A for both water and LiBr-water solution enthalpies were used [14]. These equations require the pressure distribution in the tube . To calculate the pressure drop in the boiling tube , the vapor quality must be known at each section which makes

the problem difficult to handle . Therefore , a special procedure was adopted to perform the calculations which will be described later.

5.5.1 Pressure Drop in the Boiling Tube

To find the pressure distribution in the test section, certain assumptions have to be made. These assumptions are given in the following section [17].

5.5.1.1 Assumptions

1- Martinelli - Nelson correlation are also valid for vertical tubes.
2- Smith correlation for the slip ratio S is valid for lithuim bromide-water mixture .

5.5.1.2 Derivation of the pressure drop equation in the tube test section

The momentum balance in the test section tube can be written as [17]

$$\frac{dP_A}{dz} + \frac{dP_S}{dz} + \frac{dP}{dz} + \frac{dP_F}{dz} = 0 \qquad (5.29)$$

where

P_A= acceleration pressure

$$P_a = \left[\frac{x^2}{\alpha_g \Gamma_g} + \frac{(1-x^2)}{(1-\alpha)\Gamma_f}\right] G^2 \qquad (5.30)$$

G=mass flux $=\Gamma V$

Γ_f ,Γ_g = densities for solution and water vapor respectivily.

α = void fraction $= \dfrac{1}{1 + (1-x)\ \beta\ /x}$

$$\beta = \frac{\Gamma_g}{\Gamma_f}\ S$$

$$S = \text{slip ratio} = e + (1-e)\left[\frac{\Gamma_f/\Gamma_g + e(1/x - 1)}{1 + e\ (1/x - 1)}\right]^{1/2}$$

e=.4

P_S=static pressure

$$= [\alpha\ \Gamma_g + (1-\alpha)\ \Gamma_f]\ \ g' \qquad (5.31)$$

P_F=frictional pressure

$$\frac{dP_F}{dz} = \theta^2 \left[f \frac{1}{D} \frac{G^2}{\Gamma_f} \right] \qquad (5.31)$$

D= tube diameter

f= frection coefficient

θ^2=Collier correlation defined as,

$$\theta^2=\left[1+ x \left(\frac{\Gamma_f-\Gamma_g}{\Gamma_g}\right)\right]\left[1+ \left(\frac{\mu_f-\mu_g}{\mu_g}\right)\right]^{-1/4}$$

μ_f , μ_g = viscocities for solution and vapor respectivily

P= total pressure

Subtituting in equation 5.29 we get

$$P_{z=z1}-P_{z=L} = G^2\left[\frac{x^2}{\alpha\,\Gamma_g} + \frac{(1-x)^2}{(1-\alpha)\Gamma_f}\right]\Bigg|_{z=z1}^{z=L}$$

$$+ \int_{z1}^{L} [\,\alpha\,\Gamma_g + (1-\alpha)\,\Gamma_f]\,dz$$

$$+ \frac{f}{2\ D\ \Gamma_f} \int_{z1}^{L} \theta^2\ dz$$

Changing the limits of integration from distance z to quality x since θ^2 is given in terms of x , we get ,

$$P_{Z=z1} - P_{Z=L} = G^2 \left[\frac{x^2}{\alpha\ \Gamma_g} + \frac{(1-x)^2}{(1-\alpha)\Gamma_f} \right] \Bigg|_{x=x1}^{x=x_L}$$

$$+ L\ g\ \frac{1}{x_L} \int_{x1}^{xL} [\ \alpha\ \Gamma_g + (1-\alpha)\Gamma_f]\ dx$$

$$+ \frac{f\ G^2\ L}{2\ D\ \Gamma_f}\ \frac{1}{x_L} \int_{x1}^{xl} \theta^2\ dx \qquad (5.32)$$

5.5.2 Steps for Calculations

1- Initially assume that the pressure drop in the tube

is mainly caused by the friction due to the liquid flow alone in the pipe and static drop is due to gravity.

2- Subtitute the pressure in step #1 in the

enthalpie equations and calculate the enthalpies at each section in the tube .

3- Assume that saturated liquid starts at the section where the fluid mean temperature gradient ≈ 0 (dTm / dz ≈ 0) .

If we apply the energy equation for any two successive sections in the tube we get ,

$$(1-x)\ h_{f1} + x\ h_{g1} + q/m = (1-x)\ h_{f2} + x\ h_{g2}$$

Where

q= heat added to each section , W

m = total mass flow rate, kg/s

Subtituting x=0 for the first section and the corresponding enthalphies for the first and second sections , we get the initial quality in each section .

4- Subtitute this quality in the two-phase pressure drop equation to get an improved values for the pressure distribution in the tube .

5- Repeat step 3 to 4 until the calculated

qualities in successive interations do not change with more than 10^{-6}.

5.5.3 Boiling Heat Transfer Coefficient Correlation

Boiling heat transfer coefficient is usually correlated by the convection heat transfer coefficint h_c in the form [17,23,24],

$$\frac{h}{h_c} = C1\ B_o + C2\ \left(\frac{1}{X_{tt}}\right)^{C3} \qquad (5.33)$$

where

X_{tt}= Lockhart Martinelli Parameter define as,

$$X_{tt} = \left(\frac{1-x}{x}\right)^{.9} \left(\frac{\Gamma g}{\Gamma f}\right)^{.5} \left(\frac{\mu f}{\mu g}\right)^{.1}$$

Bo= boiling number

$= q / (G\ h_{fg})$

C1 , C2 , C3 = constants determined from the experimental data

The term h/h_c is independent of Bo except for

the large values of Bo , in the region of large 1/Xtt where nucleate boiling is supressed and two phase flow is dominant . Therefore , equation 5.33 reduces to

$$\frac{h}{h_c} = C1 \left(\frac{1}{X_{tt}}\right)^{C2} \qquad (5.34)$$

taking logarithm,

$$\ln\left(\frac{h}{h_c}\right) = \ln(C1) + C2 \ln\left(\frac{1}{X_{tt}}\right)$$

$$H = a + b \; Xt$$

CHAPTER VI

DESIGN AND FABRICATION PROCEDURE

6.1 PREPARATION STUDY

6.1.1 BRAZING

Strong connections for copper tubes can be achieved by brazing using a filler material that melts at temperature in the range between 600 and 800°C. Suitable filler metals for joining the different parts in the apparatus is any alloy containing 30 to 60% silver (BAG series) or copper alloys containing phosphorus (BCU series) [1].

The strength of a brazed copper tube joint doesn't vary much with the filler material if we maintain the proper clearance between the outside of the tube and the joint(See Figure 6.1). The correct clearance between the tube and the joint is maintained by the joint manufacturer for standard joints.

Brazing Procedure

To braze a joint, certain procedure has to be followed [1].

1. Measure the length of the tube so that it reaches all the way into the socket. Correct measurement increases the brazing quality.
2. Cut the tube to the exact length using a square cutter.
3. Ream the cut end using the reamer attached to the cutter to remove the small burr on the end of the tube.
4. Clean both the tube outer surface and the fitting socket to be free from oil, grease and heavy oxide.
5. Apply flux to both tube outer surface and fitting socket. Covering the heated area with a flux prevent oxidation and greatly improve joint appearance. Flux is omitted when brazing copper to copper material using BCU series fillers.
6. Assemble the joint and remove any excess flux with a rag.
7. Apply heat using oxy-acetylene flame to the joint until the flux becomes quiet apply the brazing wire to the

joint. When filler material melts it flows into the capillary space (for BAG-1 filler metal, it is between 0.002 to 0.005") by means of the natural force of capillary attraction.

8. Allow the joint to cool naturally otherwise cracking may occur in the joint.

9. Clean the joint and inspect it for leakage.

Filler Material Used

A brazing filler metal is a metal that has the ability to wet the surface of the joint metal and form a strong bond [1]. It melts at a temperature above 430°C and have properties suitable for making joints by capillary attraction between closed-fitted surfaces.

In fabricating the apparatus, we used BAG-1 for brazing the different joints. BAG-1 is a silver alloy filler metal that contain 44 to 46% silver. It is used in plumbing, pipe fittings, refrigeration and air-conditioning. BAG-1 has the lowest melting temperature in the group and it flows freely into long and narrow capillary joints [4].

Brazing with BAG-1 requires a good ventilation since it contains cadmium in its composition. See Table 1 for more

information.

6.2 CORROSION STUDY FOR WELDED JOINTS

Corrosion of welded joints will be similar to that of the base metals if both of them have similar compositions. Small differences in composition will create differences in the electrochemical potentials that may lead to galvanic corrosion at the joint. If it is not possible to use similar materials, the weld metal should be cathodic to the base metal. It is also important to have a weld free from pinholes to prevent localized corrosion [6].

Many of the welding fluxes are corrosive to the metals where they are used. Hence they should be removed from the welded joint immediately after the welding [6].

Welding can cause high localized residual stresses which will remain in the welded structure and produce stress corrosion cracking in corrosive media. Hence the structure should be relieved from the stresses by annealing [6].

6.3 FITTINGS USED

Two types of fittings were used in fabrication, these are,

1. Compression Fittings

It is a fitting which can be connected directly to a cut tube end without flaring the tube. Instead of flaring the tube, it is equipped with a conical shaped ring that sequeezes the outer surface of the tube while tighting the coupling nut to prevent the leakage (see Figure 6.2). The ring will stick to the tube end permanently even if the coupling nut is loosened. These fittings are made from different material and for different working pressure.

2. Brazed Fitting:

It is a tight fit fitting which requires brazing to form a strong joint. For a good joint the clearance between the fitting and the tube outer surface is in the range between 0.002" to 0.005" (see Figure 6.3).

6.4 BOILING TUBE

We choose an annealed copper tube, type K with the following specifications [1] (see Table 6.1) :

Outside Diameter (1.625") 41.3 MM
Inside Diameter (1.481") 37.6 MM
Wall thickness (0.072") 1.8 MM
Rated internal working pressure (400 psi)

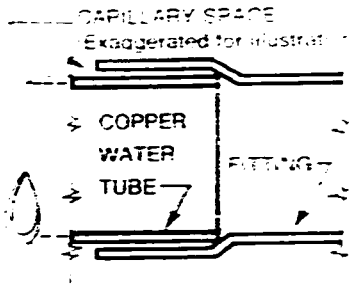

Figure 6.1. Capillary Space in Brazed Fittings [1].

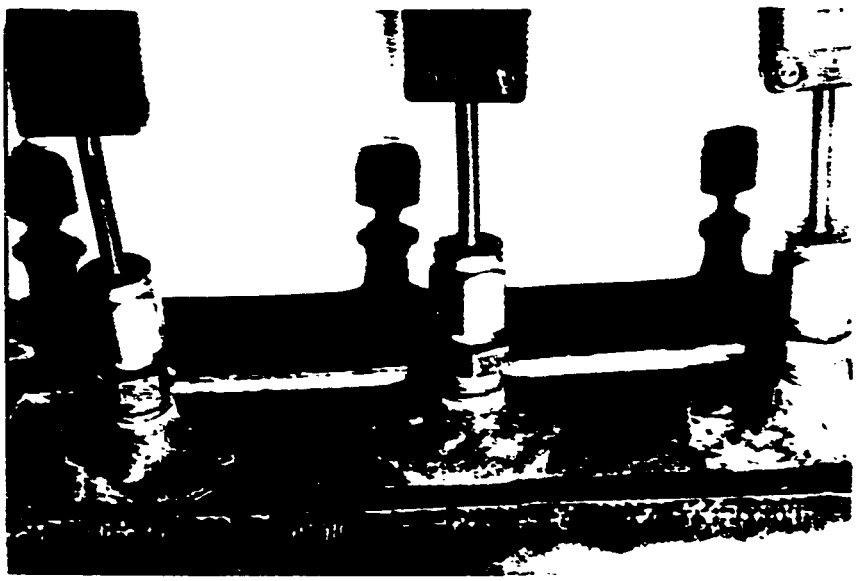

Figure 6.2. A typical Compression Fitting.

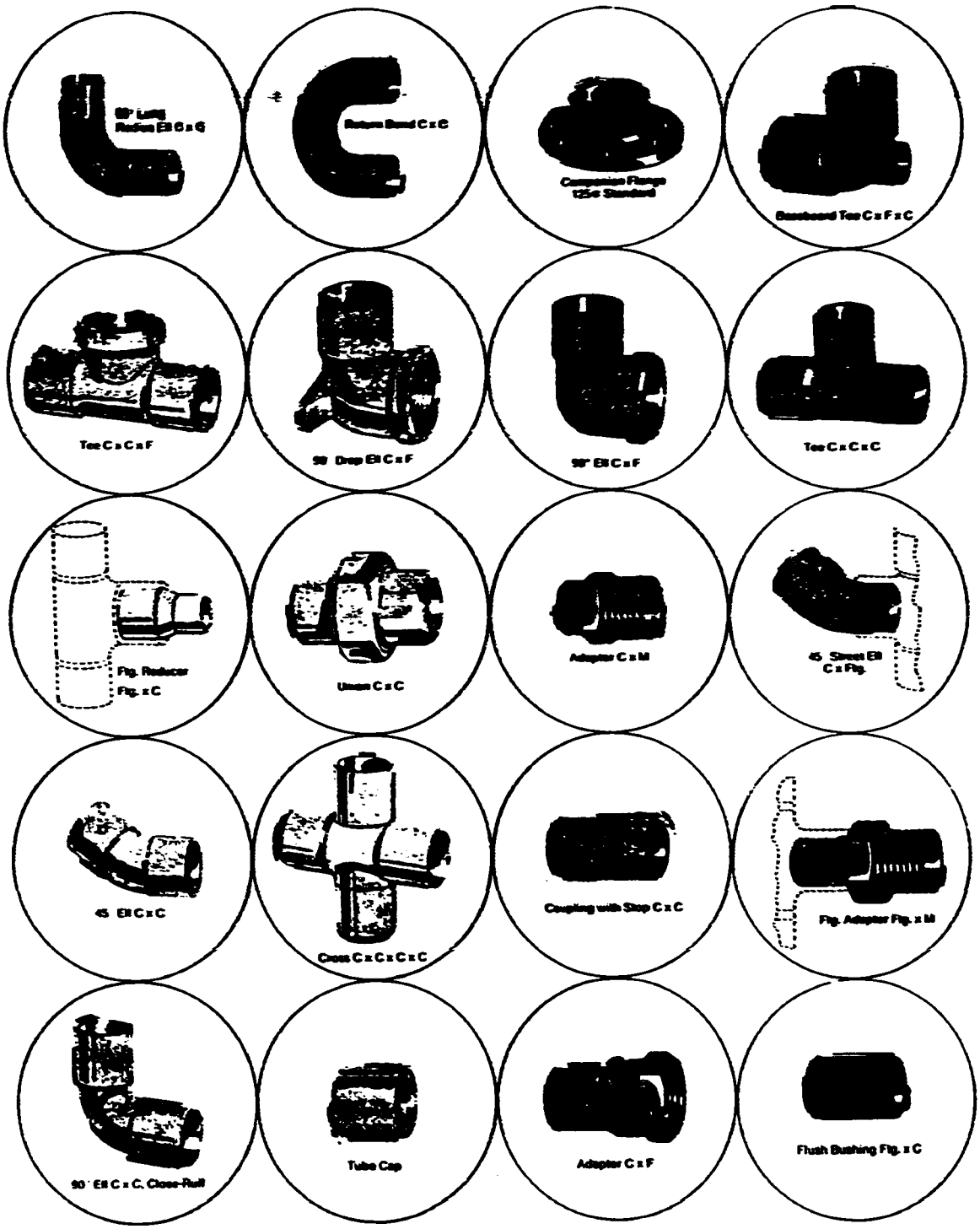

Figure 6.3 Typical brazed fittings [1].

Table 6.1 Rated Internal Working Pressures for Copper tube [1].

Types K, L, M and DWV

Size, inches	Rated Internal Working Pressures, psi							
	Type K		Type L		Type M		DWV	
	Annealed	Drawn	Annealed	Drawn	Annealed	Drawn	Annealed	Drawn
	Service Temperature up to 150F (S=5,100 psi, annealed; 9,000 psi, drawn)							
¼	900	1595	810	1350	—	—	—	—
⅜	990	1745	675	1195	475	840	—	—
½	780	1375	625	1105	430	760	—	—
⅝	640	1135	545	965	—	—	—	—
¾	750	1315	495	875	350	610	—	—
1	575	1010	440	770	295	515	—	—
1¼	465	820	385	680	295	515	275	490
1½	435	765	355	630	290	510	245	435
2	380	665	315	555	300	450	185	325
2½	355	520	295	520	235	410	—	—
3	340	605	275	490	220	385	135	240
3½	325	570	270	470	215	385	—	—
4	315	555	255	450	215	380	130	225
5	305	540	235	410	205	355	130	225
6	305	540	215	385	190	335	130	225
8	325	580	240	420	200	350	125	220
10	330	585	240	425	205	355	—	—
12	330	585	225	395	205	360	—	—
	Service Temperature 300F (S=4,700 psi, annealed; 8,700 psi, drawn)							
¼	830	1540	705	1305	—	—	—	—
⅜	910	1690	625	1155	435	815	—	—
½	720	1330	580	1065	395	735	—	—
⅝	590	1095	505	930	—	—	—	—
¾	685	1275	455	845	320	590	—	—
1	525	980	405	745	270	500	—	—
1¼	430	795	355	660	270	500	260	470
1½	400	740	330	610	270	490	225	420
2	235	645	290	540	235	435	170	315
2½	325	600	275	500	215	400	—	—
3	315	585	255	470	200	375	125	230
3½	295	550	245	455	200	370	—	—
4	290	535	235	435	195	370	120	220
5	280	520	215	395	190	345	120	220
6	280	525	200	370	175	325	120	215
8	300	560	220	405	185	340	115	210
10	305	565	220	410	190	345	—	—
12	305	565	205	385	190	345	—	—

Source: *Copper/Brass/Bronze Product Handbook*, Copper Development Assn. Inc.

2757.9 KPa for service temperature (300°F) 148°C.

Allowable stress = (4700 psi) 32405 KPa

Thermal conductivity:

K = 395.7 W/m.k. at 100°C

= 400.7 W/m.k. at 50°C

In Chapter II, in the corrosion section, it was stated that copper nickel alloys, especially alloy 706 (copper nickel, 30%) is the best choice for an apparatus which utilizes lithium bromid-water solution as a working fluid. However, if we look at Table 6.2 we see that the thermal conductivity for copper nickel, 30% is only 8% of that for pure copper. This makes copper nickel alloy a poor choice at least for the boiling tube heat flux which is limited to 1200 W only.

Calculation for the maximum difference between inner tube and outer surface temperature for pure copper and copper nickel alloy .

Given :

The specified heater capacity = 1200 W

Boiling tube outer surface Area $=\pi DL=$

$= \pi\ (41.3 \times 10^{-3})\ 1.250 = 0.162\ m^2$

Heat flux = $1200/0.162 = 7399\ W/m^2$

Tube thickness = 1.8×10^{-3} m

Steady- state condition

Table 6.2 Compositions , Thermal Conductivity and Melting Points for Copper and Copper Alloys.

Alloy No.	Alloy name	Nominal composition, %	Melting point (Temelec), F	Relative thermal conductivity(a)
		OF and ETP Coppers		
102	Oxygen-free copper (OF)	99.95 Cu	1981	100
110	Electrolytic tough pitch copper (ETP)	99.90 Cu, 0.04 O_2	1981	100
		Deoxidized Coppers		
120	Phosphorus-deoxidized copper, low-P (DLP)	99.9 Cu, 0.008 P	1981	99
122	Phosphorus-deoxidized copper, high-P (DHP)	99.9 Cu, 0.02 P	1981	87
		Beryllium Coppers		
175	High-conductivity beryllium copper, 0.6%	96.9 Cu, 0.6 Be, 2.5 Co	1955	53-66(c)
170	High-strength beryllium copper, 1.7%	98.3 Cu, 1.7 Be	1800	27-33(c)
172	High-strength beryllium copper, 1.9%	98.1 Cu, 1.9 Be	1800	27-33(c)
		Low-Zinc Brasses		
210	Gilding, 95%	95 Cu, 5 Zn	1950	60
220	Commercial bronze, 90%	90 Cu, 10 Zn	1910	48
230	Red brass, 85%	85 Cu, 15 Zn	1880	41
240	Low brass, 80%	80 Cu, 20 Zn	1830	36
		High-Zinc Brasses		
260	Cartridge brass, 70%	70 Cu, 30 Zn	1750	31
268, 270	Yellow brass, 65%	65 Cu, 35 Zn	1710	30
280	Muntz metal, 60%	60 Cu, 40 Zn	1660	31
		Tin Brasses		
442-445	Admiralty	71 Cu, 28 Zn, 1 Sn(d)	1720	28
464-467	Naval brass	60 Cu, 39.25 Zn, 0.75 Sn(d)	1650	30
		Special Brasses		
675	Manganese bronze A	58.5 Cu, 39 Zn, 1.4 Fe, 1 Sn, 0.1 Mn	1630	27
687	Aluminum brass, arsenical	77.5 Cu, 20.5 Zn, 2 Al (0.06 As)	1780	26
		Nickel Silvers		
745	Nickel silver, 65-10	65 Cu, 25 Zn, 10 Ni	1870	12
752	Nickel silver, 65-18	65 Cu, 17 Zn, 18 Ni	2030	8
754	Nickel silver, 65-15	65 Cu, 20 Zn, 15 Ni	1970	9
757	Nickel silver, 65-12	65 Cu, 23 Zn, 12 Ni	1900	10
770	Nickel silver, 55-18	55 Cu, 27 Zn, 18 Ni	1930	8
		Phosphor Bronzes		
505	Phosphor bronze, 1.25% E	98.7 Cu, 1.3 Sn (0.2 P)	1970	53
510	Phosphor bronze, 5% A	95 Cu, 5 Sn (0.2 P)	1920	18
521	Phosphor bronze, 8% C	92 Cu, 8 Sn (0.2 P)	1880	16
524	Phosphor bronze, 10% D	90 Cu, 10 Sn (0.2 P)	1830	13
		Aluminum Bronzes		
613	Aluminum bronze D, Sn-stabilized	89 Cu, 7 Al, 3.5 Fe (0.35 Sn)	1950	14
614	Aluminum bronze D	91 Cu, 6-8 Al, 1.5-3.5 Fe, 1 max Mn	1915	17
		Silicon Bronzes		
651	Low-silicon bronze B	98.5 Cu, 1.5 Si	1940	15
655	High-silicon bronze A	97 Cu, 3 Si	1880	9
		Copper Nickels		
706	Copper nickel, 10%	88.6 Cu, 9-11 Ni, 1.4 Fe, 1.0 Mn	2100	12
715	Copper nickel, 30%	70 Cu, 30 Ni	2260	8

(a) Based on the thermal conductivity of alloy 102 (226 Btu/sq ft/ft/hr/°F at 68 F) as 100. For comparison, carbon steel has a thermal conductivity of 30 Btu/sq ft/ft/hr/°F, which is 13 on this scale. (b) E excellent, G good, P fair, NR not recommended; for gas tungsten-arc welding (GTAW), gas metal-arc welding (GMAW), or shielded metal-arc welding (SMAW). (c) In the precipitation-hardened condition (d) Alloys 443 and 465 contain a nominal 0.06%. As: alloys 444 and 466, a nominal 0.06%. Sb: alloys 445 and 467, a nominal 0.06% P.

i- **Temperature difference between the inner and the outer tube surface for pure copper tube**

$$\Delta T = T_{SO} - T_{SI} = \frac{q'' \Delta X}{k} = \frac{7399(1.8X10^{-3})}{395.7} = 0.03\ ^{\circ}C$$

ii- **Temperature difference between the inner and the outer tube surface for copper nickel tube**

$$\Delta T = T_{SO} - T_{SI} = \frac{q'' \Delta X}{k} = \frac{7399\ (1.8X10^{-3})}{395.7\ (0.08)} = 0.42^{\circ}C$$

Therefore, higher thermal conductivity reduces the difference between the inner surface temperature and the outer surface temperature for a specific heat flux so that we can measure the outer surface temperature instead of the inner one. In addition to that, high conductivity materials provide uniform heating and response quickly to any change in the heating load [1].

6.4.1 Pressure Safety Factor and Corrosion Allowance

To find the safety factor and corrosion allowance thickness for the boiling tube, we have to find the rated internal working pressure for the tube joints since they are the weakest part in the tube. From Table 6.1 we find that the rated internal working pressure equals to (190 psi) 1310 KPa

for joints brazed with alloys melted at or above (1000°F) 538°C and have a diameter in the range (125^{-2} inch) 31.8 - 50.8 MM and service temperature equal to (350°F) 176.7°C.

Since the design pressure in the apparatus is 75 psi, the tube safety factor = 190 ÷ 75 = 2.53 The corrosion allowance thickness may be calculated by the folklowing equation [1].

$$P = \frac{2\ S\ (tm - C)}{D - 0.8\ (tm - C)} \qquad (6.1)$$

Where:

P = Tube allowable pressure, psi

S = Tube allowable stress, psi

tm = Wall thickness, inch

D = Diameter, inch

C = Corrosion allowance thickness

Subtituting the coresponding values of the tube , we get

$$190 = \frac{2\ (4700)\ (0.072 - C)}{1.625 - 0.8\ (0.072 - C)}$$

Solving this equation, we get

C = (0.040 Inch) 1.0 MM

The pressure at which the tube and its brazed joints burst is as many times that of the rated working

Table 6.3 Rated Pressures Againest Brust Pressures for Type M tube [1].

Tube Size, inches	Tube Temper	Rated Pressure, psi			Measured Burst Pressure* psi
		Annealed Tube	Drawn Tube	50-50 Solder	
½	Drawn	505	760	200	5900
¾	Drawn	410	610	200	4750
1	Drawn	345	515	200	4150

*Tube had soldered end closures.

Table 6.4 Copper Constantan Thermocouple Descriptions [3].

THERMO-COUPLE	TEMP. RANGE °C	ERROR %	COLOR CODE	SYMBOL	POSITIVE (+)	NEGATIVE (-)
Copper-Consta-ntan	0-350	± 0.75	BLUE	T	COPPER	CONSTANTAN

Table 6.5 Variation of the Electric Response with Wire Sizes [3].

Wire size in inch	0.005	0.015	0.032
Response in Sec	1.0	10.0	90.0

Figure 6.4. T-type copper constantan thermocouple.

Table 6.6 Thermocouple Service Temperature Versus Its Wire Diameter [3].

Service temp. °F	400	450	700
Wire Diameter	0.005	0.015	0.032

pressure given in the Table 6.3.

6.4.2 Thermocouple Construction

6.4.2.1 Thermocouple used

The thermocouple used in the apparatus is a T-Type copper-constantan thermocouple (see figure 6.4). It reads temperature in the range between 0 to 350°C with an error of ± 0.75%. Table 6.4 gives more information about this type [3].

6.4.2.2 Correct Wire Diameter Selection

To choose the correct wire diameter two factors have to be considered carefully. First is the maximum service temperature, second is the response time of the probe. A thin thermocouple wire has a faster response than a thick one but its service temperature and life expectancy is lower. Table 6.5 shows the thermocouple response as a function of wire diameter for type 5, iron-constantan thermocouple.

Table 6.6 shows the recommended maximum service temperature for different diameters of copper-constantan, T-Type wires [3].

6.4.2.3 Selecting the Measuring Junction Type

There are two types of measuring junctions these are exposed and closed end junction. The exposed one response faster but it cannot be used for measuring temperature in systems with pressurized liquid or gas [3].

6.4.2.4 Protection Tube Material

To protect a thermocouple, stainless steel 304 or inconel is used to protect mechanical damage or to prevent contamination of the thermocouple. The 304 stainless steel has a maximum service temperature of 927°C while inconel has a maximum service temperature of 1150°C. Inconel tube is used in general in gas furnaces, lead baths, etc, while stainless tube is used in chemical applications, oil refineries and food chemical applications [3]. In low temperature applications with low flow rates similar to the apparatus under design where the maximum temperature does not exceed 200°C and flow rate of 1GPM , copper tubes is almost ideal because of its higher thermal conductivity and inexpensive (see figure 6.5).

6.4.2.5 Ceramic Insulators

To insert a thermocouple into the protection tube

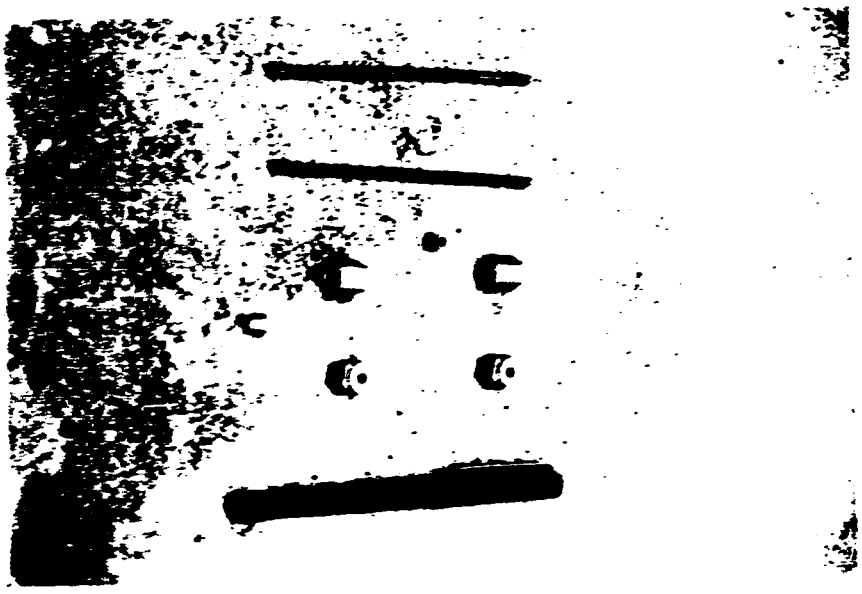

Figure 6.5.Thermocouple protection copper tube.

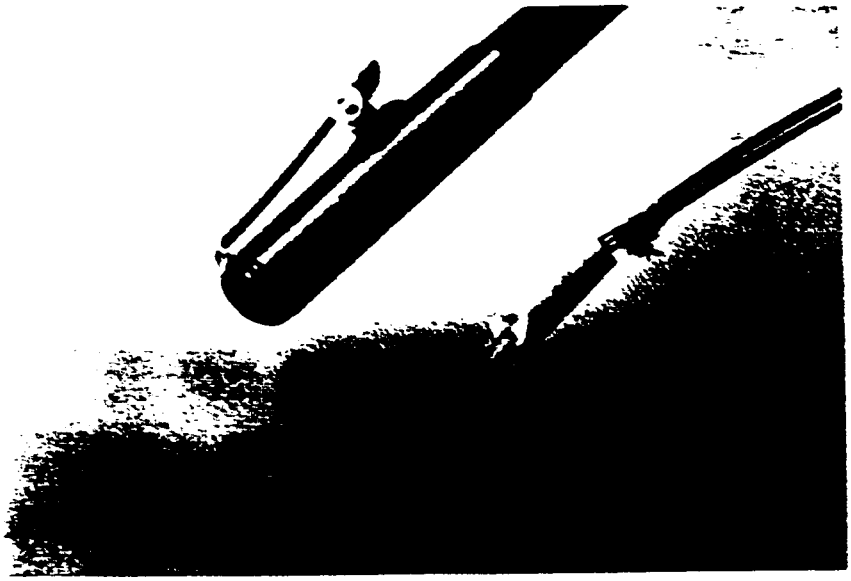

Figure 6.6.a Thermocouple ceramic insulator size 3/16 ".

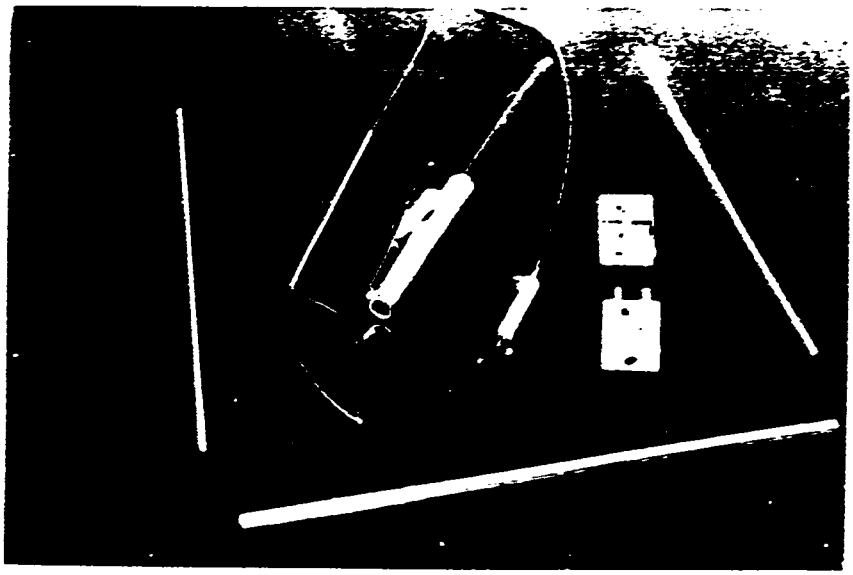

Figure 6.6.b Thermocouple ceramic insulator size 1/16".

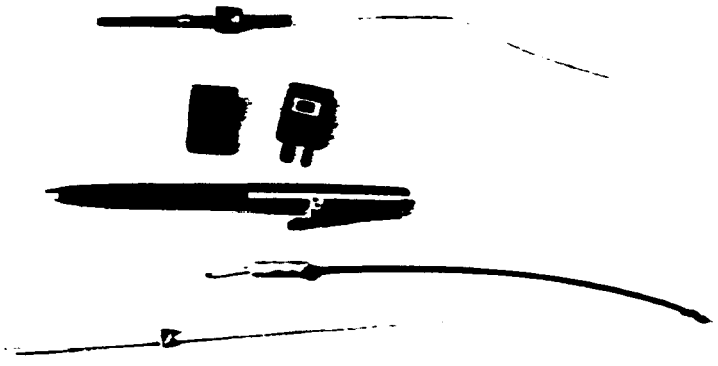

Figure 6.7 T-Type thermocouple connector.

special tube type insulator is used to prevent shorting the thermocouple wire with each other and with the protecting tube (see figure 6.6). This insulator is made of ceramic bar with two longitudinal holes and it withstands a temperature as high as 1650°C [3]. Three sizes are usually used which depends on the thermocouple wire diameter. These are 3/64, 1/16 and 3/16 inch outside diameter, which are used with 0.005, 0.015 and 0.032 inch diameter wires respectively.

6.4.2.6 Thermocouple Conectors

Special connectors are used to connect the thermocouple probes to the measuring instrument (see figure 6.4 and 6.7). These connectors are designed according to the type and size of the thermocouple. They are made of the same materials as the thermocouple and they are given the same color code to distinguish the different types. While assembling, the polarity of the thermocouple connector and the extension wires should be the same.

6.4.2.7 OMEGA CC High Temperature Cement

It is a Zircon base, two part ceramic cement which has many exceptional characteristics such as it withstands temperature upto 1100°C and adheres to metal,

Table 6.7.Pysical properties for OMEGA CC High Temperature Cement [7].

Color	Beige
Compressive strength	3900 psi
Tensile strength	425 psi
Absorption (water)	10 to 12%
Shrinkage	0.50%
Dielectric strength ASTM D-149	
at 70°F	25.0 to 51.0 volts/mil
at 750°F	12.5 to 25.0 volts/mil
at 1475°F	up to 1.3 volts/mil
Volume resistivity ASTM D-1829	
at 70°F	10^{13}-10^{14} ohm-cm
at 750°F	10^{11}-10^{12} ohm-cm
at 1475°F	10^{7}-10^{8} ohm-cm
Dielectric constants	5.0-7.0
Thermal conductivity (K factor) at 500°F	~3.41 Btu/hr/ft²/°F/in
Coefficient of thermal expansion	4.6 x 10⁻⁶ in/in/°F
Density	141 lb/ft³
Specific gravity	1.92 ± 0.05 g/cc
Maximum service temperature	2000°F

Figure 6.8. OMEGA CC high Temperature Cement [7].

glass ceramic and most surfaces [7]. Also it resists oil, water, electricity, and most solvents and acids. Furthermore, it withstands thermal shocks and it is an excellent electric insulator (see figure 6.8). See Table 6.7 for physical properties of the cement.

Direction for Use

Omega CC consists of two parts. These are a power filler and liquid binder. They are mixed in a ratio of two parts powder to one part liquid by volume. The initial set time is approximately 30 minutes and it solidifies completely in 18 to 24 hours under normal room condition [7].

6.4.3 Thermocouple Fabrication

A specific procedure was followed in assembling the thermocouple used in the apparatus. It can be described as follows:

6.4.3.1 Thermocouple Fabrication

1.1 60 pieces of (0.015 inch) 0.381 mm diameter, T-type thermocouple wires were cut in equal length of 200 mm.

1.2 Wires end insulations were scraped and

removed.

1.3 Both copper and constantan wires were twisted and wound on each other for 5 MM length.

1.4 The terminals of the copper and constantan wires were fused using a thermocouple fusing machine forming the thermocouple head.

1.5 The thermocouple head should look like a small round ball with two separated wires coming out of it (see Figure 6.4 and 6.6). Therefore, all the thermocouple heads were inspected under the microscope looking for malfunctions.

6.4.3.2 Thermocouple Probe Fabrication

2.1 Mean temperature thermocouple probes:

To measure the mean temperature of the fluid inside the boiling tube, the thermocouple must be inserted into a closed end tube forming what is called a thermocouple probe.

The following procedure was used for fabricating the probes .

2.1.1 30 thermocouples prepared in section 6.4.3.1 were inserted into (1/16 inch) 1.6 mm diameter and 60 mm long ceramic insulators (see figure 6.4 and 6.6).

2.1.2 30 pieces of (1/8 inch) 3.2 MM straight copper tube were cut to equal length of 60 MM (see figure 6.5).

2.1.3 The end of each tube was brazed and the tube was cleaned inside by drilling and outside by sanding paper so that the tube thickness is maintained at the brazed tip.

2.1.4 Small quantity of Omega CC high temperature cement, enough for few thermocouples, was mixed.

2.1.5 Small quantity of the cement was used, just enough to cover the tip and the insulator. Then both the insulator and the thermocouple were inserted into the prepared tube (see figure 6.7).

2.1.6 These thermocouple were left to dry for a day then they were fitted with thermocouple

connectors and the propes were ready.

2.1.7 Each probe was connected to OMINI-CALTH thermometer and immersed into boiling water at which the boiling temperature was recorded by each thermocouple. All of them read within 0.1°C difference. The reading of these probes were compared with the reading of a probe made by Omega group company which gave a reading within the probes range.

2.2 Surface Temperature Thermocouple Probes

30 thermocouples prepared in section 6.4.3.1 were inserted into (3/16 inch) 4.8 mm in diameter and 25 mm long ceramic insulators. Then they were inserted into (1/4 inch) 6.4 mm in diameter and 25 mm long copper tube as will be mentioned later in detail.

6.4.3 Boiling Tube Fabrication

The procedure for fabricating the boiling tube is as follows:

1 - Two reducers from (1½ inch) 38 mm to (3/8 inch) 9.5 mm were brazed at both end of an annealed Type-K

copper tube, 41.3 mm outside diameter and 1500 mm long . Then the tube was divided into 29 longitudinal sections each 50 mm long starting from a point 25 mm from one end. After that two lines were marked at 0° and 180° which intersected the 29-circumferential lines.

2 - The intersections of the lines at 0° (or 180°) were drilled with 4 mm drilling pit while the other side was indented at each intersection and drilled slightly to reduce the tube thickness to minimize the temperature difference between the inner and outer surface.

3 - Thirty (1/8 inch) 3.2 mm male compression fittings were drilled very carefully by (1/8 inch) 3.2 mm drill pit so the copper tube can go all the way through the fitting.

4 - The fittings prepared in step # 3 were brazed to the boiling tube with their holes centered to the ones drilled (see figure 6.9).

5 - The thirty probes fabricated in Section 5.4.3.2 were inserted into the boiling tube so that their tips were adjusted to be in the center of the tube.

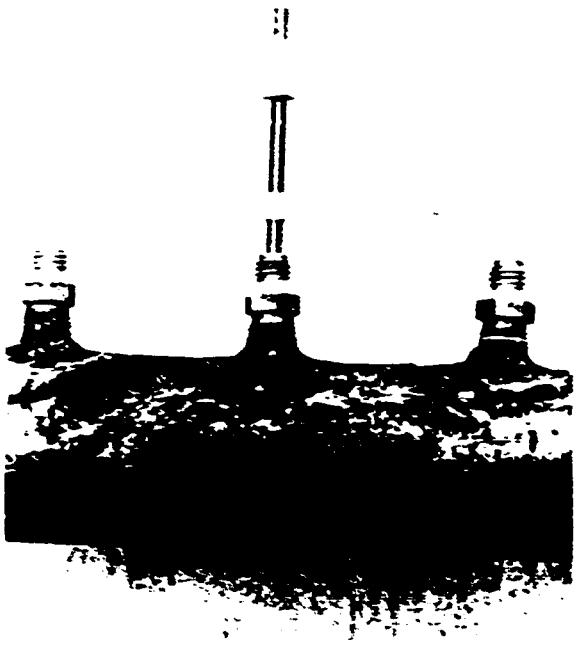

figure 6.9.a

Figure 6.9.b

Figure 6.9.a and b . Compression fittings brazed to the boiling tube

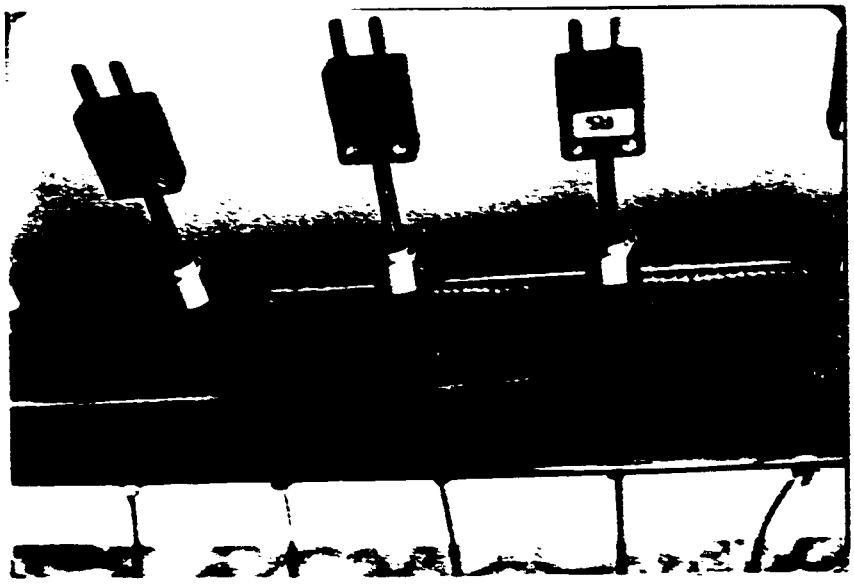

Figure 6.10.Complete thermocouple mean temperature probes inserted into the boiling tube.

Then the coupling nuts were tightened as seen in Figure 6.10.

6 - For the surface thermocouples, thirty pieces 25 MM in length and 6.4 MM in diameter were brazed to the boiling tube and centered on the indented area. Then the inner surfaces of the tubes were cleaned thoroughly.

7 - Enough quantity of the ceramic cement was used to cover the tips of the thermocouples prepared in section 6.4.3.2.2 then they were inserted into the 25 mm tubes which were brazed on the boiling tube. After that thirty thermocouple connectors were fitted on these thermocouples as can be seen in figure 6.11.

8 - 1200 W heater wire was inserted in 2 mm fiber glass insulator tube . Then the heater was wound around the boiling tube in a Helical shape with an angle less than 4° to the X-Y plane assuming that the tube axis was parallel to the Z-axis and spacing of 15 mm between rings. The heater started 250 mm away from the entrance to insure that the flow is dynamically fully developed (See figure 6.12).

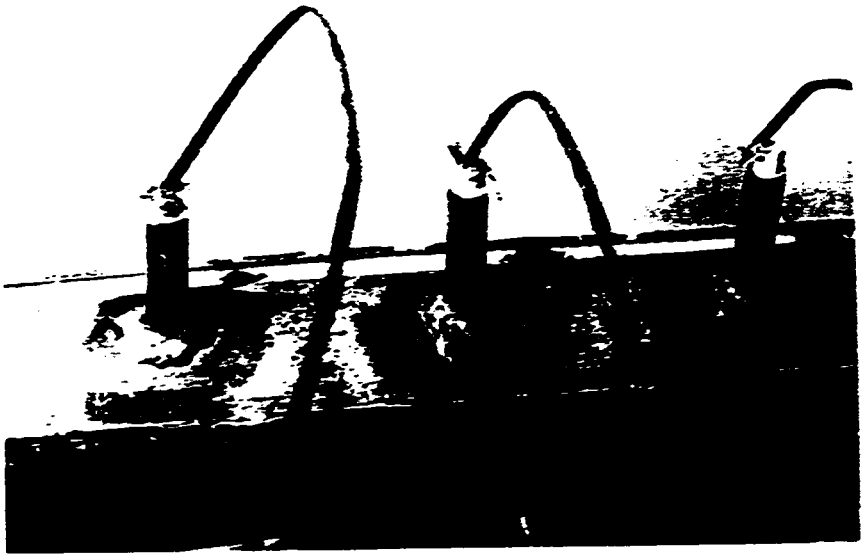

Figure 6.11.a

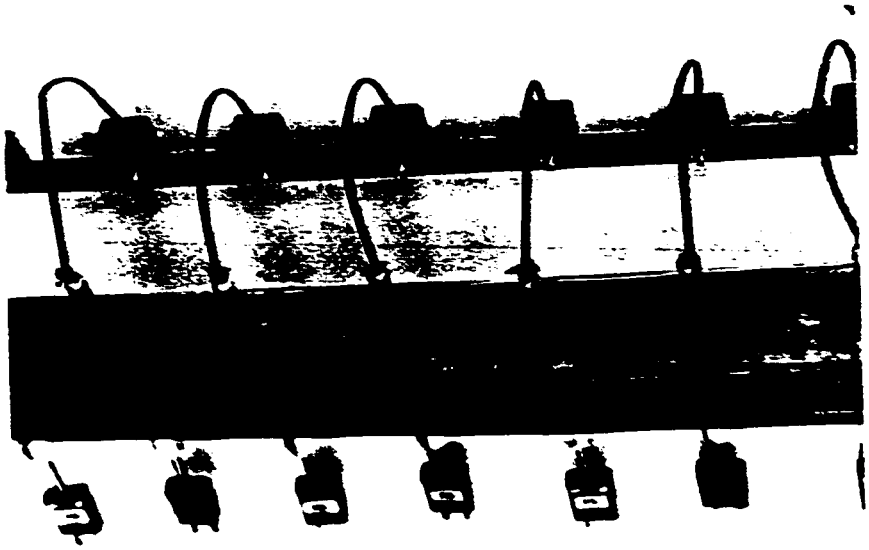

Figure 6.11.b

Figure 6.11.a and b. Complete surface thermocouple probes fitted to the boiling tube.

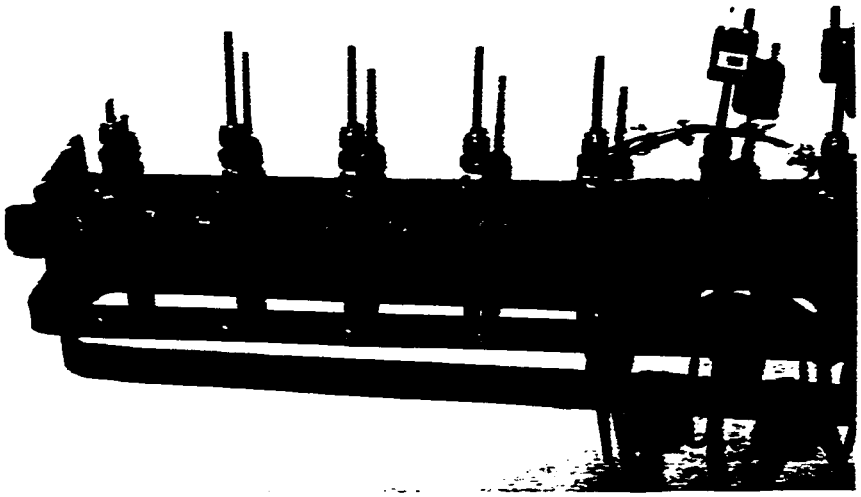

Figure 6.12 Boiling tube entrance.

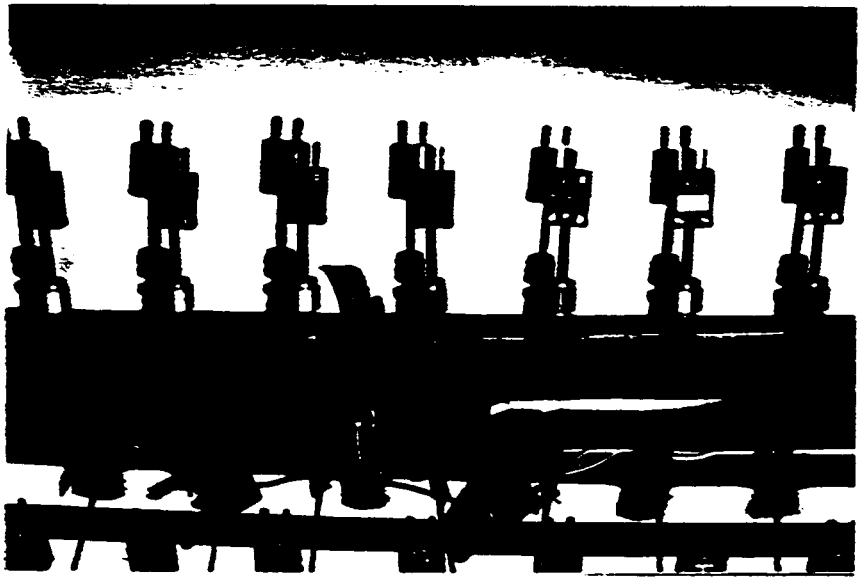

Figure 6.13.a

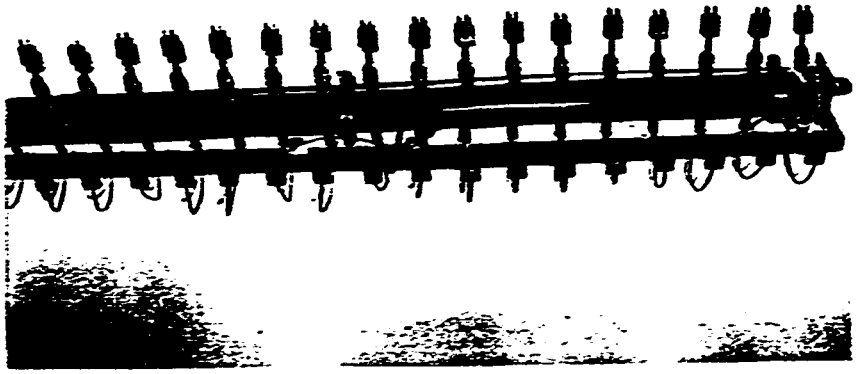

Figure 6.13.b

Figure 6.13.a and b. Complete boiling tube.

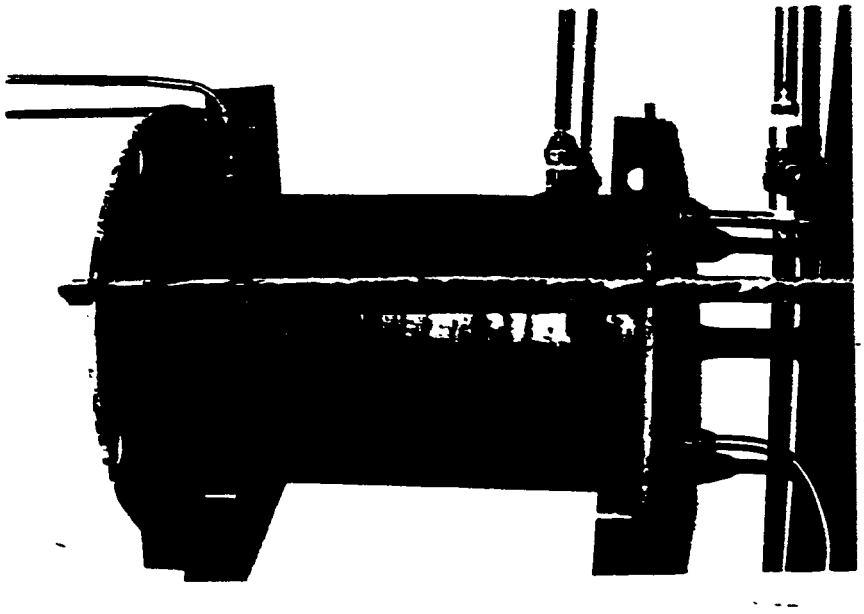

Figure 6.14.Liquid reservoir.

9 - 30 mm ceramic fiber insulator sheet was used to cover the whole tube . See figure 6.13 for the complete boiling tube .

6.5 PREHEATER FABRICATION

The preheater consists of three Type-K copper tubes which are 50 mm in diameter and 500 mm long . Steps in the fabrication of each tube are as follows.

1 - Two 9.5 mm holes are drilled on the preheater copper tube, one at each end.

2 - Two 9.5 mm compression coupling are brazed on the holes on the tube.

3 - One of the tube ends is plugged while the other is fitted with a reducer from (2" to 1.25") 50.8 mm to 31.75 mm and threaded internally in the 31.75 mm side.

4 - 1200 W and 110V heater is inserted into the preheater tube and tightened into the thread.

5 - 30 mm ceramic insulator sheet is used to insulate the preheater.

6 - The three preheater tubes are connected vertically in series so that both the heater and the inlet are at the bottom.

6.6 LIQUID RESERVOIR FABRICATION

The liquid reservoir is a 4 mm thick mild steel cylinder whose length is 290 mm and 170 mm diameter. It has an inlet, an outlet, a filler, a drainage and a feedback from the pump. All have the size of 9.5 mm inner diameter as can be seen in Figure 6.14.

6.7 PUMPS

6.7.1 Lithium Bromide Solution Pumps

It is a magnetic drive pump in which the conventional shaft seals found in most pumps is eliminated. The only seal in the pump is a stationary viton "O" ring seal between the front and the rear housings. The impeller which rotates on a stationary ceramic spindle and up against a ceramic thrust washer is fitted with a magnetic bushing. Six magnetic slices which were glued to the motor shaft create a magnetic

Table 6.8 Lithium bromide solution pump specifications.

MODEL NO.	CONNECTIONS		ELECTRICAL			GPM-AT LISTED HEAD (60 Hz)					
	INLET	OUTLET	HP	VOLTS	AMPS	1 FT.	10 FT.	20 FT.	30 FT.	40 FT.	PSI GAGE
TE-5536MB	1" FPT	¾" MPT	1/3	115/230	4.8/2.8	27	23	18.2	11.7	1.5	17.5

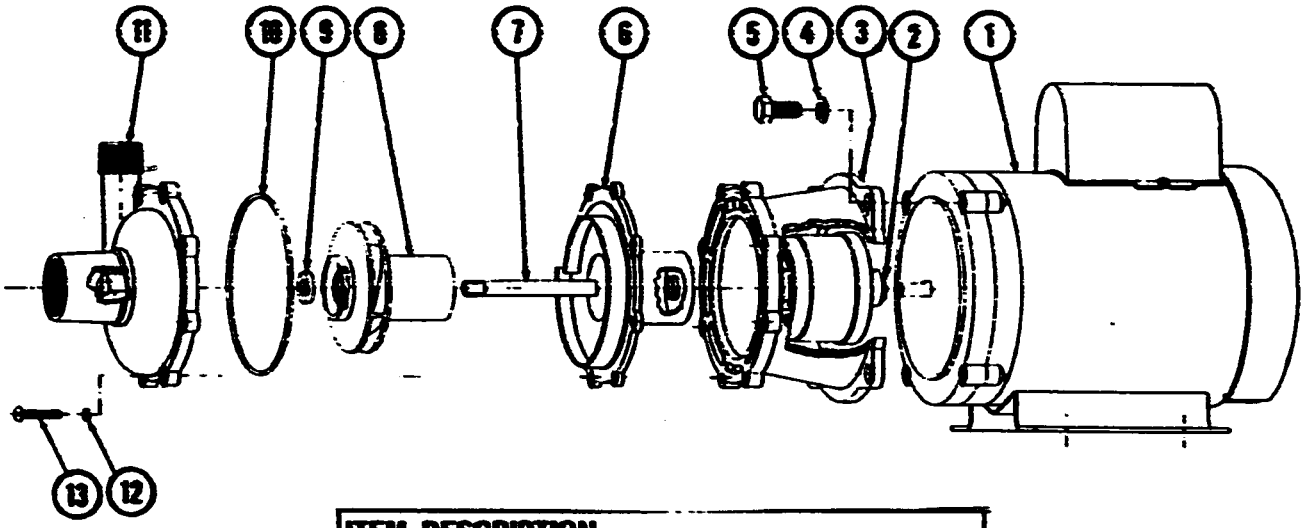

ITEM	DESCRIPTION
1	Motor, 115/230 Volt, 1 Phase
2	Drive Magnet Assembly
3	Motor Connecting Bracket
4	3/8 I.D. x 5/8 O.D. Stainless Washer
5	3/8-16 x 3/4 Long Screw
6	Rear Housing, Type 316 Stainless
7	Impeller Shaft, Ceramic
8a	Impeller Ass'y., Type 316 S.S. w/Std. Bushing
8b	Impeller Ass'y., Type 316 S.S. w/Chemloy Bushing
8c	Impeller Ass'y., Type 316 S.S. w/Carbon Bushing
9	Thrust Washer, Ceramic
10	4-1/4 I.D. x 3/32 Thick "O" Ring, Viton
11	Pump Housing, Type 316 Stainless
12	#10 I.D. Stainless Lock Washer
13	#10-32 X 1 Long Stainless Screw

Figure 6.15 Lithium bromide pump components.

field that influences the impeller magnetic and drive the impeller. See Figure 6.15 and Table 6.8 for more details [15].

Head Losses Estimation in the System

Assumptions

1- Assume that the fluid is water .

2- Neglect the losses inside the reservoir , preheater, and the heat exchanger since the velocities in these components are very low due to the relatively large diameters with respect to the tubes .

Calculations

The velocity in the 9.5mm tubes=0.89 m/s

Total length of the tubes = (22 ft)=6.65 m

Pressure loss per 100 Ft for 3/8" tube given by the manufacturer of the tube = (4.5 psi)=31 kpa

pressure loss in 22 ft =4.5 *22/100 =(1 psi)=6.895 kPa

head loss = 1(2.31)= (2.31 ft) = 0.7 m

head loss in elbows= number of elbows * 2k $v^2/2g$

head loss in the entrance =

= number of entrances * ke $v^2/2g$

Applying the energy equation [16] between the heat

exchanger and the reservoir in the apparatus

$$P_1/\alpha+V_1^2/2g+Z1=P_2/\alpha+V_2^2/2g+Z_2+\Sigma h_1$$

P1=P2=0 V1=0

Z2=1.5 m V2=0.89 m/s

elbows with(k=.19) = 17

elbows with(k=.32) = 8

entrances with (ke=.5) = 6

Substituting the above equation we get the minimum required pump head Z1=2.8 m

Since the pump available has flow rate of 23 GPM at this head, a feed back must be designed to minimize the load on the pump and to control the flow to the boiling tube.

6.7.2 Cooling System Water Pump

It is an ordinary water pump with the following specifications :

Horse power = 1/3

Voltage = 120 - 220 v

Capacity GPM at

6.8 HEAT EXCHANGER DESIGN

The heat exchanger used in this appratus is a U-Tube heat exchanger made of brass and it was designed previously for the following conditions [42].

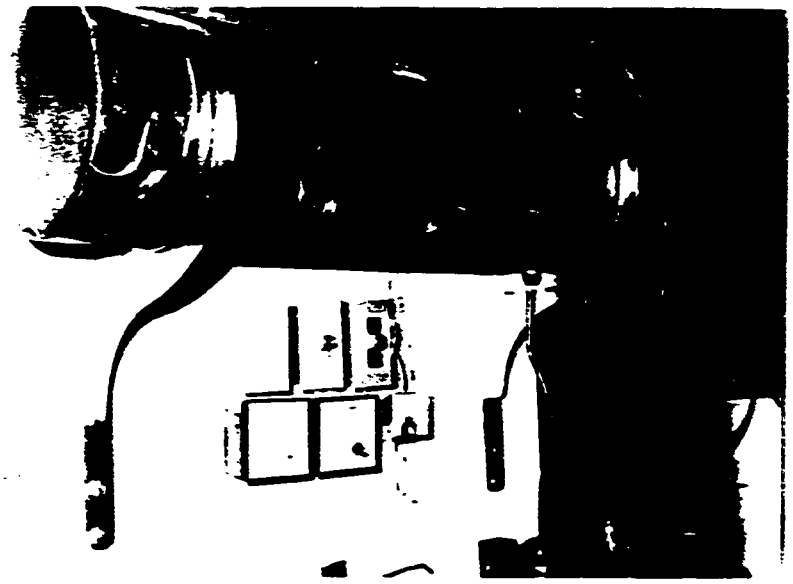

Figure 6.16 Lithium bromide solution-water heat exchanger.

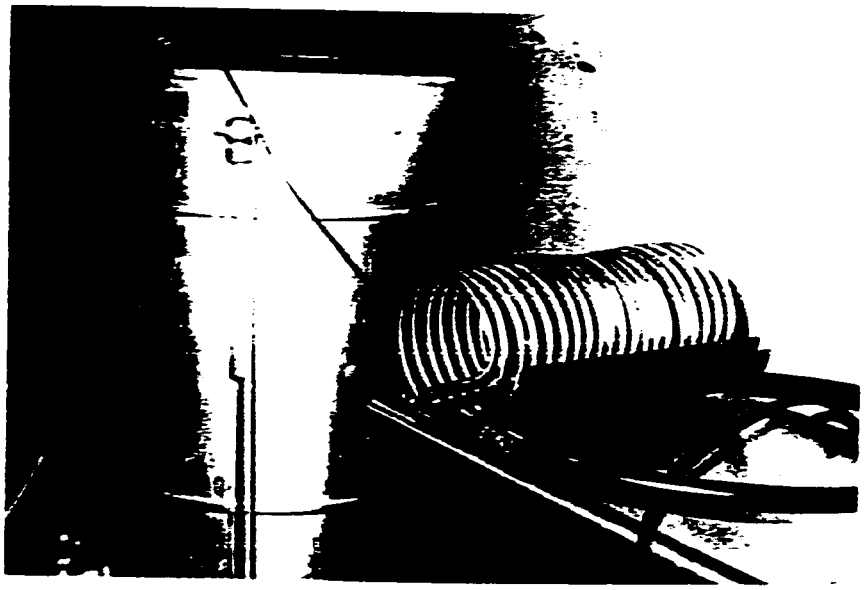

Figure 6.17.a. Cooling system reservoir.

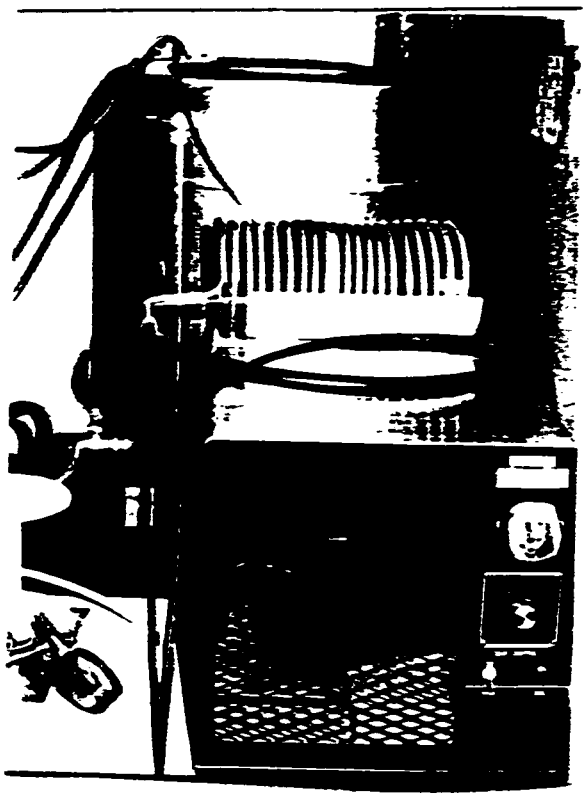

Figure 6.17.b. Apparatus cooling system .

Hot side	Cooled side
Water	Water
T_{hi}=100 °C vapor	T_{ci}=25 °C
T_{ho}=100 °C subcooled	T_{co}=40 °C
flow rate = 3 GPM	

Although the specified flow rate of the heat exchanger and its cooling capacity is much more than the one required for the apparatus, the cooling capacity can be minimized by lowering the flow rate of the cooling water by introducing a feedback from the pump outlet to its inlet .

6.9 COOLING SYSTEM

The cooling system consists of a water pump that sucks the water from a reservoir and pumps it to the heat exchanger after which it returns to the reservoir. A half-ton cooling capacity is used to keep the temperature of the cooling water in the reservoir at approximately constant temperature which is specified by adjusting its thermostat as seen in Figure 6.17.

6.10 DESIGN SIMPLIFICATION

To simplify the design, certain assumptions were made . These are ,

1. Negligible heat lost through the insulation.

2. The fluid mean temperature thermocouples will read the fluid temperature rather than the surface temperature.

3. The heat is uniformly distributed on the tube test section surface.

To justify these assumptions the following calculations was performed.

6.10.1 Heat lost calculation

Due to the large number of connections to the boiling tube , the insulation of the tube was not very effective . Therefore , heat lost to the surrounding was found by by calculating the heat added to pure water flowing through the tube at different inlet temperatures. Then the heat lost was ploted against the difference between the surface temperature of the tube and the ambient temperature . By interpolation , the heat lost at any temperature within the range can be found .The calculation is summarized in table 6.9 .

Heat added to water = $Q = m\ C_p\ (\ T_{mi} - T_{mo}\ )$

water flow rate $= 6.308 * 10^{-5}\ m^3 / s$

Heat lost throw the insulation = $1200 - Q$ Watt

6.10.2 Mean temperature thermocouple reading

If we assume that the thermowell tubes will act as fins

TABLE 6.9. Boiling Tube Heat Lost Through the insulation

T_s °C	T_m °C	C_p J/kg k	Γ kg/m^3	m kg/s	$T_i - T_o$ °C	Q Watt	Q_{lost} Watt
70.5	65	4184	980	.062	4.40	1141	59
77.8	71	4190	978	.062	4.39	1140	60
90.5	82	4199	971	.061	4.13	1058	142
102.8	94.5	4212	962	.061	4.08	1048	152

inside the boiling tube , then the reading of the thermocouples will not be the temperature of the fluid but a value between the surface temperature and the fluid mean temperature . The heat transfer inside the tube will be the main factor that govern the reading to be either close or far away from the temperature of the fluid .

For a circular cross section fin with convection heat transfer at the tip , the temperature distribution is given by [2],

$$\frac{T - T_m}{T_s - T_m} = \frac{\text{COSH}(m(L-X)) + h/(mk)\ \text{SINH}(m(L-X))}{\text{COSH}(mL) + h/(mk)\ \text{SINH}(L-X)} \qquad (6.3)$$

Since the thermocouple is effected by the tip temperature only which is at X=L ,the above expression is reduced to

$$T = T_m + (T_s - T_m)/(\text{COSH}(mL) + h/(mk)\text{SINH}(mL))$$

where $m^2 = hp/(kA_c) = 4.238\ h$ (6.5)

Figure 6.18 shows the thermocouple reading for 92 °C fluid mean temperature versus the difference between the surface and the mean temperature as it is inrceased from 1 to 15 °C for different heat transfer coefficients in the range

between 500 to 32,000 W/m^2k .From the figure we see that if $h=500\ W/m^2k$, the thermocouple will read the surface temperature rather than the mean temperature of the fluid as (T_S-T_m) approach 15 °C. But at $h\geq20000$ the reading error will be less than 0.4 °C for $(T_S-T_m)=15$ °C . Since the temperature difference in this experiment will not be more than 15 °C , the mean factor that affects the reading is the heat transfer coefficient h . Notice that the heat transfer coefficient is not necessary. It is the one for the whole flow and not that which effects the transfer of heat in the neighborhood of the thermowell tube .Therefore , if we imagine that the thermowell tube is a cylinder in a single phase cross flow , then the heat transfer coefficient is given by the following expression [2]:

$$hD/k=C\ Re_D^M\ Pr^{1/3} \qquad (6.6)$$

For water mean temperature $T_m=$ 92 °C , and flow rate Q=.5 GPM,

$k=677*10^{-3}$ W/mk $\mu=366*10^{-6}$ NS/m² Pr=2.02 $\Gamma=963$ kg /m³	$Re_D=4Q\Gamma/\pi D\mu=33034$ h=32026 W/m²k

For $T_m=$ 32 °C

$k=620*10^{-3}$ $\mu=769*10^{-6}$ Pr= 5.2 $\Gamma=995$	$Re_D=16239$ h=25917 W/m²k

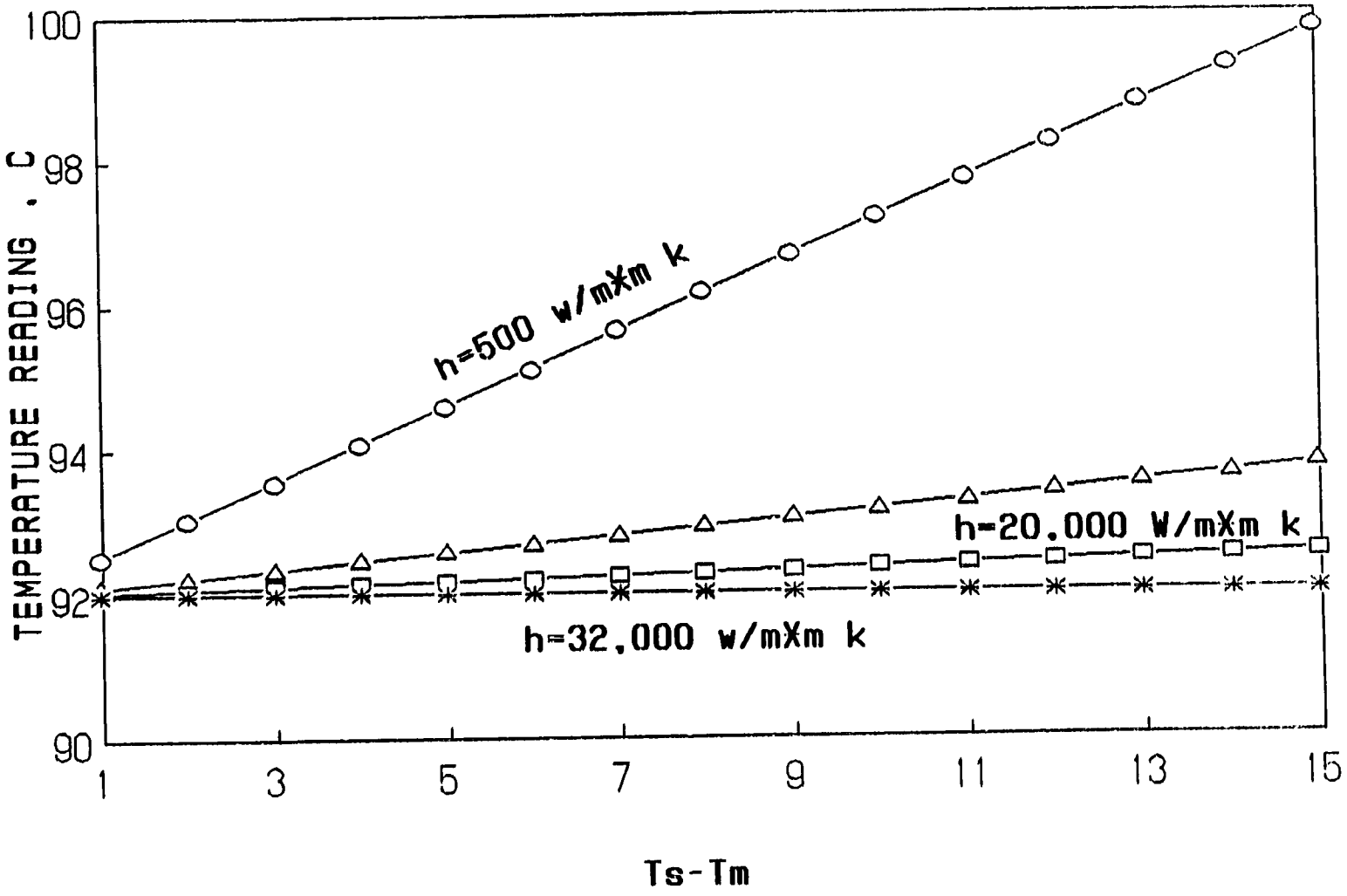

Figure 6.18. Thermocouple reading for 92 C fluid mean temperature .

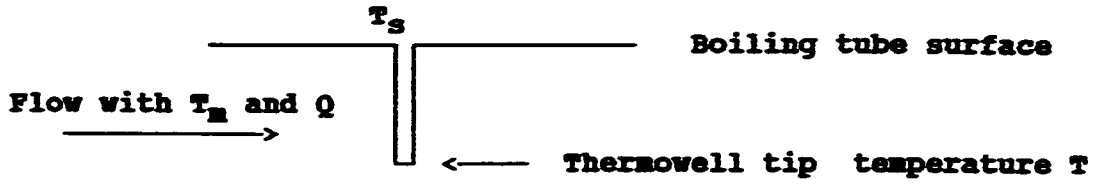

Figure 6.19. Representation of a thermocouple as a fin inside the boiling tube

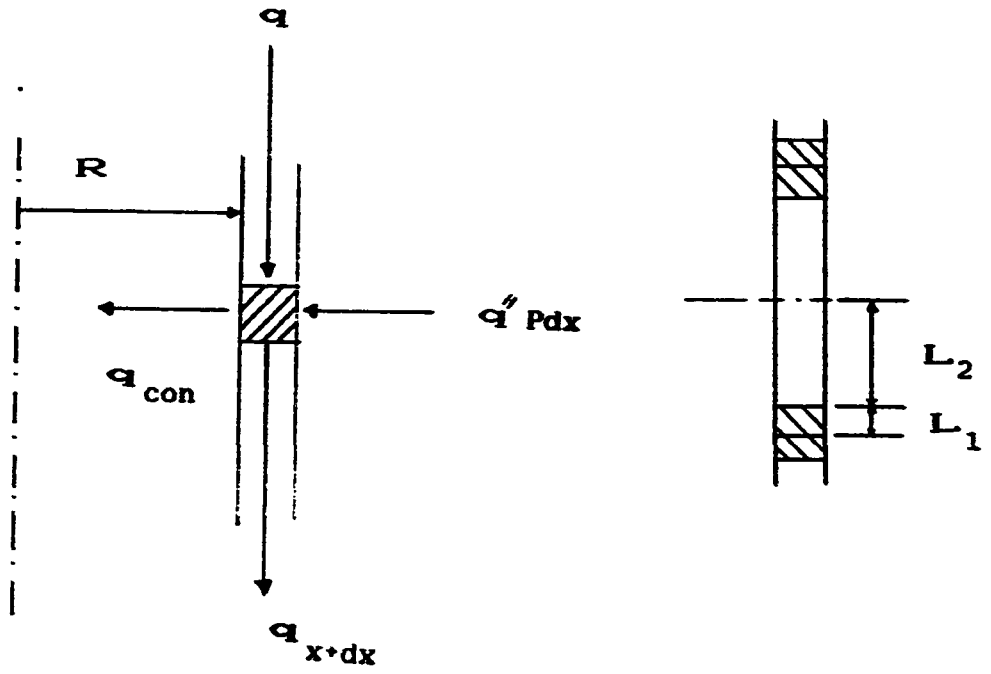

Figure 6.20. Differential element of the boiling tube cross setion.

From table 6.10 we get

C=0.193 and m=0.618

When we substitute the values in equation 6.5 , we get the thermocouple temperature reading T=92.022°C for T_m=92°C in the first case and T=32.046 °C for T_m= 32 °C in the second case . Because the minimum flow rate in this experiment is approximately 0.5 GPM , it is safe to say that the thermocouples will read the mean temperature with an error that is less than 0.05 °C .

6.10.3 Boiling tube surface temperature distribution

The heater used in the boiling tube is an electrical wire heater which is 1 mm diameter and 19000 mm long .It was wound in a helical shape around the tube with 100 turns on 1500 mm long tube. Because the pitch angle of the spiral shape is less than 4.5 °, we can approximate the problem as a tube with 100 ring shape heaters each 2 mm thick (including the elecrical insulation) and a space of 15 mm between every two heaters .In this case the heat suplied by each heater is 12 watt .

heat flux $q = Q/A_s$ =12 /(π 0.041*0.002)=46.58 kw/m²

To find out the effect of axial conduction by the fluid, the Peclet number Pe=Γ C_p V A_c /k P should be greater or

equal to 100 .

For water at 92 °C

Γ=965 kg/ m3 , C_p=4209 J/kg k , k=0.677 W/mk

the velocity of water inside the tube =0.0556 m/s

$A_C=\pi D^2/4=\pi(.038)^2/4 = 0.00115\ m^2$

$P= \pi\ D=\pi*0.041=0.1288\ m$

subtituting these numbers, we get Pe=2978 which means that the axial conduction by the fluid is negligible.

Assumptions

1- Steady state one dimentional conduction in the x direction along the tube .

2- Constant fluid mean temperature for at least a distance of 15 mm to cover the distance half way from the heater in both directions , T_m = constant.

3- Any two successive heaters supply heat in a way such that there is no net conduction at the center point between them, that is dT/dx = 0.0 .

This proplem is a two domain problem one with heat input and the other with out heat input . Hence , we solve the one with the heat input then we set q=0 for the second part .

Summing energy in and out of the element dx in figure 6.20, we get ,

$$-q_{con} + q_x + q''' p\,dx - q_{x+dx} = 0$$

$$- h(T_s - T_m)p\,dx - k A_c\, dT/dx + A_c k \left(dT/dx + d^2T/dx^2\, dx \right) + q''' P\,dx = 0$$

$$d^2\theta/dx^2 - m^2 \theta = -M$$

where $m^2 = Ph/A_c k$, $M = q''' P/A_c k$, $\theta = T_s - T_m$

The solution for this equation is given by

$$\theta_1(x) = C_1 \cosh m x + C_2 \sinh m x + M/m^2$$

For the second part M=0 and the solution of the problem is

$$\theta_2(x) = C_3 \cosh mx + C_4 \sinh mx$$

Boundary conditions

1. $\theta_1 = \theta_2$ and $d\theta_1/dx = d\theta_2/dx$ at $x=0$
2. $d\theta_1/dx = 0$ at $x = L_1 = 1$ mm
3. $d\theta_2/dx = 0$ at $x = L_2 = 7.5$ mm

Solving the equation we get

$$C_2 = C_4 \quad , \quad C_1 + M/m^2 = C_3 \quad , \quad C_1 = C_2 * \cosh mL_1 / \sinh mL_1$$

$$C_3 = - C_4 * \cosh mL_2 / \sinh mL_2$$

Let $\alpha = \text{Cosh } mL_1 / \text{Sinh } mL_1$, $\beta = -\text{Cosh } mL_2 / \text{Sinh } mL_2$

$H = \alpha - \beta$ and $B = -M/m^2H$ then the solution of the problem

$$\theta_1(x) = \alpha B \text{ Cosh } mx + B \text{ Sinh } mx + M/m^2 \qquad (6.7)$$

$$\theta_2(x) = \beta B \text{ Cosh } mx + B \text{ Sinh } mx \qquad (6.8)$$

Figure 6.21 shows the temperature distribution for the boiling tube surface from the heater center to the center between the two heater for h= 500 W/m^2k . We see that the temperature difference between the heater center A and a point at the center between the two heaters B is about .05 °C . Since the lowest heat transfer coefficient that we expect in this experiment is about 500 W/m^2 k , and hence, the maximum temperature difference between any two points on the tube surface is about .05 °C, we can assume that the heat is uniformly distributed on the tube surface and the surface temperature whether it is close or away from the heater, is almost the same .

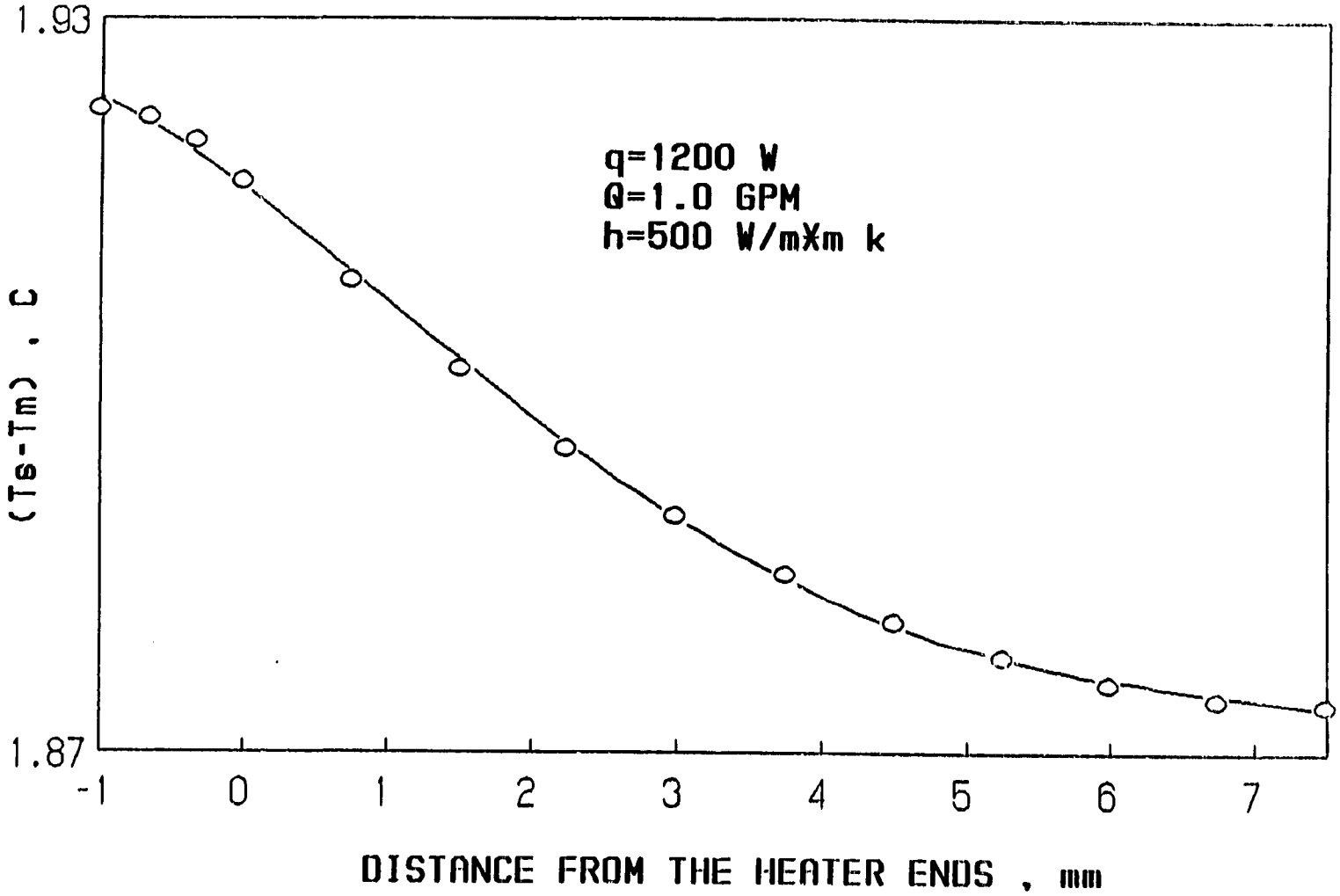

Figure 6.19 Tube test section surface temperature distribution.

CHAPTER VII

INSTRUMENTATION

7.1 DATA ACQUISITION COMPUTER

description of the computer usewd to collect the experimental data is given below.

7.1.1 Its Components

It consists of the following (see figure 7.1):

1-Listener : A device that receives data from another instrument like printer .

2- Talker : A device that transmits data to another instrument like counter and voltmeter.

3- Controller : A device that manages communications such as addressing and sending information .

7.1.2 How It Reads the Data

In the case of the temperature reading, the data acquisition controler scans the 50 thermocouple terminals

(see Figure 7.2) within 25 seconds and reads and displays their voltages on its panel . After it converts the voltage data to temperature values in °C it sends them to the computer where they are displayed on the terminal screen.

In the case of the flow rate reading , the controller receives the data from the counter as number of pulses per unit time which is usually specified by the controller . These pulses are sent to the counter by a turbine flow meter after amplification of the signal voltage which is usually very weak . The number of pulses received is converted into the flow rate in gallon per minutes by multiplying it by a factor usually supplied with the turbine flow meter .

7.2 TURBINE FLOWMETER

It is a mechanical flow meter in which a small magnetic turbine impeller rotates by the force exerted by the flow [17]. When the impeller rotates, it sends a weak magnetic signal picked up by an electronic sensor which in turn, sends it to an amplifier before it goes to the data acquisition system.

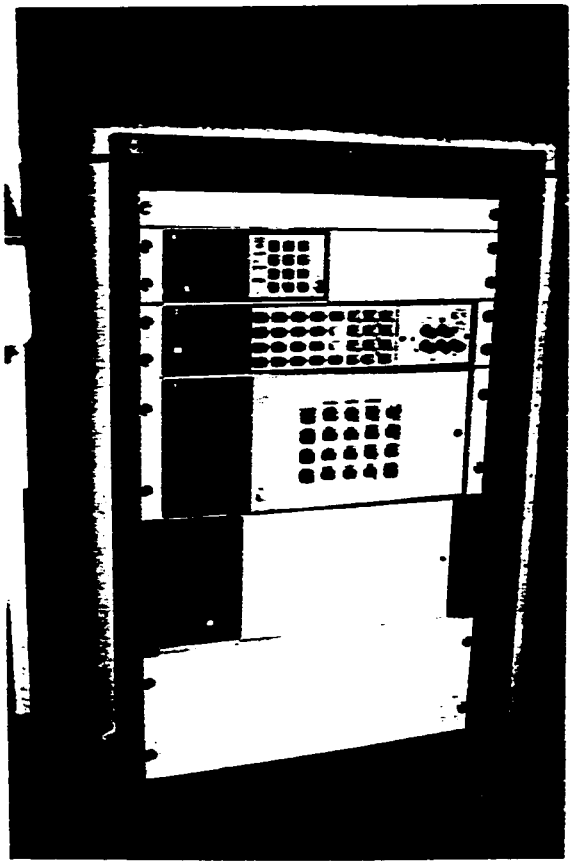

Figure 7.1 Data acquistion computer.

Figure 7.2.Thermocouple terminals.

THEORY:

1. Single Phase

In single phase flow one can define the following:

$$\text{Rotation Reynolds number } Re = \frac{MD^2}{v} \qquad (7.1)$$

$$\text{Flow coefficient } C = \frac{Q}{MD^3} \qquad (7.2)$$

Q = Flow rate

M = Rotational frequency

D = Pipe diameter

v = Kinematic Viscosity

Although Hochreiter (1958)[17] has shown that the flow coefficient is a function of Renolds number, the flow coefficient appears to be constant over a wide range of Renolds number. This means that the rotational frequency M is proportional to the volumetric flowrate.

$$n = C\, m / \Gamma \qquad (7.3)$$

where,

m= mass flow rate

Γ= fluid density

C= calibration constant

2- Two Phase Flow

For two phase flow ,the same formula is used with the following changes .

m= total mass flow rate

Γ= two phase density

C= calibration constant for single phase liquid flow

To find the two phase density Γ ,analysis of the force acting on the turbine blades is required . Popper (1961)[17]found the following relation for the acting forces.

$$n = C\ A\ W_L \frac{(1-R)\ \Gamma_L + R\ \Gamma\ v\ \alpha^2}{(1-R)\ \Gamma_L + R\ \Gamma v\ \alpha} \qquad (7.4)$$

where,

A= Pipe cross section area

R= Area void fraction

α= slip ratio= W_V/W_L

where,

W_L, W_V =area averaged velocity of the liquid and the vapor phase respectevely

If the vapor quality x is subtituted in the above equation with the help of the expression $(1-x)m=(1-R)\Gamma_l W_L$, we get the following .

$$n=C\ A\ W_1\ [1+(x-1)] \qquad (7.5)$$

comparing equation 7.3 with 7.4 we get an expression for the equivalent density [17].

$$\frac{1}{\Gamma} = \frac{(1-x)^2}{(1-R)\Gamma_L} + \frac{x^2}{R\ \Gamma_V} \qquad (7.6)$$

7.3 OMEGA TEMPERATURE CALIBRATOR (OMINI-CALTH)

OMINI-CALTH is a multi-function microprocessor package. First, it can be used as thermometer when connected to a thermocouple and it provides a direct °F or °C readout. Second, it can be used as a calibrator. It provide a precise voltage outputs equivalent to the tubular value for a specific thermocouple. Third, it can be used as a voltmeter with a range of ± 101 mv. Fourth, it can be used as a self-tester which provides for a complete check up of the system performance. It provides reading for seven thermocouple types (J, K, T, E, R, S, C). It is battery powered and supplied with a rechargable NiCadmium battery and an integral battery charging circuit which uses 110V AC source power. See instrument specification for more detail [8].

7.3.1- Using OMINI-CALTH for Calibration

1.1 To obtain the maximum benefit from the calibrator perform the following before using it [8].

1.1.1 °F - °C switch must be in the °C position.

1.1.2- Select the test function.

1.1.3- Rotate the range selector through its eight range positions starting with mV.

1.1.4- Compare the display value for each range with the given reading found on the calibrator cover.

1.2. Disconnect the thermocouple leads from the instrument which will be calibrated.

1.3. Connect the instrument to the calibrator using good quality thermocouple wire.

1.4. Select calibrate function.

1.5. Select the appropriate OMINI-CALTH range.

1.6. Use the coarse and fine output adjust controls for zero degree display value.

1.7. Adjust the instrument for zero degree value.

1.8. Use OMINI-CALTH "output adjust" controls for calibrating the full scale range of the instrument.

1.9. Adjust the instrument range control for equal display.

7.4- OMEGA NON-INVASIVE ULTRASONIC VELOCITY MONITOR

It is an instrument that measure the velocity of flowing liquids inside pipes by means of reflected ultrasonic signals. The monitor requires at least 30 PPM of 30 micron or larger suspended solids. The monitor consists of a portable transducer which sends continuous ultrasonic signal through the pipe wall and into the liquid stream. When these signals are reflected back from particles in the stream the detected signals will be proportional to the velocity of the fluid and it is to be displayed as velocity in feet per second [51].

7.4.1- How to Measure a Flow

To measure a flow certain conditions should be known to get the maximum benefit from the instrument. Some pipe materials diffuse or transmit sound more than the other. Thus, for best performance of the instrument, recommended piping materials should be used:

7.4.1.1 Poor Materials:

Concrete, rubber, galvanized, lead, soft plastic and heavily painted pipes.

7.4.1.2- Good Materials:

PVC, CPVC, and other hard plastic pipes, aluminum, carbon steel, cast iron, stainless steel, ductile iron and copper pipes.

7.4.2- Necessary Conditions for Measurements

1. The media to be measured must be a liquid.

2. The pipe should be full or at a constant depth.

3. Pipe material should allow penetration of the ultrasonic signal.

4. Should have sufficient straight pipe before and after the transducer.

5. Fluids flow horizontally or upward vertically.

6. The flow must be uniform and has particles in it.

7.4.3 Weak Signals

Weak signal usually caused by the following [51]:

1. Clean fluids.
2. Low velocity.
3. Pipe inner surface contains scales.

7.4.4- Transducer Mounting

Before transducer mounting, clean an area slightly larger than the transducer, then apply a heavy coat of the couplant compound supplied with the unit to the face of the transducer. The

transducer must be parallel to the pipe axis with its arrow towards the direction of the flow. Some precautions must be kept in mind when mounting the transducer. They are the following [51]:

7.4.4.1 - Do not mount

1. On hot or vibrating pipe
2. Near high heat source, AC motor, transformer, transmitter or antenna.
3. On bottom of pipe (it may pick up sediments).
4. On top of pipe (pipe may be not full).
5. Avoid air bubbles within the couplant jelly.

7.4.4.2 - Do mount

1. High and dry pipes.
2. Easily accessible pipes.
3. Near the 3 O'clock or 9 O'clock position on pipe.

7.4.5- Operation instructions

1 - Put sufficient couplant jelly to transducer and mount it to the pipe.

2 - Press the ON-button and hold until a steady reading is shown supported with a green light from the indicator.

3 - A number of readings should be taken to obtain an average flow velocity in feet per second.

7.4.6- Converting a Velocity reading into GPM

To convert a velocity reading into GPM use the following equation:

$$Q = CVD^2 \qquad (7.7)$$

Where:

V = Velocity of flow in feet/second.

D = Internal pipe diameter.

C = A constant = 2.45.

Q = Flow rate in GPM

7.4.7- Precautions

The monitor is calibrated on water. Therefore there may be an error in the reading if the fluid being monitored has the following [51]:

1 - High solid particles about 10%.
2 - High viscosity.
3 - Density is not in the same order of magnitude as of water that cause a change in refraction.

7.5 THERMOCOUPLE WELDER

It is an arc welder in which high current fuses the thermocouple wires togeather under the shielding of argon gas to prevent oxidation of the thermocouple tip see figure 7.3 .

7.5.1 Specification

voltage 110-220 v
Amp 15 A
Argon flow pressure 2 - 4 psig
Welding time 2 - 4 Sec.

7.5.2 How to Use the Welder

1- Clean the holding gun for good electrical contact .

2- Turn the welder on .

4- Adjust the argon gas pressure to 4 psig and purge the system to get rid of air in the system.

2- Hold the thermocouple wires so that the starting of the twested wires is exactly at the end of the holding gun .

5- Insert the gun and apply the arc to fuse the two wires and form the thermocouple tip.

7.6 TUBE CUTTER

Used to cut steel, copper or brass tubes with diameter in the range between 3 to 30 mm by rotating it around the tube and gradually tightening the lead screw . The cutter wheels cause fracture of the tube material because of the highy localized stress under the wheel edges .

7.7 ACETYLINE GAS WELDER

Acetyline gas welder consists of two bottle of acetyline and oxygen ,extension hoses and a torch in which the acetyline gas burns in a stream of oxygen giving off very high heat energy which is used to melt steel , copper or other materials for cutting or welding .

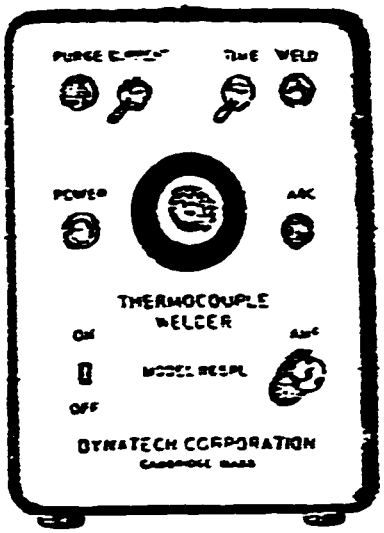

WELDER WITH CONTROLS DEFINED

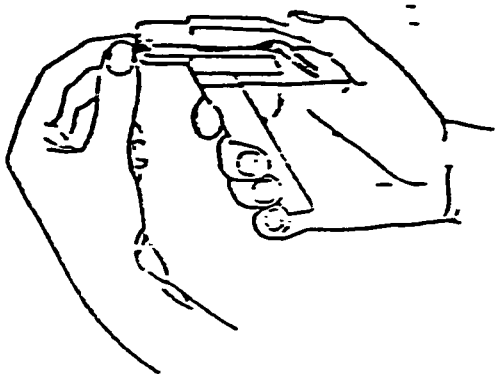

HOLDING GUN

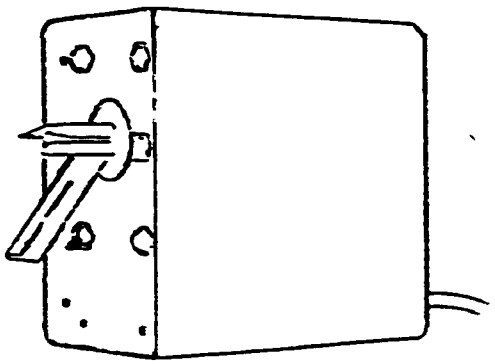

GUN IN WELDING RECEPTACLE

Figure 7.3 Thermocoupole welder.

CHAPTER VIII

EXPERIMENTAL RESULTS AND DATA REDUCTION

The heat transfer of seven samples of LiBr-water solutions having concentration ranging from 10% to 50% by weight were studied in the present investigation. Starting with a concentration of 50%, three readings were taken for each solution, two of which were for convection at two different inlet temperatures and one for boiling . Readings were taken at steady state condition where the mean temperatures remained almost constant . The data were collected after it was ascertained that the readings did not fluctuate by more than ±.8°C during boiling, and ±.5°C in convection. Although ±.8°C change may seem to be relatively large, it is worth noting that the boiling phenomena is typically characterized by fluctuations and as such it is rather difficult to obtain the ideal steady condition. This is further detailed later in Chapter 9 related to error discussion. All data collected from the system were analyzed and a number of plots showing the temperature distribution,

heat transfer coefficient and quality were generated. The methodology of data reduction and subsequent heat transfer formulations are now detailed below.

8.1 CONVECTION

8.1.1 Temperature Distribution:

All convection temperature distribution plots in Figs. 8.2 to 8.13 (data for these Figs. are given in tables 8.1 to 8.7) show two distinct regions, namely, the entry length region where the temperature profile is developing, and the fully developed region. As such the discussions below is carried out separately for these two regions.

i. Entry region

The above mentioned temperature and heat transfer coefficient plots given in Figs 8.2 to 8.17 clearly show the existence of an entry length varying from 30 to 40 cm from the tube inlet inspite of the difference in flow rates and the thermal properties due to different concentrations. In fact the average distance is about 37 cm which is almost 10 times the tube diameter. This result is consistent in turbulent flow where the temperature profiles are expected to fully develop withen 10 to 15 tube diameter. The development of such boundary

layer is, however, strongly dependent on the geometry of the entrance conditions. Usually, the boundary layer develops very quickly if the tube entrance is sharp and Re > 2300, which is the case in the present investigation.

In order to have a hydrodynamically fully developed flow before the heating starts, the test section was preceeded by an entrance length of 25 cm as shown in Fig. 8.1. For the range of Re and Pr studied, this length is well within the required 10 D for hydrodynamically fully developed flow. The results presented in the entrance region, thus, represents the developing thermal profile in the presence of a hydrodynamically fully developed flow. Note also that the first temperature reading is taken at a distance of 5 cm away from the point where the heating begins. Since in most cases the working fluid was preheated before it was introduced to the test section, the temperature of the working fluid was actually higher than the surface temperature in the entrance length of 25 cm, as shown in Fig. 8.1.

ii. Fully developed region

After the heating begins, the thermal boundary layer starts to grow and it becomes fully developed within a distance of 35 to 40 cm. The temperature profile remains invariant thereafter in the tube and the difference

between the surface temperature and the mean fluid temperature also remains invariant, as was discussed earlier in section 3 and shown in Fig. 8.1. All the convection temperature distribution of Figs. 8.2 to 8.13 show that after about 10 tube diameter, both the surface and the mean fluid temperature increase linearly, parallel to each other, the slope of which is given by the expression:

$$\frac{dT_m}{dx} = \frac{\pi D q_{con}}{m Cp} \qquad (8.1)$$

This equation is useful in calculating the actual amount of heat added to the fluid , i.e.,

$$q_{con} = m Cp dT_m / \pi D dx$$

8.1.2 Heat Transfer Coefficient Distribution

Heat transfer coefficient in all the runs was calculated by using equation 5.13. Figures 8.14 to 8.17 (the corresponding data are given in tables 8.1 to 8.7) show the variations in h and they show two distinct regions reflecting the entrance region, where the temperature profile is developing, and the fully developed profile.

In the first case, the heat transfer coefficient decreases sharply starting from the inlet upto a distance of about 10 to 15 diameters, as expected, after which it

approaches a constant value corresponding to fully developed temperature profile. Usually the entry region is not important in turbulent flow since its length is small compare to that in laminar flow. One important conclusion which can be drawn by inspecting the Fig. 8.14 to 8.17 is that for a given heat flux , flow rate and concentration , heat transfer coefficients remain almost the same in spite of the difference in the inlet temperatures. For example, Figure 8.14 shows such runs both at 1 GPM and 10%LiBr but with inlet temperatures of 66°C and 83°C and heat input of 1120 W and 1025 W . Ispite of the relatively large difference in the inlet temperature (17°C), both curves predict almost the same heat transfer coefficient which is about 700 W/m^2K. Whatever deviation is observed between the two curves, for the entire length, it cannot be attributed to the difference in the heat flux applied, as calculations show that such difference may cause only a deviation of ±35 W/m^2K. This deviation in fact is within the calculated standard deviation of ± 35.5 W/m^2K for the entire data set. Similar trend is displayed by Fig. 8.15, which is for a concentration of 20% LiBr . It is seen that the heat transfer coefficient for both the runs level off to the same value of 600 W/m^2K as the flow becomes fully developed. Similar trend is displayed by the remaining plots. This behavior tends to conclude that the total effect of increasing the inlet temperatures on the physical properties related to the heat transfer coefficient, such

as k, Cp, μ and Γ is negligible in spite of the big difference in the mean fluid temperature. In the fully developed region some fluctuations in the value of the heat transfer coefficient can be observed. This is due mainly to the consistent computer card reading error for the surface temperatures at location of 95 cm to 110 cm. This is further detailed in the Chapter related to error analysis.

8.1.3 Convective Heat Transfer Correlations

Comparing Figures 8.14 and 8.15, it is evident that the heat transfer coefficient changes significantly as the lithium bromide water concentration is changed keeping the flow rate and heat flux the same. This suggests that the heat transfer coefficient is a strong function of concentration. Therefore, the correlation that can best describe the heat transfer mechanism is of the form,

$$Nu=C\ Re^{m}\ Pr^{n}\ F \qquad (8.2)$$

where the F factor introduces the effect of concentration. As a first step towards obtaining the factor F, the effect of concentration of LiBr on viscosity μ , specific heat Cp, density Γ, and thermal conductivity K, the dimensionless parameters μ/μ_w , Cp/Cp_w , Γ/Γ_w and k/k_w were plotted against LiBr concentration X, shown in figure 8.18 . The

subscript w refers to water properties under the same conditions as LiBr-water solution . The figure shows that the viscosity is very sensitive to concentration change while the change of the other properties are not appreciable. It is thus possible to say that $F=f(\mu)$.

Hence, $$Nu=C\ Re^{m}\ Pr^{n}\ f(\mu) \qquad (8.3)$$

The function $f(\mu)$ can be represented by a dimensionless $f(\mu^*)$

where,

$$\mu^* = \mu_{LiBr}/\mu_{water} \qquad (8.4)$$

It is observed in equation (8.3) that there are four unknowns (c,m,n and f) which needs to be determined experimentaly. However, if we consider commonly assigned values of m=0.8 and n=0.4 for heating and incorporate the effect of the constant C in the functional relation $f(\mu^*)$, then equation (8.3) can be written as ,

$$Nu=hD/k= Re^{.8}\ Pr^{.4}\ f(\mu^*)$$

or

$$Nu/Re^{.8}\ Pr^{.4}=f(\mu^*)$$

Taking ln on both sides,

$$\ln(Nu/Re^{.8}\ Pr^{.4})=\ln(f(\mu^*)) \qquad (8.5)$$

From experimental measurements the heat transfer coefficient was calculated by writing h= q/(Ts-Tm), which in turns give the Nu . Re and Pr also calculated since the flow rate and other physical propertis were available beforehand .To find the function $f(\mu^*)$, the left side of equation 8.5 was ploted against the corresponding values of μ^* for 140 data point that represent the fully developed flow. The plot Figs 8.19, show a linear relationship between $\ln(Nu/Re^{.8}\ Pr^{.4})$ and $\ln(\mu^*)$. A regressaion analysis with such data yields an equation of the form,

$$\ln(Nu/\ Re^{.8}\ Pr^{.4})= C1+C2\ \ln\ (\mu^*)$$

i.e.

$$\ln(Nu/\ Re^{.8}\ Pr^{.4})= C1+\ \ln\ (\ (\mu^*)^{C2}\ )$$

Taking exponents on both sides and rearranging one obtains,

$$Nu=0.02844\ Re^{.8}\ Pr^{.4}\ (\mu^*)^{.327} \qquad (8.6)$$

$$2300 \leq Re \leq 6000$$

$$1 \leq Pr \leq 6$$

Equation 8.6 fits the data with mean square error of 8.6 and standard deveation of ± 2.9 . In order to chek the accuracy futher, equation 8.6 was ploted againest the measured Nu as shown in figure 8.20 and table 8.8 , where

it can be seen that 86% of the data fall withen ± 12% . Equation 8.6 is applicable to both LiBr solution and Pure water where in the later case only the viscosity μ_{LiBr} is replaced by μ_{water} and doing so equation 8.6 is reduced to,

$$Nu = .02844\ Re^{.8}\ Pr^{.4} \qquad (8.7)$$

The above equation is very similar to the Dittus-Boelter equation (equation 5.11), and we find that equation (8.7) will differ from equation (5.11) by only 7% .

8.2 SUBCOOLED BOILING (SBC)

When the temperature of the surface exceeds the saturation temperature of the fluid, vapor bubbles starts generate in the surface cavitation of the tube . As the bubbles reach their critical diameter , they detach from the surface and collapse in the sub-cooled liquid in the mean core without affecting any net vapor generation. The process of generation of disappearance of the bubble transport more energy to the mean fluid than that caused by convection alone.

8.2.1 Temperature Distribution

Subcooled boiling can be visualized as a transition zone between convection and fully developed boiling . The

mean fluid temperature distribution in subcooled boiling (see Fig. 5.6) is an extension of that in convection which increases linearly until it changes completely to saturated temperature as saturated boiling begins. Therefore the mean temperature in subcooled boiling can be calculated by using equation (5.5) which assumes linear distribution . However the surface profiles of temperature in SBC is completely different from both convection or boiling . The shape of the curve depends mainly on the length of the subcooled region . The longer the region , the smoother the change from convection to boiling. Figure 8.21 and table 8.9 represent such a case where subcooled boiling gently transitions from convection to boiling . This may not be very apparent from the temperature distribution plot, but once the heat transfer coefficient is obtained from this data and plotted, as shown in Fig. 8.22 (data are given in table 8.9), the presence of subcooled boiling become evident. The plot with Ti= 107 °C (curve A) has higher coefficient than that for Ti=82 °C (curve B) even though the flow rate in the former situation is lower. This can not have happened if convection was the only mode. In both situations the heat transfewr coefficient decays in the entry length of approximately 30 cm . However, in curve A, nuclation starts initiating the subcooled boiling and boosting its heat transfer, whereas curve B does not experience any subcooled boiling at all.

A somewhat different picture is presented in Fig. 8.23 and Fig. 8.24 (corresponing data are given in table 8.5) , where the presence of subcooled boiling is much more pronounced . The two curves are seperated right from the inlet suggesting that curve A does not have thermal entry length convection alone but also experiences surface nucleation in this region. Incontrast curve B has the usual pattern of entrance length convectin followed by fully developed convectioin and not reach nucleation.

Similarly , figure 8.25 and table 10 represent the case where the subcooled boiling starts right at the tube inlet and continues up to the exit. In this figure the surface temperature changes gently similar to figure 8.23 suggesting the presence of subcooled region . and the only differance being that in this run the entry length region could not be detected even from the heat transfer coefficient distribution graph in figure 8.26 . This behavior is due mainly to nucleation which started exactly at the tube inlet . Therefore , the transfer of heat from the surface due to nucleation exceeds the transfer of heat that is due to convection . Also to be noted here that the net vapor generation in the SCB is zero and was also verified in the runs by calculating the vapor quality, which was found to be less than zero.

Figures 8.27, 8.28 and 8.29 (data are given in table

8.11 to 8.13) are further extensions of the above phenemenon in that they show all three zones of heat transfer : convection , subcooled boiling and saturated boiling . From these figures we find that the subcooled region starts when the surface temperature Ts becomes equal to the saturated temperature T_{sat}. The surface temperature further increases upto a degree of superheat of about 4°C declining again to about 2°C superheat, where saturated boiling begins. It is also striking to note that in all the runs the distance between the point of maximum superheat and the initiating of fully developed boiling remained approximately the same, about 6 tube diameter .This particular behavior can be explained by noting that the location of the maximum superheat primarily depends on heat flux and the tube geometry and not on the flow properties . In these runs the heat flux remained approximately the same .

8.2.2 Heat Transfer Coefficient

Figure 8.31 and table 8.14 show the heat transfer regions convection , subcooled and saturated boiling for the case of 35% by wt. LiBr water mixture . In this figure we see that for most part the heat transfer coefficient for subcooled boiling remain fairly costant , but rising sharply as it approaches fully developed boiling . As the

surface temperature increases above saturation , the frequency of vapor bubbles formation increases boosting the transport of heat from the surface to the bulk flow and thus increasing the heat transfer coefficient almost exponentially until it reaches to a point where its value is about 5 times that for convection calculated using equation (8.6) while the convection' calculation predicts a coefficient of 420 W/m^2k , the actual coefficient is almost 2300 W/m^2K , shown in Fig.8.31. It was earlier mentioned that the surface temperature in subcooled boiling attains a maximum degree of superheat of about 4 °C , at which point the heat transfer coefficient shoots up, while before this point the heat transfer coefficient can be assumed as constant approximately two times that for convection shown in figure 8.32. Similarly , figure 8.33 shows the same trend as 8.32 in which we find that the heat transfer coefficient starts with a constant value of 800 W/m^2 k and at z=80 cm , the curve starts to shoot up as in the first case . This location also coincides with the point of the maximum surface temperature as can be seen in figure 8.28. It can be further noticed from Figs 8.28 and 8.35 that at z=100 cm , where saturated boiling initiates, the heat transfer coefficient h_{SCB} is about 1600 W/m^2 k . If we calculate the coefficient for convection h_c at what point, using equation (8.6), we get $h_c \approx 300$ W/m^2k which is one fifth the value due to subcooled boiling.

8.3 BOILING

8.3.1 Temperature Distribution

When the fluid mean temperature reaches the saturated temperature , important changes in both surface and mean temperatures occur shown in Figs 8.27 to 8.30 and tables 8.11 to 8.14. First of all the mean temperature changes from linearly increasing in the convection and subcooled region to a constant temperature ,i.e., the saturation temperature . While, the surface temperature profile shown a gradual decrease gradually from 4 °C superheat to about 2 °C near the point of zero quality and further continues to decrease slightly until it approaches a limit where it becomes parallel to the mean fluid temperature .

Figure 8.27 shows the boiling regions in which the vertical line that separates the subcooled from saturated boiling is the location where vapor quality is zero. There the slope of the mean fluid temperature changes from $dt_m/dx=(\pi D\ q\ /\ m\ Cp)$ to $dt_m/dx \approx 0$ and the surface temperature approaches the mean fluid temperature.

Figure 8.34 shows the data for saturated boiling region only where both surface and fluid mean temperature

decrease almost parallel to each other along the tube. The decreasing of the temperature curves is due to the pressure reduction as the flow moves up . The decrease is about 1°C between the tube inlet and outlet which corresponds to pressure reduction in the tube of about 5.5 kPa. From the figure we see that the surface temperature somewhat fluctuates and the curve is not smooth as in the subcooled region while the mean fluid temperature remains almost constant or equal to saturated temperature. The fluctuation in the surface temperature is due mainly to the vapor bubble generation which is usually larger in low pressure flow . Fiori and Bergles [31] had observed this phenomena prior to critical heat flux (CHF) of subcooled or low quality flow boiling in uniformly heated tube. This was observed through photography and other means that vapor slugs or thin vapor layers exist near the wall .

In Fig. 8.34 and table 8.15 some scatter in the surface temperature reading is observed at locations 90 cm to 105 cm .This happened consistently in all temperature plots for convection , subcooled and saturated boiling where these thermocouples always gave readings less than the nearby thermocouples . This is attributed to the malfunction of the thermocouple card which was detected only after all the data had been collected and the plots were done . Figure 8.30 distenctly shows two regions of boiling : subcooled and saturated boiling . In the

saturated zone which starts from the line of zero vapor quality , we notice the same trend as discussed before .

As the fluid moves up , more and more vapor bubbles are generated at the surface . The increase in vapor bubbles consumes the water from the solution leaving a sublayer containing high concentrated LiBr solution which require higher heat to boil . The concentration of the sublayer depends on the diffusion rate of water to the sublayer. The sublayer acts as a resistance that retards the flow of heat , increasing the surface temperature . At the same time , as the fluid moves up there is a decrease in pressure which increases the bubble growth due to the decrease in saturated temperature of the bulk flow . This in turn, decreases the surface temperature, which is more than the increase caused by the sublayer resistance mentioned earlier.

8.3.2 Heat Transfer Coefficient

Theoretically it is expected that the heat transfer coefficient will increases linearly in the subcooled region, later becoming constant in the saturated boiling region due to the fixed difference between the surface and mean fluid temperature. However, in case of LiBr solution, the heat transfer coefficient plot , shown in Fig. 8.35 and table 8.14, obtainwed from the temperature plot of Fig.

8.30, shows that h remain fairly constant in the subcooled boiling ,but changes sharply in the region around x=0 due to increase bubble activity and later assumes a linear increase after quality of .3 % . The region 55 cm and 95 cm can thus be treated as the transition zone between subcooled and fully developed boiling . This observation is further supported by the temperature and heat transfer coefficient plot of Fig. 8.36 (data are given in table 8.13), where the SCB and the transition from the SCB is illustrated.

Figure 8.37 and table 15 represent fully developed boiling data for 10% LiBr solution. From the appearance , the heat transfer coefficient seems to be fluctuating for the entire data set . However these fluctuations are rather normal and are explainable by observing the corresponding surface and fluid mean temperature plot. It is seen that while the fluid mean temperature remains rather steady , the surface temperature displays irregular fluctuations for reasons explained earlier. Since heat transfer coefficient is calculated based on (Ts-Tm) , also known as wall superheat. Tese fluctuations become highly pronounced when (Ts-Tm) becomes very close to zero. In most boiling data the wall superheat usually are very low. For this reason , the surface temperature data was smoothened using the least square method after which the heat transfer coefficient h_b was calculated using equation (5.13) and shown by the solid line. In the same figure , the dashed line represents the

best fit of h obtained from the raw data. Both regression show an increase in h_b along the tube test section.

8.3.3 Vapor Quality

Calculating the vapor quality is not a simple task . It involves a trial and error procedure because the calculation the vapor quality requires the enthalpy for both vapor and liquid . For enthalpy calculation, the system pressure must be known which by in turn requires the vapor quality . Due to the low qualities encountered in these experiments ($x \approx 1\ \%$) and the smoothness in the boiling tube, the pressure drop in the vertical test section is mainly dominated by gravity.

In addition to that the location where saturated boiling begins (x=0 location) must also be known, which makes the problem even more complicated . Fortunately, the location for x=0 can be estimated first from the temperature distribution graph since at this location the slope of the mean fluid temperature changes from $dT/dx=\pi Dq/mCp$ to $dT/dx\approx 0$. Then an itrative method was used as outlined below:

1.from the temperature distribution plot find the initial approximate location , L_o , where x=0

2. calculate the pressure drop between the inlet and L_o by using single phase equation

3. calculatwe pressure at L_o by writing

$$P=P_{inlet}- \delta P$$

4. assume a single-phase flow from Lo to tube outlet and obtain a pressure distribution at each location
5. by knowing the pressure at each location obtain the enthalpy value to calculate the quality x
6. use this quality value and calculate a new pressure distribution by considering two phase flow equations
7. the steps 1 to 6 is repeated untill the calculation change in quality at each location does not differ by more than .00005%

Notice that the iteration was initiated starting from an approximate location L_o where x=0. If the above described routine resulted into negative value of x (x< 0), it means that the location of L_o is subcooled. In orther to determine the exact location of L_o, the entire iteration was repeated for the next higher location and so on. On the other hand , if a positive value (x > 0) resulted dowwnward until the desired convergence was achieved. The entire procedure is desicribed in the flow chart given in Fig. 8.38.

All vapor quality vs. distance plots of Figs.8.39 to 8.43 (corresponding data are given in tables 8.11 to 8.15) show linear increase of vapor quality with distance. This is expected since heat flux is constant and the pressure is almost linearly distributed .

Figs 8.44 to 8.48 (tables 8.11 to 8.15 represents the data for these plots) also show linear variation of heat transfer coefficient with vapor quality . Usually in low heat flux-two phase flow , heat transfer coefficient increasese linearly in the subcooled region then it becomes constant in the saturated boiling region as was described in section 5.3.3. However, figures 8.44 to 8.48 show the heat transfer coefficient increasing almost linearly with the vapor quality . In the present ivestigation the highest quality was achieved was only 2%, which is due to the limited heater capacity of the system. As the LiBr concentration increases, it makes the solution more difficult to boil . In fact the exit quality of the high concentration solution was only .035%. The observed linear variation of the heat transfer coefficient thus concides with that expected from subcooled or low quality boiling. It is further observed in figure 8.44 to 8.48 that as the LiBr concentration increases, the fluctuations in the heat transfer coefficient diminishes for almost the same heat flux. This is due the increase of vigour of boiling as the concentration is lowered.

8.4 HEAT TRANSFER COEFFICIENT CORRELATION

In addition to what was discribed in the previous section about the linearity of heat transfer

coefficient, h with vapor quality x , the rate of change of heat transfer coefficient with respect to quality (dh/dx) changes from one concentration to another. Therefore , a good two-phase boiling correlation should include both the vapor quality x and the concentration X in it. One of the correlations which is widely used in correlating binary mixture boiling data is equation (5.34) which can be restated here,.

$$h_b/h_c=C1(1/xtt)^{C2} \qquad (8.8)$$

Attempt was made to obtain similar correlation in this study from the experimentally determined data by keeping in mind that the present investigation incorporates two-phase components flow.

8.4.1 Determining the Constants C1 and C2

In order to determine the constants C1 and C2 in the above equation, the convective heat transfer coefficient h_c was calculated for each concentration assuming superficial liquid flow. It means that the calculation of Reynolds number and velocity was based on the liquid component only . Equation (8.6) was used for such calculation. Calculation of the boiling heat transfer coefficient is now carried as was earlier mentioned in section 5.5.3. The experimental data were

next used to calculate ln(h/hc) and ln(1/Xtt) for each concentration and the result plotted in figure 8.49, which shows an almost linear relation between the two variables . Similar plots also made for other concentrations . By the method of the lest square fit , the follwing equations were obtained for each individual concentration,

1. $h/hc=29.25\ (1/Xtt)^{.2048}$ X=10% (8.11)
2. $h/hc=29.42\ (1/Xtt)^{.4333}$ X=20% (8.12)
3. $h/hc=20.77\ (1/Xtt)^{.2595}$ X=35% (8.13)
4. $h/hc=25.02\ (1/Xtt)^{.3229}$ X=40% (8.14)
5. $h/hc=26.09\ (1/Xtt)^{.3692}$ X=50% (8.15)

In order to see the variation of h_{exp}/hc with Lockhart-Martinlli parameter, Figure 8.50 was ploted .h_{exp} is the measured boiling coefficient while hc and Xtt were calculated by equation (8.10) and (8.6) respectively .

Since the constants C1 ands C2 in equation (8.11) to (8.15) are dependent on concentration , they were plotted against concentration X and were fitted with third order polynomials. The resulting equations are ,

$$C1=24.922+46.175\ (X/50) - 126.699(X/50)^2 +82.036(X/50)^3 \qquad (8.16)$$

$$C2=-.48568+5.07046(X/50) - 8.9137(X/50)^2 + 4.70605(X/50)^3$$

for $10 \leq X \leq 50$

(8.17)

It is know possible to use equation (8.8) alone for all concentration range from 10% to 50% with equation (8.16) and (8.17).

To test the result correlation , the experimental heat transfer coefficient ratio h_{exp}/h_c was plotted against the calculated heat transfer coefficient ratio h_{cal}/h_c in figure 8.51 . The percentage of error between the two was found to be withen ± 12 % .

In figure 8.52 the calculated heat transfer coefficient was plotted against concentration starting from 10% to 50 % Libr by wt, for vapor quality of 0.5 and 1% . Data points which were within 90% of the given quality are shown in the same figure .They are in good agreement with the calculated curves . It can further be observed that the boiling heat transfer coefficient decreases as concentration increases. This agrees with other experiment results in binary system reported in references [23 , 24] and others . Some detailed sample calculations are given in appendex B.

8.5 SOURCE OF ERROR AND ERROR ANALYSIS

It is rather a challenging task to make a single error analysis in this invistigation because the experiment and the analysis depend on many factors for which the individual errors are not clearly known . A list of the sources of error that caused different magnitudes of error in the experimental data are below .

1- Data acquisition computer cards are needed to be calibrated every time a new set of data have to be read because those cards were in transition mode as the computer warmed up .In some instances , cards read more than 4° C higher than the actual reading due to improper resistor in the card. This required the computer to be switched off just after the reading and manual thermometer multiplixer used to read the first and the last thermocouple in each card . The error obtained in this reading were subtracted from the previously collected data. The error in these cards are constant for that individual card and it was found to be in the order of magnitude of 0.8°C.

2- In some instances , the physical properties which are

needed for calculation are beyond the data available in the properties table . So interpolation beyond these data had to be performed. In addition to that , since all the calculations in this invistigation was performed on a computer , physical properties had to be available in the form of equations .Therefore , all the properties were curve fitted with equations using the least square method. To improve the accuracy, a set of functions were used for each concentration, thus minimizing the data points handled by each correlation. The R square coefficients of these equations are within 98 % and are deemed satisfactory. For the thermodynamic properties ,equations which are available in refrences [14] and [43] were used . A list of these equations are given in appendex A.

3- Design simplifications malfunctions and their justifications are given in section 6.10 . The contributionb of such factors to the overall reading error are in the range of 0.1° C, as discussed before.

To detirmine the uncertainity in the data, Kaline and McClintock [52] method was used as follows.

1. The power input to the test section q= I E

where,

I= current, A ± 2%

E= voltage, V ± 1%

The percentage uncertainity in the heat added (W_q/q) can be calculated as,

$$\frac{W_q}{q} = \left[\left(\frac{W_V}{E}\right)^2 + \left(\frac{W_I}{I}\right)^2 \right]^{\frac{1}{2}} * 100$$

$$= [(.01)^2 + (.02)^2]^{\frac{1}{2}} *100 = 2.23 \%$$

2. The heat transfer coefficient $h = q/ A_S \Delta T$

where,

q= heat added, W ± 2.23 %

A_S = surface area, m^2

ΔT= (Ts-Tm)= temperature difference, °C ± .75 %

The percentage uncertainity in calculating the heat transfer coefficient (W_h / h) can be found as,

$$\frac{W_h}{h} = \left[\left(\frac{W_q}{q}\right)^2 + \left(\frac{W_{\Delta T}}{\Delta T}\right)^2 \right]^{\frac{1}{2}} *100$$

$$=[(.0223)^2 + (.0075)^2]^{\frac{1}{2}} *100 = 2.35 \%$$

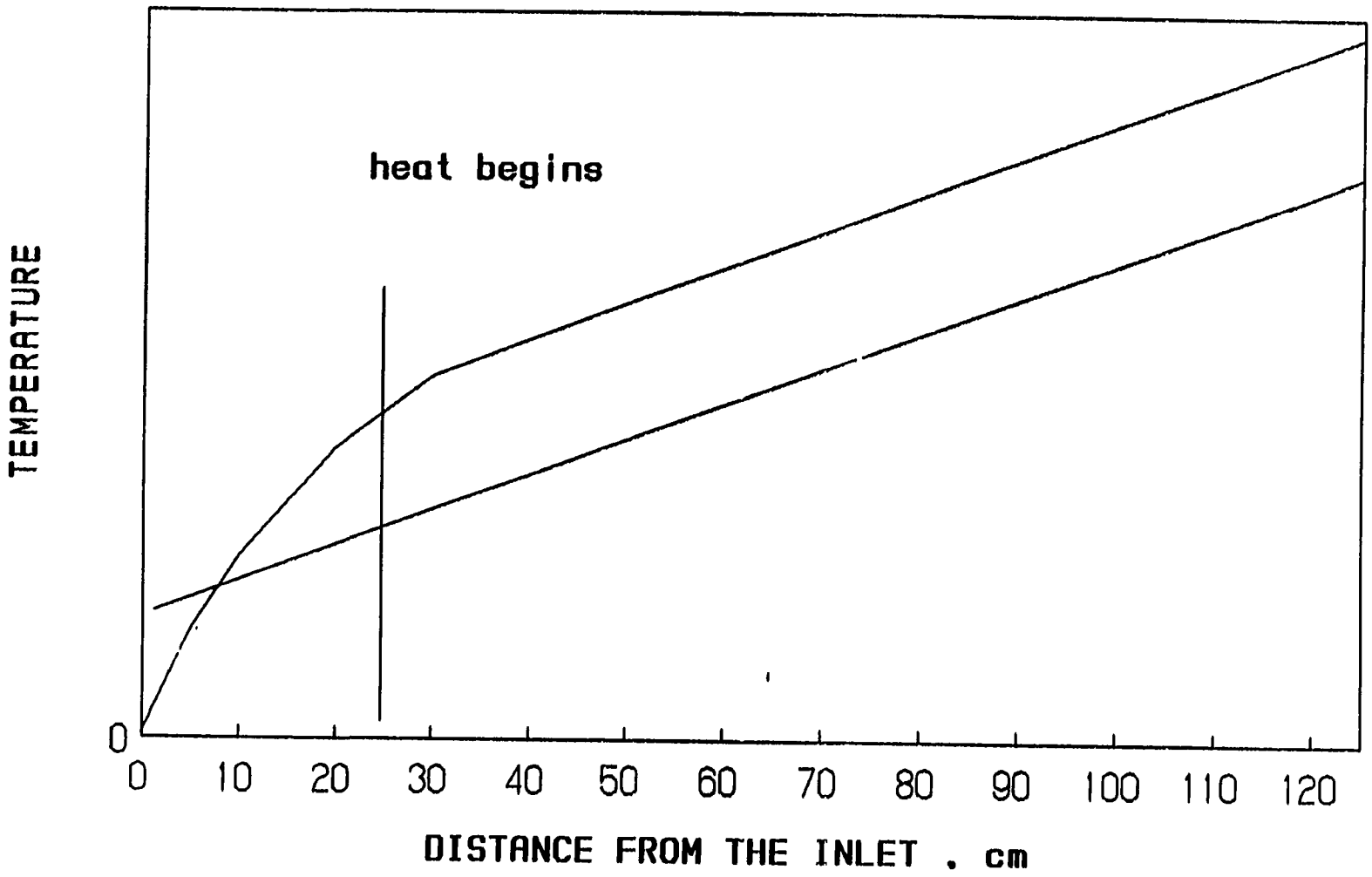

Figure 8.1 Temperature distribution along the tube test section in convection mode.

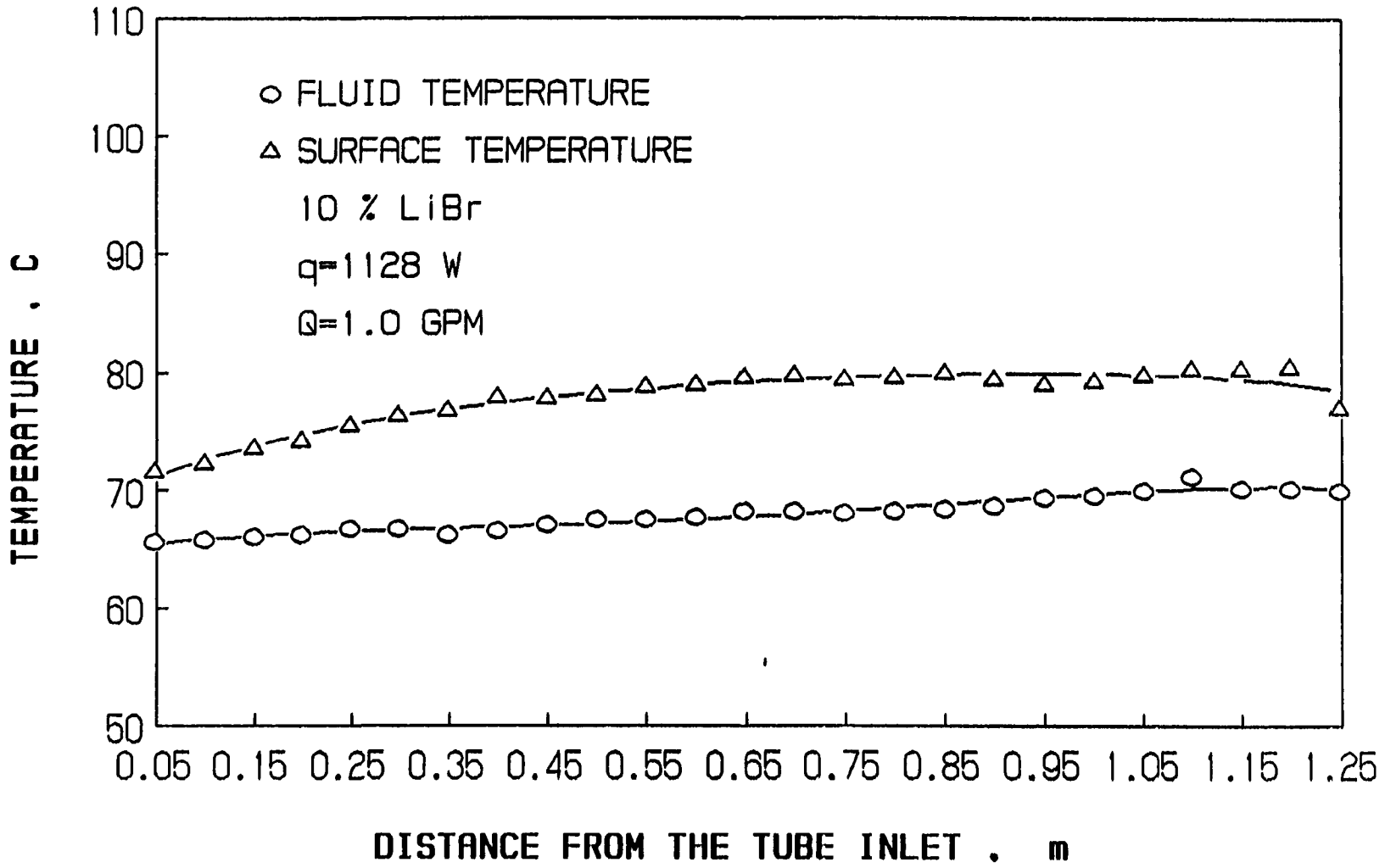

Figure 8.2 Temperature distribution in convection

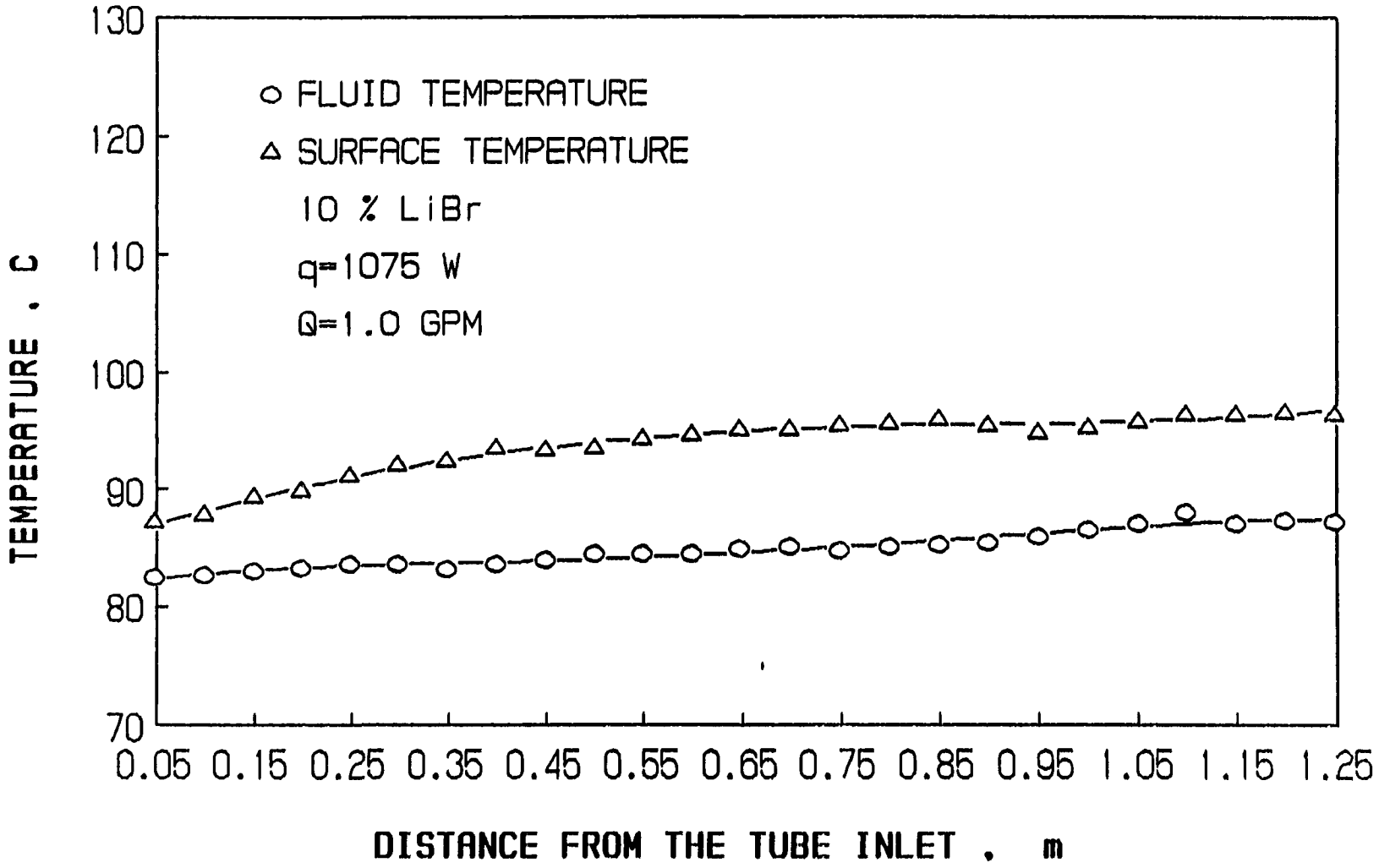

Figure 8.3 Temperature distribution in convection.

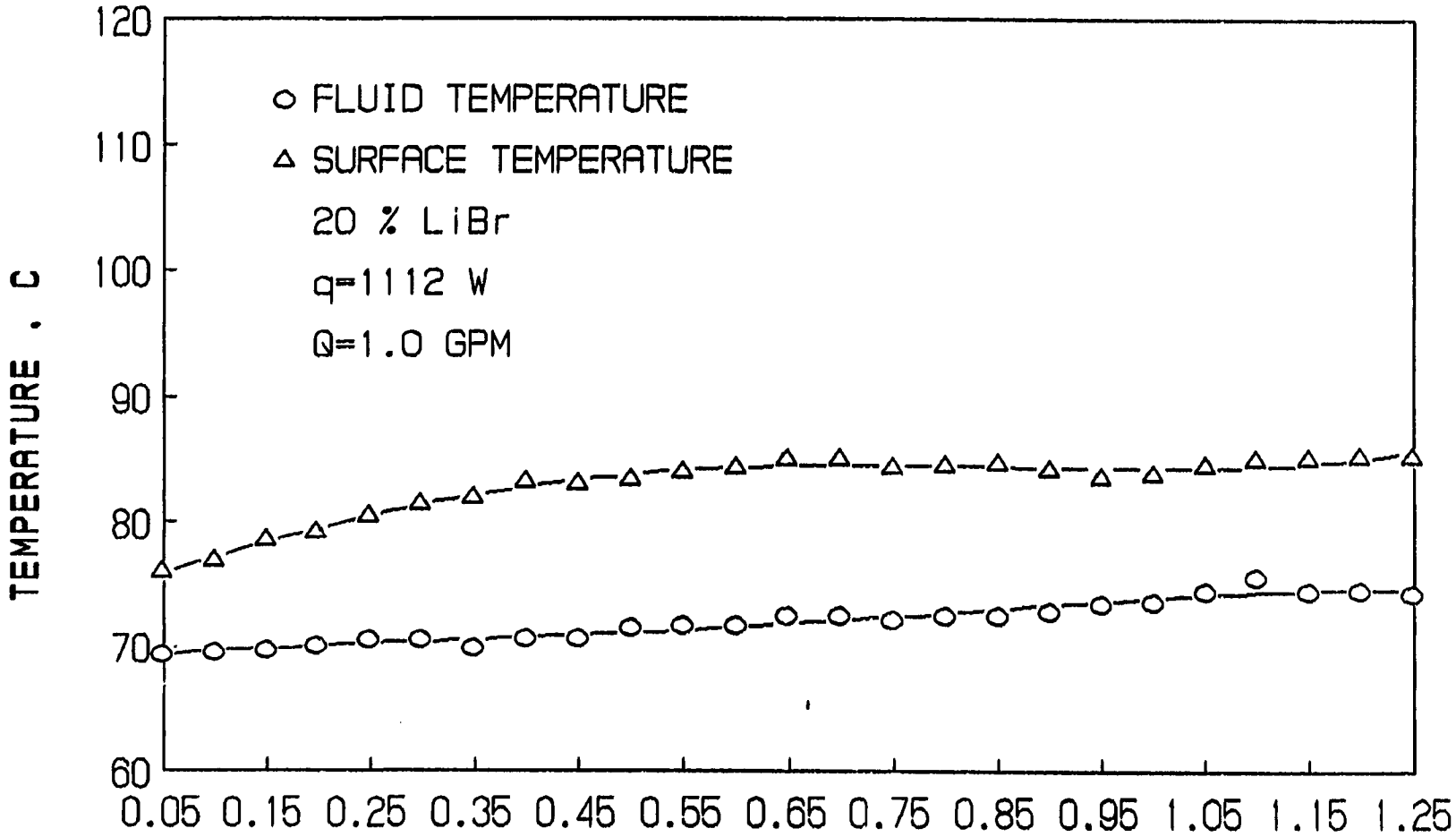

Figure 8.4 Temperature distribution in convection.

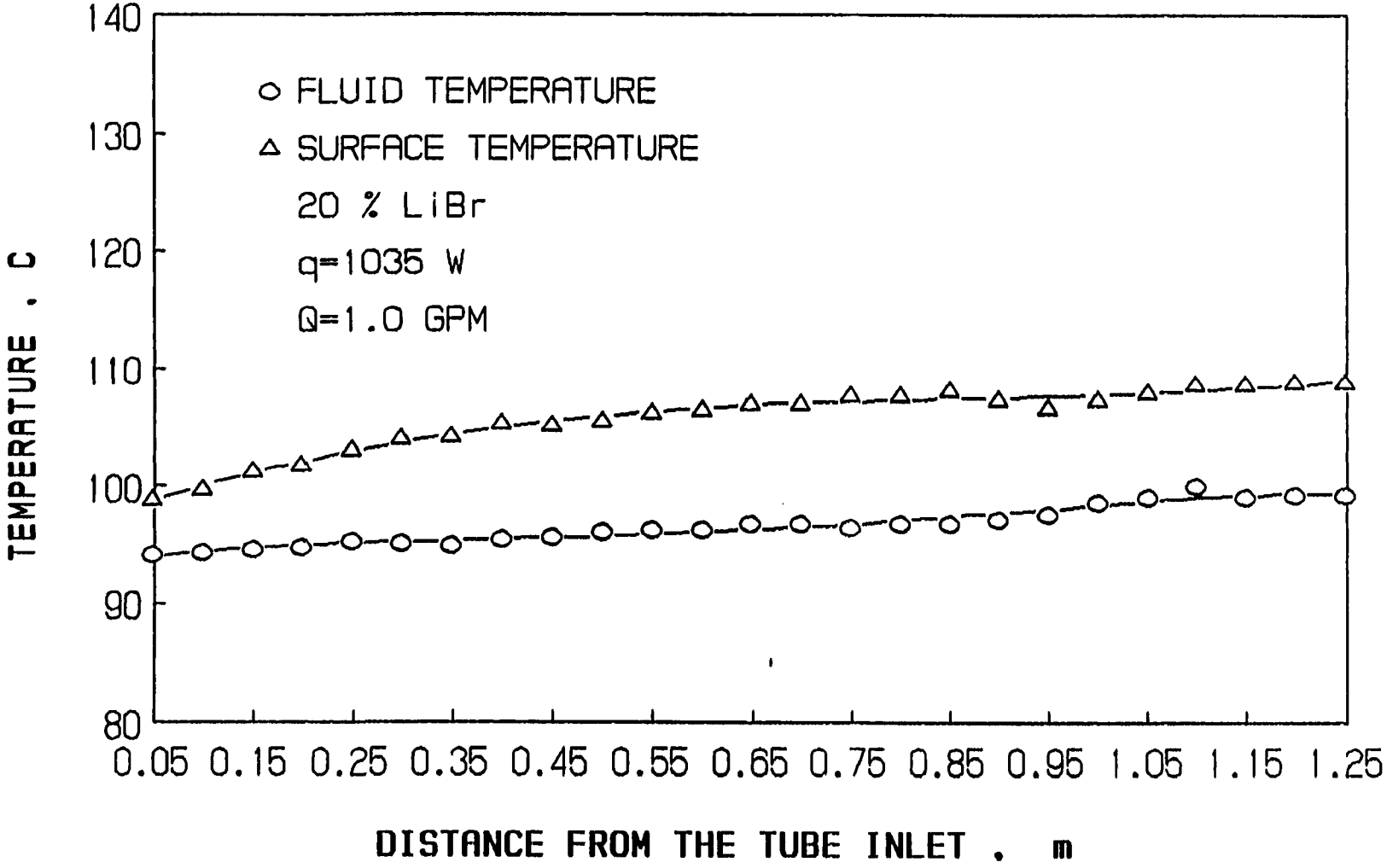

Figure 8.5 Temperature distribution in convection.

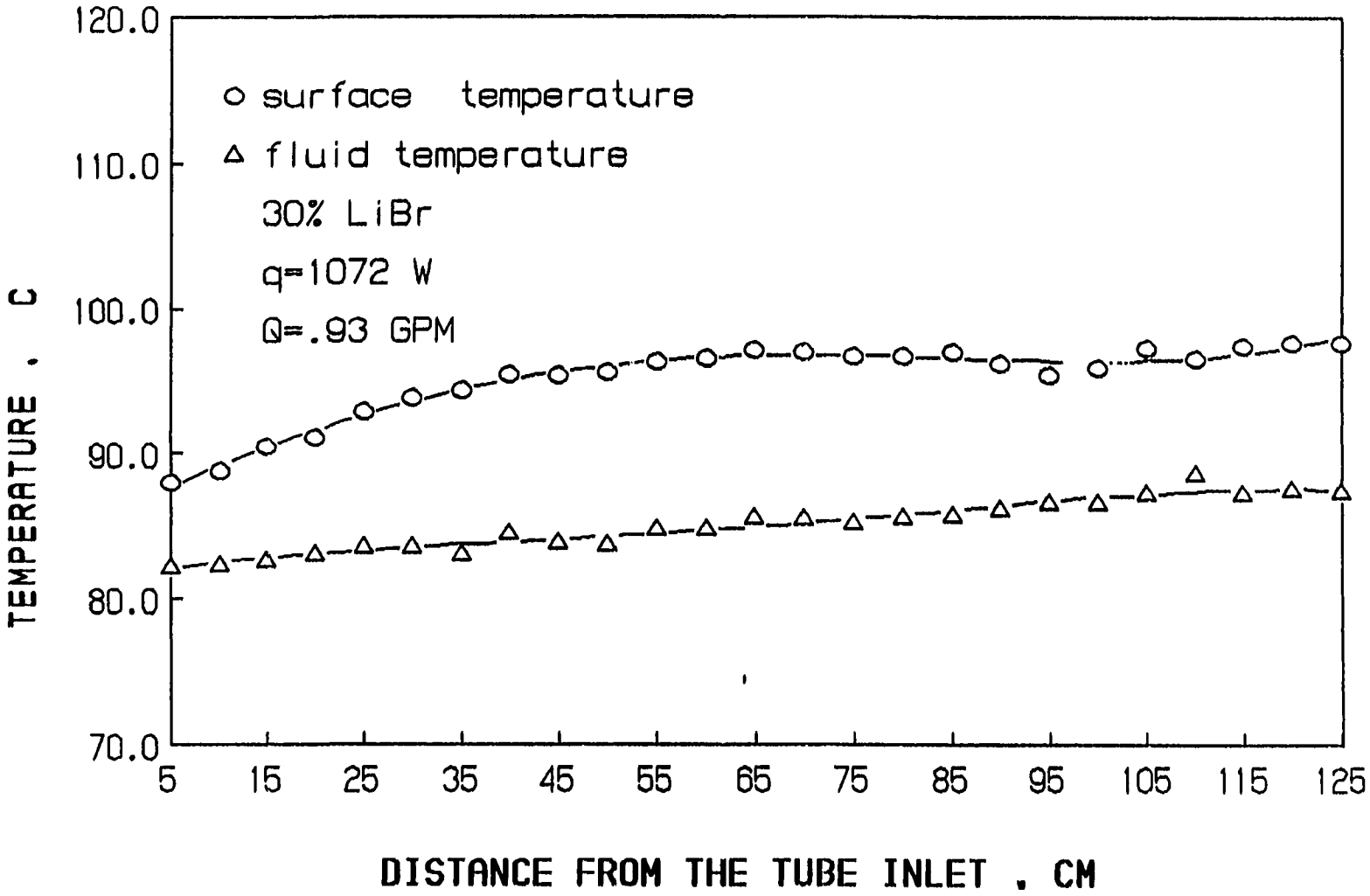

Figure 8.6 Tempwerature distribution in convection.

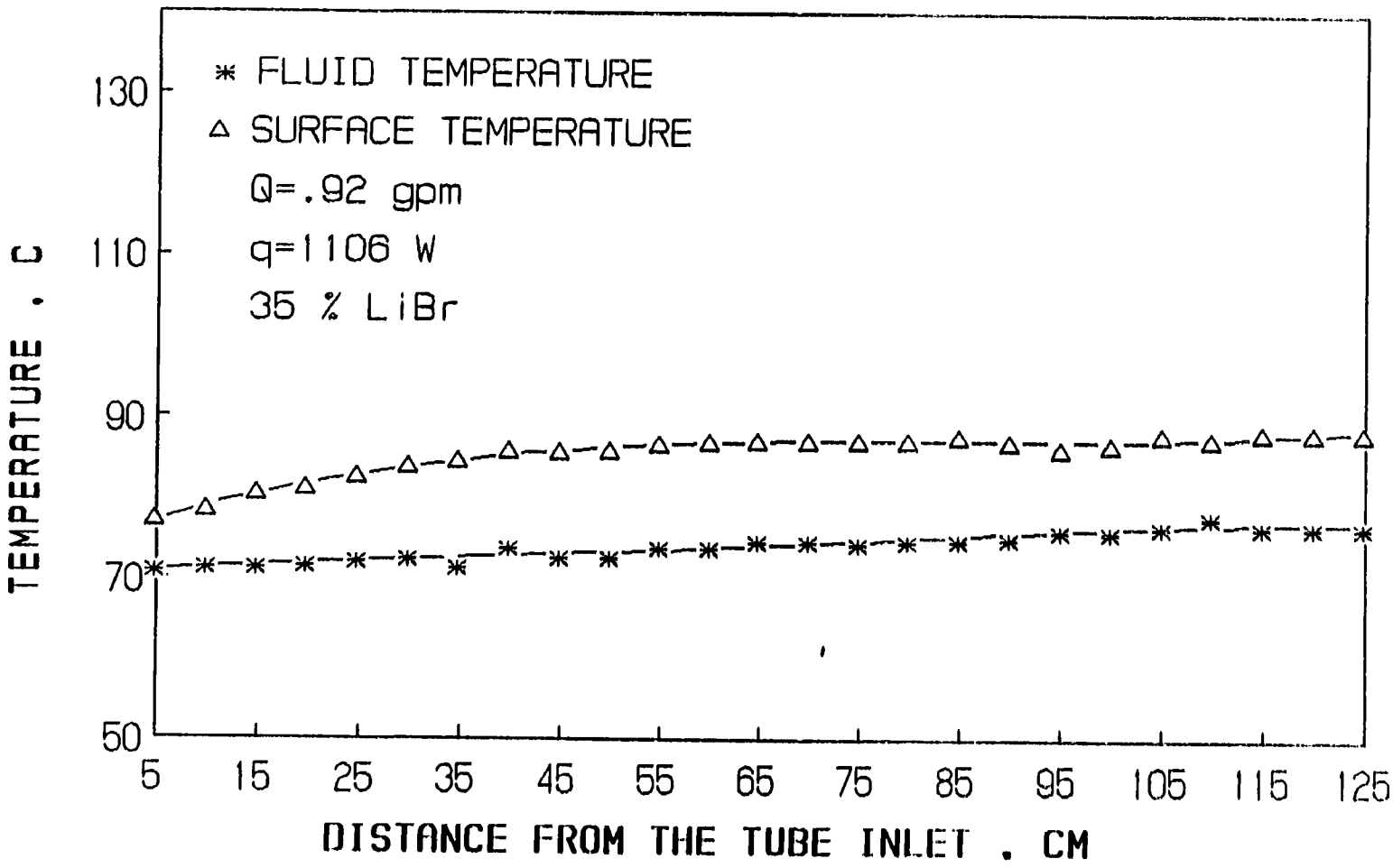

Figure 8.7 Temperature distribution during convection.

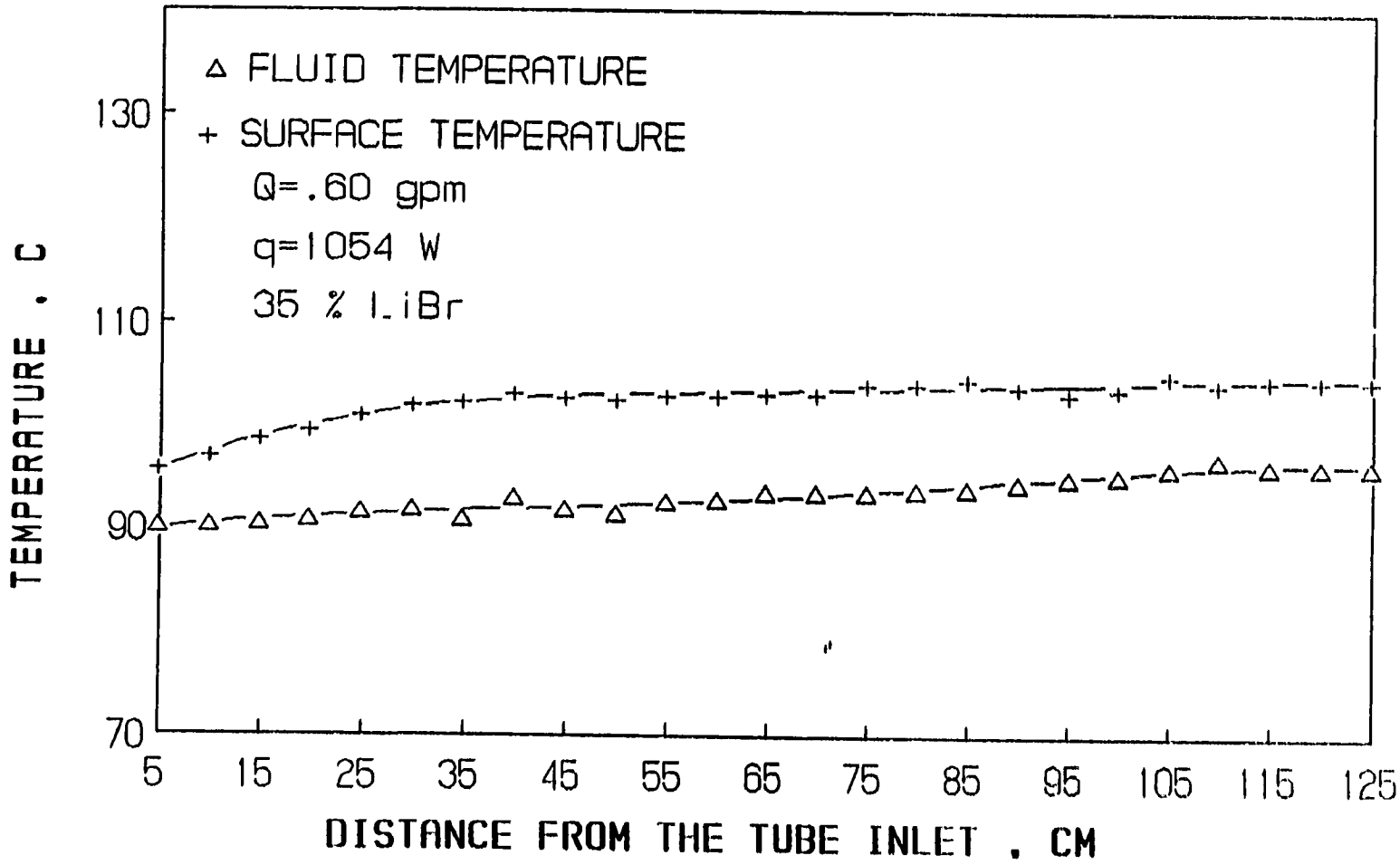

Figure 8.8 Temperature distribution during convection.

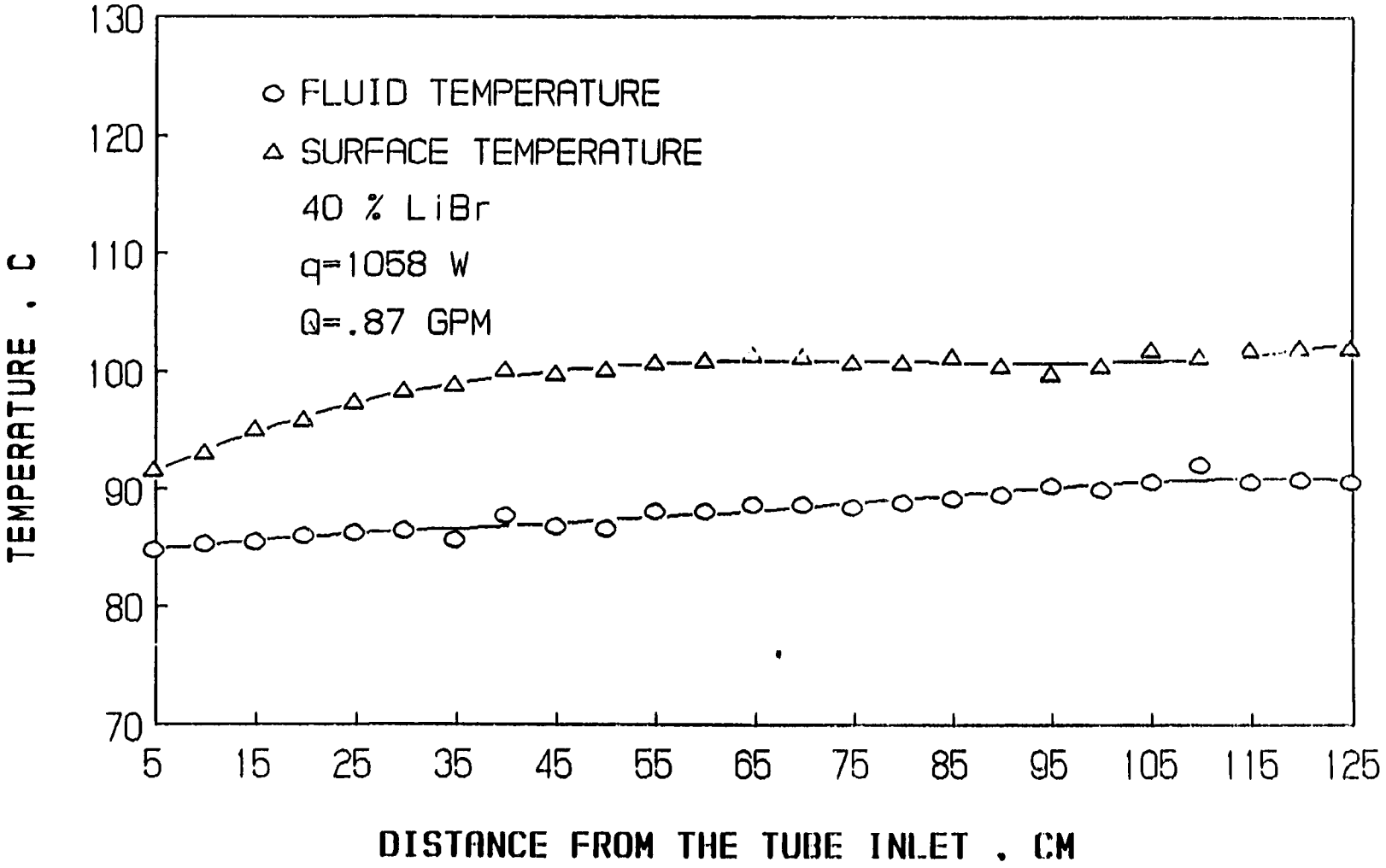

Figure 8.9 Temperature distribution in convection.

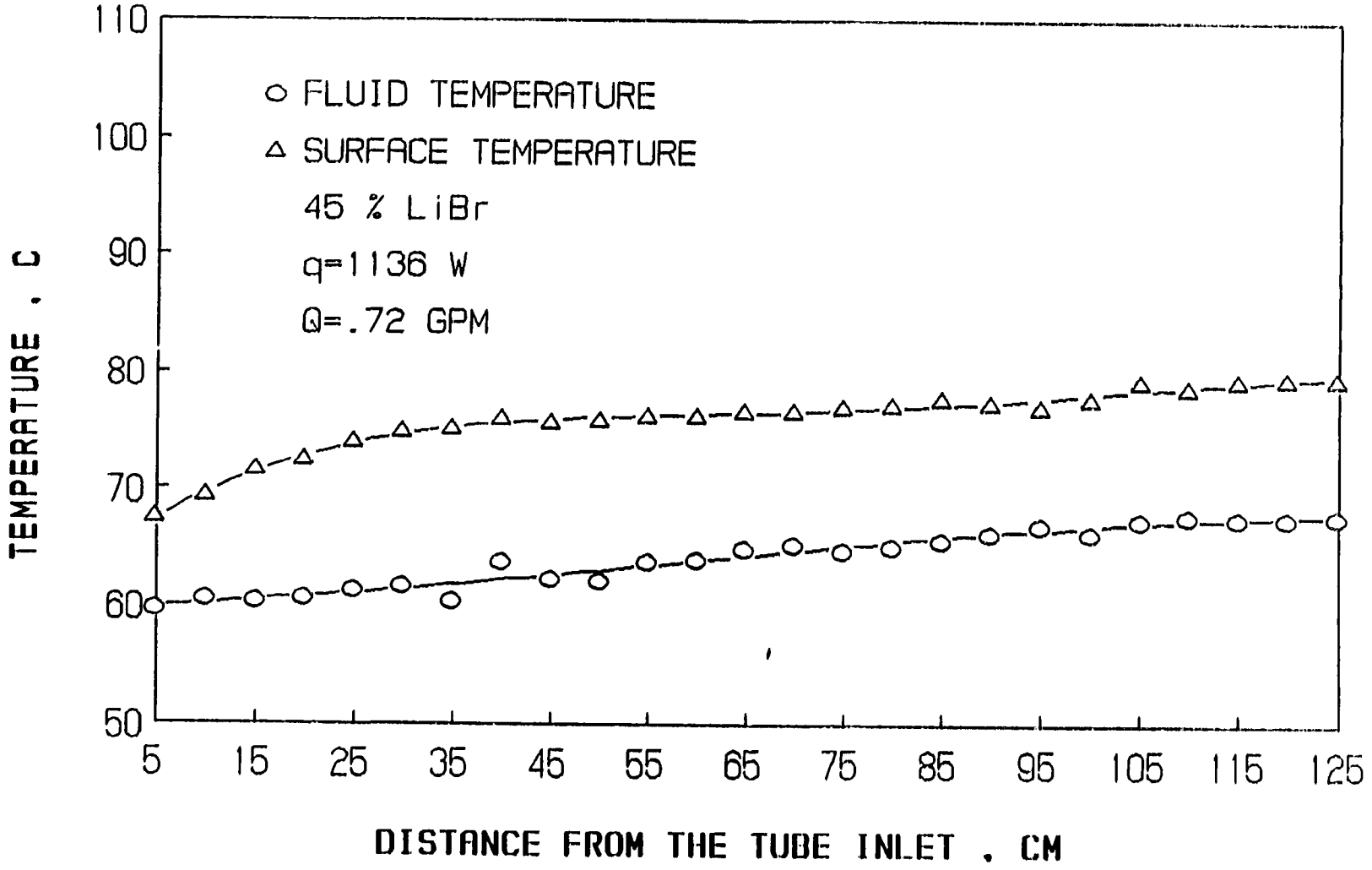

Figure 8.10 Temperature distribution in convection.

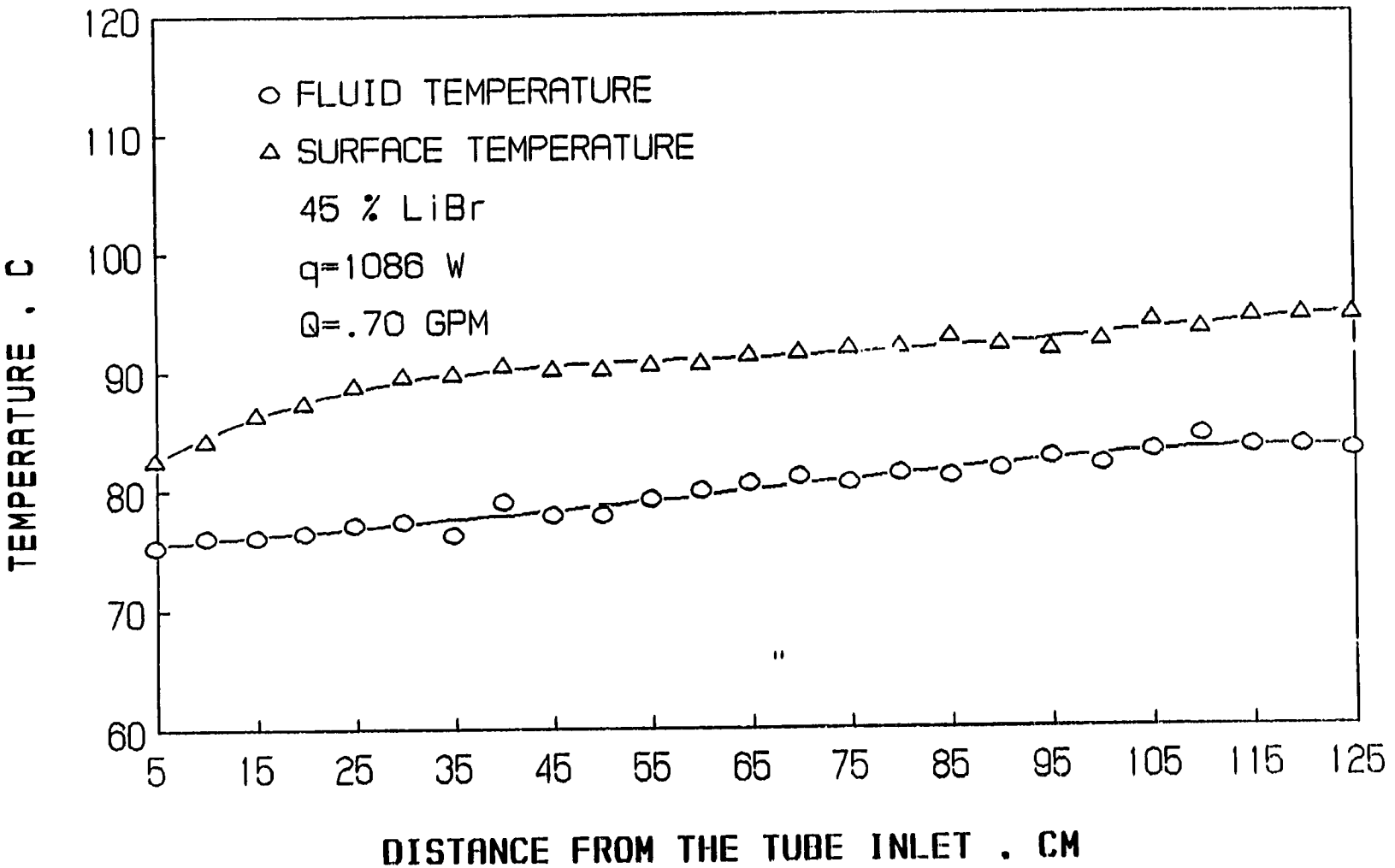

Figure 8.11 Temperature distribution in convection.

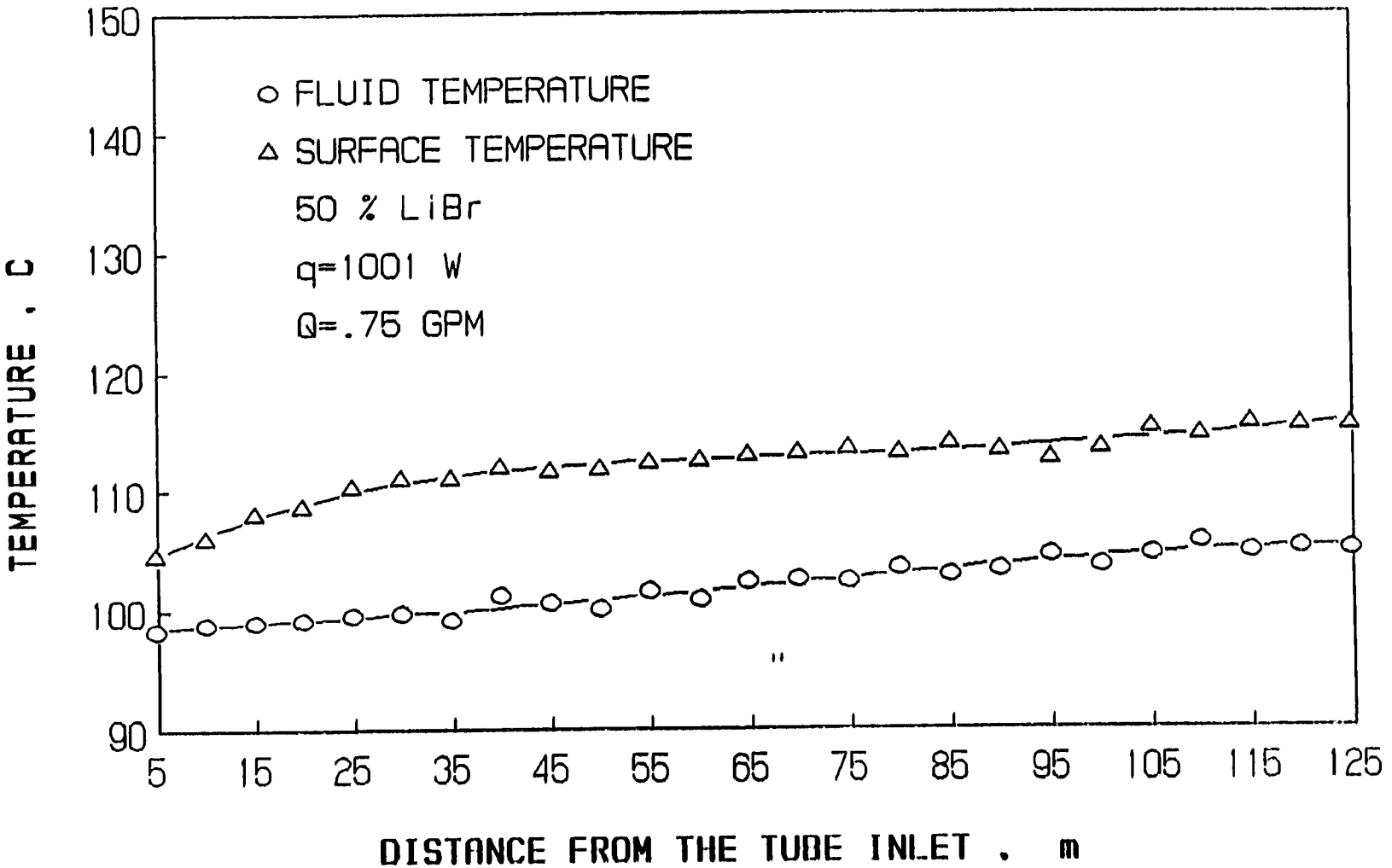

Figure 8.12 Temperature distribution in convection.

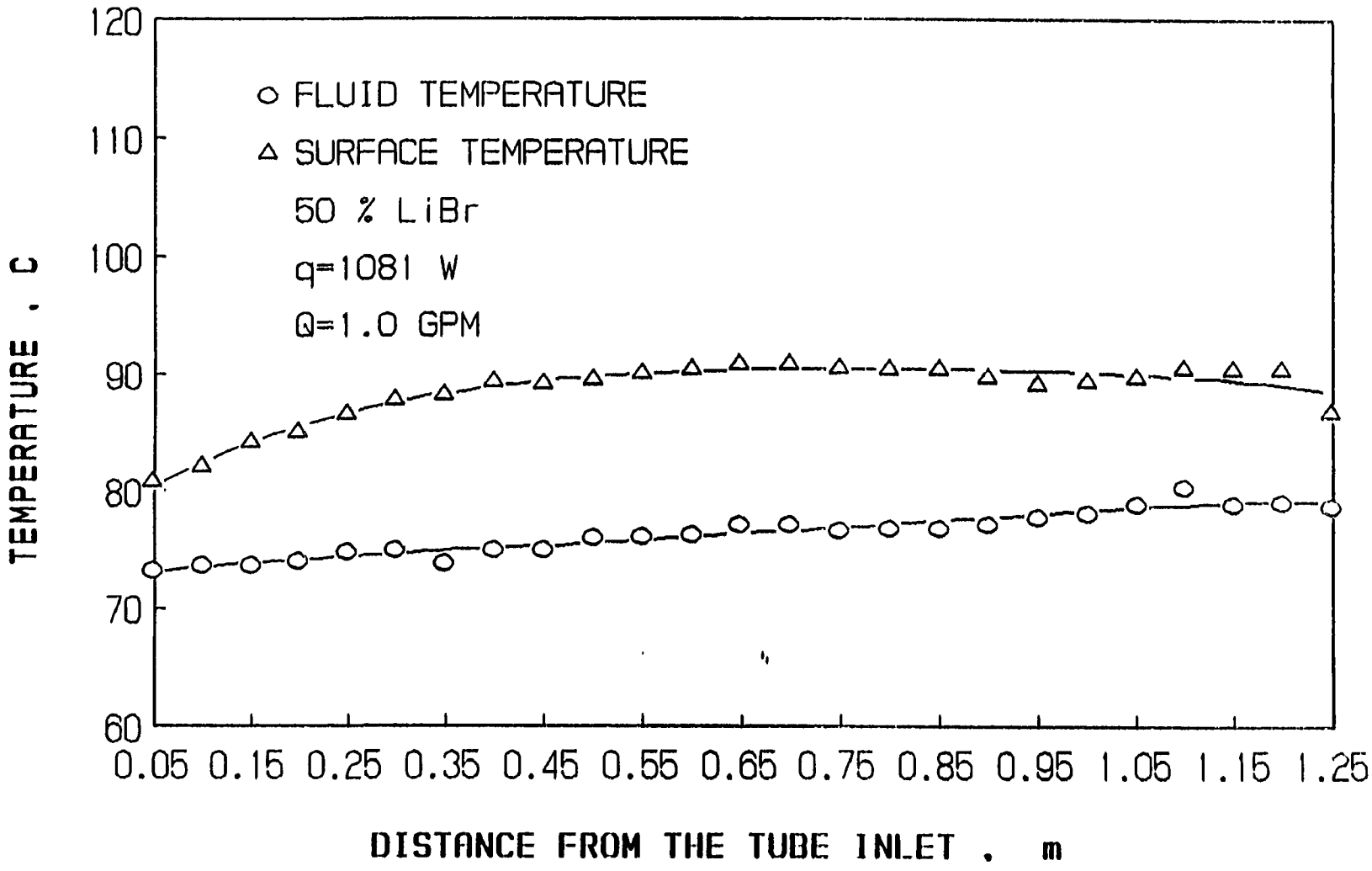

Figure 8.13 Temperature distribution in convection.

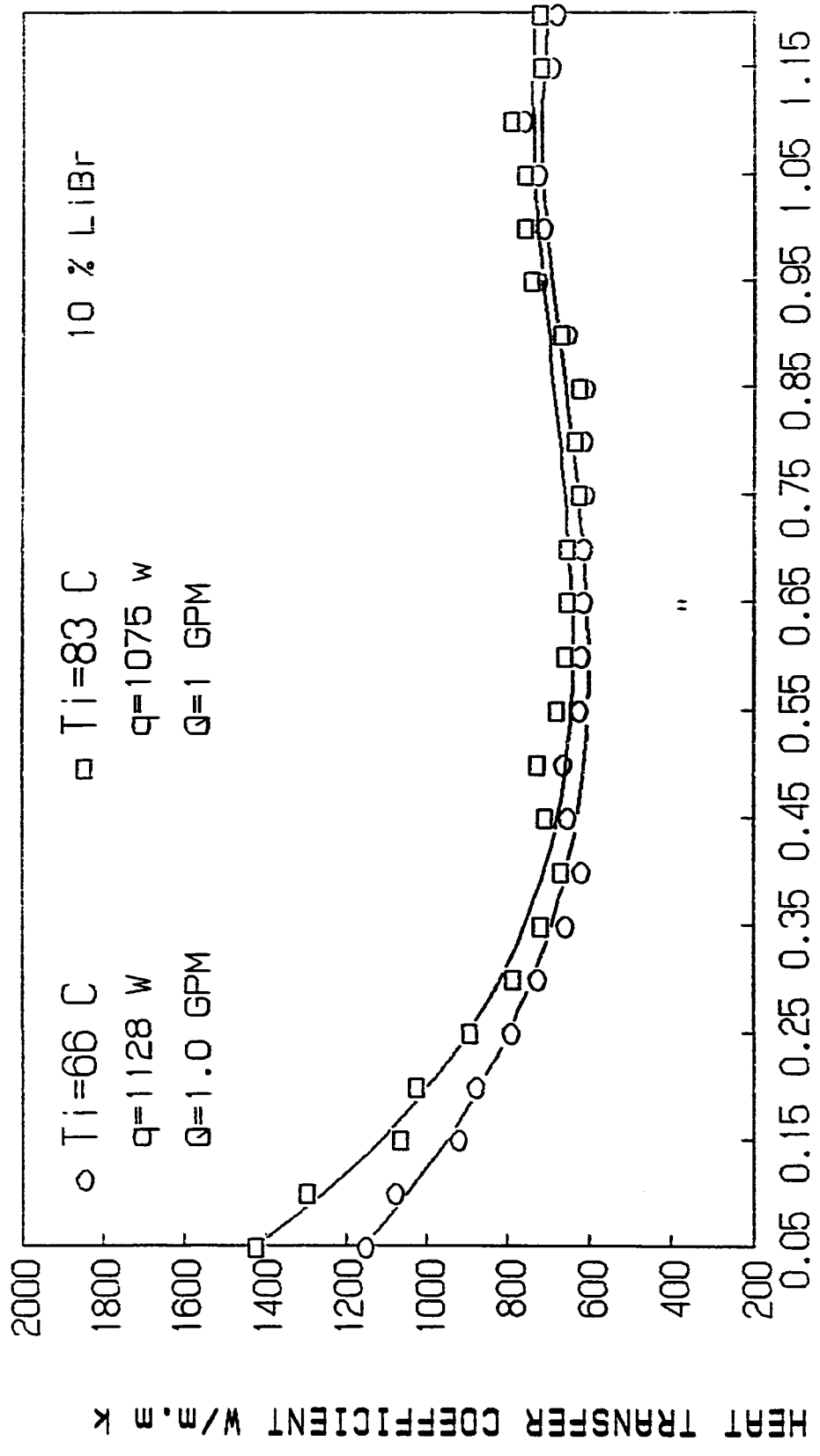

Figure 8.14 Heat transfer coefficient in convection.

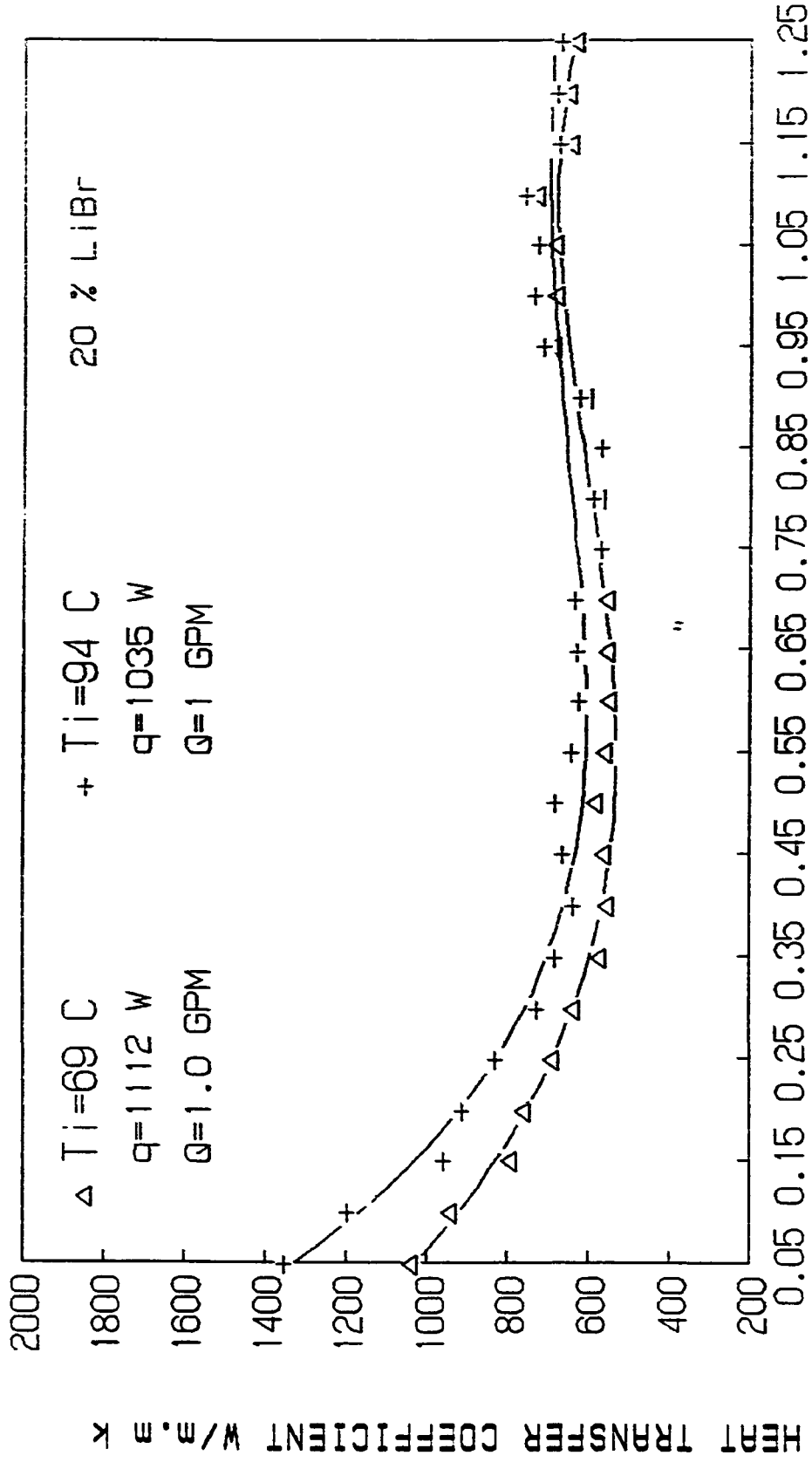

Figure 8.15 Heat transfer coefficient distribution in convection .

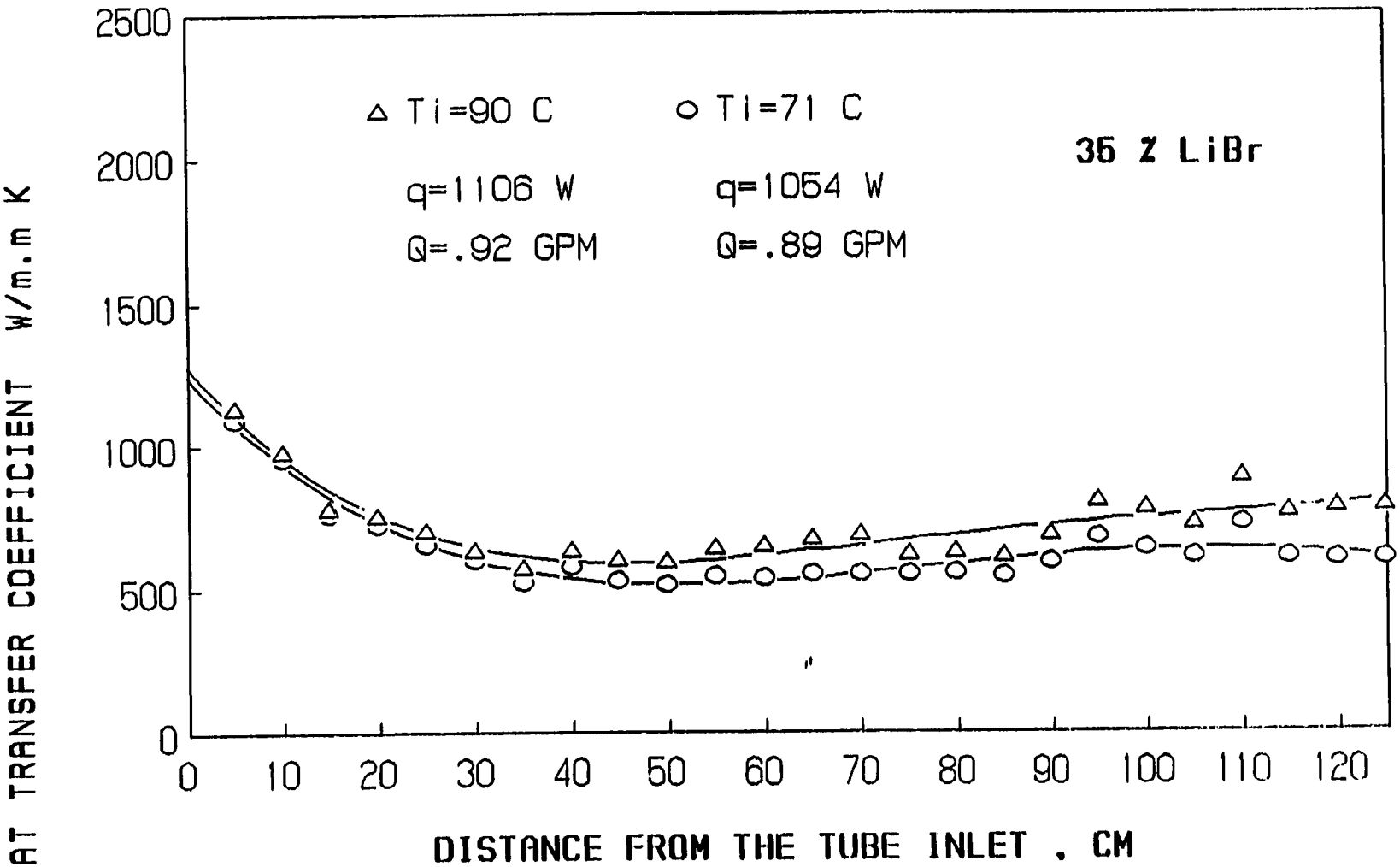

Figure 8.16 Heat transfer coefficient distribution during convection.

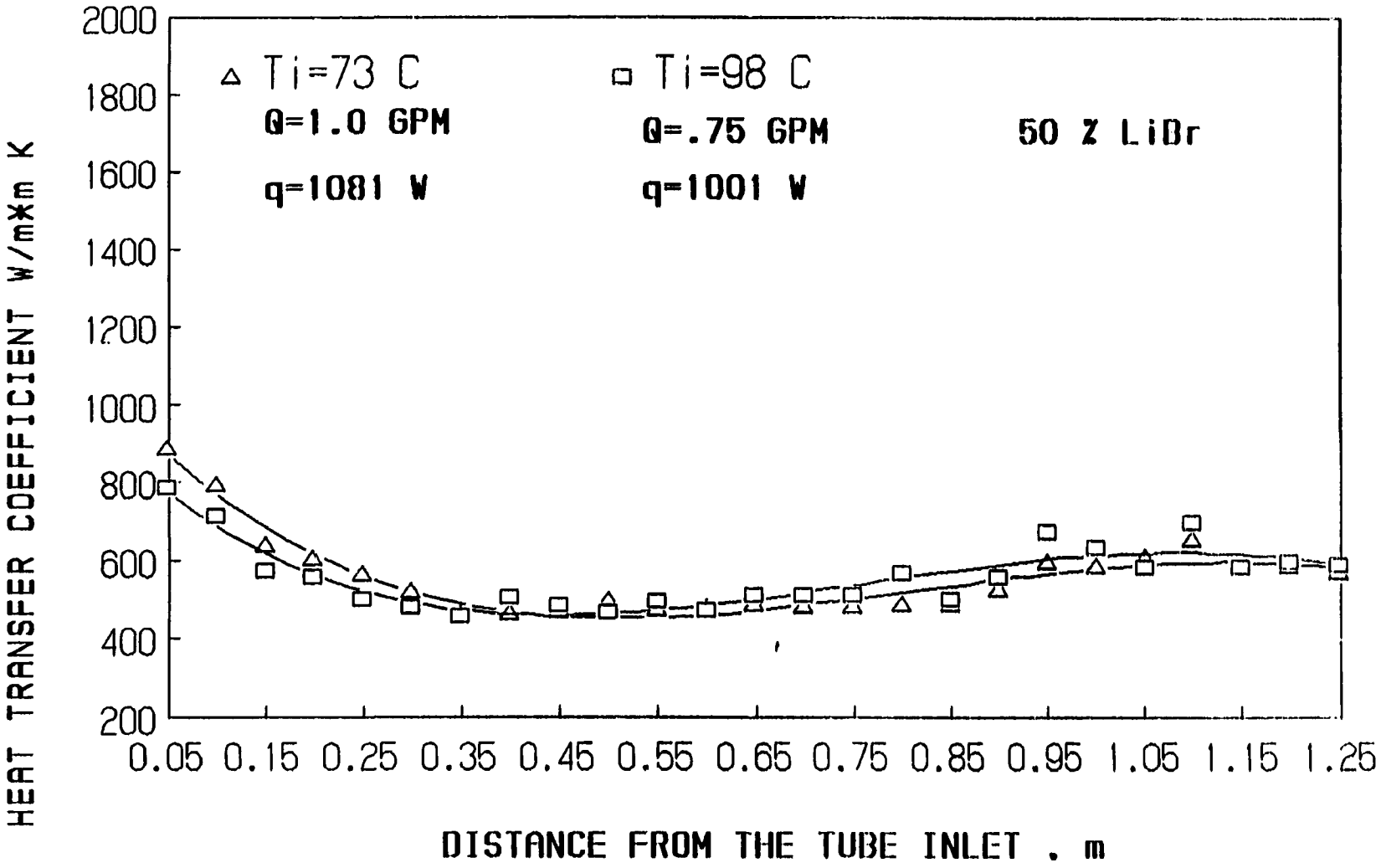

Figure 8.17 Heat transfer coefficient distribution during convection along the tube test section.

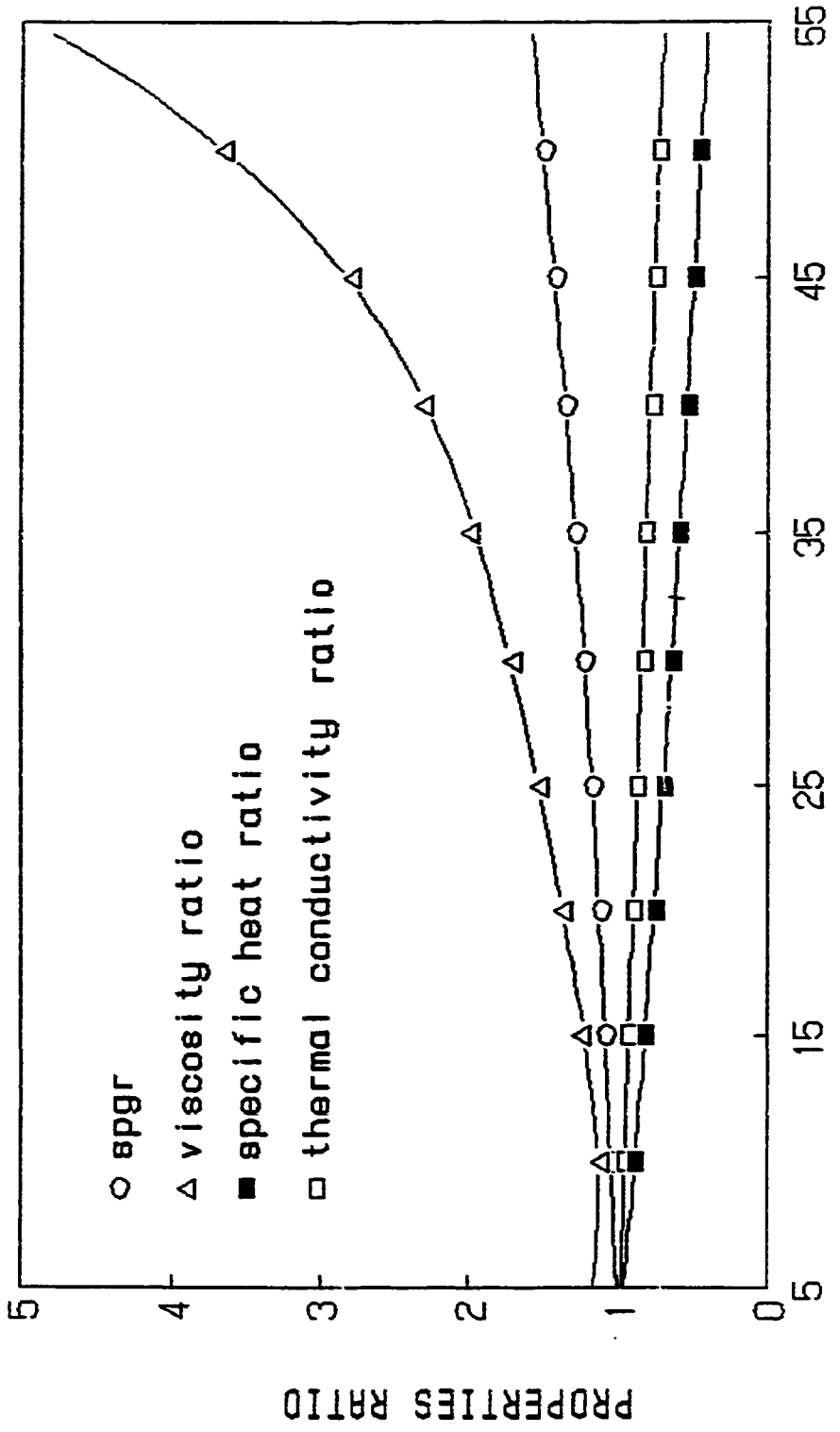

Figure 8.18 Variation of LiBr solution physical properties with concentration.

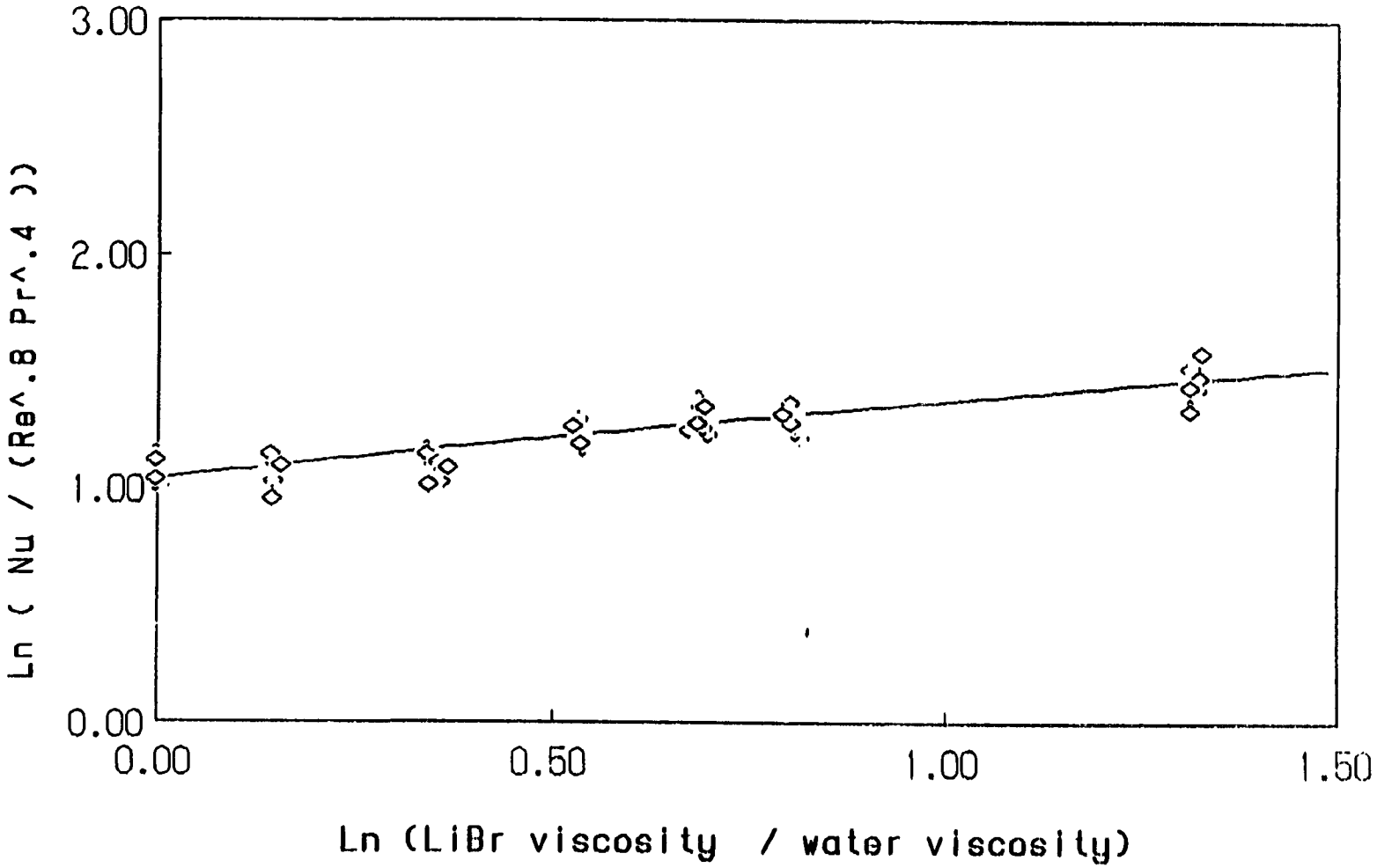

Figure 8.19 Variation of Nusselt number with viscosity ratio for water and LiBr-water solutions data.

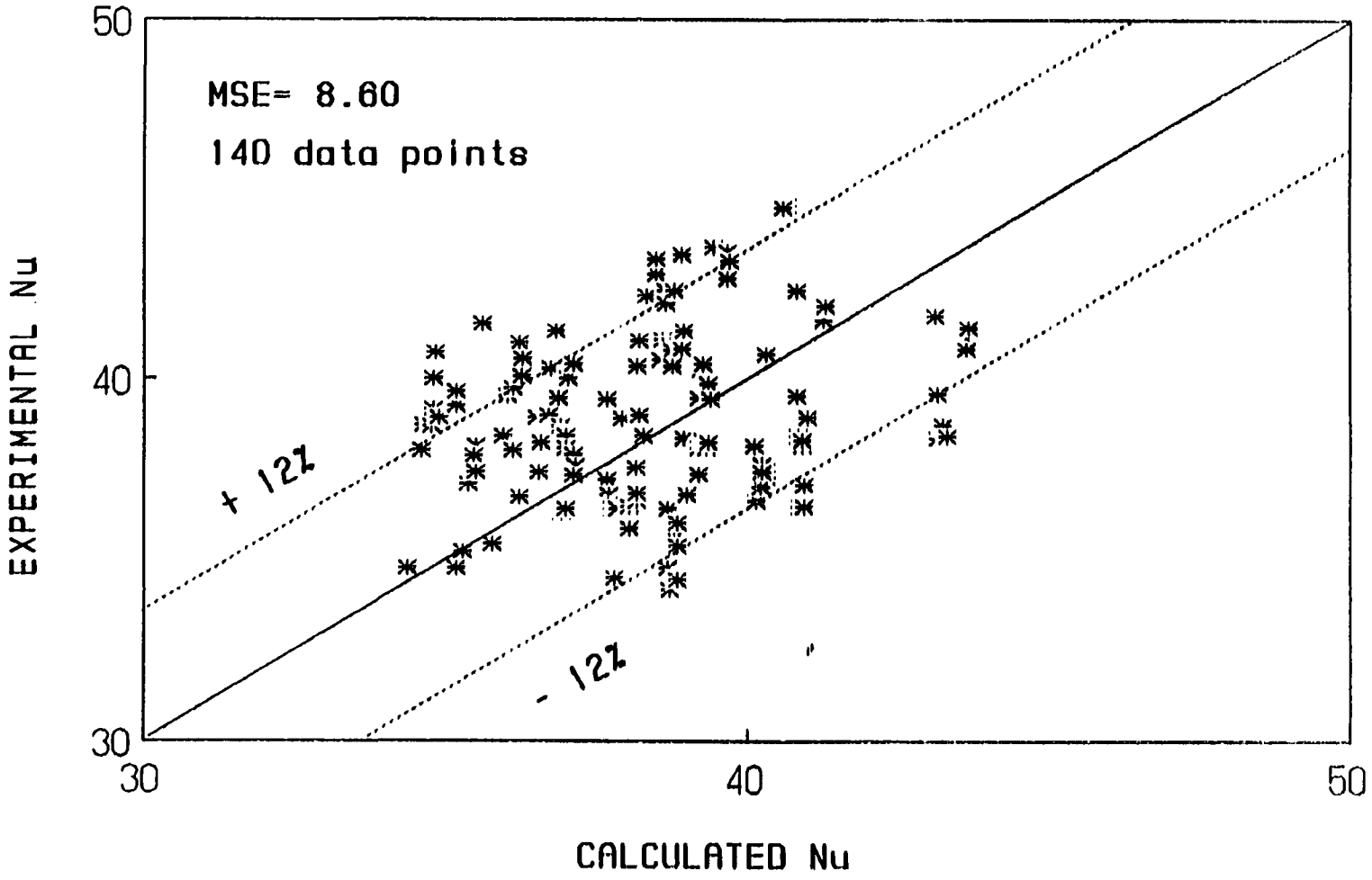

Figure 8.20 Comparison of predected and measured Nu number.

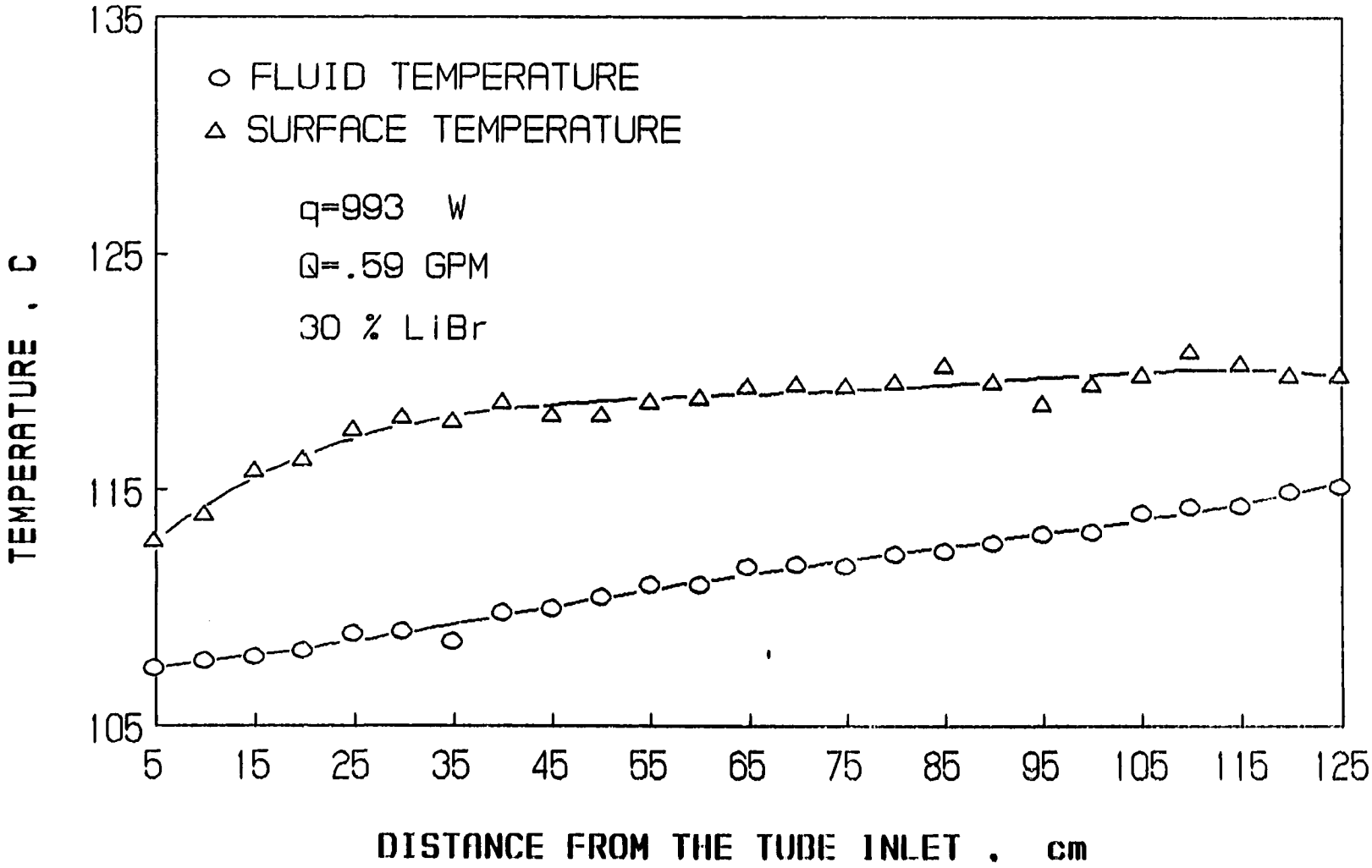

Figure 8.21 Temperature distribution during subcooled boiling.

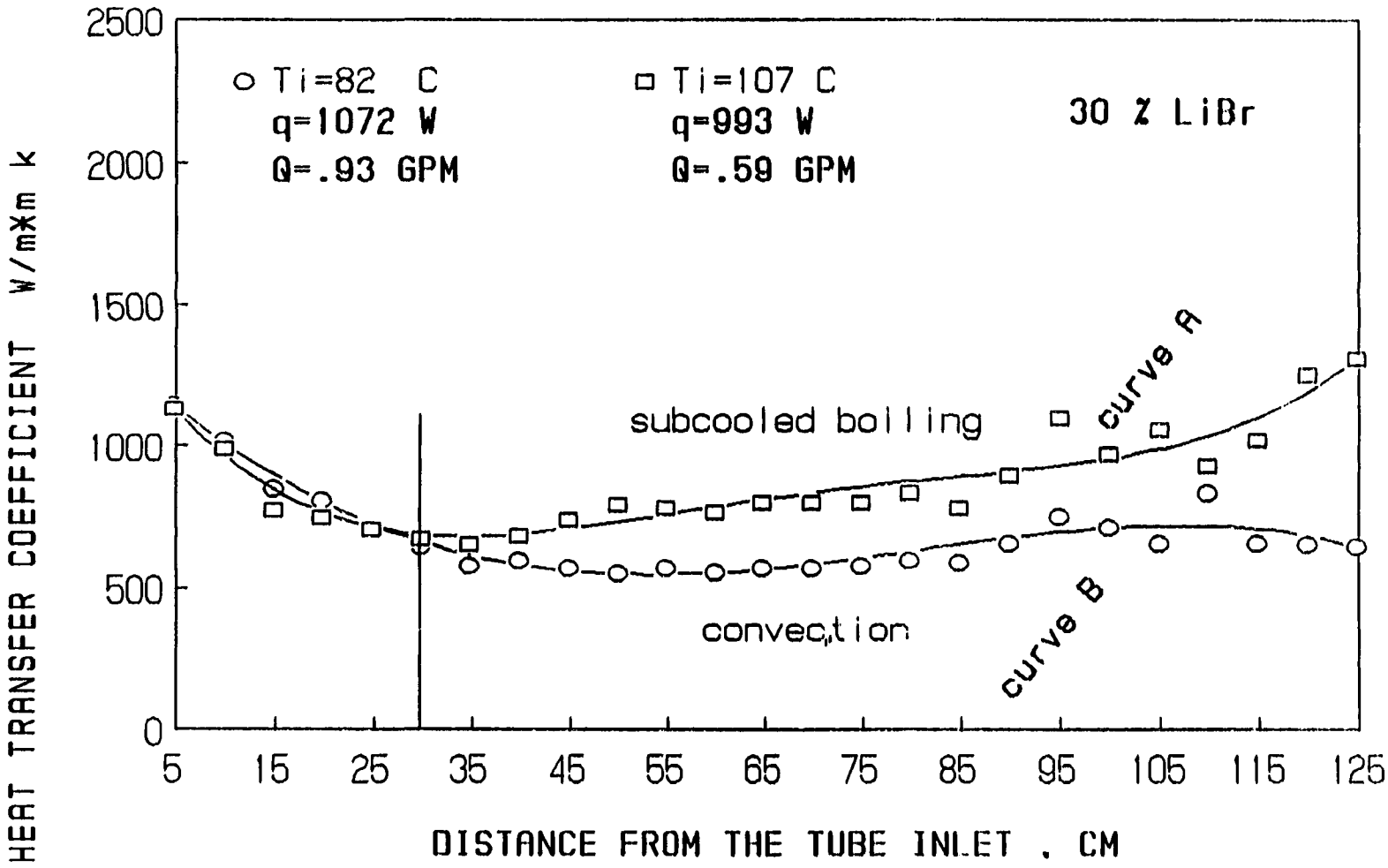

Figure 8.22 Heat transfer coefficient distribution during convection and subcooled boiling along the tube test section .

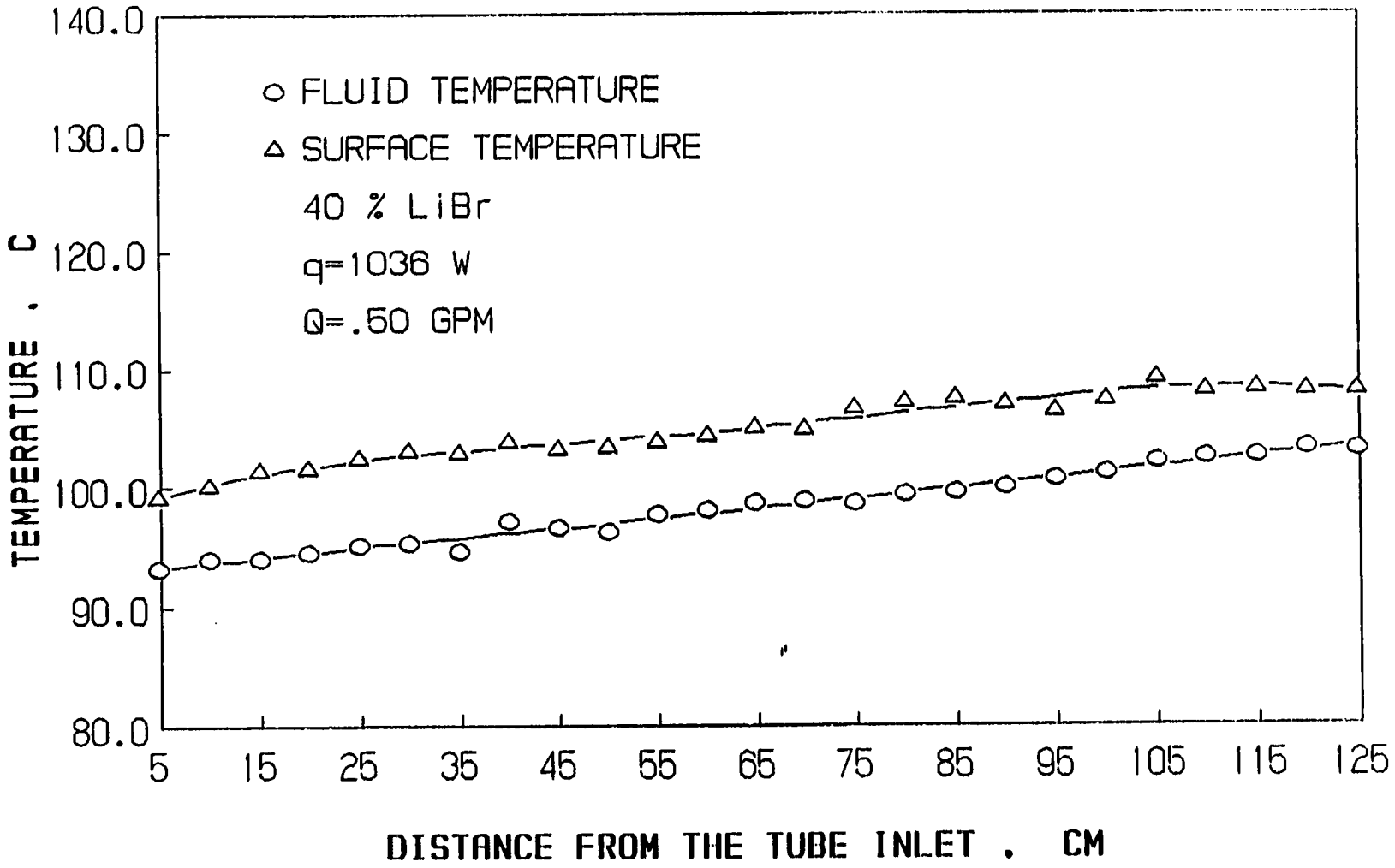

Figure 8.23 Temperature distribution in subcooled boiling in a vertical tube.

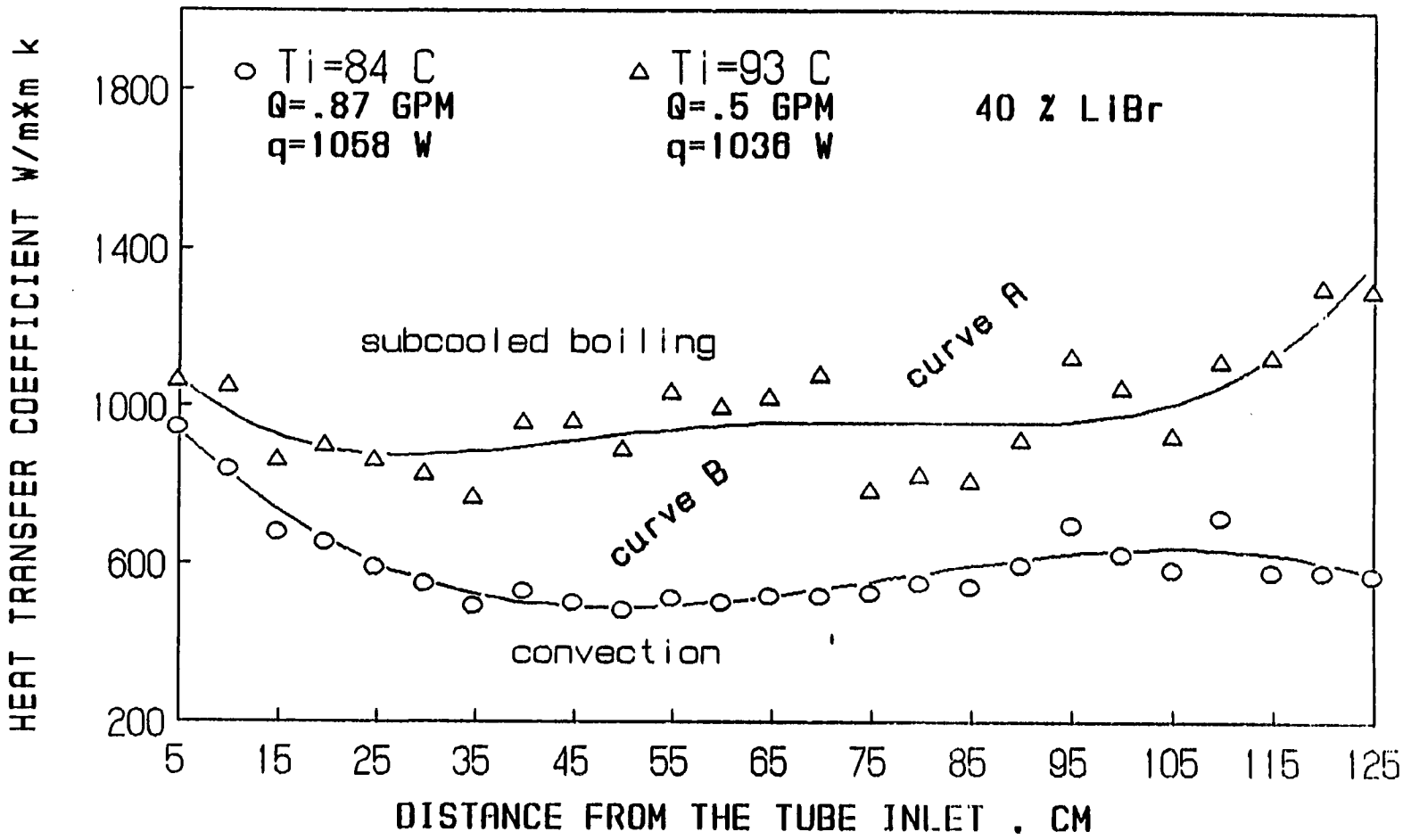

Figure 8.24 Heat transfer coefficient distribution for convection and subcooled boiling along the tube test section .

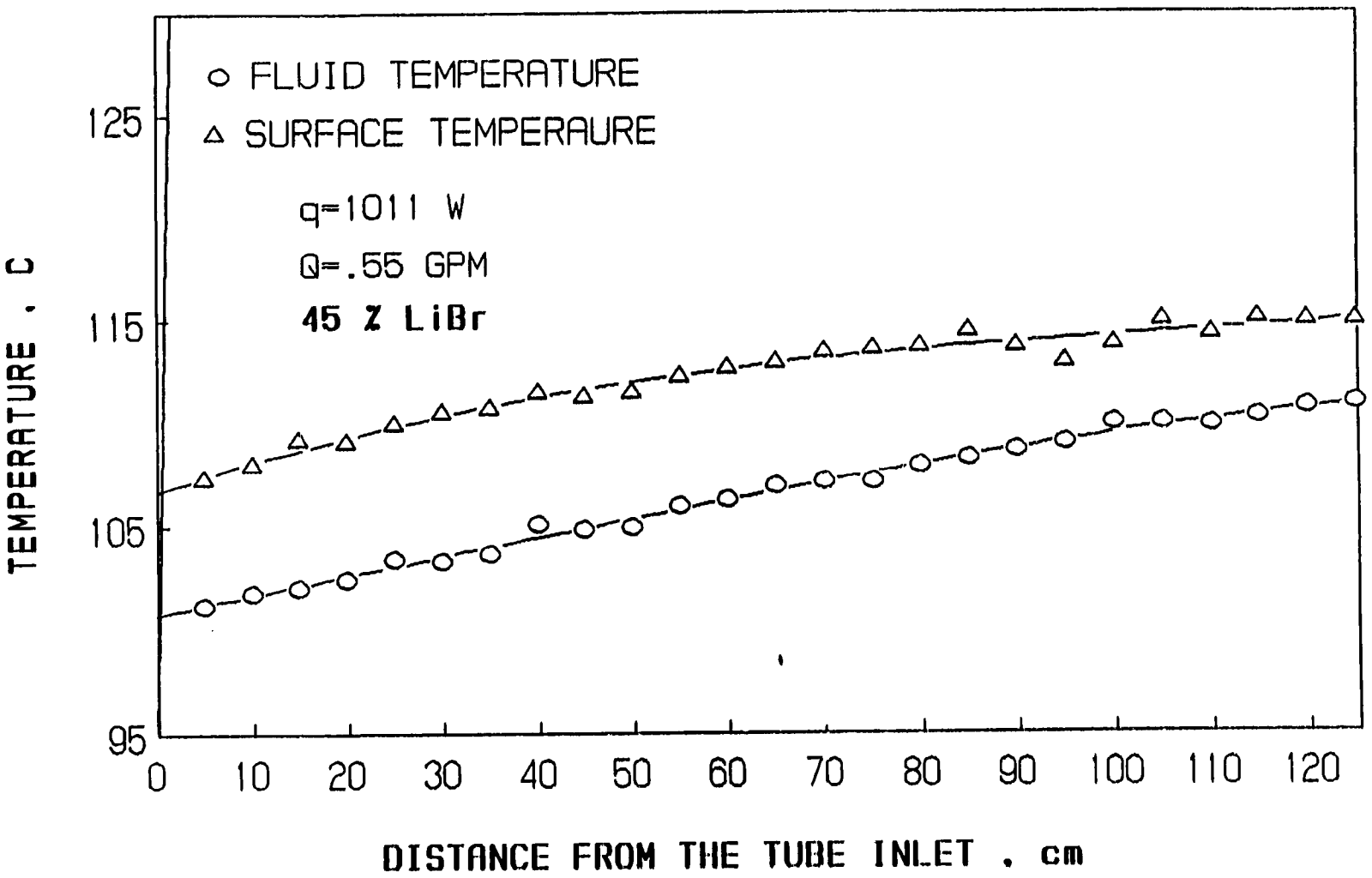

Figure 8.25 Temperature distribution during subcooled boiling.

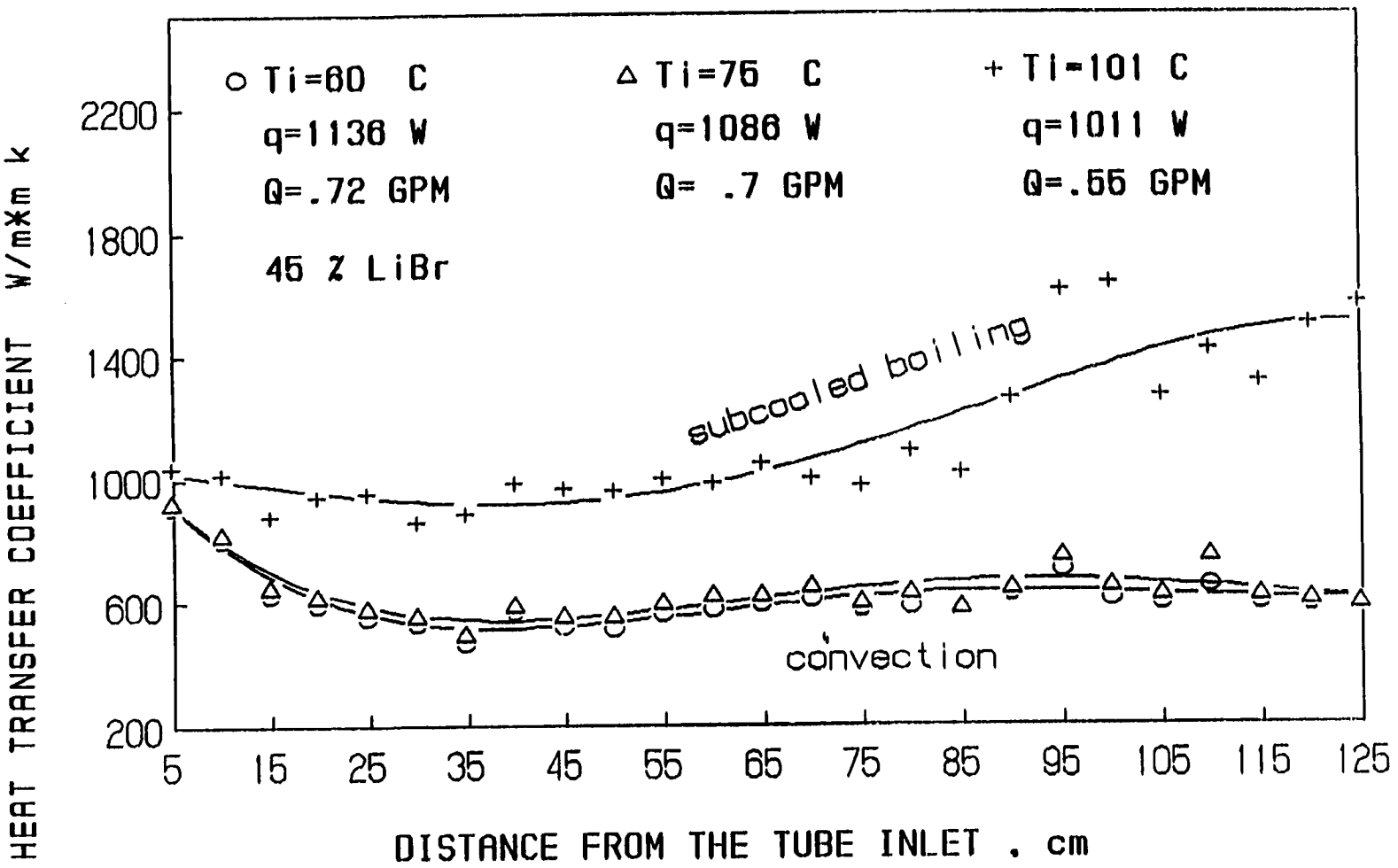

Figure 8.26 Heat transfer coefficient during convection and subcooled boiling .

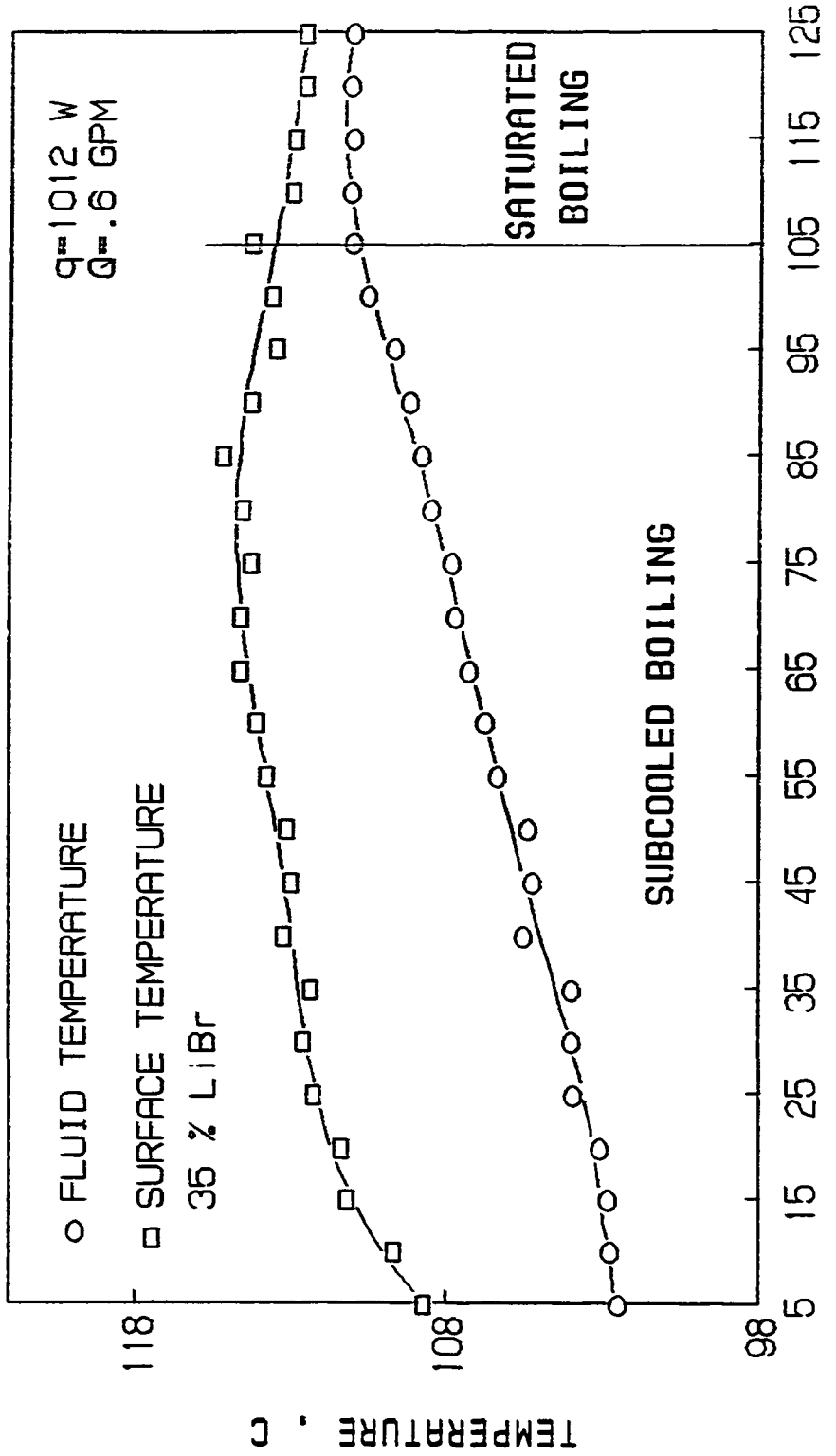

Figure 8.27 Temperature distribution during boiling.

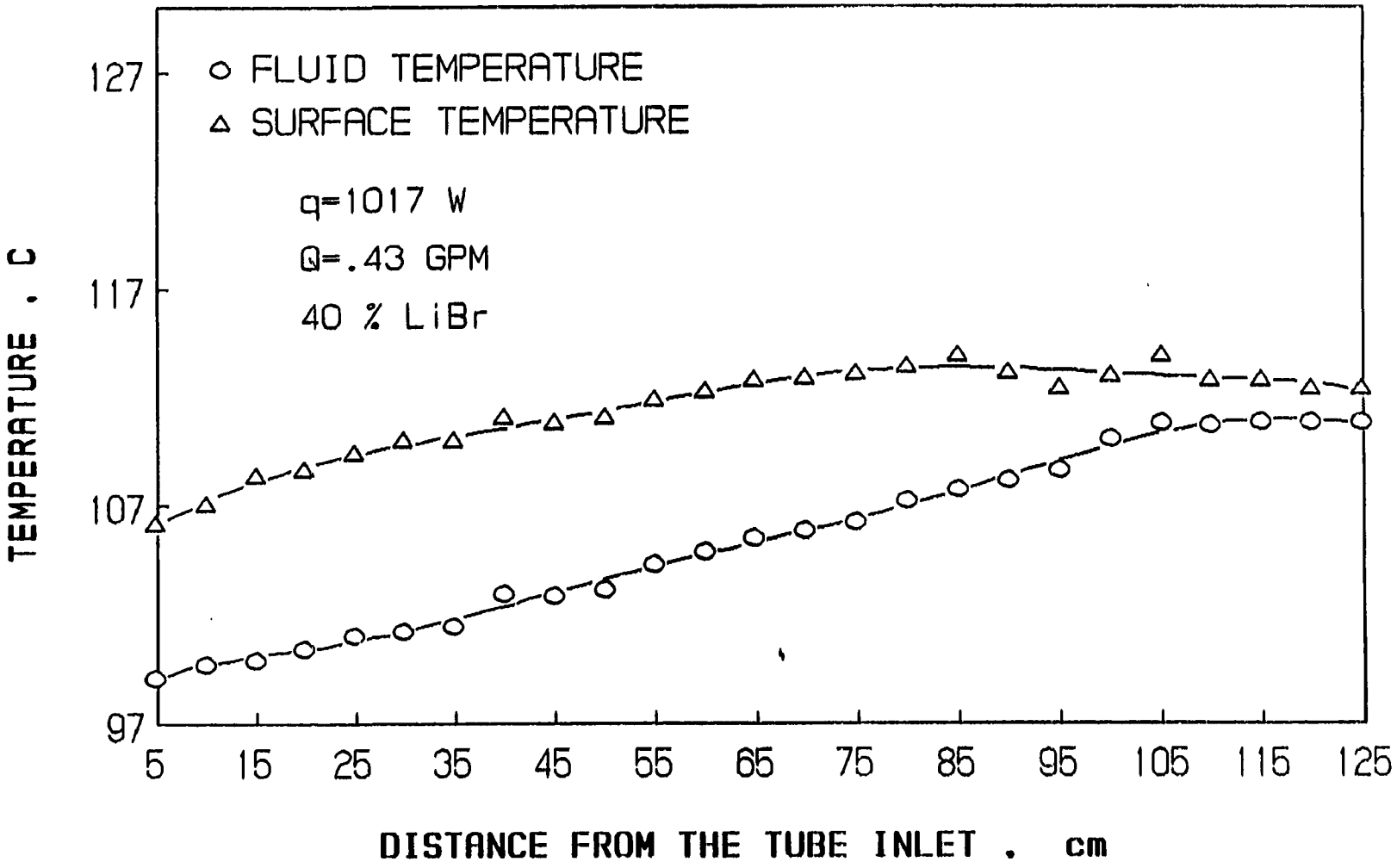

Figure 8.28 Temperature distribution during boiling.

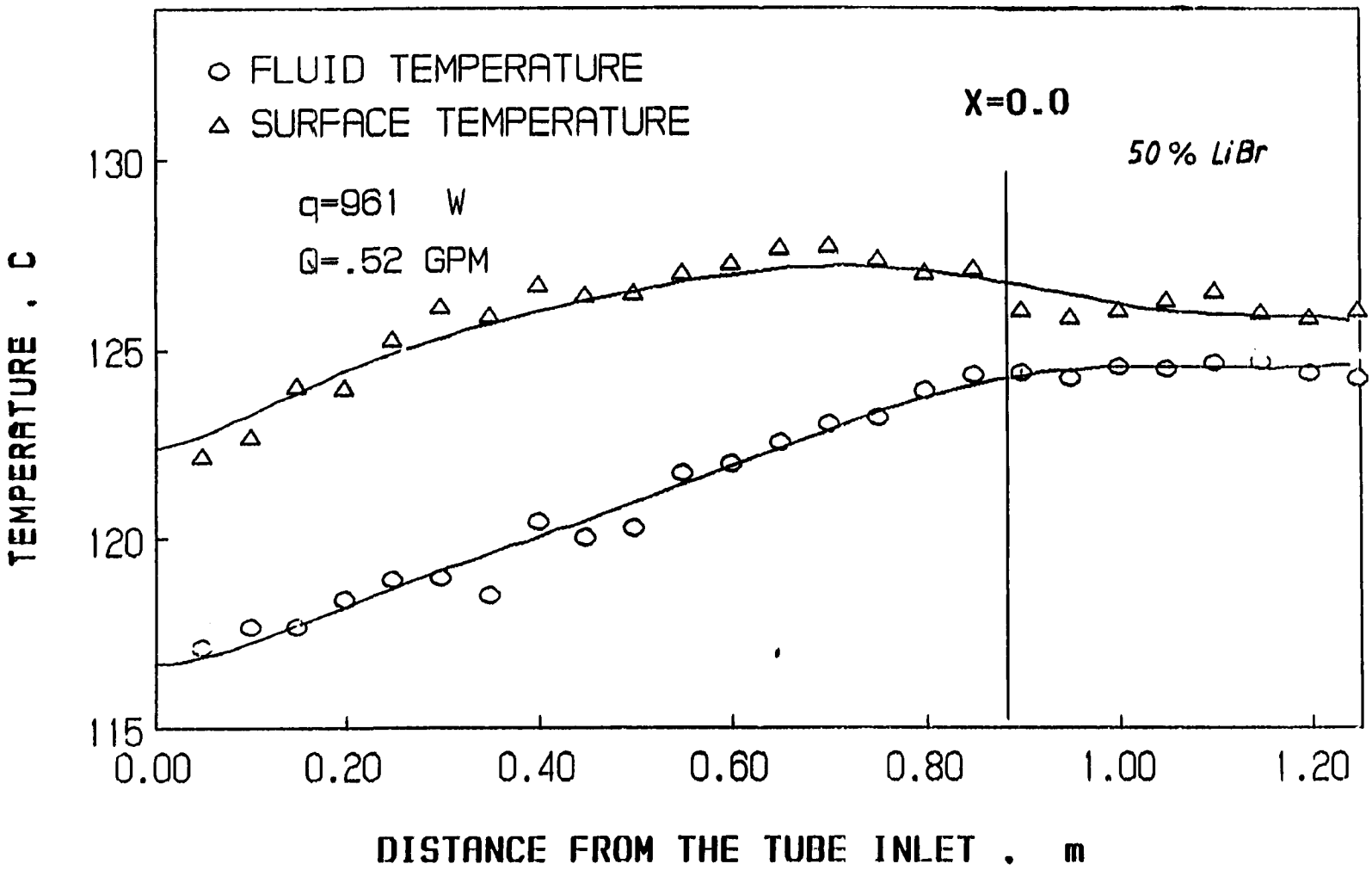

Figure 8.29 Temperature distribution during boiling.

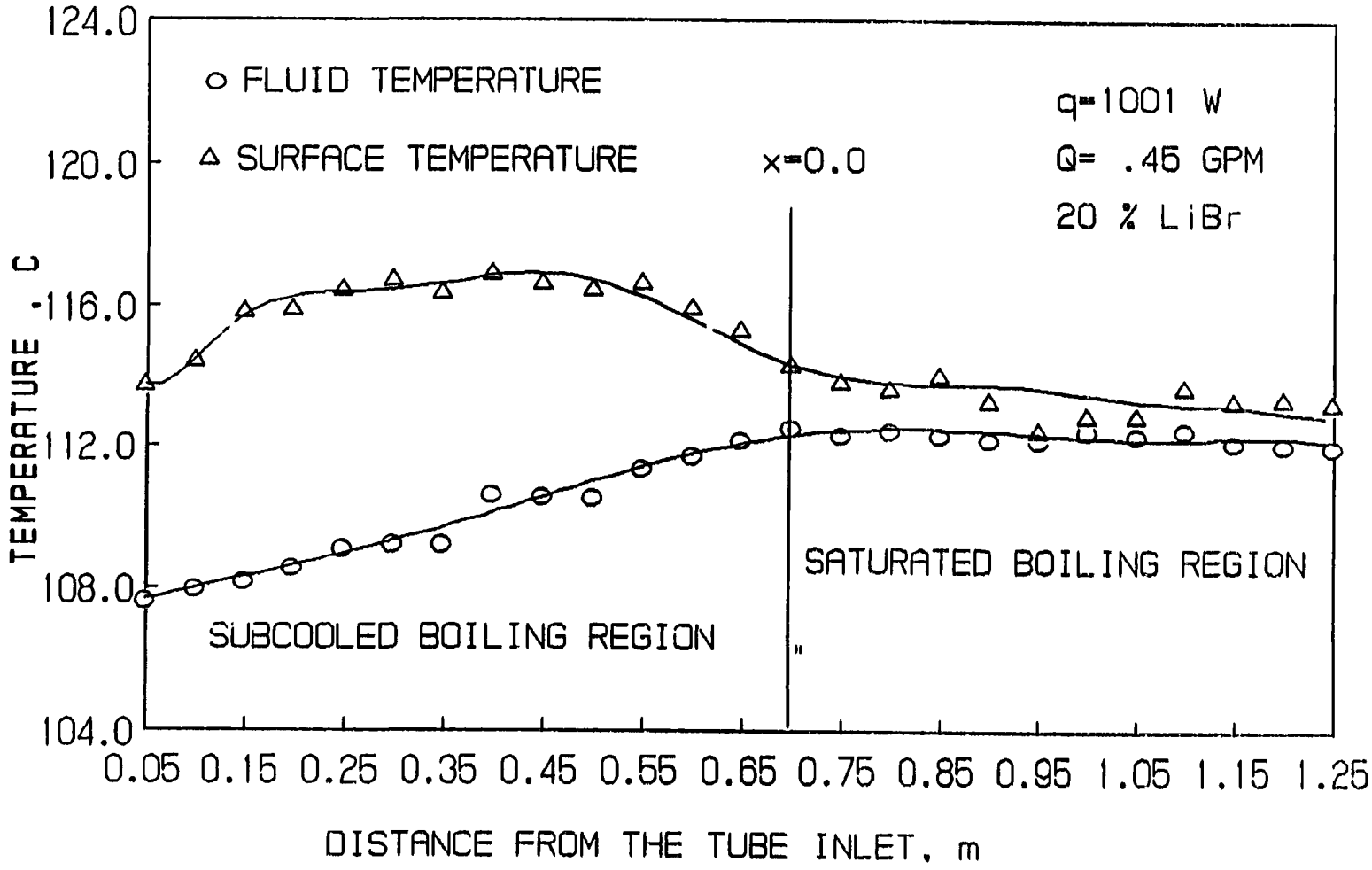

Figure 8.30 Temperature distribution during boiling.

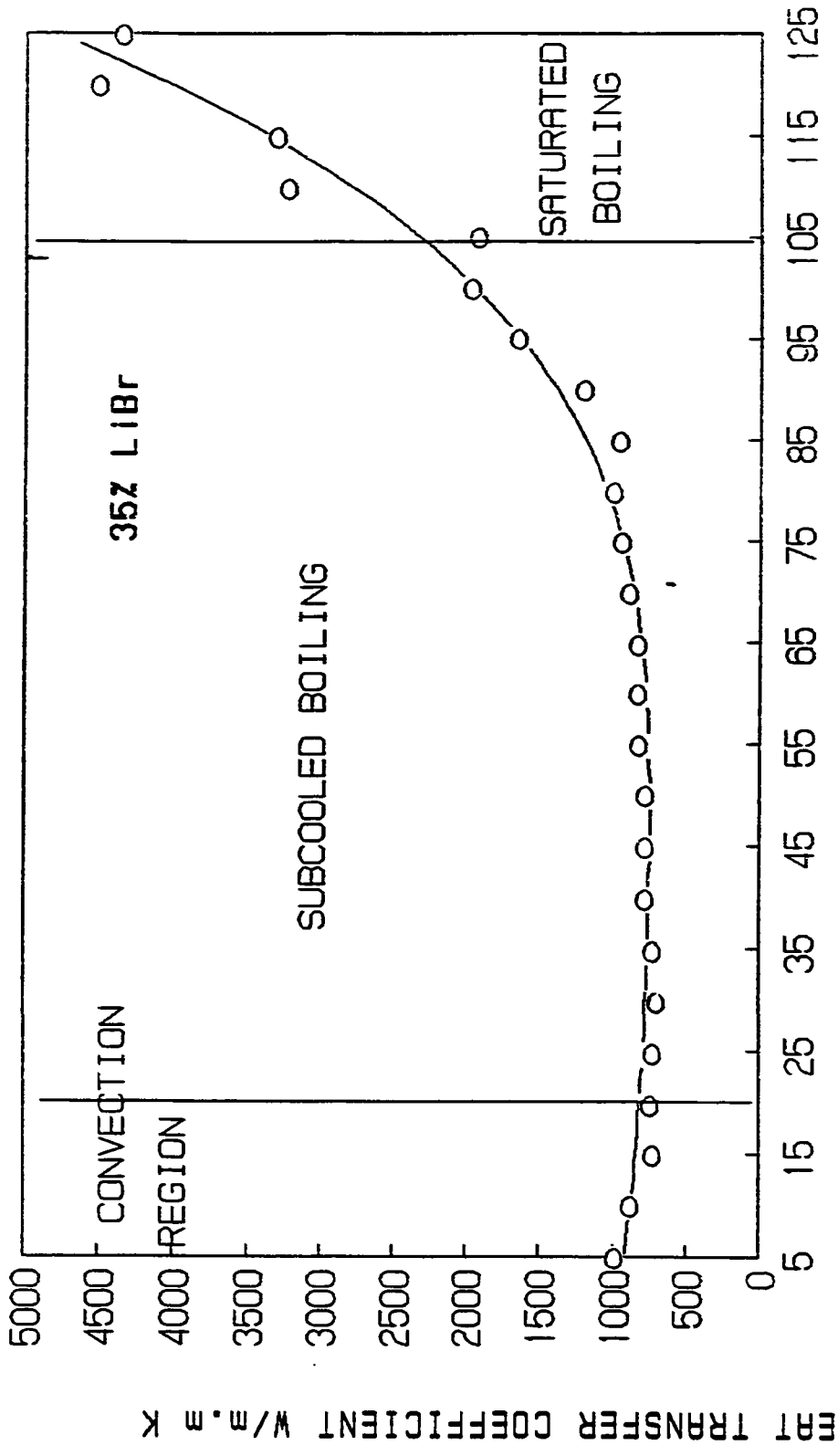

Figure 8.31 Heat transfer coefficient distribution .

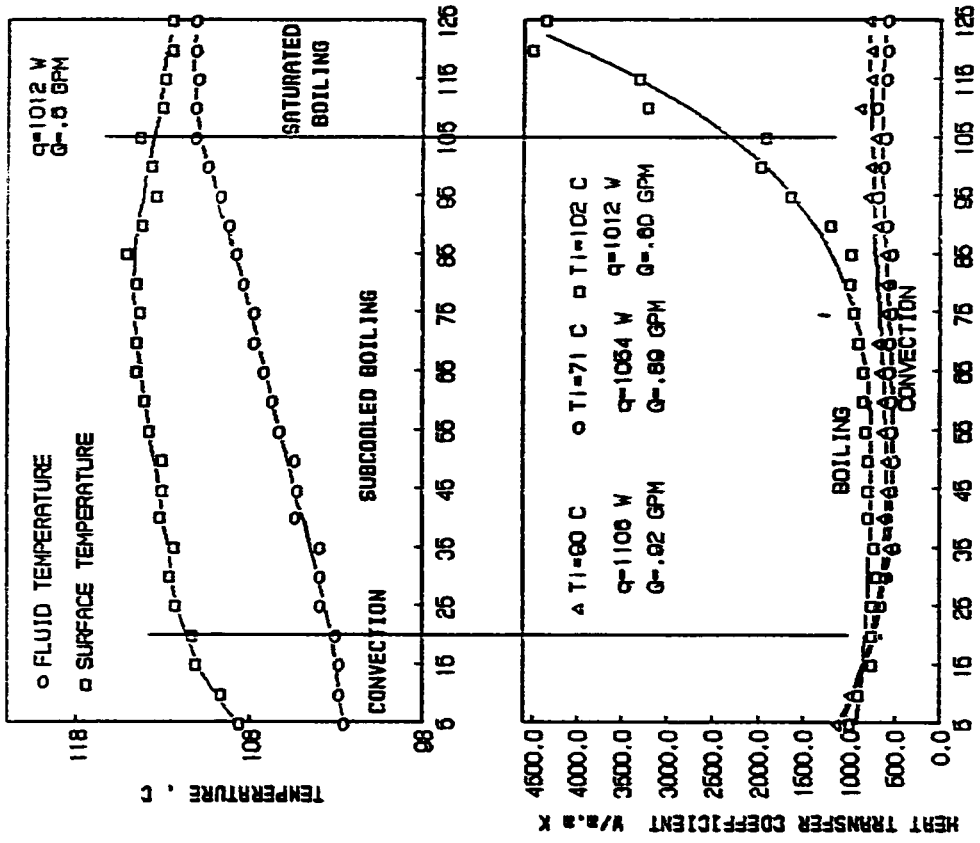

Figure 8.32 Heat transfer coefficient distribution during convection and boiling.

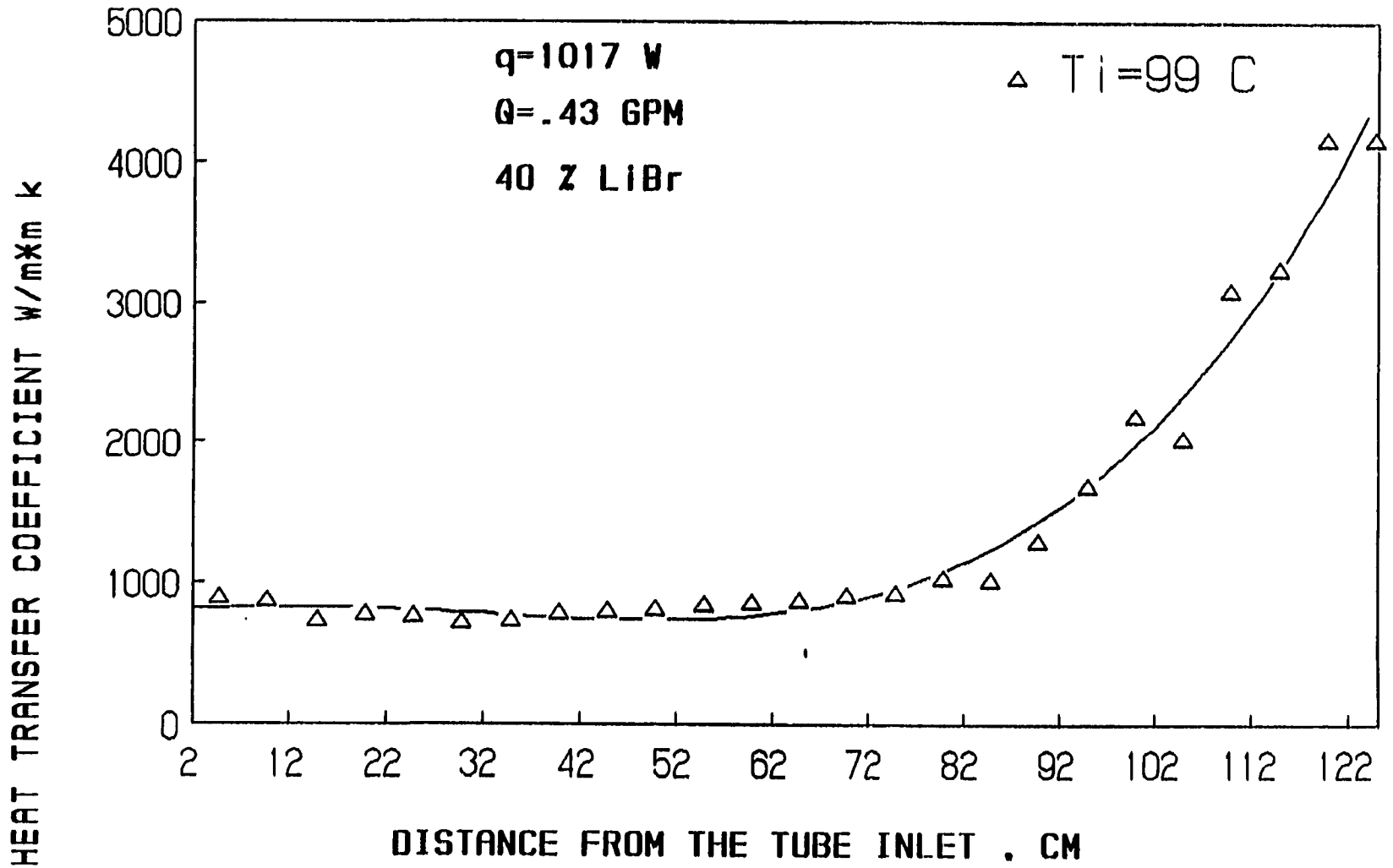

Figure 8.33 Heat transfer coefficient distribution during boiling.

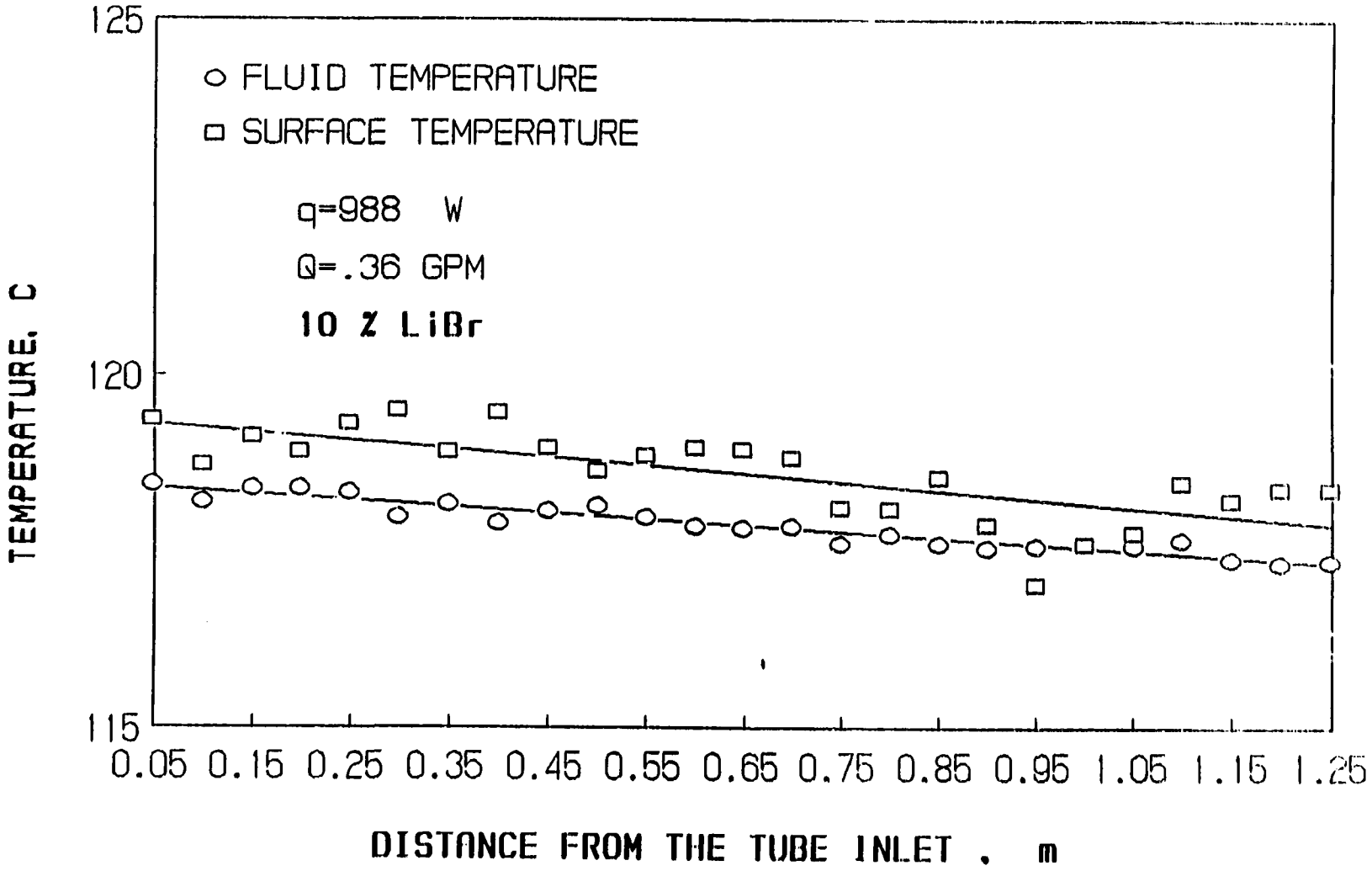

Figure 8.34 Temperature distribution during boiling.

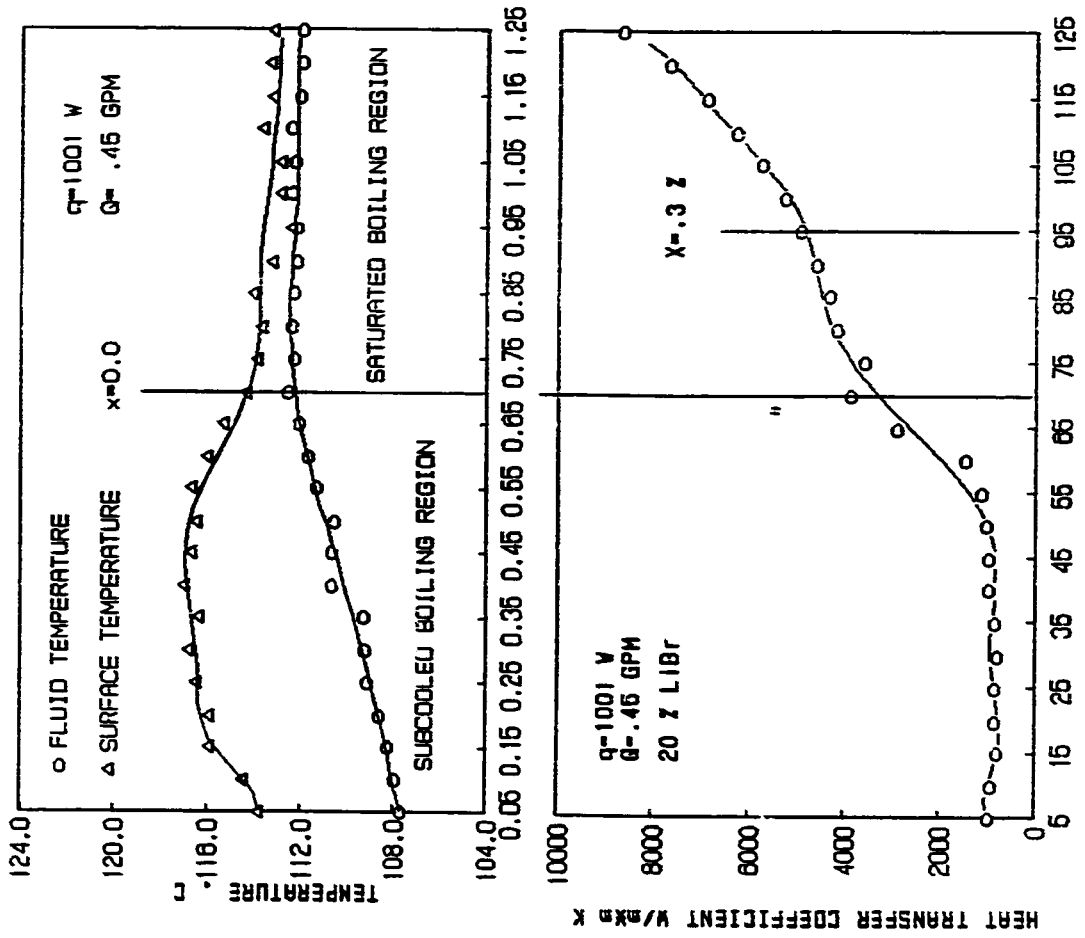

Figure 8.35 Heat transfer coefficient distribution along the tube test section during boiling.

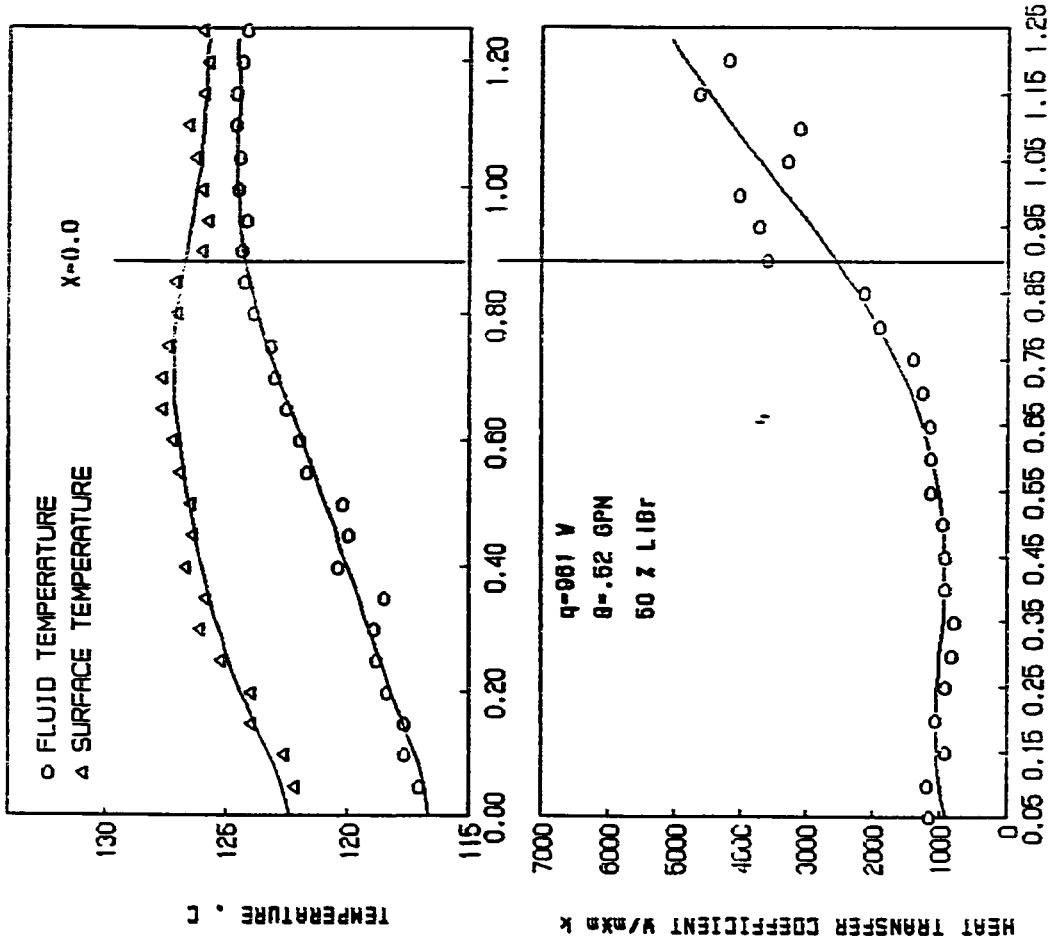

Figure 8.30 Heat transfer coefficient distribution during boiling.

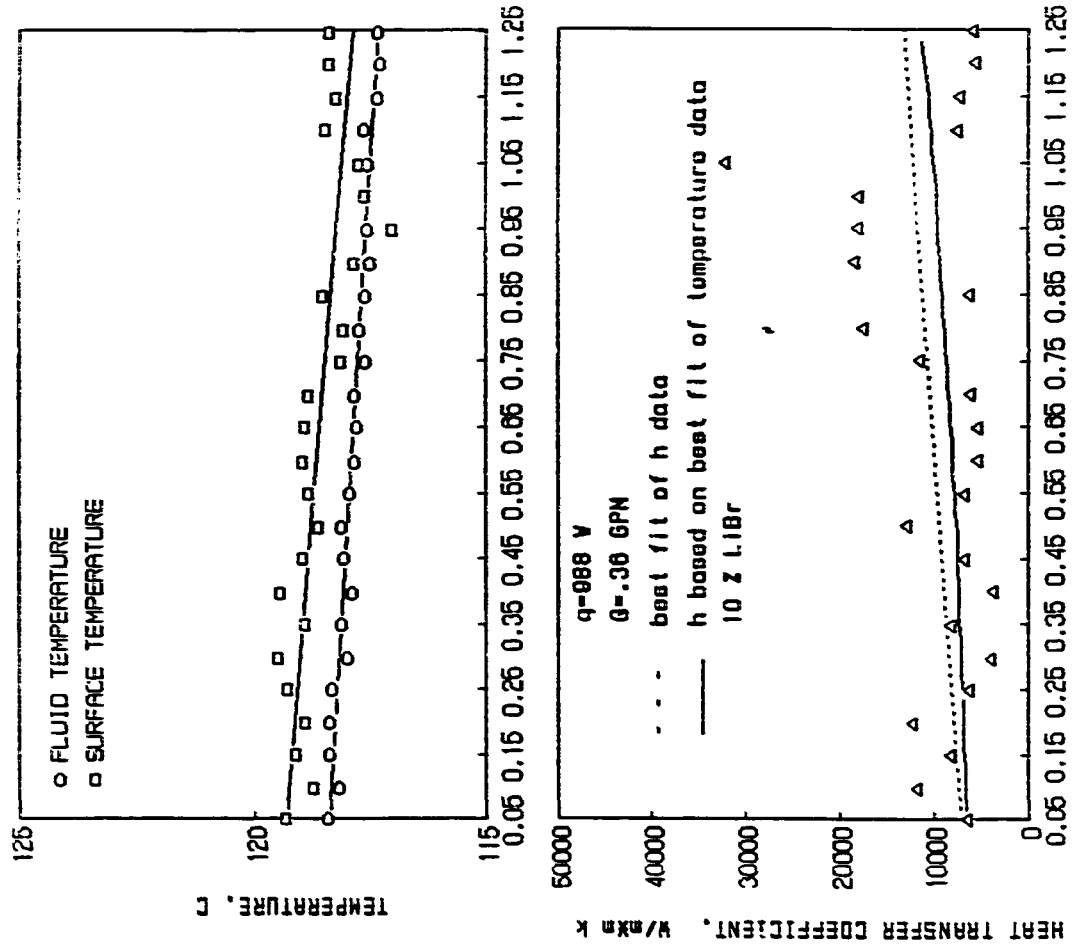

Figure 8.37 Heat transfer coefficient distribution during boiling.

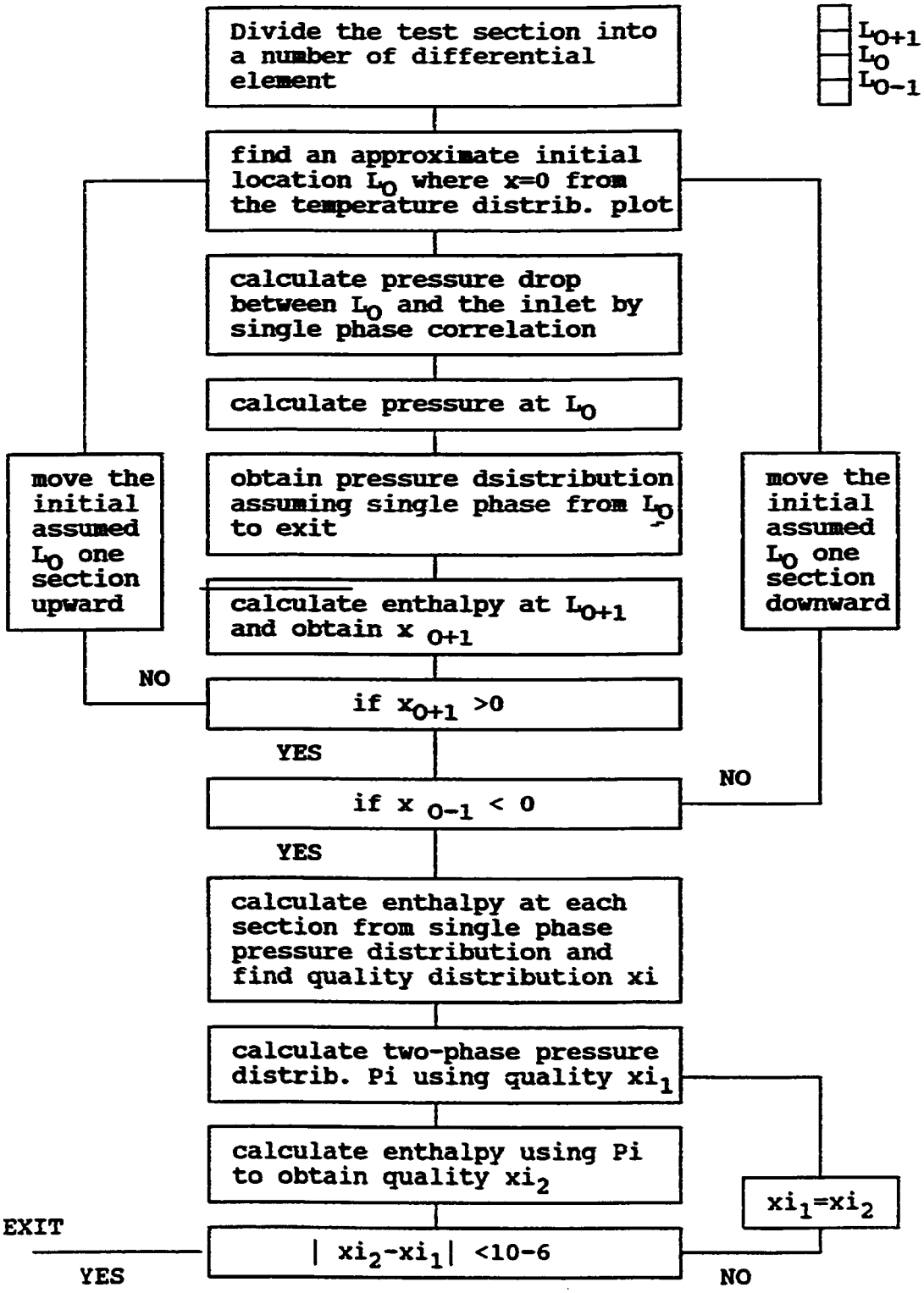

Figure 8.38 Vapor quality calculation flow diagram.

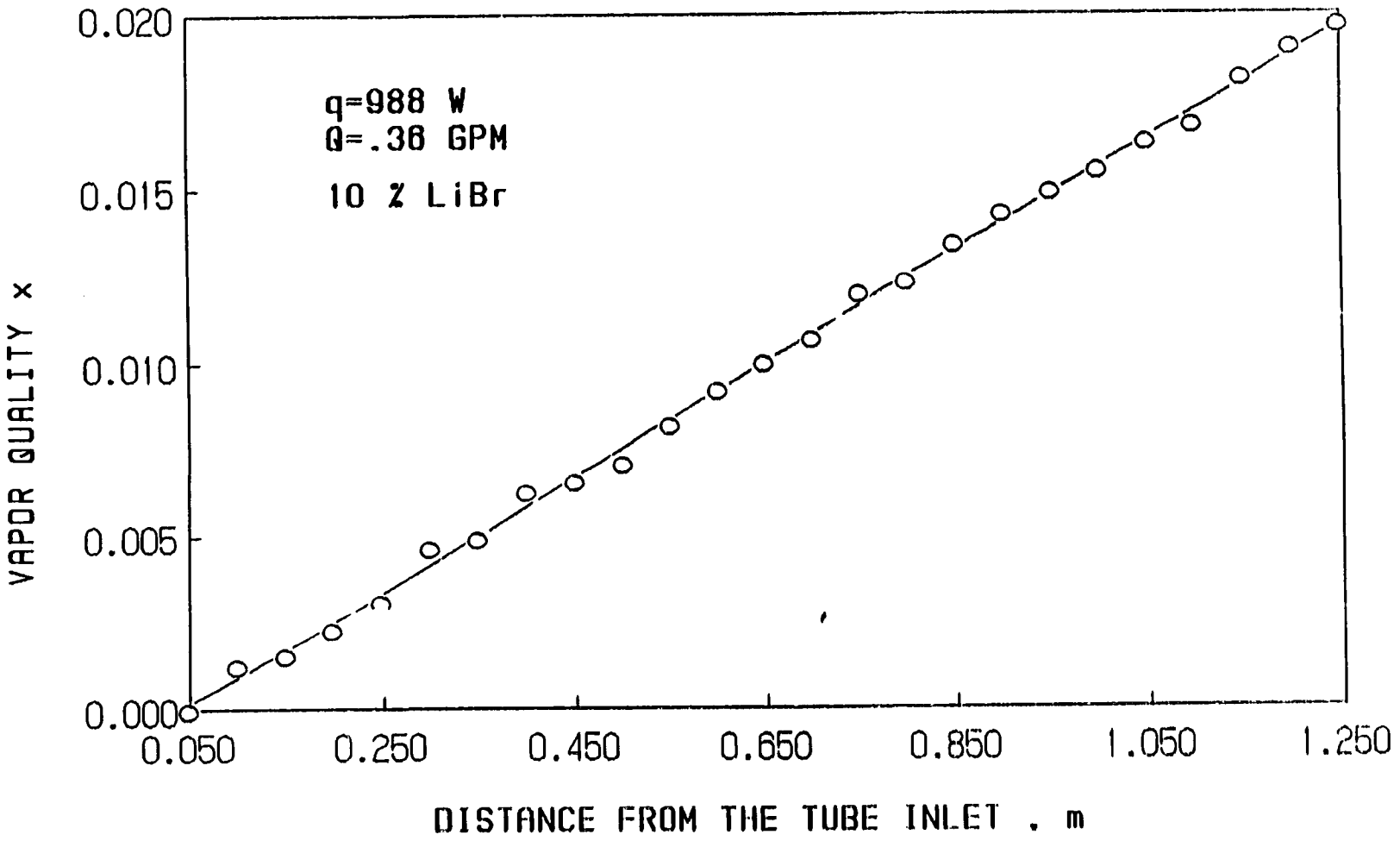

Figure 8.39 Variation of vapor quality along the tube test section.

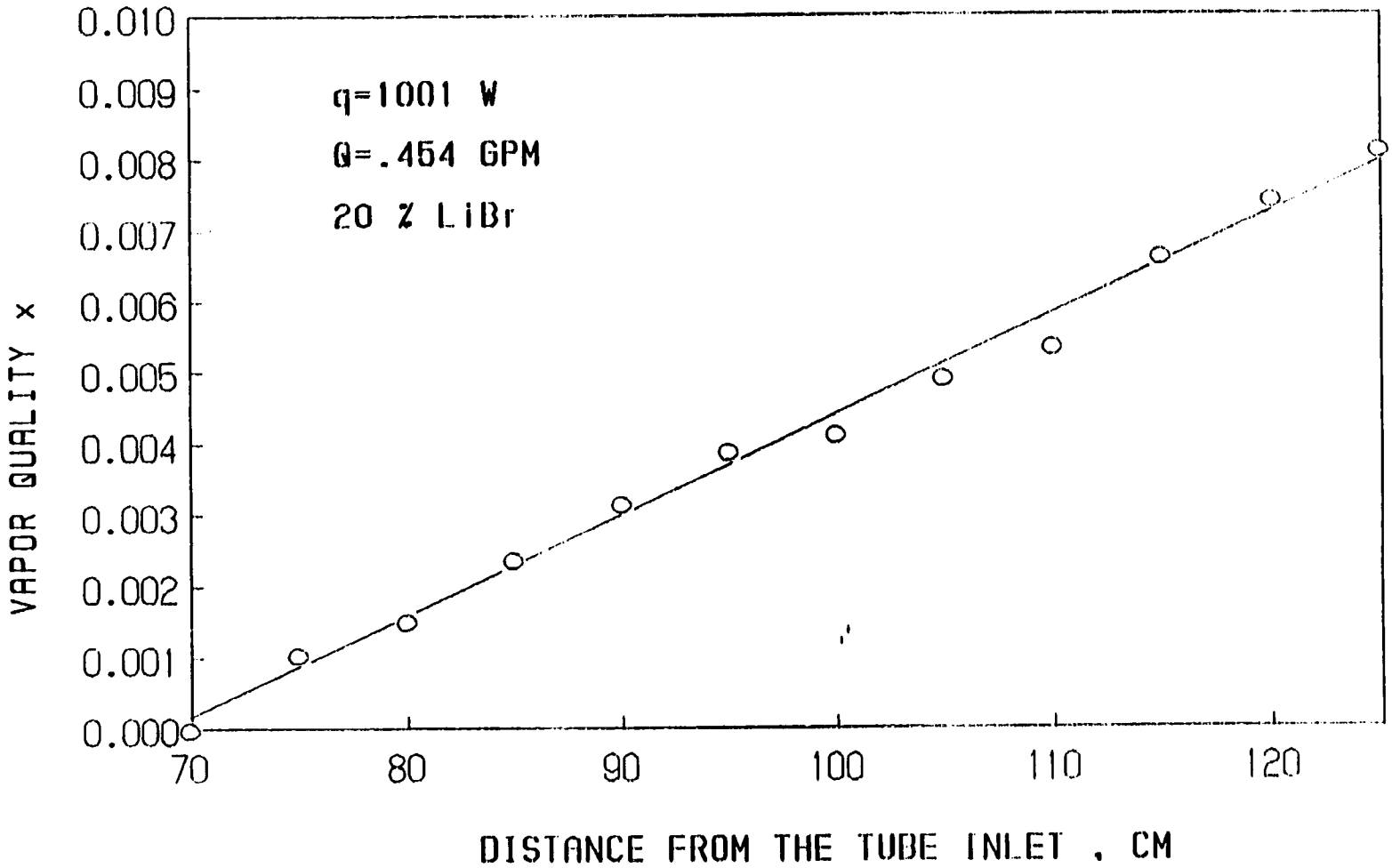

Figure 8.40 Vapor quality distribution along the boiling tube.

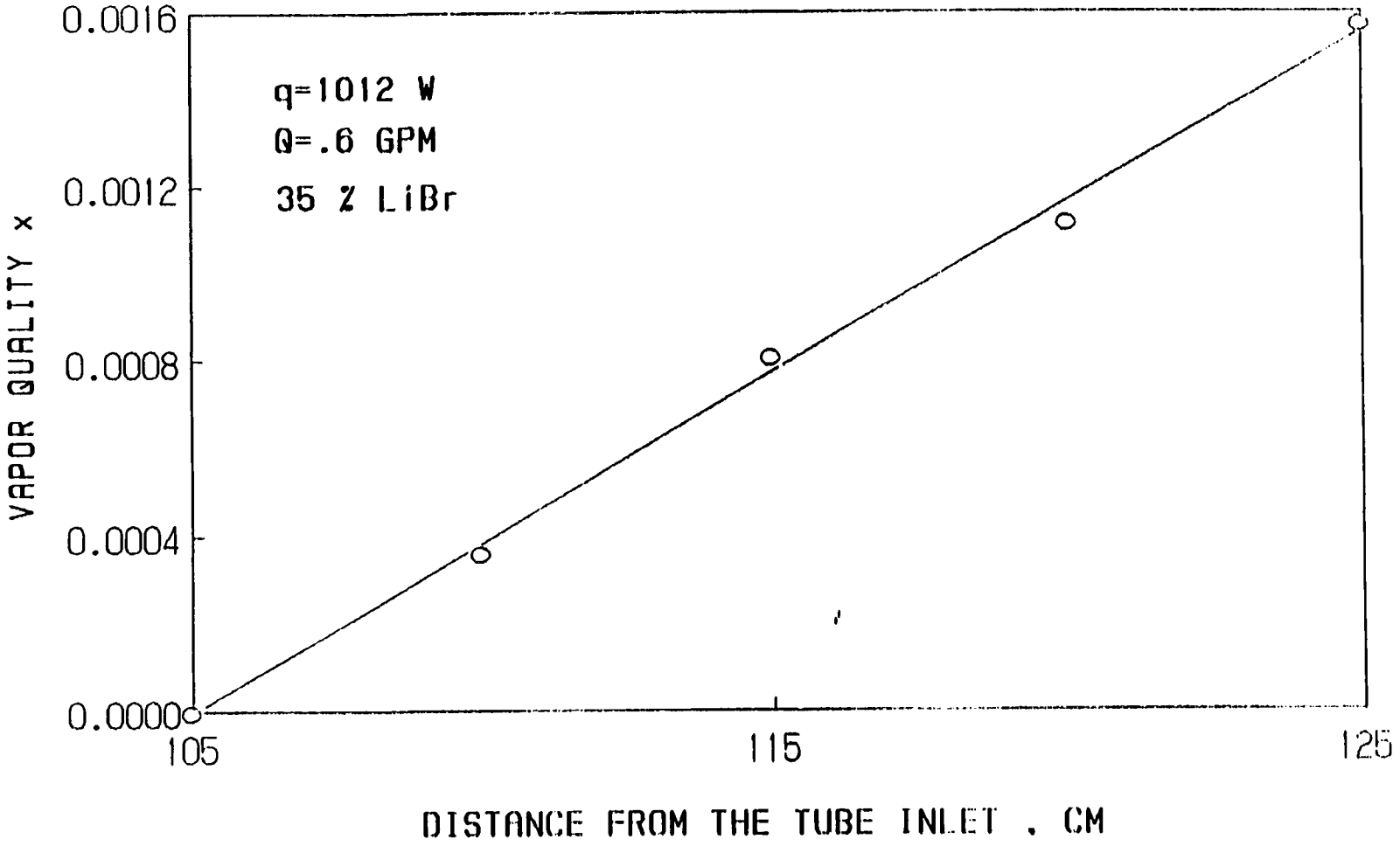

Figure 8.41 Vapor quality distribution along the boiling tube.

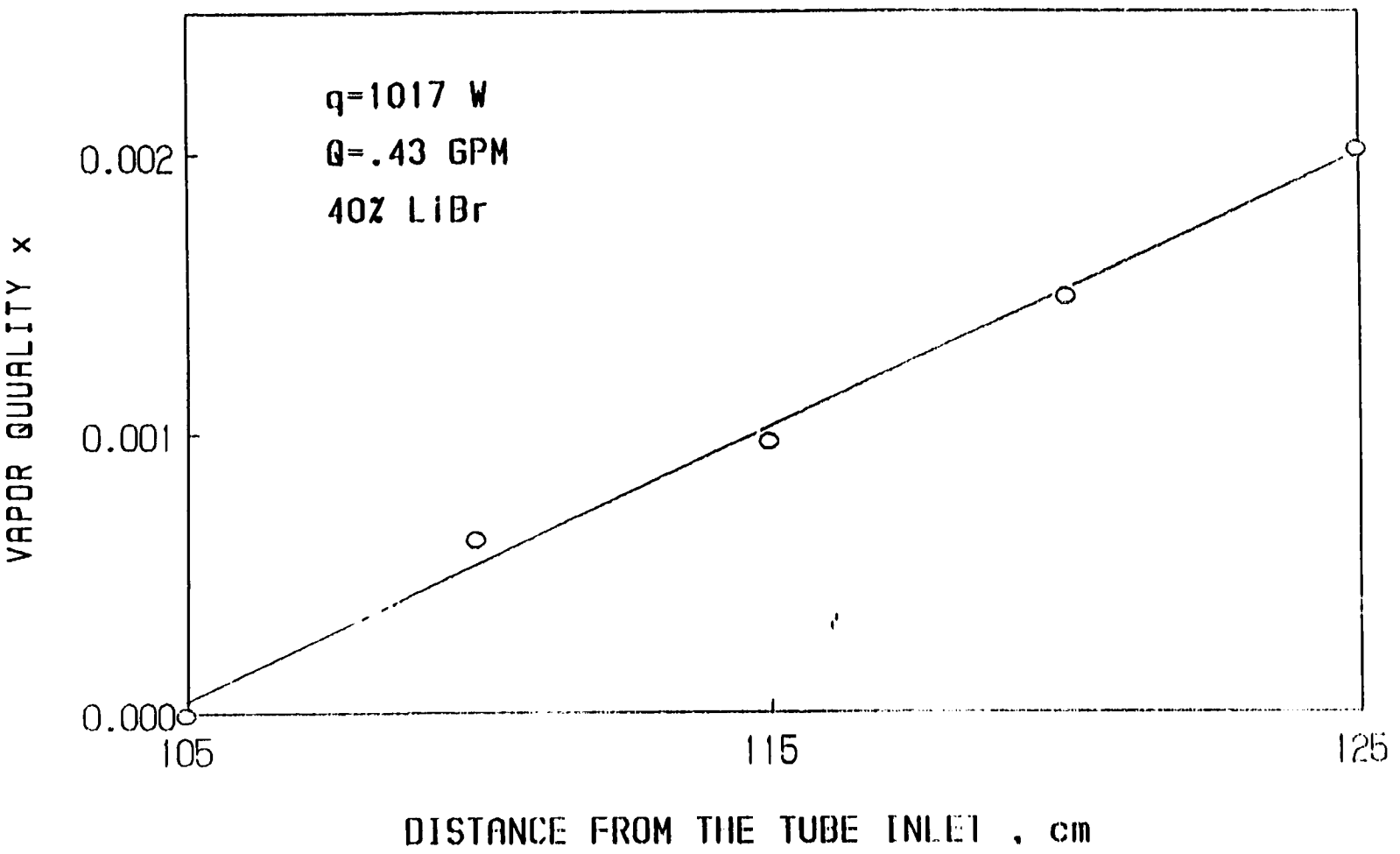

Figure 8.42 Vapor quality distribution in a vertical tube.

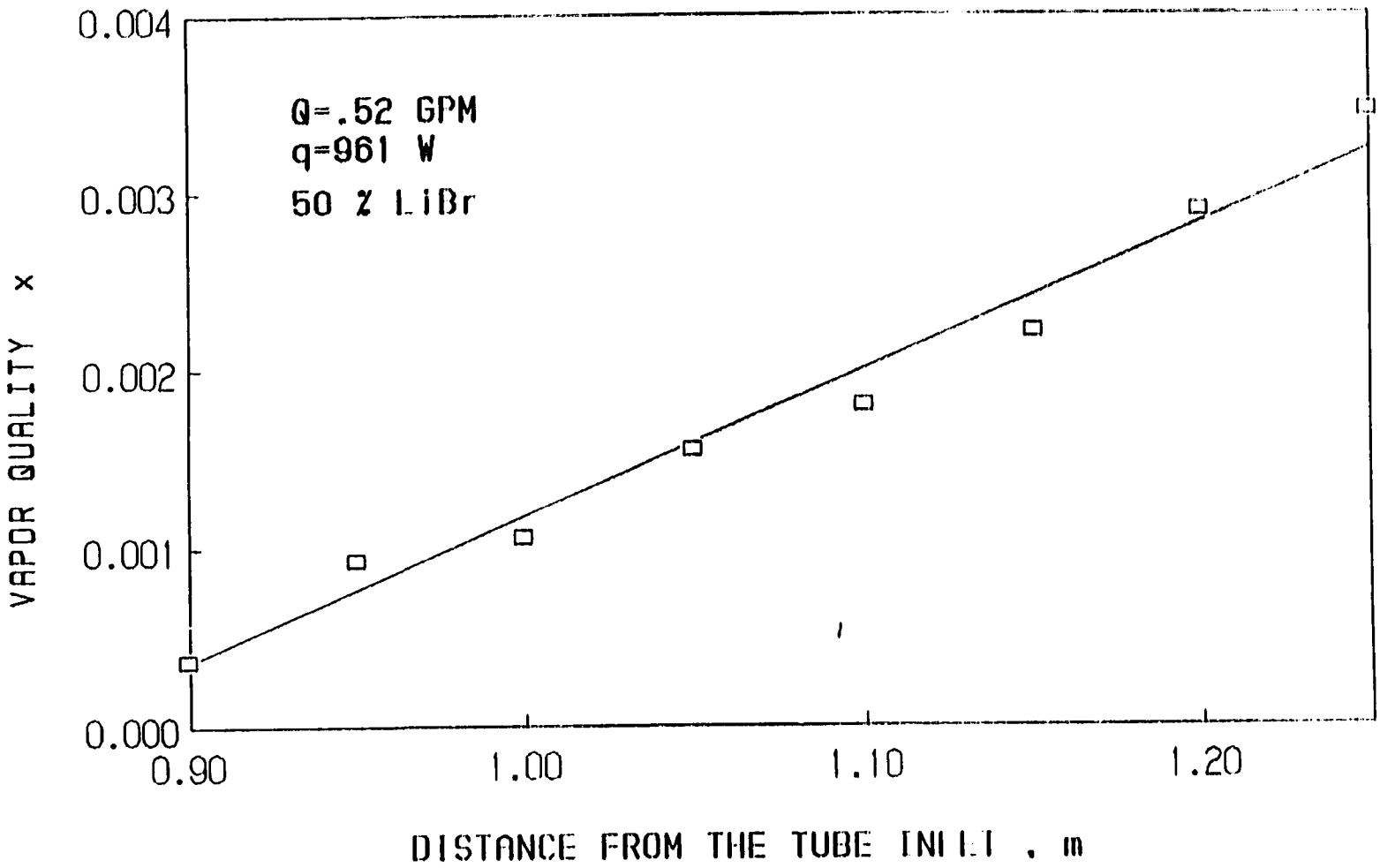

Figure 8.43 Vapor quality distribution in a vertical tube.

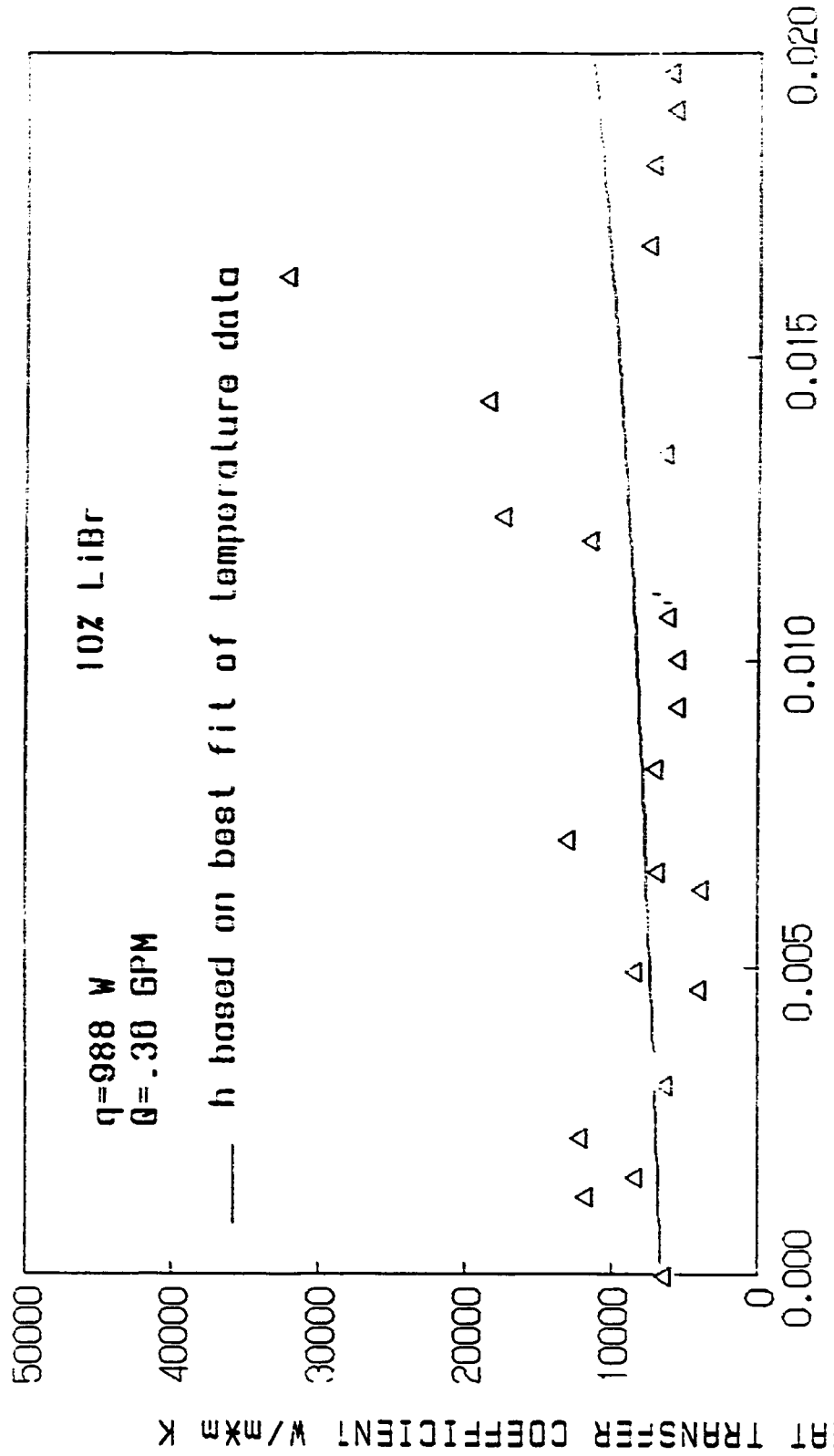

Figure 8.44 Variation of heat transfer coefficient with vapor quality.

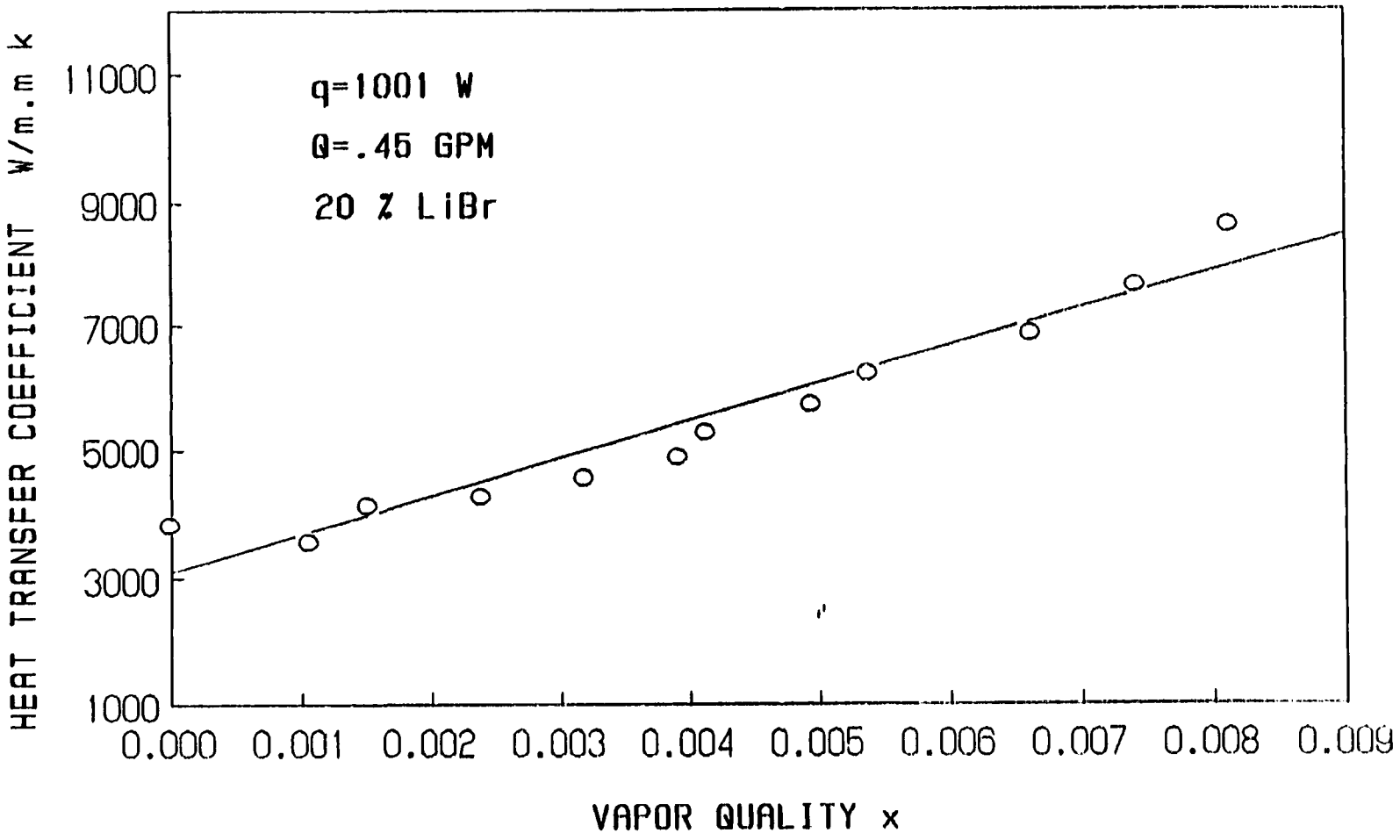

Figure 8.45 Variation of heat transfer coefficient with vapor quality .

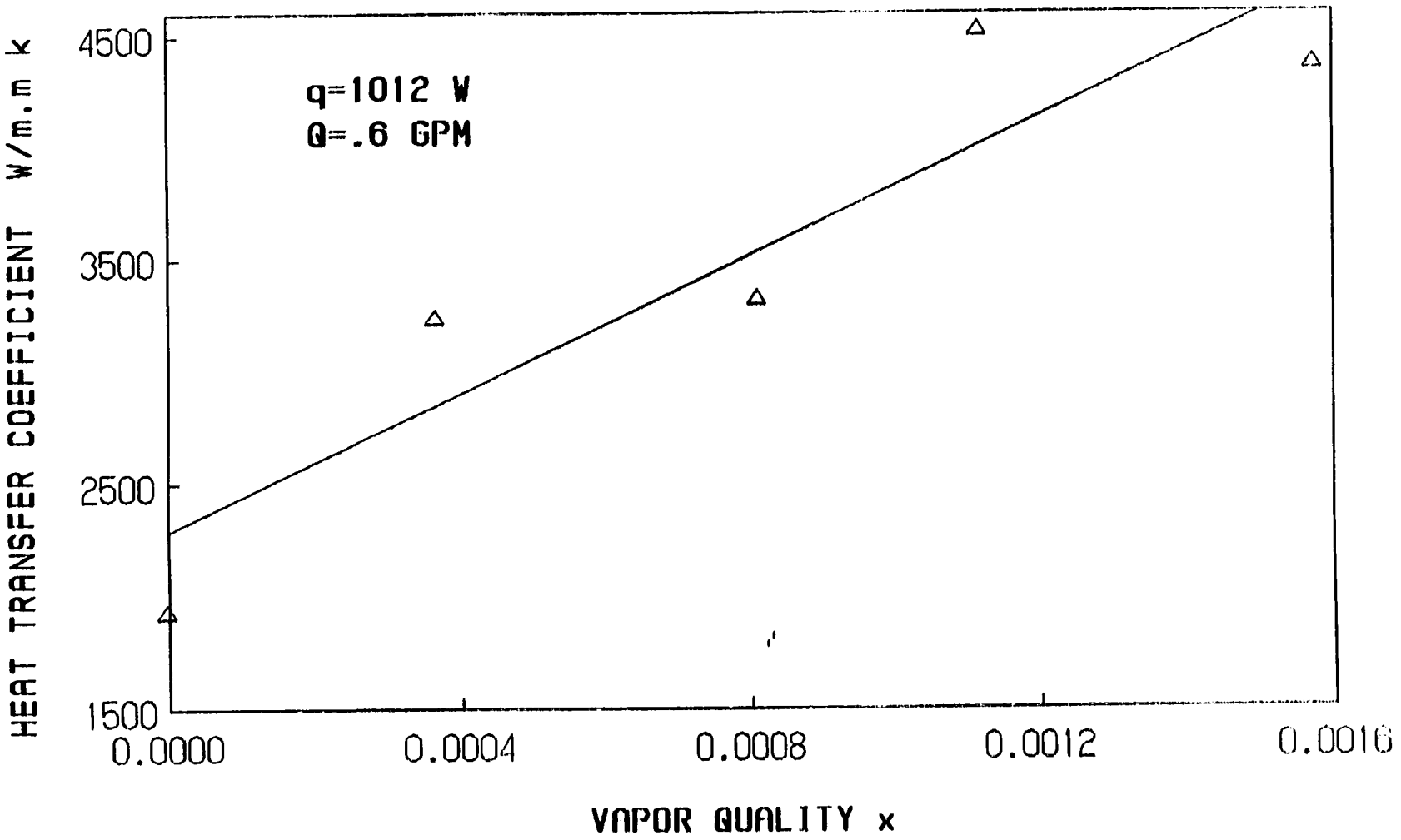

Figure 8.46 variation of heat transfer coefficient with vapor quality for 35Z LiBr by wt.

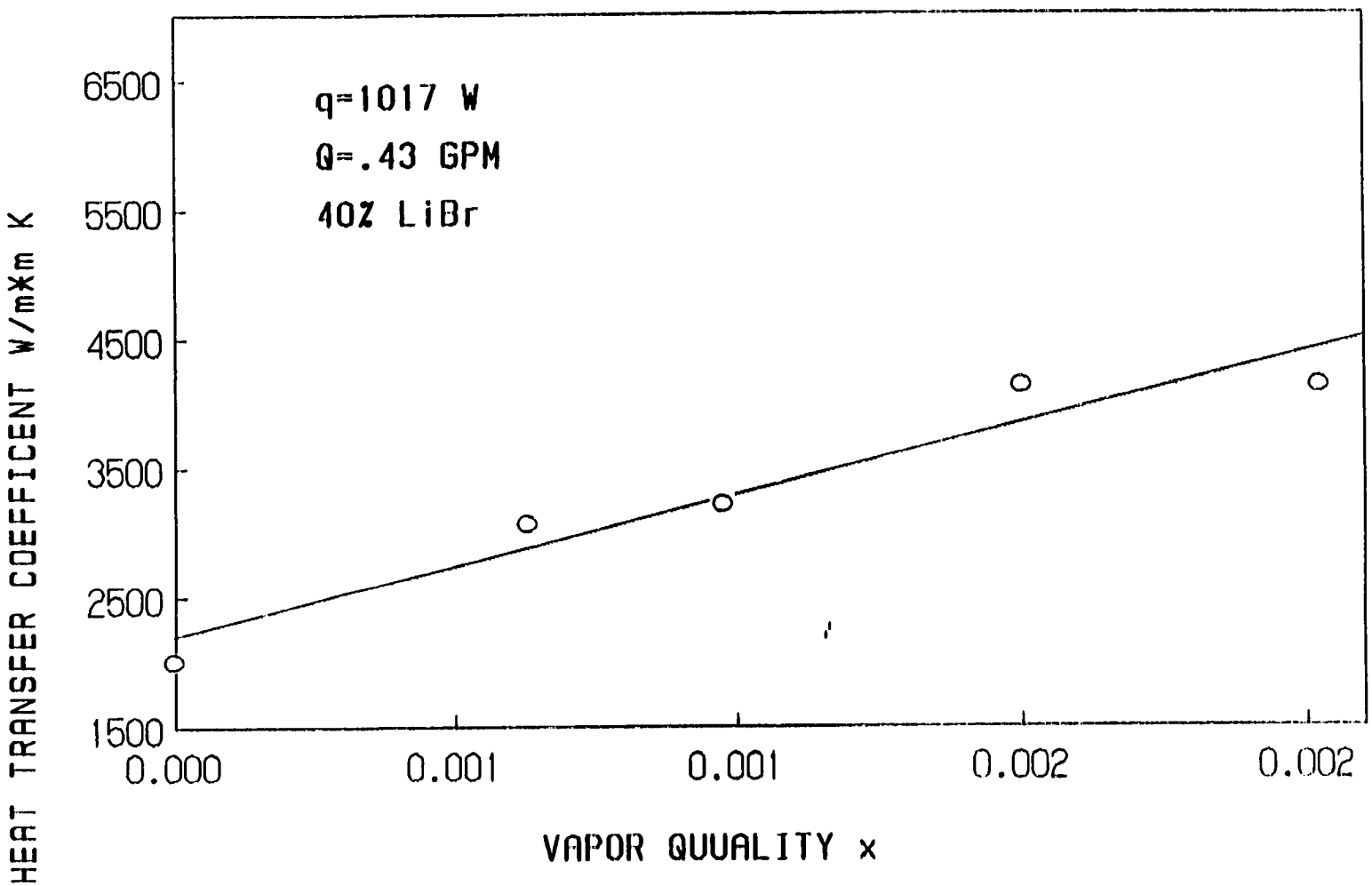

Figure 8.47 Vapor quality versus heat transfer coefficient.

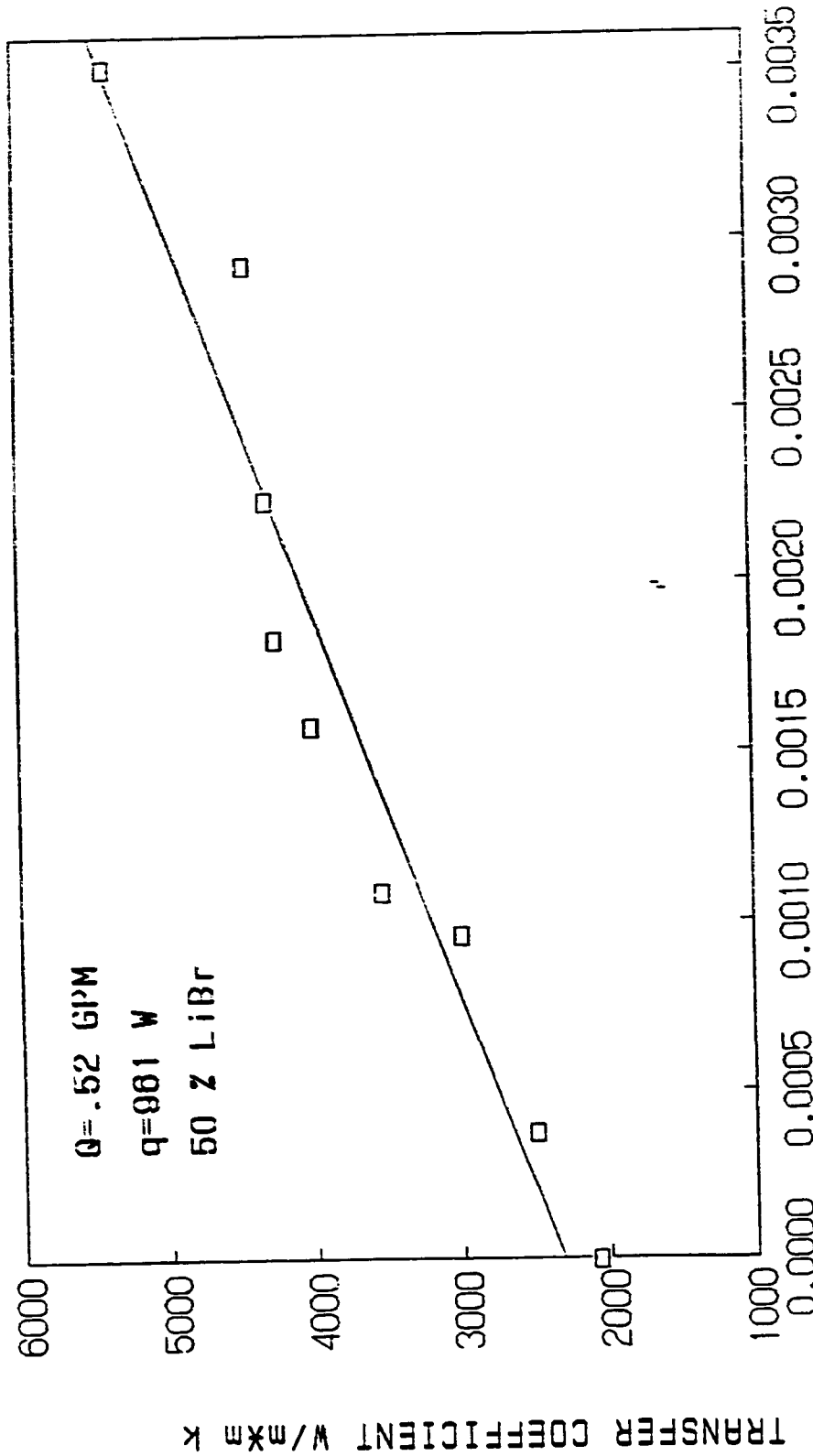

Figure 8.48 Heat transfer coefficient versus vapor quality.

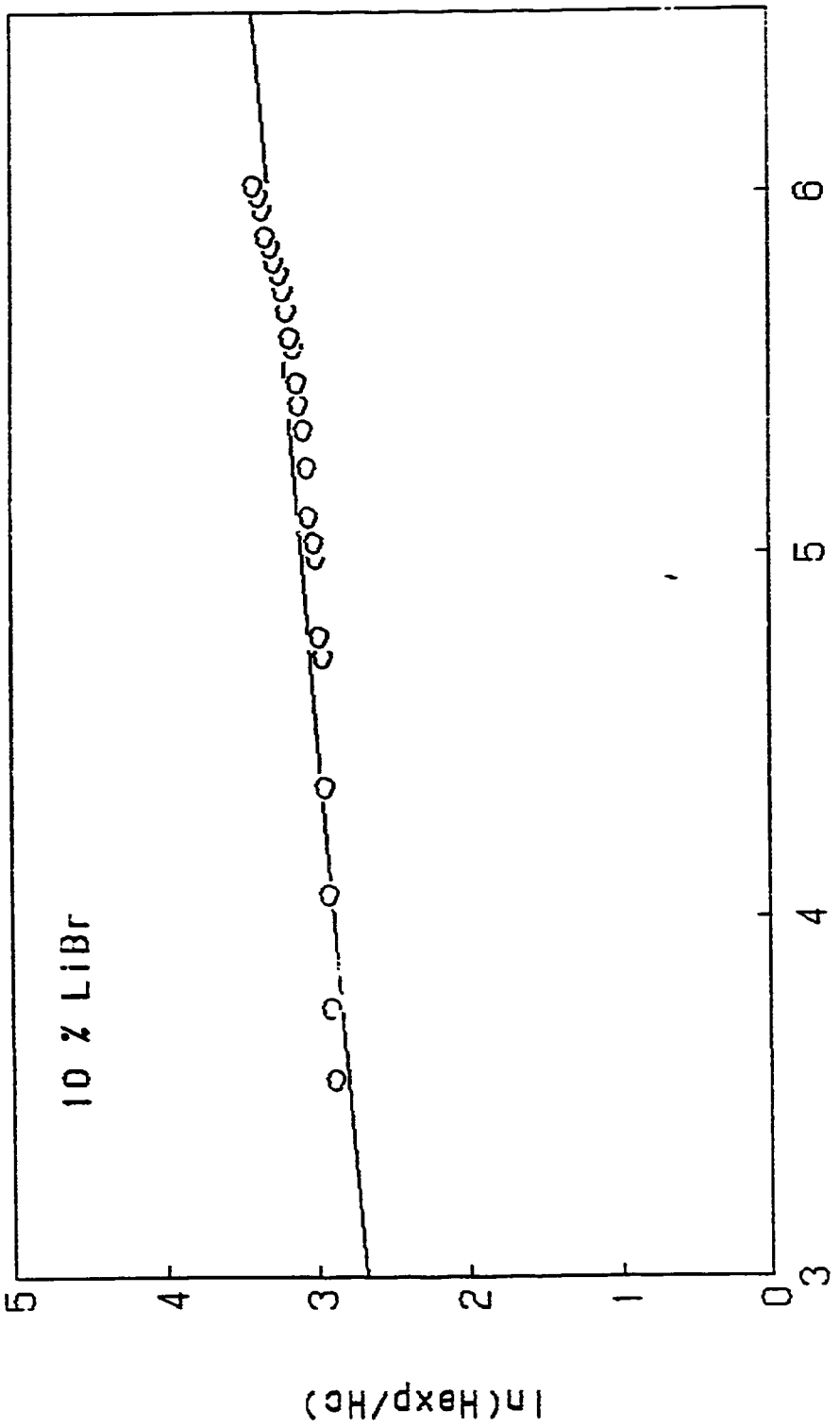

Figure 8.49 Variation of heat transfer coefficient with Lockhart Martinlli Parameter .

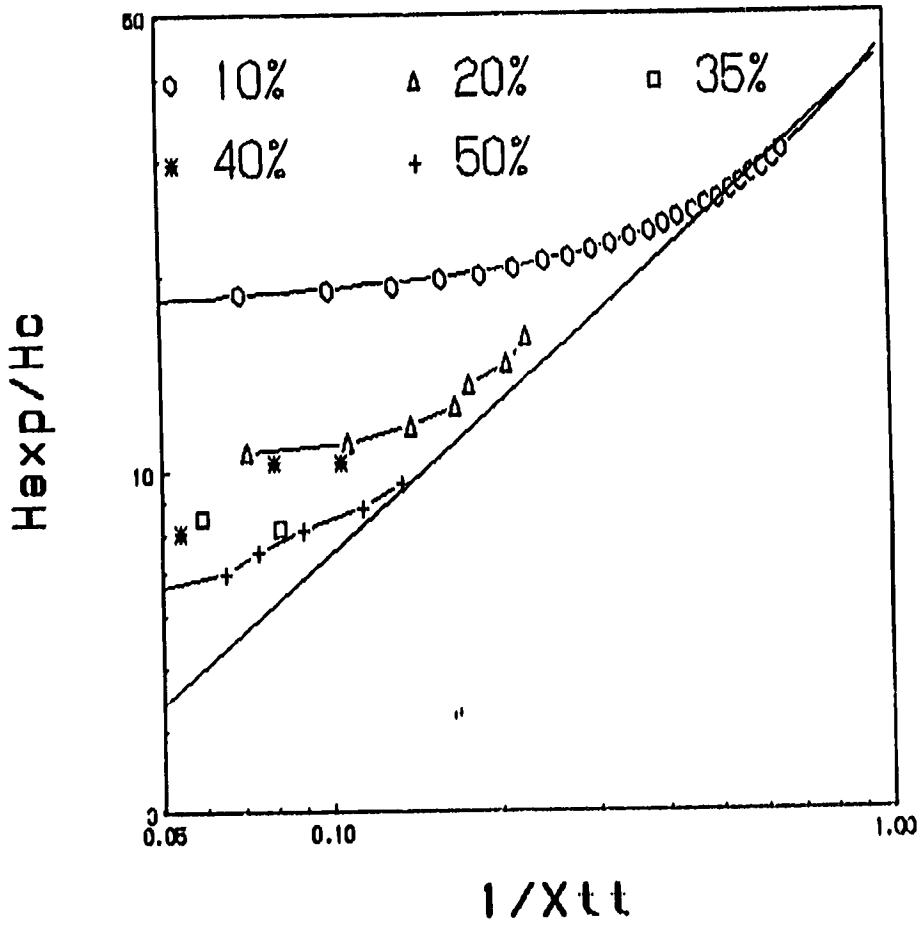

Figure 8.50 variation of heat transfer coefficient with Lockhart-Martinelli parameter.

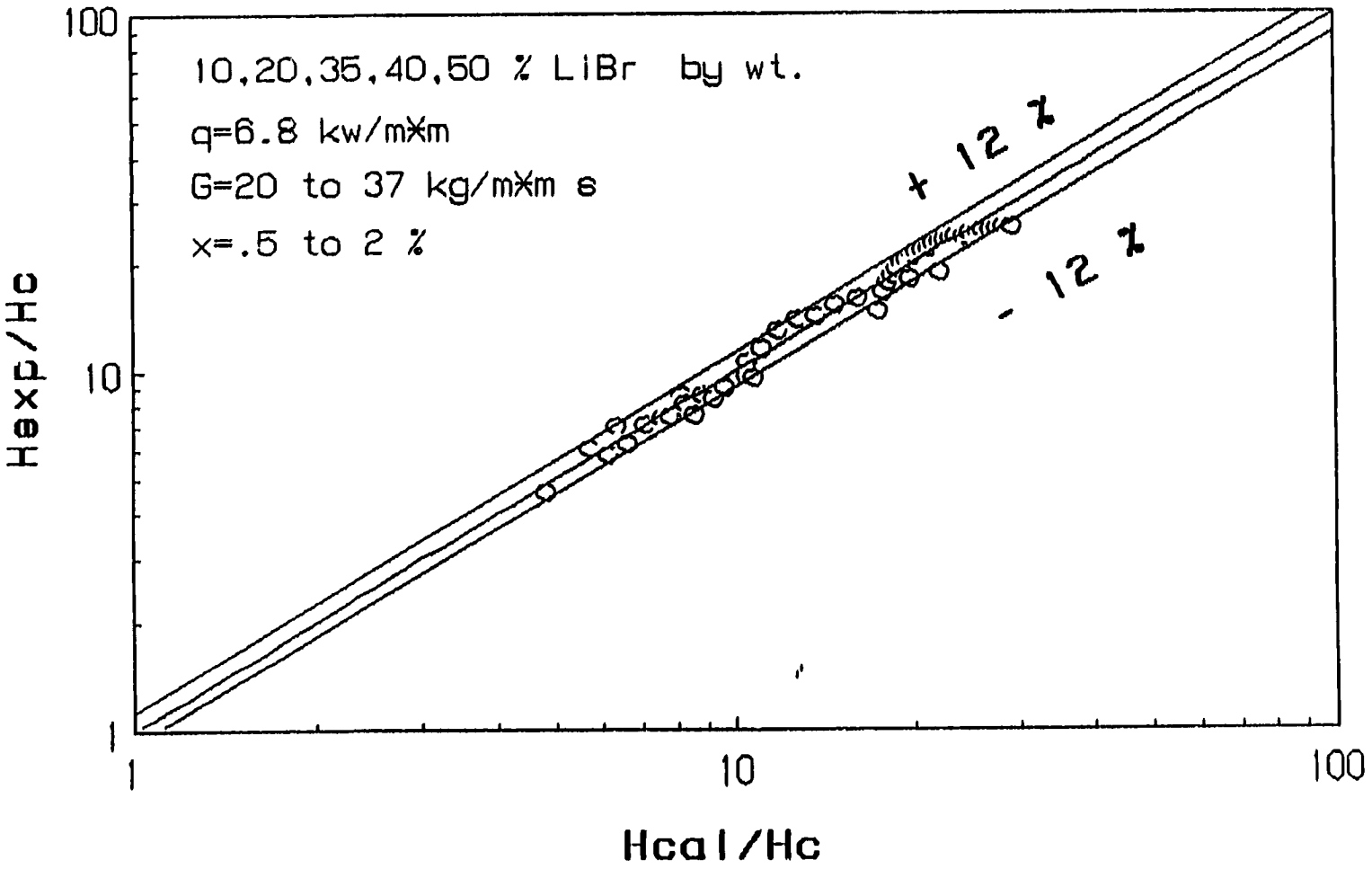

Figure 8.51 Comparison of predected and measured heat transfer coefficient ratio.

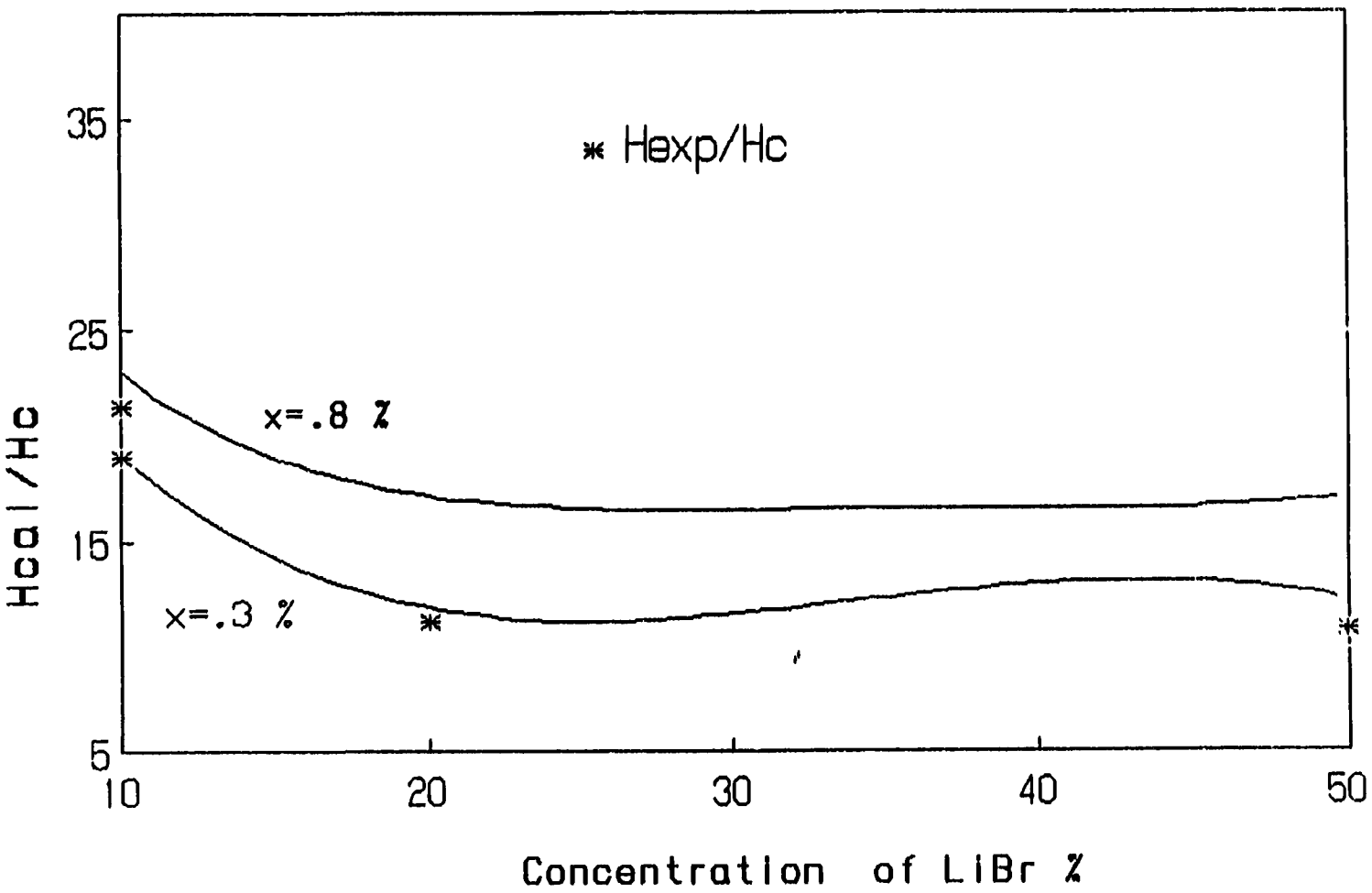

Figure 8.52 Calculated and experimental heat transfer coefficient ratio for different compositions.

TABLE 6.1 Variation of Fluid and Surface Temperatures and Heat transfer Coefficient Along the Tube Test Section in Convection for 10 % by wt. LiBr Solution .

	CONVECTION DATA FOR 10% BY WT. LiBr AT Q=1.0 GPM AND q=1128 W			CONVECTION DATA FOR 10 % BY WT LiBr AT Q=1.0 GPM AND q=1075 W		
DISTANCE FROM TUBE INLET IN m	FLUID MEAN TEMPERATURE IN °C	SURFACE TEMPERATURE IN °C	HEAT TRANSFER COEFFICIENT W/m²K	FLUID MEAN TEMPERATURE IN °C	SURFACE TEMPERATURE IN °C	HEAT TRANSFER COEFFICIENT W/m²K
0.05	65.59	71.67	1,152.34	82.60	87.28	1,426.71
0.10	65.83	72.32	1,079.54	82.79	87.94	1,296.51
0.15	66.07	73.66	923.08	83.03	89.31	1,063.22
0.20	66.29	74.27	877.97	83.31	89.83	1,024.08
0.25	66.73	75.57	792.56	83.76	91.22	895.04
0.30	66.74	76.36	728.30	83.68	92.16	787.38
0.35	66.26	76.85	661.59	83.23	92.53	717.96
0.40	66.68	77.93	622.77	83.64	93.59	671.06
0.45	67.11	77.80	655.40	83.97	93.38	709.57
0.50	67.54	78.11	662.84	84.47	93.64	728.14
0.55	67.61	78.81	625.55	84.51	94.36	677.87
0.60	67.68	79.00	618.92	84.54	94.68	658.48
0.65	68.27	79.68	614.04	85.04	95.25	653.97
0.70	68.32	79.72	614.58	85.11	95.28	656.54
0.75	68.04	79.48	612.43	84.79	95.48	624.60
0.80	68.27	79.68	614.04	85.13	95.64	635.30
0.85	68.44	79.87	612.97	85.30	95.98	625.19
0.90	68.76	79.45	655.40	85.53	95.52	668.37
0.95	69.32	78.95	727.54	86.00	94.97	744.37
1.00	69.53	79.33	714.92	86.61	95.42	757.89
1.05	70.10	79.70	729.81	87.10	95.91	757.89
1.10	71.10	80.27	764.04	88.13	96.55	793.00
1.15	70.18	80.30	692.31	87.18	96.51	715.65
1.20	70.14	80.43	680.88	87.36	96.61	721.84
1.25	70.00	77.06	992.38	87.31	93.07	1,159.20

TABLE 6.2 Variation of Fluid and Surface Temperatures and Heat transfer Coefficient Along the Tube Test Section in Convection for 20 % by wt. LiBr Solution .

	CONVECTION DATA FOR 20% BY WT. LiBr AT Q=1.0 GPM AND q=1112 W			CONVECTION DATA FOR 20% BY WT. LiBr AT Q=1.0 GPM AND q=1035 W		
DISTANCE FROM TUBE INLET IN m	FLUID MEAN TEMPERATURE IN °C	SURFACE TEMPERATURE IN °C	HEAT TRANSFER COEFFICIENT W/m²K	FLUID MEAN TEMPERATURE IN °C	SURFACE TEMPERATURE IN °C	HEAT TRANSFER COEFFICIENT W/m²K
0.05	69.48	76.13	1,038.62	94.23	98.97	1,356.24
0.10	69.65	76.97	943.56	94.36	99.72	1,199.36
0.15	69.84	78.57	791.16	94.62	101.31	960.92
0.20	70.07	79.21	755.67	94.85	101.88	914.45
0.25	70.53	80.54	689.99	95.31	103.07	828.42
0.30	70.57	81.44	635.40	95.22	104.03	729.69
0.35	69.95	82.05	570.81	94.93	104.32	684.62
0.40	70.72	83.22	552.55	95.42	105.45	640.93
0.45	70.83	83.16	560.16	95.60	105.30	662.74
0.50	71.59	83.48	580.89	96.10	105.52	682.44
0.55	71.71	84.16	554.77	96.28	106.22	646.74
0.60	71.77	84.43	545.56	96.28	106.54	626.57
0.65	72.50	85.04	550.78	96.84	107.01	632.11
0.70	72.50	85.06	549.91	96.81	106.97	632.73
0.75	72.18	84.34	568.00	96.42	107.64	572.96
0.80	72.49	84.50	575.09	96.74	107.63	590.32
0.85	72.57	84.79	565.21	96.85	108.08	572.45
0.90	72.93	84.20	612.85	97.15	107.39	627.79
0.95	73.54	83.58	687.93	97.60	106.64	711.13
1.00	73.77	83.96	677.80	98.56	107.26	738.92
1.05	74.48	84.55	685.88	99.09	107.95	725.57
1.10	75.62	85.10	728.57	100.10	108.62	754.53
1.15	74.47	85.19	644.29	99.05	108.61	672.44
1.20	74.65	85.32	647.31	99.28	108.76	678.12
1.25	74.40	85.32	632.49	99.14	108.76	668.25

TABLE 6.3 Variation of Fluid and Surface Temperatures and Heat transfer Coefficient Along the Tube Test Section in Convection for 30 % by wt. LiBr Solution .

	CONVECTION DATA FOR 30 % BY WT. LiBr AT q=1072 W AND Q=.93 GPM		
DISTANCE FROM TUBE INLET IN m	FLUID MEAN TEMPERATURE IN °C	SURFACE TEMPERATURE IN °C	HEAT TRANSFER COEFFICIENT W/m²K
0.05	82.24	88.02	1,151.97
0.10	82.41	88.92	1,022.79
0.15	82.69	90.50	852.55
0.20	82.99	91.16	814.98
0.25	83.58	92.87	716.73
0.30	83.60	93.86	648.97
0.35	82.99	94.35	586.13
0.40	84.56	95.55	605.86
0.45	83.80	95.36	575.98
0.50	83.68	95.63	557.19
0.55	84.79	96.33	576.98
0.60	84.81	96.56	566.67
0.65	85.58	97.06	580.00
0.70	85.50	97.03	577.48
0.75	85.19	96.65	581.01
0.80	85.64	96.65	604.76
0.85	85.78	96.91	598.24
0.90	86.14	96.18	663.19
0.95	86.60	95.35	760.96
1.00	86.61	95.86	719.83
1.05	87.21	97.20	666.51
1.10	88.61	96.54	839.65
1.15	87.27	97.33	661.87
1.20	87.48	97.59	658.59
1.25	87.36	97.59	650.87

TABLE 6.4 Variation of Fluid and Surface Temperatures and Heat transfer Coefficient Along the Boiling Tube in Convection for 35 % by wt. LiBr Solution .

	CONVECTION DATA FOR 35 % BY WT. LiBr AT Q=.95 GPM AND q=1106 W			CONVECTION DATA FOR 35 % BY WT. LiBr AT Q=.89 GPM AND q=1054 W		
DISTANCE FROM TUBE INLET IN m	FLUID MEAN TEMPERATURE IN °C	SURFACE TEMPERATURE IN °C	HEAT TRANSFER COEFFICIENT W/m²K	FLUID MEAN TEMPERATURE IN °C	SURFACE TEMPERATURE IN °C	HEAT TRANSFER COEFFICIENT W/m²K
0.05	71.06	77.34	1,093.88	90.12	95.90	1,132.63
0.10	71.41	78.58	958.10	90.40	97.10	977.10
0.15	71.52	80.53	762.44	90.56	98.95	780.28
0.20	71.74	81.24	723.11	90.88	99.60	750.76
0.25	72.30	82.84	651.76	91.74	101.06	702.42
0.30	72.44	83.88	600.49	91.77	102.12	632.52
0.35	71.46	84.55	524.79	90.92	102.37	571.75
0.40	74.00	85.86	579.22	92.91	103.29	630.69
0.45	72.79	85.68	532.94	91.85	102.77	599.50
0.50	72.68	85.98	516.51	91.56	102.65	590.31
0.55	73.95	86.60	543.05	92.68	102.97	636.21
0.60	73.88	86.75	533.77	92.84	102.99	644.98
0.65	74.75	87.17	553.11	93.57	103.30	672.82
0.70	74.68	87.12	552.22	93.63	103.20	684.07
0.75	74.46	87.00	547.81	93.49	104.08	618.19
0.80	74.75	87.11	555.79	93.73	104.26	621.71
0.85	74.85	87.49	543.48	94.00	104.72	610.69
0.90	75.27	86.86	592.71	94.42	103.95	686.94
0.95	76.05	86.20	676.80	95.01	103.20	799.34
1.00	75.85	86.66	635.48	95.32	103.81	771.09
1.05	76.64	87.93	608.46	96.02	105.15	717.04
1.10	77.82	87.30	724.64	96.86	104.28	882.29
1.15	76.66	87.97	607.39	96.18	104.80	759.46
1.20	76.72	88.20	598.39	96.23	104.69	773.83
1.25	76.66	88.20	595.28	96.30	104.69	780.28

TABLE 6.5 Variation of Fluid and Surface Temperatures and Heat transfer Coefficient Along the Boiling Tube in Convection and Subcooled Boiling for 40 % by wt. LiBr Solution .

	CONVECTION DATA FOR 40 % BY WT. LiBr AT Q=.87 GPM AND q=1058 W			SUBCOOLED DATA FOR 40 % BY WT. LiBr AT Q=.50 GPM AND q=1036 W		
DISTANCE FROM TUBE INLET IN m	FLUID MEAN TEMPERATURE IN °C	SURFACE TEMPERATURE IN °C	HEAT TRANSFER COEFFICIENT W/m²K	FLUID MEAN TEMPERATURE IN °C	SURFACE TEMPERATURE IN °C	HEAT TRANSFER COEFFICIENT W/m²K
0.05	84.82	91.71	953.76	93.14	99.15	1,070.68
0.10	85.29	93.05	846.83	94.02	100.11	1,056.61
0.15	85.46	95.07	683.81	93.99	101.44	863.73
0.20	85.89	95.89	657.14	94.53	101.66	902.49
0.25	86.37	97.37	597.40	95.08	102.53	863.73
0.30	86.51	98.33	555.96	95.30	103.06	829.22
0.35	85.65	98.81	499.35	94.69	103.01	773.41
0.40	87.81	100.02	538.20	97.16	103.86	960.42
0.45	86.81	99.78	506.66	96.57	103.24	964.74
0.50	86.65	100.06	490.04	96.21	103.40	894.96
0.55	88.04	100.71	518.66	97.70	103.90	1,037.87
0.60	88.08	100.95	510.60	98.05	104.48	1,000.74
0.65	88.77	101.37	521.54	98.73	105.00	1,026.28
0.70	88.72	101.25	524.46	98.97	104.92	1,081.48
0.75	88.48	100.77	534.70	98.58	106.76	786.65
0.80	88.88	100.71	555.49	99.35	107.13	827.09
0.85	89.15	101.16	547.16	99.52	107.48	808.39
0.90	89.61	100.50	603.44	99.98	107.00	916.64
0.95	90.39	99.73	703.58	100.61	106.32	1,126.93
1.00	89.97	100.38	631.26	101.23	107.36	1,049.72
1.05	90.71	101.83	590.96	102.15	109.07	929.88
1.10	92.10	101.19	722.93	102.41	108.18	1,115.21
1.15	90.75	101.94	587.26	102.61	108.31	1,128.91
1.20	90.87	102.07	586.73	103.20	108.12	1,307.88
1.25	90.71	102.07	578.47	103.17	108.12	1,299.96

TABLE 6.6 Variation of Fluid and Surface Temperatures and Heat transfer Coefficient Along the Boiling Tube in Convection for 45 % by wt. LiBr Solution .

	CONVECTION DATA FOR 45 % BY WT. LiBr AT Q=.72 GPM AND q=1136 W			CONVECTION DATA FOR 45 % BY WT. LiBr AT Q=.70 GPM AND q=1086 W		
DISTANCE FROM TUBE INLET IN m	FLUID MEAN TEMPERATURE IN °C	SURFACE TEMPERATURE IN °C	HEAT TRANSFER COEFFICIENT W/m²K	FLUID MEAN TEMPERATURE IN °C	SURFACE TEMPERATURE IN °C	HEAT TRANSFER COEFFICIENT W/m²K
0.050	59.860	67.560	916.351	75.370	82.640	927.832
0.100	60.680	69.350	813.829	76.050	84.260	821.601
0.150	60.430	71.580	632.816	76.050	86.400	651.724
0.200	60.760	72.490	601.526	76.390	87.290	618.839
0.250	61.440	74.150	555.146	77.140	88.730	581.997
0.300	61.810	74.890	539.442	77.440	89.550	557.006
0.350	60.460	75.290	475.786	76.280	89.770	500.025
0.400	63.780	76.030	575.992	79.080	90.490	591.178
0.450	62.350	75.740	526.953	77.980	90.100	556.546
0.500	62.220	75.820	518.816	77.920	90.090	554.260
0.550	63.850	76.230	569.944	79.290	90.470	603.340
0.600	64.050	76.210	580.255	79.820	90.660	622.264
0.650	64.960	76.690	601.526	80.470	91.240	626.308
0.700	65.240	76.750	613.024	80.960	91.380	647.346
0.750	64.820	76.960	581.211	80.490	91.740	599.586
0.800	65.130	77.100	589.465	81.260	91.910	633.365
0.850	65.670	77.690	587.013	81.020	92.650	579.995
0.900	66.230	77.350	634.523	81.600	92.110	641.802
0.950	67.020	76.990	707.713	82.580	91.550	751.989
1.000	66.220	77.710	614.091	81.990	92.390	648.591
1.050	67.360	79.080	602.039	83.120	93.940	623.414
1.100	67.830	78.560	657.586	84.430	93.420	750.316
1.150	67.560	79.330	599.482	83.390	94.300	618.271
1.200	67.600	79.460	594.933	83.410	94.510	607.688
1.250	67.730	79.460	601.526	83.170	94.510	594.827

TABLE 6.7 Variation of Fluid and Surface Temperatures and Heat transfer Coefficient Along the Boiling Tube in Convection for 50 % by wt. LiBr Solution .

	CONVECTION DATA FOR 50 % BY WT. LiBr AT Q=1.0 GPM AND q=1081 W			CONVECTION DATA FOR 50 % BY WT. LiBr AT Q=.75 GPM AND q=1001 W		
DISTANCE FROM TUBE INLET IN m	FLUID MEAN TEMPERATURE IN °C	SURFACE TEMPERATURE IN °C	HEAT TRANSFER COEFFICIENT W/m²K	FLUID MEAN TEMPERATURE IN °C	SURFACE TEMPERATURE IN °C	HEAT TRANSFER COEFFICIENT W/m²K
0.050	73.210	80.760	889.309	98.340	106.230	788.009
0.100	73.630	82.130	789.916	98.840	107.570	712.187
0.150	73.690	84.190	639.456	98.900	109.660	577.824
0.200	73.980	85.040	607.078	99.180	110.290	559.621
0.250	74.760	86.640	565.176	99.630	111.960	504.249
0.300	74.990	87.770	525.374	99.720	112.540	484.976
0.350	73.910	88.330	465.623	99.070	112.640	458.172
0.400	74.910	89.370	464.335	101.220	113.490	506.715
0.450	74.940	89.260	468.875	100.570	113.290	488.789
0.500	76.020	89.550	496.252	100.150	113.440	467.825
0.550	76.060	90.170	475.853	101.540	113.970	500.192
0.600	76.270	90.350	476.867	101.000	114.110	474.248
0.650	77.110	90.850	488.667	102.410	114.500	514.259
0.700	77.040	90.870	485.487	102.550	114.630	514.685
0.750	76.570	90.510	481.656	102.450	114.610	511.299
0.800	76.780	90.480	490.094	103.480	114.320	573.560
0.850	76.730	90.500	487.602	102.800	115.100	505.479
0.900	77.100	89.770	529.936	103.390	114.470	561.136
0.950	77.760	89.060	594.185	104.490	113.690	675.803
1.000	78.010	89.480	585.378	104.830	114.640	633.781
1.050	78.890	89.850	612.617	105.740	116.380	584.341
1.100	80.280	90.530	655.052	106.810	115.690	700.157
1.150	78.850	90.350	583.851	106.040	116.610	588.211
1.200	78.980	90.460	584.868	106.240	116.600	600.134
1.250	78.740	90.400	821.822	106.100	116.600	1,157.801

Table 8.8 Experimental and Predicted Nusselt Number and the Percentage Difference Between Them.

Nu EXPERIMENTAL	Nu CALCULATED	% ERROR	Nu EXPERIMENTAL	Nu CALCULATED	% ERROR
34.25	39.44	15.15	39.61	36.11	8.84
38.46	44.17	14.87	38.20	41.52	8.71
34.49	39.58	14.77	38.34	41.53	8.32
38.40	44.02	14.64	40.64	37.26	8.32
34.54	39.58	14.58	36.86	39.91	8.27
36.63	41.80	14.12	38.76	35.56	8.25
36.70	41.84	14.02	39.02	35.82	8.20
38.73	44.12	13.92	42.54	39.06	8.18
36.51	41.57	13.86	41.15	44.50	8.15
38.77	44.11	13.80	39.31	36.12	8.11
36.49	41.48	13.68	36.48	39.40	8.02
34.83	39.42	13.19	40.34	37.12	7.96
37.05	41.90	13.09	38.73	35.68	7.87
34.54	38.92	12.69	42.50	39.19	7.77
37.32	41.99	12.51	38.48	41.44	7.69
40.80	35.75	12.38	43.74	40.37	7.69
37.10	41.54	11.95	42.45	39.19	7.67
37.56	42.00	11.82	41.49	44.54	7.35
37.50	41.93	11.81	36.50	39.18	7.35
35.44	39.59	11.71	40.15	37.21	7.31
37.69	41.94	11.28	42.16	39.09	7.29
39.64	44.02	11.06	40.44	37.52	7.24
40.07	35.71	10.89	36.67	39.32	7.22
35.64	39.52	10.89	37.44	40.12	7.18
41.58	37.08	10.82	43.58	40.59	6.88
43.38	38.92	10.28	42.39	39.48	6.87
41.39	37.22	10.06	39.79	37.09	6.79
36.07	39.58	9.73	38.10	35.53	6.73
41.07	37.16	9.51	40.09	37.41	6.68
38.21	41.80	9.40	39.02	41.61	6.63
42.95	38.92	9.38	39.61	36.99	6.61
35.93	39.19	9.07	36.88	39.31	6.60
39.72	36.14	9.03	43.36	40.62	6.30
39.24	35.73	8.95	39.53	37.26	5.75
40.89	44.52	8.87	41.09	38.73	5.74

Continuation of Table 8.8

Mu EXPERIMENTAL	Mu CALCULATED	% ERROR
38.12	40.25	5.61
44.84	42.36	5.54
44.79	42.31	5.53
44.77	42.33	5.44
38.98	36.88	5.39
42.86	40.60	5.26
34.82	36.65	5.26
38.12	40.12	5.25
36.46	38.38	5.25
38.28	40.27	5.20
41.83	43.99	5.17
39.08	37.10	5.08
36.45	38.30	5.06
36.54	38.35	4.95
36.54	38.35	4.95
41.41	39.37	4.92
36.57	38.36	4.89
38.36	40.20	4.77
39.61	41.43	4.60
40.99	39.14	4.53
37.61	39.26	4.40
35.26	36.76	4.27
40.42	38.70	4.26
40.41	38.72	4.18
40.86	39.15	4.17
38.47	36.91	4.04
40.90	39.32	3.86
38.75	37.27	3.82
36.86	38.22	3.71
41.20	39.69	3.65
38.94	37.53	3.63
41.15	39.72	3.49
35.48	36.71	3.46
38.41	39.66	3.26
39.48	38.20	3.25

Mu EXPERIMENTAL	Mu CALCULATED	% ERROR
38.18	36.97	3.17
38.16	36.95	3.16
40.43	39.17	3.11
40.74	42.00	3.11
38.57	37.38	3.08
38.49	37.39	2.86
42.55	41.42	2.64
38.09	37.09	2.62
36.37	37.32	2.60
37.93	36.96	2.58
37.26	38.21	2.56
36.47	37.37	2.47
38.45	39.39	2.43
36.51	37.35	2.29
40.58	39.69	2.21
39.47	40.31	2.12
38.14	37.37	2.01
38.27	37.53	1.96
38.97	38.45	1.35
37.48	37.00	1.29
34.86	35.27	1.19
40.48	40.00	1.19
37.95	37.50	1.17
36.79	37.17	1.04
39.56	39.95	0.97
39.91	40.28	0.93
37.16	36.84	0.87
40.30	39.96	0.84
39.05	39.34	0.74
42.08	41.91	0.39
37.38	37.52	0.39
41.72	41.88	0.38
37.67	37.53	0.38
42.03	41.90	0.30
37.49	37.50	0.01

TABLE 6.9 Variation of Fluid and Surface Temperature and Heat Transfer Coefficient Along the Tube Test Section in Subcooled boiling for 30% by wt. LiBr .

SUBCOOLED BOILING DATA FOR 30% BY WT. LiBr AT Q=.59 GPM AND q=993 W			
DISTANCE FROM TUBE INLET IN m	FLUID MEAN TEMPERATURE IN °C	SURFACE TEMPERATURE IN °C	HEAT TRANSFER COEFFICIENT W/m² K
0.05	107.44	112.85	1,140.06
0.10	107.78	113.95	999.63
0.15	107.93	115.81	782.70
0.20	108.19	116.35	755.85
0.25	108.93	117.59	712.21
0.30	108.98	118.07	678.52
0.35	108.61	117.95	660.35
0.40	109.83	118.71	694.56
0.45	109.97	118.22	747.60
0.50	110.50	118.22	798.93
0.55	110.96	118.77	789.72
0.60	110.99	118.94	775.81
0.65	111.75	119.39	807.29
0.70	111.87	119.48	810.47
0.75	111.78	119.39	810.47
0.80	112.22	119.58	838.00
0.85	112.41	120.27	784.69
0.90	112.73	119.56	903.03
0.95	113.12	118.69	1,107.31
1.00	113.20	119.51	977.45
1.05	114.04	119.85	1,061.57
1.10	114.29	120.90	933.09
1.15	114.35	120.39	1,021.14
1.20	114.97	119.86	1,261.29
1.25	115.16	119.86	1,312.28

TABLE 6.10 Variation of Fluid and Surface Temperature and Heat Transfer Coefficient Along the Test Seaction Tube in Subcooled Boiling for 45% by wt. LiBr .

SUBCOOLED BOILING DATA FOR 45% BY WT. LiBr AT Q=.55 GPM AND q=1011 W			
DISTANCE FROM TUBE INLET IN m	FLUID MEAN TEMPERATURE IN °C	SURFACE TEMPERATURE IN °C	HEAT TRANSFER COEFFICIENT W/m² K
0.050	101.310	107.340	1,041.377
0.100	101.840	107.970	1,024.389
0.150	102.160	109.220	889.448
0.200	102.540	109.160	948.565
0.250	103.430	109.960	961.639
0.300	103.360	110.610	866.138
0.350	103.730	110.760	893.244
0.400	105.170	111.480	995.167
0.450	104.890	111.340	973.566
0.500	104.980	111.470	967.566
0.550	106.030	112.260	1,007.946
0.600	106.310	112.620	995.167
0.650	106.960	112.920	1,053.608
0.700	107.190	113.440	1,004.720
0.750	107.180	113.580	981.172
0.800	107.920	113.680	1,090.192
0.850	108.340	114.480	1,022.720
0.900	108.700	113.660	1,266.029
0.950	109.020	112.910	1,614.268
1.000	109.990	113.820	1,639.557
1.050	110.030	114.960	1,273.733
1.100	109.860	114.280	1,420.702
1.150	110.250	115.030	1,313.704
1.200	110.730	114.900	1,505.876
1.250	110.910	114.900	1,573.810

TABLE 6.11 Variation of Fluid and Surface Temperature and Heat Transfer Coefficient Along the Test Seaction Tube in Saturated Boiling for 35% by wt. LiBr .

SATURATED BOILING DATA FOR 35% BY WT. LiBr AT Q=.6 GPM AND q=1012 W				
DISTANCE FROM TUBE INLET IN m	FLUID MEAN TEMPERATURE IN °C	SURFACE TEMPERATURE IN °C	HEAT TRANSFER COEFFICIENT W/m² K	VAPOR QUALITY x
0.050	102.570	108.800	1,008.943	0.000
0.100	102.630	109.800	901.824	0.000
0.150	102.900	111.270	750.981	0.000
0.200	103.180	111.460	759.144	0.000
0.250	104.010	112.360	752.780	0.000
0.300	104.030	112.730	722.496	0.000
0.350	104.080	112.470	749.191	0.000
0.400	105.550	113.340	806.895	0.000
0.450	105.320	113.120	805.861	0.000
0.500	105.450	113.220	808.972	0.000
0.550	106.400	113.890	839.214	0.000
0.600	106.820	114.200	851.723	0.000
0.650	107.340	114.710	852.878	0.000
0.700	107.790	114.710	908.340	0.000
0.750	107.870	114.400	962.590	0.000
0.800	108.520	114.660	1,023.732	0.000
0.850	108.880	115.300	979.083	0.000
0.900	109.230	114.390	1,218.162	0.000
0.950	109.810	113.580	1,667.298	0.000
1.000	110.600	113.770	1,982.875	0.000
1.050	111.150	114.400	1,934.066	0.000
1.100	111.180	113.120	3,240.059	0.037
1.150	111.140	113.030	3,325.775	0.081
1.200	111.220	112.610	4,522.097	0.112
1.250	111.170	112.610	4,365.079	0.158

TABLE 6.12 Variation of Fluid and Surface Temperature and Heat Transfer Coefficient Along the Test Seaction Tube in Saturated Boiling for 40% by wt. LiBr .

SATURATED BOILING DATA FOR 40% BY WT. LiBr AT G=.43 GPM AND q=1017 W				
DISTANCE FROM TUBE INLET IN m	FLUID MEAN TEMPERATURE IN °C	SURFACE TEMPERATURE IN °C	HEAT TRANSFER COEFFICIENT W/m² K	VAPOR QUALITY x
0.050	99.080	106.160	892.199	0.000
0.100	99.710	107.010	865.311	0.000
0.150	99.860	108.410	738.804	0.000
0.200	100.460	108.600	776.016	0.000
0.250	101.070	109.410	757.406	0.000
0.300	101.210	109.940	723.570	0.000
0.350	101.480	110.020	739.669	0.000
0.400	102.990	111.040	784.692	0.000
0.450	102.900	110.800	799.591	0.000
0.500	103.230	111.030	809.842	0.000
0.550	104.360	111.840	844.488	0.000
0.600	104.890	112.220	861.769	0.000
0.650	105.510	112.750	872.482	0.000
0.700	105.890	112.850	907.582	0.000
0.750	106.190	113.030	923.504	0.000
0.800	107.250	113.400	1,027.117	0.000
0.850	107.750	113.920	1,023.788	0.000
0.900	108.150	113.070	1,283.896	0.000
0.950	108.600	112.350	1,684.472	0.000
1.000	110.040	112.930	2,185.734	0.000
1.050	110.780	113.910	2,018.137	0.000
1.100	110.680	112.720	3,096.456	0.063
1.150	110.840	112.790	3,239.369	0.098
1.200	110.840	112.360	4,155.770	0.150
1.250	110.840	112.360	4,155.770	0.202

TABLE 6.13 Variation of Fluid and Surface Temperature and Heat Transfer Coefficient Along the Test Seaction Tube in Saturated Boiling for 50% by wt. LiBr .

	SATURATED BOILING DATA FOR Q=.52 GPM AND q= 961 W			SMOOTH BOILING DATA			
DISTANCE FROM TUBE INLET IN m	FLUID MEAN TEMPERATURE IN °C	SURFACE TEMPERATURE IN °C	HEAT TRANSFER COEFFICIENT W/m² K	FLUID MEAN TEMPERATURE IN °C	SURFACE TEMPERATURE IN °C	HEAT TRANSFER COEFFICIENT W/m² K	VAPOR QUALITY x
0.050	117.130	122.190	1,179.633	116.874	122.743	1,016.907	0.000
0.100	117.710	122.660	1,205.847	117.264	123.299	988.977	0.000
0.150	117.710	124.010	967.451	117.743	123.886	971.639	0.000
0.200	118.390	123.990	1,065.883	118.238	124.433	963.451	0.000
0.250	118.910	125.250	961.474	118.715	124.915	962.818	0.000
0.300	118.970	126.140	832.489	119.168	125.330	968.554	0.000
0.350	118.520	125.870	812.101	119.602	125.692	980.156	0.000
0.400	120.410	126.680	951.985	120.032	126.013	997.963	0.000
0.450	120.000	126.420	929.742	120.470	126.303	1,023.236	0.000
0.500	120.240	126.470	958.097	120.925	126.566	1,058.234	0.000
0.550	121.710	127.000	1,128.345	121.401	126.796	1,106.325	0.000
0.600	121.980	127.270	1,128.345	121.892	126.984	1,172.211	0.000
0.650	122.550	127.660	1,168.091	122.387	127.116	1,262.330	0.000
0.700	123.030	127.730	1,269.988	122.870	127.178	1,385.497	0.000
0.750	123.190	127.380	1,424.569	123.320	127.161	1,553.748	0.000
0.800	123.900	127.010	1,919.275	123.717	127.065	1,783.072	0.000
0.850	124.320	127.100	2,147.102	124.045	126.897	2,092.865	0.000
0.900	124.370	126.030	3,595.749	124.291	126.678	2,500.756	0.038
0.950	124.200	125.800	3,730.590	124.451	126.437	3,005.833	0.096
1.000	124.530	126.000	4,060.506	124.531	126.210	3,555.136	0.109
1.050	124.460	126.270	3,297.759	124.547	126.032	4,020.074	0.158
1.100	124.650	126.550	3,141.550	124.527	125.926	4,266.002	0.183
1.150	124.670	125.950	4,663.238	124.507	125.888	4,319.259	0.224
1.200	124.380	125.800	4,203.482	124.528	125.868	4,455.767	0.293
1.250	124.220	125.900	3,552.943	124.635	125.740	5,402.004	0.351

TABLE 6.14 Variation of Fluid and Surface Temperature and Heat Transfer Coefficient Along the Test Seaction Tube in Saturated Boiling for 20% by wt. LiBr .

	ACTUAL BOILING DATA AT Q=.45 GPM AND q= 1001 W			SMOOTH BOILING DATA			
DISTANCE FROM TUBE INLET IN m	FLUID MEAN TEMPERATURE IN °C	SURFACE TEMPERATURE IN °C	HEAT TRANSFER COEFFICIENT W/m² K	FLUID MEAN TEMPERATURE IN °C	SURFACE TEMPERATURE IN °C	HEAT TRANSFER COEFFICIENT W/m² K	VAPOR QUALITY x
0.05	107.68	113.78	1,019.24	107.68	113.78	1,019.24	0.00
0.10	108.02	114.49	960.96	108.02	114.49	960.96	0.00
0.15	108.23	115.89	811.67	108.23	115.89	811.67	0.00
0.20	108.63	115.94	850.53	108.63	115.94	850.53	0.00
0.25	109.18	116.53	845.90	109.18	116.53	845.90	0.00
0.30	109.27	116.82	823.50	109.27	116.82	823.50	0.00
0.35	109.29	116.39	875.69	109.29	116.39	875.69	0.00
0.40	110.70	116.98	990.03	110.70	116.98	990.03	0.00
0.45	110.64	116.68	1,029.37	110.64	116.68	1,029.37	0.00
0.50	110.57	116.53	1,043.19	110.57	116.53	1,043.19	0.00
0.55	111.37	116.70	1,166.49	111.37	116.70	1,166.49	0.00
0.60	111.76	115.98	1,473.32	111.76	115.98	1,473.32	0.00
0.65	112.17	115.32	1,973.78	112.17	114.30	2,916.99	0.00
0.70	112.58	114.38	3,454.11	112.58	114.18	3,881.70	0.00
0.75	112.34	113.85	4,117.48	112.34	114.06	3,610.56	0.11
0.80	112.46	113.67	5,138.34	112.46	113.94	4,194.48	0.15
0.85	112.33	114.05	3,614.76	112.38	113.82	4,319.49	0.23
0.90	112.25	113.34	5,704.03	112.35	113.70	4,607.80	0.30
0.95	112.21	112.45	25,905.80	112.32	113.58	4,937.34	0.37
1.00	112.46	112.90	14,130.43	112.29	113.46	5,317.65	0.44
1.05	112.37	112.90	11,730.93	112.26	113.34	5,761.43	0.51
1.10	112.50	113.69	5,224.70	112.23	113.22	6,286.03	0.58
1.15	112.15	113.34	5,224.70	112.21	113.10	6,915.74	0.65
1.20	112.07	113.39	4,710.14	112.18	112.98	7,685.66	0.72
1.25	112.04	113.30	4,934.44	112.15	112.86	8,648.48	0.79

TABLE 6.15 Variation of Fluid and Surface boiling Temperature and Heat Transfer Coefficient Along the Tube Test Section in Saturated Boiling for 10% by wt. LiBr .

	ACTUAL BOILING DATA AT Q=.36 GPM AND q= 988 W			SMOOTH BOILING DATA			
DISTANCE FROM TUBE INLET IN m	FLUID MEAN TEMPERATURE IN °C	SURFACE TEMPERATURE IN °C	HEAT TRANSFER COEFFICIENT W/m² K	FLUID MEAN TEMPERATURE IN °C	SURFACE TEMPERATURE IN °C	HEAT TRANSFER COEFFICIENT W/m² K	VAPOR QUALITY x
0.05	118.45	119.38	6,598.54	118.39	119.32	6,602.45	0.00
0.10	118.21	118.73	11,801.24	118.35	119.26	6,719.20	0.13
0.15	118.38	119.11	8,406.36	118.30	119.20	6,840.16	0.16
0.20	118.40	118.90	12,273.29	118.26	119.14	6,965.55	0.23
0.25	118.34	119.30	6,392.34	118.22	119.08	7,095.62	0.31
0.30	117.99	119.51	4,037.27	118.17	119.02	7,230.64	0.47
0.35	118.17	118.90	8,406.36	118.13	118.96	7,370.90	0.50
0.40	117.90	119.47	3,908.69	118.08	118.90	7,516.71	0.63
0.45	118.08	118.97	6,895.11	118.04	118.84	7,668.41	0.66
0.50	118.16	118.63	13,056.69	118.00	118.78	7,826.36	0.71
0.55	117.98	118.85	7,053.62	117.95	118.72	7,990.94	0.83
0.60	117.85	118.95	5,578.77	117.91	118.66	8,162.60	0.93
0.65	117.83	118.92	5,629.95	117.86	118.60	8,341.80	1.01
0.70	117.84	118.83	6,198.63	117.82	118.54	8,529.04	1.07
0.75	117.60	118.13	11,578.58	117.78	118.48	8,724.88	1.20
0.80	117.75	118.10	17,533.27	117.73	118.42	8,929.93	1.24
0.85	117.61	118.55	6,528.35	117.69	118.36	9,144.84	1.34
0.90	117.54	117.87	18,595.90	117.65	118.30	9,370.36	1.43
0.95	117.57	117.04	(11,578.58)	117.60	118.24	9,607.27	1.50
1.00	117.62	117.61	(613,664.60)	117.56	118.18	9,856.48	1.55
1.05	117.58	117.77	32,298.14	117.51	118.12	10,118.96	1.64
1.10	117.67	118.48	7,576.11	117.47	118.06	10,395.81	1.69
1.15	117.40	118.23	7,393.55	117.43	118.00	10,688.23	1.82
1.20	117.33	118.38	5,844.42	117.38	117.94	10,997.57	1.91
1.25	117.37	118.38	6,075.89	117.34	117.88	11,325.36	1.97

CHAPTER IX

CONCLUSION AND RECOMMENDATION

9.1 CONCLUSION

The present investigation consisted mainly of two parts, the first was to fabricat an apparatus which can be utilized to collect forced convection and boiling data , and the second was to collect the heat transfer data for different concentrations of lithium bromide-water solutions followed by analysing and correlating these data .

In the design part, the apparatus shown in figure 2.1 was fabricated with 75 psi working pressure and flow rate of 1 GPM. The heater in the test section is 1200 W and that in the preheater is 3600 W.

The important part of the apparatus is the tube test section in which 25 thermocouples were used to measure the fluid temperature while another 25 thermocouples were used to

measure the surface temperature . These thermocouples were connected to a computer system which converts the input data to a temperature data and saves them . The apparatus was tested in the begining then it was used to collect the experimental data.

In the study , two heat transfer regions were identified in convection . These are the entrance region where the temperature profile is developing and the fully developed region where the difference between the tube surface temperature and the fluid mean temperature is constant . In the entrance region, heat transfer , for example , for 20% LiBr by weight , decreased sharply from 1350 W/m^2 k until it reached a constant value of about 650 W/m^2k corresponding to the fully developed region . Data for convection heat transfer were correlated by equation (8.6) which described the data with mean squre error of 8.6 and standard deviation of ± 2.9 . Almost 86 % of the calculated data fall withen ±12 % of the experimental values. Equation 8.6 agrees with Dittus and Boelter equation withen 7 % in case of water.

In boiling also two heat transfer regions were detected. These are subcooled boiling and saturated boiling region . Subcooled boiling zone started, where convection terminated, at a point where surface temperature is almost equal to the saturated temperature of the fluid. Saturated boiling started at a point where the fluid temperature gradient is almost zero or the mean temperature of the fluid is equal to the

saturated temperature. The degree of superheat at this point is about 3° C .

In case of surface boiling , it was found that the maximum heat transfer coefficient that can be reached in this case is about five times that of convection with approximately the same flow rate and concentration . For example, the maximum heat transfer coefficient in the SCB for 35% LiBr by weight is 2300 W/m^2 k while the calculated one for convection at the same flow rate and heat added is only 420 W/m^2 k .

Boiling heat transfer data were correlated to the convection heat transfer coiefficient by equation (8.7) which describes the experimental data within ± 12% .

In both convection and boiling , the heat transfer coefficient was a strong function of concentration . The effect of concentration was included in the correlations.

9.2 RECOMMENDATION

The main objective of this project is to study the heat transfer of lithium bromide water solutions in order to understand their behavior in the generator and absorber.Such a knowledge may help to increase the coefficient of

performance of the heat pumps utilizing such solutions. Thus, a study on LiBr-water solution need to be conducted with higher vapor quality solutions . For this reason, some design modifications are needed to be able to utilize the apparatus more efficiently . These modifications are listed in the following points .

1- Improve the data acquisition system to read the data more accurately as the present system needed calibration each time data have to be taken . In addition to that, data which are taken by the computer are stored in a tape which is not compatible with other computers . This necessitated manual data punching in this invistigation.

2- In order to operate the apparatus at higher quality , high power heaters are needed to be installed. Special care must be taken when installing these heaters to maintain uniform heating on the entire tube .

APPENDEX A

PROPERTIES OF LiBr-WATER SOLUTION

In this appendex , various properties of LiBr-water solution are presented to support the calculation in the data reduction chapter.

Table A4.3. Dew Point and Solution Temperature of Lithium Bromide Solutions [14].

% LiBr	A	B	Solution Temperatures, °F (t) 40	80	120	160	200	240	280	320	360
			Dew point Temperatures, °F (t')								
0	1.0000	0.00	40.0	80.0	120.0	160.0	200.0	240.0			
5	1.0033	0.56	39.3	79.2	119.1	158.9	198.8	238.7			
10	1.0072	1.21	38.5	79.2	118.0	157.7	197.4	237.1			
15	1.0113	2.01	37.6	77.1	116.7	156.2	195.8	235.3			
20	1.0170	3.11	36.3	75.6	114.9	154.3	193.6	232.9			
25	1.0248	4.75	34.4	73.4	112.5	151.5	190.5	229.6			
30	1.0348	7.00	31.9	70.6	109.2	147.9	186.5	225.2			
35	1.0497	10.4	28.2	66.3	104.4	142.5	180.6	218.7			
40	1.0678	15.0	23.4	60.9	98.3	135.8	173.2	210.7	248.2		
45	1.0906	21.7	16.8	53.4	90.1	126.8	163.5	200.1	236.9		
50	1.1164	33.0	6.2	42.1	77.9	113.7	149.6	185.4	221.2		
51	1.1216	35.6		39.6	75.2	110.9	146.6	182.2	217.9		
52	1.1265	38.4		37.0	72.5	108.0	143.5	179.0	214.5	250.0	
53	1.1318	41.3		34.2	69.6	104.9	140.3	175.6	210.9	246.3	
54	1.1364	44.3		31.4	66.6	101.8	137.0	172.2	207.4	242.6	
55	1.1410	47.4		28.6	63.6	98.7	133.7	168.8	203.9	238.9	
56	1.1457	50.7		25.7	60.6	95.5	130.4	165.3	200.2	235.1	
57	1.1506	53.9		22.7	57.5	92.2	127.0	161.8	196.5	231.3	
58	1.1556	57.2		19.7	54.3	88.9	123.6	158.2	192.8	227.4	
59	1.1611	60.5		16.8	51.2	85.7	120.1	154.6	189.0	223.5	
60	1.1673	63.9		13.8	48.0	82.3	116.6	150.8	185.1	219.4	
									181.1		
61	1.1747	67.3		10.8	44.9	78.9	113.0	147.1	181.1	215.1	249.2
62	1.1833	70.5		8.0	41.8	75.6	109.4	143.2	177.0	210.8	244.6
63	1.1926	73.9		5.1	38.7	72.2	105.8	139.3	172.8	206.4	239.9
64	1.2031	77.2		2.4	35.6	68.9	102.1	135.4	168.6	201.9	235.1
65	1.2154	80.3			32.6	65.6	98.5	131.4	164.3	197.2	230.1
66	1.2298	83.4			29.8	62.3	94.8	127.3	159.9	192.4	224.9
67	1.2465	86.4			27.0	59.1	91.2	123.2	155.3	187.4	219.5
68	1.2648	89.3			24.3	55.9	87.6	119.2	150.8	182.4	214.0
69	1.2840	92.2			21.6	52.8	83.9	115.1	146.2	177.3	208.5
70	1.3049	95.1			19.1	49.8	80.4	111.1	141.7	172.4	203.1

EQUATIONS

$$t = (a_0 + a_1X + a_2X^2 + a_3X^3)t' + b_0 + b_1X + b_2X^2 + b_3X^3$$

where $a_0 = -2.00755$, $a_1 = 0.16976$, $a_2 = -3.133362E\text{-}3$, $a_3 = 1.97668E\text{-}5$

$b_0 = 321.128$, $b_1 = -19.322$, $b_2 = 0.374332$, $b_3 = -2.0637E\text{-}3$

Range: $0 \leq t' \leq 230F$, $40 \leq t \leq 350F$, $45\% \leq X \leq 70\%$

Table A4.4. Boiling Points of LiBr Solutions-Dew Point Comparison [14].

% LiBr X	Solution Temp. °F	Pressure Psia	Dew Point (observed)	Pennington Eq. D.P.	Pennington Eq. Dev.	Dühring Eq. D.P.	Dühring Eq. Dev.
50.31	270.31	14.52	211.4	211.7	0.3	211.4	0.0
50.57	270.81	14.49	211.3	211.2	-0.1	211.0	-0.3
52.55	278.50	14.57	211.6	211.2	-0.4	211.2	-0.4
54.06	283.51	14.33	210.7	210.3	-0.4	210.5	-0.2
55.28	289.39	14.44	211.1	211.1	0.0	211.3	0.2
56.71	296.07	14.41	211.0	211.6	0.6	211.9	0.9
57.29	298.22	14.48	211.3	211.3	0.0	211.6	0.3
58.60	304.78	14.56	211.5	211.9	0.4	212.2	0.7
59.67	308.61	14.42	211.1	210.9	-0.2	211.2	0.2
60.07	310.42	14.49	211.3	211.3	-0.4	211.1	-0.2
			Maximum deviation		0.6		0.9
			Average deviation		0.3		0.3

Table A4.5. Vapor Pressure of LiBr Solutions at 30.4 °C-Dew Point Comparison [14].

% LiBr	Pressure mm Hg.	Dew Point (observed)	Pennington Eq. D.P.	Pennington Eq. Dev.	Dühring Eq. D.P.	Dühring Eq. Dev.
50.00	8.39	47.5	49.3	1.8	48.1	0.6
51.30	7.76	45.5	45.2	-0.3	44.7	-0.8
52.02	7.02	42.9	43.1	0.2	42.7	-0.2
53.30	6.23	39.8	39.2	-0.6	39.2	-0.6
54.49	5.38	36.0	35.7	-0.3	35.9	-0.1
56.00	4.54	31.8	31.4	-0.4	31.5	-0.3
57.03	3.96	28.4	28.5	0.1	28.5	0.1
57.62	3.67	26.6	26.8	0.2	26.7	0.1
58.27	3.36	24.5	25.0	0.1	24.8	0.3
60.00	2.77	19.9	20.3	0.4	19.6	0.3
61.09	2.35	16.1	17.3	1.2	16.4	0.3
			Maximum deviation	1.8		0.8
			Average deviation	0.5		0.3

Table A4.6 Comparison of Equilliometric and Calculated Dew Points [14].

% LiBr X	Solution Temp. °F t	Pressure Psia P	Dew-point (actual) t'	Pennington eq. D.P. t'	Pennington eq. Dev. Δt'	Dühring Eq. D.P. t'	Dühring Eq. Dev. Δt'
50.10	175.30	2.03	126.6	127.7	1.1	127.1	0.5
	203.90	3.95	152.4	153.2	0.8	152.6	0.2
	222.27	6.09	170.7	169.6	1.1	169.1	1.6
	236.92	7.94	182.5	182.6	0.1	182.2	-0.3
	246.68	9.72	191.9	191.3	-0.6	190.9	-1.0
			Maximum deviation		1.1		1.6
			Average deviation		0.7		0.7
53.98	190.58	2.12	128.2	128.2	0.0	128.8	0.6
	217.90	3.99	152.8	152.3	-0.5	152.9	0.1
	236.72	5.92	169.4	169.0	-0.4	169.5	0.1
	250.35	7.77	181.5	181.1	-0.4	181.5	0.0
	263.99	10.11	193.7	193.2	-0.5	193.6	-0.1
			Maximum deviation		0.5		0.6
			Average deviation		0.4		0.2
56.02	194.60	1.97	125.5	125.0	-0.5	125.7	0.2
	224.70	3.90	151.9	151.3	-0.6	152.1	0.2
	243.50	5.80	168.6	167.9	-0.7	168.5	-0.1
	259.72	8.00	182.8	182.1	-0.7	182.7	-0.1
	270.39	9.87	192.6	191.5	-1.1	192.0	-0.6
			Maximum deviation		1.1		0.6
			Average deviation		0.7		0.2
58.06	209.14	2.22	129.9	130.9	1.0	131.5	1.6
	240.12	4.44	157.2	157.8	0.6	158.3	1.1
	258.67	6.53	173.7	173.2	-0.5	174.4	0.7
	272.18	8.51	185.7	185.6	-0.1	186.1	-0.4
	283.20	10.46	195.3	195.2	-0.1	195.6	0.3
			Maximum deviation		1.0		1.6
			Average deviation		0.6		0.6
60.73	215.45	1.99	125.8	127.5	1.7	127.3	1.5
	245.78	3.96	152.5	153.2	0.7	153.2	0.7
	263.10	5.68	167.7	167.9	0.2	167.9	0.2
	279.40	7.84	181.9	181.8	-0.1	181.8	-0.1
	290.34	9.64	191.5	191.1	-0.4	191.2	-0.3
			Maximum deviation		1.7		1.5
			Average deviation		0.6		0.6

Table A4.7 Summary of Deviation Per Tables A4.4 to A4.6 [14].

	Log P = A+B/T'+C/T'^{2}		t = At' + B	
	Ave. dev.	Max. dev.	Ave. dev.	Max. dev.
Table 3 Atmospheric boiling point, Δt'	0.3	0.6	0.3	0.9
Table 4 Vap. press. at 86.7°F, Δt'	0.5	1.8	0.3	0.8
Table 5 Ebullioscopic data, Δt'	0.6	1.7	0.5	1.6

Table A4.8 E.M Greeley Vapor Pressure Tata [14].

% LiBr X	Solution Temp. °F t	Dew Point observed t'	Dühring Eq. D.P. t'	Dühring Eq. Dev. Δt'
57.96	111.2	46.6	46.9	0.3
	103.8	40.0	40.5	0.5
	96.8	32.4	32.7	0.3
	90.5	29.0	29.0	0.0
	89.2	27.9	27.8	-0.1
	80.3	20.2	20.1	-0.1
	Maximum deviation			0.5
	Average deviation			0.2
59.52	109.4	40.6	40.5	-0.1
	106.5	39.1	39.0	-0.1
	100.0	32.5	32.5	0.0
	95.0	28.3	28.2	-0.1
	89.9	23.4*	22.1	-2.3*
	78.4	13.0*	10.5	-2.5*
	Maximum deviation			0.1
	Average deviation			0.1
60.29	121.2	48.0	48.3	0.3
	111.0	39.2	39.6	0.4
	98.8	29.0	29.1	0.1
	91.2	22.4	22.6	0.2
	81.0	12.0*	13.9	1.9*
	Maximum deviation			0.4
	Average deviation			0.3
61.30	123.0	46.0	46.6	0.6
	119.6	43.2	43.7	0.5
	118.0	42.0	42.4	0.4
	113.0	37.6	38.1	0.5
	110.4	35.2	35.9	0.7
	107.5	32.7	33.4	0.7
	Maximum deviation			0.7
	Average deviation			0.5
64.00	129.8	43.3	43.9	0.6
	122.0	36.7	37.4	0.6
	117.8	33.4	33.9	0.5
	110.0	27.0	27.4	0.4
	106.0	23.4	24.1	0.7
	99.5	18.2	18.7	0.5
	Maximum deviation			0.7
	Average deviation			0.6

* These values are not used in consideration of maximum or minimum deviations.

Table A4.9 Enthalpy of LiBr Solutions [14].

% LiBr	0	10	20	30	35	40	45	50	55	60	65	70
°C	Solution Temperature vs Enthalpy, kJ/kg (Isotherm Plot)											
0	0	-3.4	-8.0	-11.3	-11.9	-11.2	-9.2	0.0	17.0	45.0*	80.8*	116.9*
10	42.0	31.9	22.0	14.1	11.6	10.6	12.1	18.8	34.4	60.8	95.1*	130.3*
20	84.0	67.4	52.6	40.4	36.1	33.5	33.5	38.9	53.2	78.0	111.0*	145.0*
30	125.9	103.3	84.0	68.6	62.6	58.3	56.8	60.5	73.5	96.8	128.4*	161.7*
40	167.6	139.5	115.8	96.0	88.6	82.5	79.7	82.2	93.5	115.4	146.0*	178.3*
50	209.3	175.2	147.0	123.4	113.9	106.7	102.6	103.8	114.0	134.5	163.5	195.0*
60	251.1	211.7	179.1	151.4	140.0	131.7	125.8	125.8	134.7	153.7	181.4	211.9*
70	293.0	247.7	210.5	178.8	166.0	155.7	148.9	148.0	155.6	173.2	199.4	228.8*
80	334.9	287.8	243.6	207.3	193.0	181.0	172.8	170.0	176.2	192.6	217.2	245.7*
90	376.9	321.1	275.6	235.4	219.8	206.1	195.8	192.3	197.1	212.2	235.6	262.9*
100	419.0	357.6	307.9	263.8	246.2	231.0	219.9	214.6	218.2	231.5	253.5	279.7
110	461.3	394.3	340.1	292.4	272.8	255.9	243.3	236.8	239.1	251.0	271.4	296.3
120	503.7	431.0	372.5	320.9	299.6	281.0	267.0	259.0	260.0	270.2	289.5	313.4
130	546.3	468.0	404.5	349.6	326.3	306.2	290.7	281.0	280.4	289.1	306.9	330.2
140	589.1	505.6	437.8	377.9	353.2	331.3	314.2	303.2	301.1	308.1	324.7	346.9
150	632.2	542.7	470.5	406.8	379.8	356.6	337.8	325.5	321.6	327.3	342.7	363.6
160	675.6	580.8	503.1	435.4	406.6	381.9	361.2	347.7	342.2	346.1	360.3	380.1
170	719.2	618.9	536.1	464.3	433.6	406.8	384.9	369.9	362.9	365.4	378.3	396.0
180	763.2	657.1	569.4	493.4	460.8	432.1	408.8	392.1	383.4	384.3	395.8	411.3
	Saturated Dew Point Temperature vs Enthalpy, kJ/kg (Isobar Plot)											
10	42.0	35.0	28.7	26.8	29.1	34.0	44.4	63.8	94.0	134.8	182.5	231.0*
20	84.0	70.8	60.1	55.3	56.5	60.5	69.4	88.3	117.4	157.4	205.3	253.0*
30	125.8	107.0	91.8	83.9	84.0	86.3	94.2	112.7	141.5	180.3	226.3	275.0*
40	167.6	143.3	123.8	112.0	110.3	112.3	119.5	137.1	164.8	202.6	248.3	297.1
50	209.3	179.4	155.9	140.9	137.8	138.7	144.7	161.7	188.4	225.5	270.1	319.1
60	251.1	216.2	188.8	169.4	165.1	164.8	170.6	186.4	212.5	248.1	291.9	341.2
70	293.0	252.4	221.1	198.5	193.4	191.8	195.8	211.4	236.4	270.6	313.1	362.8
80	334.9	288.7	254.6	227.8	221.5	218.3	222.0	236.2	260.3	292.7	334.9	384.2
90	376.9	326.5	287.5	257.0	249.2	245.1	247.7	261.2	283.5	314.9	356.4	404.6
100	419.0	363.1	319.3	286.7	277.1	271.7	273.5	285.3	307.2	337.1	378.3	
110	461.3	400.2	352.8	316.2	305.3	298.8	299.2	310.3	330.6	359.6	399.7	
120	503.7	437.0	385.3	345.8	333.5	325.4	325.0	335.3	354.0	381.6		

Solution Concentration vs Enthalpy at Crystallisation Point

% LiBr	57	58	59	60	61	62	63	64	65	66	67	68	69	70
kJ/kg	10.5	22.5	34.5	62.2	85.4	104.2	120.9	136.9	155.3	189.7	217.1	239.3	264.8	282.4

Enthalpy Equations for SI Units

$h = 2.326(a + B(1.8t + 32) + C(1.8t + 32)^2)$ kJ/kg solution where t = °C

$A = -1015.07 + 79.5387X - 2.358016X^2 + .03031583X^3 - (1.400261E\text{-}4)X^4$

$B = 4.64108 - (3.037766E\text{-}1)X + (8.448453E\text{-}3)X^2 - (1.047721E\text{-}4)X^3 + (4.80097E\text{-}7)X^4$

$C = -4.9107E\text{-}3 + (3.831845E\text{-}4)X - (1.078963E\text{-}5)X^2 + (1.31528E\text{-}7)X^3 - (5.897E\text{-}10)X^4$

Table A4.10. Simplified Steam Table Equations and Constants [14].

1. $\text{Log } P = k_o + k_1/T' + k_2/T'^2$
2. $t' = (-2k_2/(k_1 + (k_1^2 - 4k_2(k_o - \text{Log } P))^{.5} - 459.7$
3. $\Delta H' = H_v' - H_f$
4. $H_f = 1.001t' - 32.05$
5. $H_v' = (.00274t' - .989805)P + (.44942t' + 1060.8)$
6. $H_v = (.00274t - .989805)P + (.44942t + 1060.8)$
7. $V' = (-.000013t'^2 + .008082t' - 1.52167) + (.59553t' + 273.845)/P$
8. $V = (-.000013t^2 + .008082t - 1.52167) + (.59553t + 273.845)/P$

$k_o = 6.21147$

$k_1 = -2886.373$

$k_2 = -337269.46$

$T = t + 459.7$ absolute temperature, ^oR

where $\Delta H'$ = latent heat of saturated water at temp. t', Btu/lb
H_f = enthalpy water at t', Btu/lb
H_v' = enthalpy of saturated water vapor at temp. t', Btu/lb
H_v = enthalpy superheated water vapor (t-t'= deg. superheat), Btu/lb
V' = volume of saturated water vapor at temp. t', ft^3/lb
V = volume of superheated water vapor (t-t'= deg. superheat), ft^3/lb
$P = P' = Psia$

Range: $10 < t' < 230F$; $40 < t < 360F$; $.035 < P < 21$ psia
(Below 32F vapor pressures are for subcooled water at temp. t')

Table A4.11 Viscosity of LiBr Solutions at various Temperature [43]. (C.P.)

Viscosity of lithium bromide-water solutions at various temperatures (C. P.) Smoothed values

LiBr wt% \ ℃	0	10	20	30	40	50	60	70	80	90
5	1.950	1.428	1.092	0.794	0.710	0.615	0.508	0.438	0.381	0.365
10	1.995	1.479	1.154	0.857	0.756	0.648	0.565	0.462	0.401	0.372
15	2.105	1.552	1.237	0.938	0.829	0.701	0.588	0.517	0.443	0.401
20	2.240	1.664	1.340	1.036	0.897	0.760	0.668	0.575	0.485	0.439
25	2.413	1.836	1.473	1.148	0.988	0.842	0.734	0.640	0.543	0.478
30	2.686	2.029	1.640	1.282	1.110	0.942	0.819	0.721	0.605	0.521
35	3.048	2.356	1.860	1.479	1.278	1.082	0.913	0.800	0.707	0.592
40	3.545	2.805	2.205	1.787	1.495	1.284	1.022	0.926	0.819	0.690
45	4.342	3.455	2.770	2.278	1.858	1.595	1.280	1.140	0.990	0.870
50	6.000	4.580	3.830	3.040	2.410	2.080	1.700	1.490	1.300	1.160
55	9.160	7.200	6.230	4.900	3.730	3.000	2.500	2.080	1.810	1.590
60		11.800	10.300	8.440	6.000	5.000	4.040	3.280	2.580	2.280

Table A4.12 Surface Tension of LiBr Solutions at Various Temperature [43]. (dyne/cm)

Surface tension of lithium bromide-water solutions at various temperatures (Smoothed values) (dyne/cm)

℃ / wt%	0	5	10	15	20	25	30	35	40	45	50	55	60	65	70	75	80	85	90
5	78.19	77.82	76.38	75.42	74.37	73.62	72.83	72.06	71.22	70.45	69.60	68.90	68.15	67.38	66.58	65.75	64.92	64.30	63.60
10	79.73	78.70	77.70	76.65	75.53	74.72	73.81	73.03	72.21	71.30	70.33	69.78	68.98	68.23	67.43	66.62	65.80	65.19	64.51
15	81.13	80.10	78.92	77.82	76.73	75.80	74.83	74.08	73.22	72.23	71.18	70.56	69.90	69.12	68.30	67.48	66.68	65.48	65.33
20	82.44	81.25	80.08	78.92	77.83	76.85	75.96	75.20	74.38	73.33	72.71	71.52	70.88	70.14	69.33	68.50	67.61	66.94	66.26
25	83.79	82.61	81.35	80.22	79.00	78.12	77.15	76.32	75.50	74.52	73.50	72.72	71.90	71.13	70.27	69.40	68.54	67.84	67.16
30	85.12	83.92	82.75	81.50	80.22	79.36	78.46	77.58	76.69	75.70	74.89	74.00	73.04	72.22	71.33	70.50	69.60	68.82	68.14
35	86.92	85.72	84.50	83.18	81.83	80.93	80.04	79.15	78.22	77.42	76.45	75.48	74.51	73.60	72.72	71.75	70.92	70.85	69.40
40	88.97	87.68	86.37	85.12	83.79	82.68	81.76	80.81	79.92	78.95	78.06	77.04	76.07	75.22	74.31	73.34	72.44	71.59	70.81
45	91.32	89.84	88.53	87.20	85.86	84.78	83.83	82.79	81.92	80.85	79.88	78.82	77.87	77.02	76.03	75.10	74.08	73.22	72.34
50	93.80	92.22	90.84	89.34	88.03	86.98	85.94	84.88	83.87	82.78	81.81	80.73	79.71	78.72	77.79	76.73	75.77	74.82	73.94
55	96.25	94.72	93.21	91.75	90.23	89.20	88.02	87.02	85.93	84.78	83.78	82.64	81.58	80.60	79.58	78.50	77.42	76.44	75.57
60	98.79	97.21	95.58	94.00	92.47	91.22	90.18	89.03	88.02	86.88	85.80	84.55	83.35	82.35	81.31	80.28	79.10	78.22	77.25

Table A4.13 Specific Gravity of LiBr-Water Solutions at Various Temperature [43].

Specific gravity of lithium bromide-water solutions at various temperatures (Smoothed values)

LiBr wt% \ °C	0	10	20	30	40	50	60	70	80	90	100
10	1.0862	1.0823	1.0778	1.0722	1.0674	1.0622	1.0578	1.0522	1.0473	1.0425	1.0383
15	1.1295	1.1251	1.1203	1.1154	1.1100	1.1052	1.1002	1.0952	1.0903	1.0855	1.0795
20	1.1740	1.1690	1.1640	1.1590	1.1540	1.1490	1.1440	1.1390	1.1340	1.1290	1.1240
25	1.2213	1.2159	1.2110	1.2063	1.2006	1.1959	1.1908	1.1868	1.1817	1.1762	1.1708
30	1.2730	1.2680	1.2635	1.2585	1.2535	1.2480	1.2432	1.2388	1.2335	1.2282	1.2231
35	1.3340	1.3308	1.3235	1.3200	1.3145	1.3095	1.3045	1.3000	1.2942	1.2900	1.2845
40	1.3990	1.3940	1.3890	1.3840	1.3790	1.3740	1.3690	1.3640	1.3590	1.3540	1.3490
45	1.4705	1.4660	1.4615	1.4560	1.4515	1.4460	1.4400	1.4350	1.4300	1.4265	1.4190
50	1.5530	1.5480	1.5430	1.5380	1.5330	1.5280	1.5220	1.5170	1.5120	1.5060	1.5010
55	1.6370	1.6320	1.6270	1.6210	1.6160	1.6110	1.6050	1.6000	1.5950	1.5900	1.5850
60	1.7365	1.7225	1.7160	1.7105	1.7065	1.6960	1.6910	1.6905	1.6855	1.6800	1.6745

Table A4.14 Thermal Conductivity of LiBr-Water Solutions at various temperature [43]. (Kcal/m.hr.k)

Thermal conductivity of lithium bromide-water solutions at various temp-ratures (Smoothed values). (kcal m. hr. C)

wt% \ °C	0*	10	20	30	40	50	60	70	80	90*	100*
5	0.467	0.489	0.506	0.520	0.533	0.542	0.550	0.558	0.564	0.570	0.575
10	0.455	0.477	0.494	0.507	0.520	0.530	0.536	0.545	0.550	0.555	0.559
15	0.442	0.463	0.480	0.492	0.505	0.514	0.522	0.529	0.535	0.540	0.543
20	0.429	0.450	0.466	0.478	0.490	0.499	0.505	0.513	0.520	0.525	0.528
25	0.415	0.435	0.452	0.462	0.475	0.483	0.489	0.497	0.505	0.509	0.513
30	0.403	0.421	0.436	0.447	0.460	0.466	0.473	0.481	0.484	0.494	0.498
35	0.389	0.407	0.422	0.432	0.444	0.452	0.457	0.464	0.472	0.476	0.481
40	0.376	0.392	0.407	0.417	0.429	0.435	0.442	0.448	0.455	0.460	0.465
45	0.363	0.379	0.392	0.402	0.413	0.421	0.426	0.432	0.439	0.444	0.449
50	0.350	0.364	0.377	0.387	0.397	0.405	0.410	0.416	0.423	0.427	0.434
55	0.337	0.350	0.363	0.372	0.382	0.389	0.394	0.400	0.406	0.412	0.417
60	0.323	0.336	0.349	0.357	0.366	0.373	0.378	0.385	0.390	0.396	0.401
*65	0.309	0.321	0.334	0.342	0.350	0.357	0.362	0.367	0.374	0.381	0.386

* extrapolated values

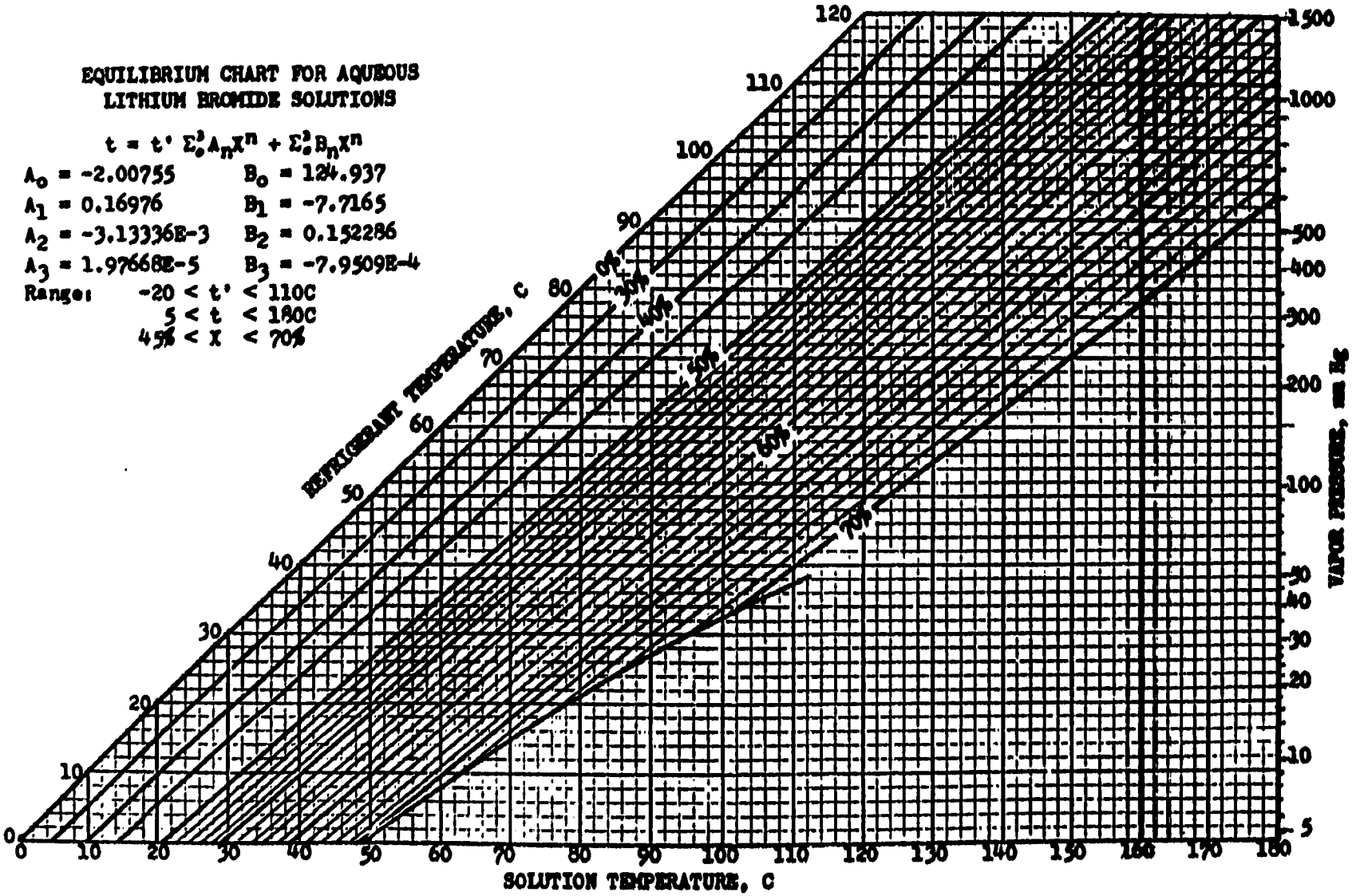

Figure A4.4 Equilibrium Chart For LiBr-water Solutions [14].

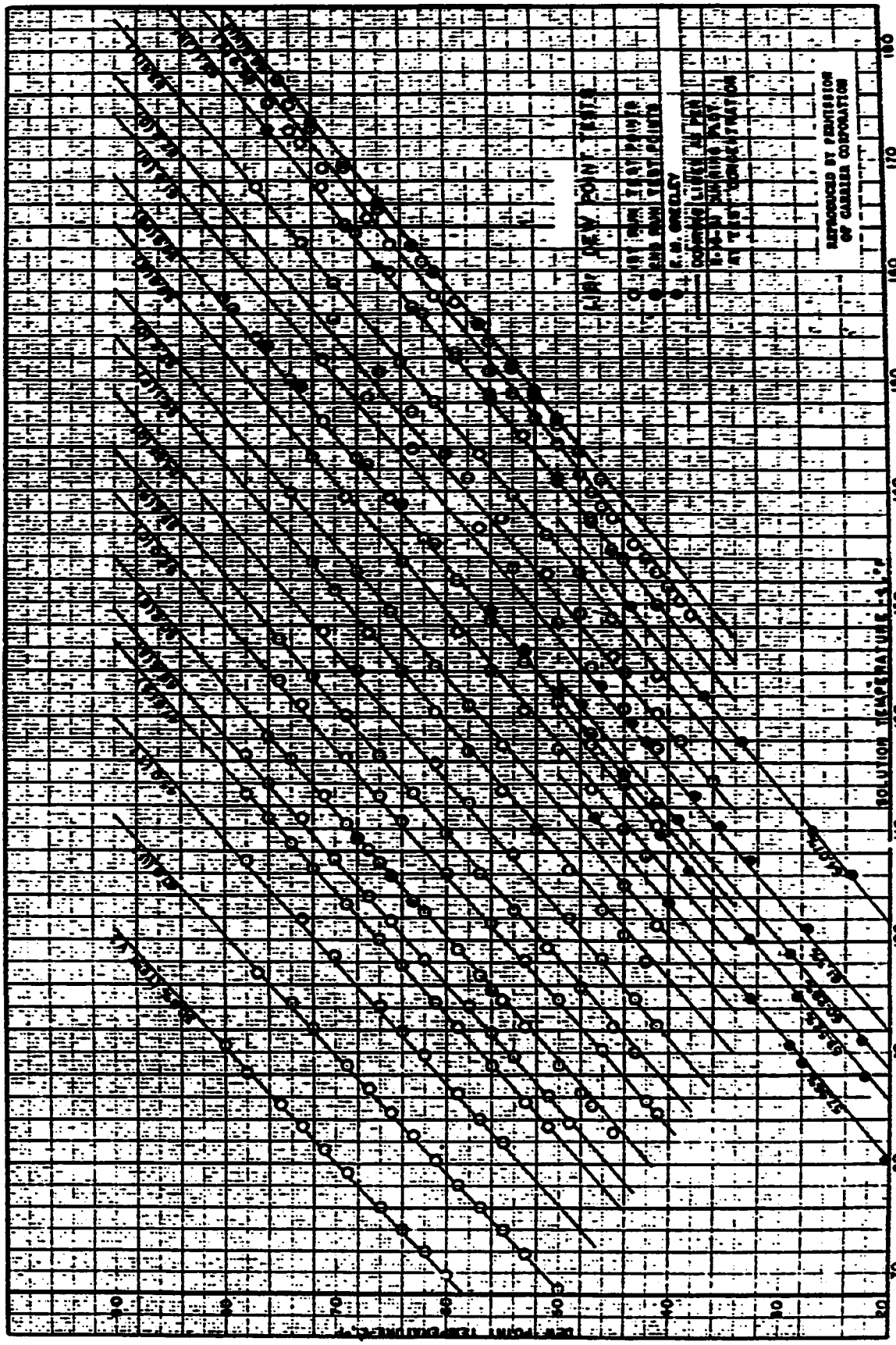

Figure A4.5 LiBr Dew Point Tests [14].

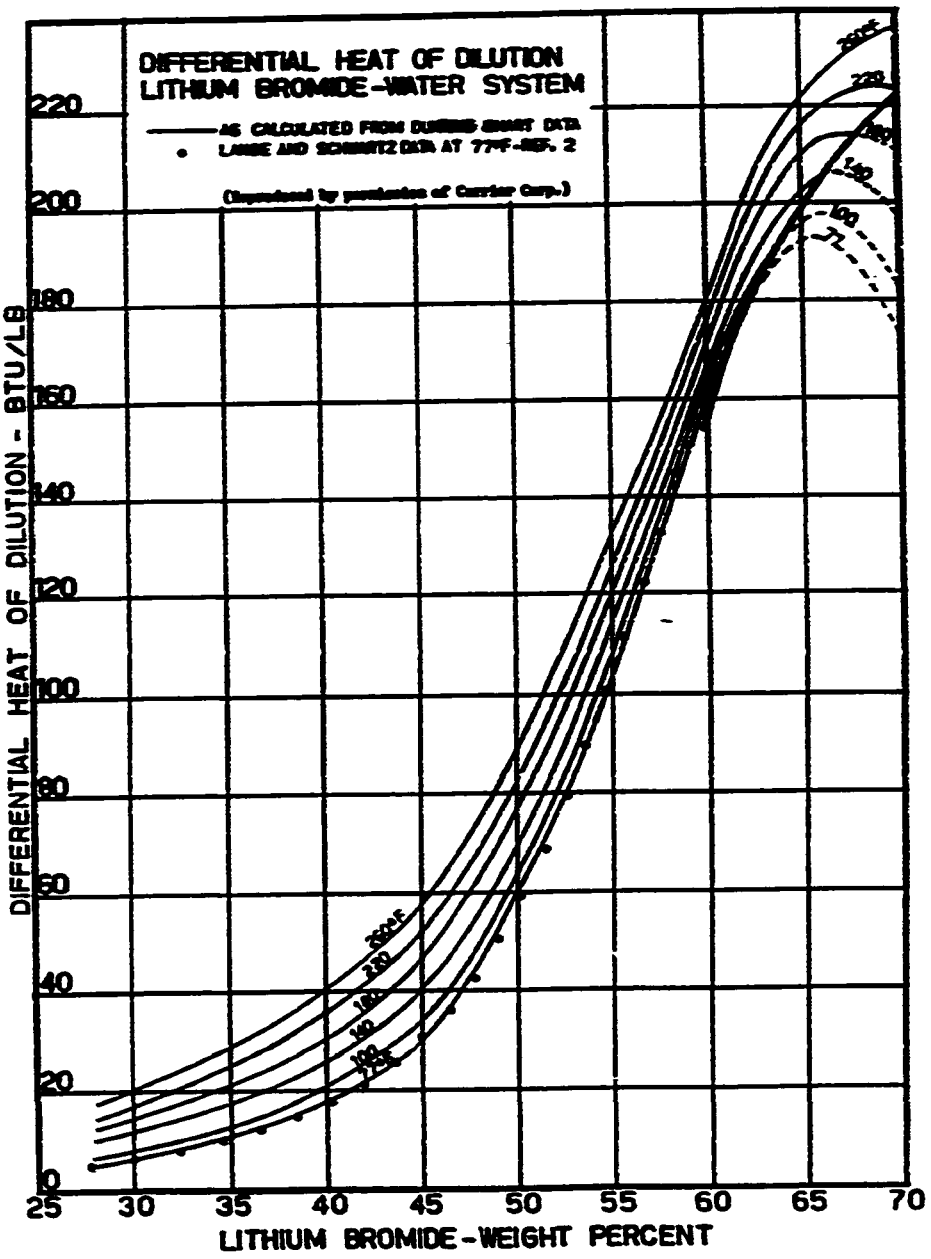

Figure A4.6 LiBr Differential Heat of Dilution [14].

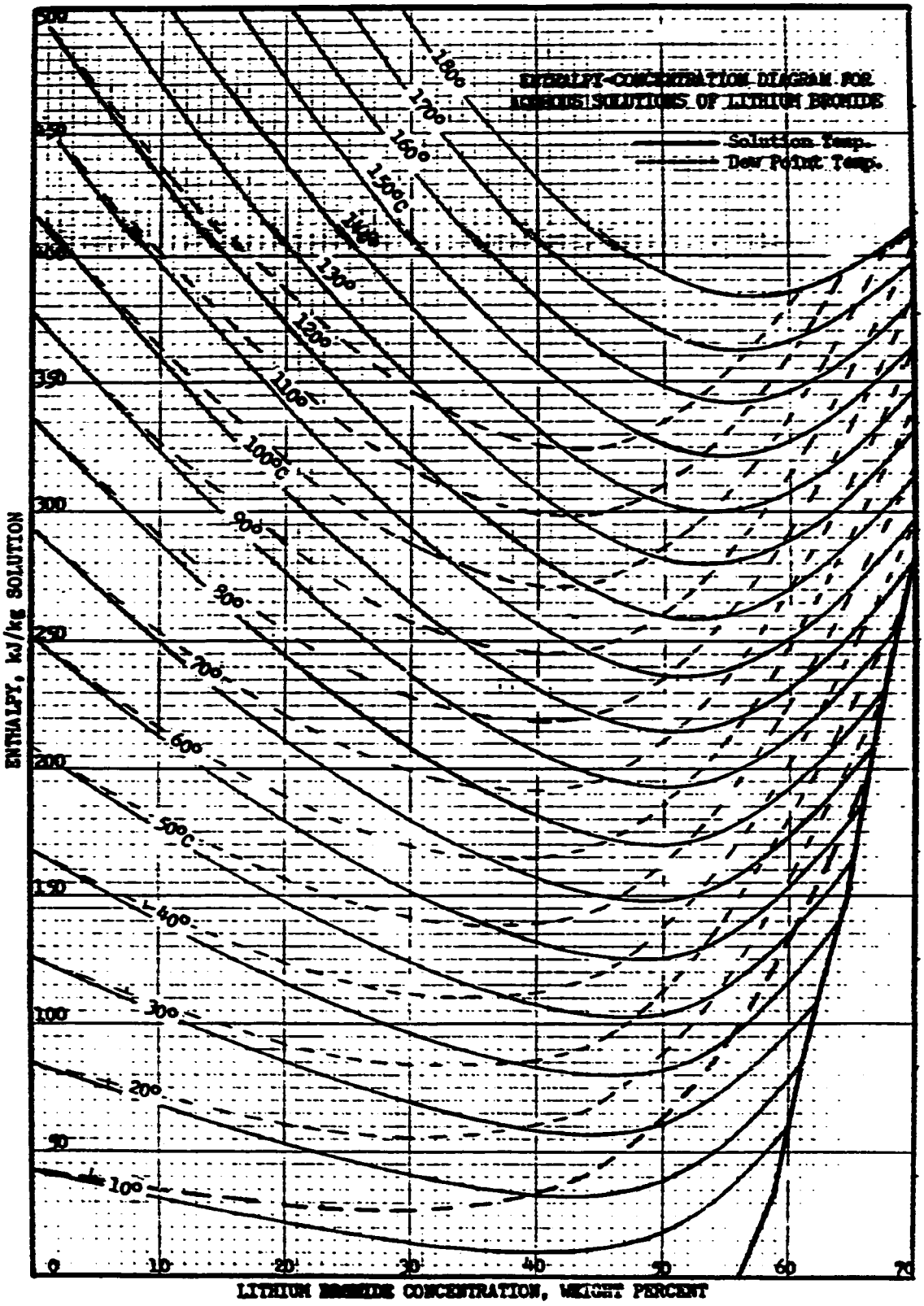

Figure A4.7 Enthalpy- Concentration Diagram for LiBr-Water Solutions [14].

The following equations can be used to calculate the properties of LiBr-water solutions at the given concentration X %.

The specific gravity is given by,

X	Sp.Gr.
10	$1.099497-8.203124*10^{-4}\ T+2.083044\ T^2$
20	$.180446*.99627^{T}+1.0$
30	$(2678-3.4802\ T-.01\ T^2)*10^{-4}+1.0$
35	$.3374\ (.9983)^{T}+1.0$
40	$(3990-5T)*10^{-4}+1.0$
45	$0.47378(.99878)^{T}+1.0$
50	$(5496-4.1665\ T-.00708\ T^2)*10^{-4}+1.0$

Thermal conductivity is calculated by,

X	k (Kal/m.hr.k
10	459.91+1.70T-7.143*10-3 T^2
20	418.651 + 1.951 T- 8.572 10-3 T^2
30	438.033 (1.0013)T
35	386.567 +1.514 T-5.715*10-3 T^2
40	389.882+ 1.037 T-2.857*10-3 T^2
45	393.855 (1.0013)T
50	377.248(1.0014)T

The viscosity is calculated by,

X	μ (C.P.)
10	1.293-1.871 (T/120) + .792$(T/120)^2$
20	1.482 -2.13 (T/120) +.977$(T/120)^2$
30	1.662-1.822(T/110)+.519$(T/110)^2$
35	2.079-2.959 (T/120) +1.316$(T/120)^2$
40	1.999-2.311(T/120)+ .775$(T/120)^2$
45	3.222-4.589(t/110)+2.067$(T/110)^2$
50	3.733 - 5.322 (T/120) +2.52$(T/120)^2$

Specific heat Cp is given by,

$$Cp=A+BT+CT^2 \qquad (Cal/g.k)$$

where,

$$A=1.098-1.529*10-2\ X+6.220*10-5\ X^2$$

$$B=-3.651*10-3+4.204*10-5\ X$$

$$C=3.576*10-5-4.238*10-7\ X$$

APPENDIX B

Some examples are given in this appendix to supplement the calculations in chapter 4 and 8.

CHAPTER 4

Example 4.1

To prepare 6 liters , 35 % lithium bromide by weight out of 50 % solution at 25 °C , proceed as follows:

1- Have a thermometer and a hydrometer to measure the temperature and the specific gravity of the solution. A container for mixing is also needed together with a specific gravity chart.

2- Estimate the required amount of the initial solution V_1 that gives the required volume and concentration using equation 2.2 . Then find the amount of water that should be added to give the final solution by subtracting the volume of the final solution V_2 from that for the initial solution V_1. In this example the estimated initial solution volume is 3.86 liter and the required amount of

water is 2.14 liter .

3- Measure the temperature of the solution and read the specific gravity for the given concentration at that temperature from the chart . For this example the final specific gravity was 1.315 for 35 % LiBr solution at 25°C .

4- Add pure water less than 2.14 liter , which was estimated in step 2 , to the solution until the specific gravity becomes 1.315 which coresponds to 35 % solution concentration. Although the final temperature of the solution may change by one or two degrees , the change will not make a sensible difference that can be read from the chart. for example, if the final solution changes to 27 °C then the specific gravity will remain 1.315 because the rate of change of specific gravity with temperature is very small , in the order of $5.94 * 10^{-4}$ / °C .

CHAPTER 8

Two examples will be used to show the the calculation procedure for convection and boiling problems.

Example 8.1

Find the heat transfer coefficient for 35% LiBr by wt. solution flowing at .90 GPM and an average mean temperature of 74° C .

Solution :

Physical properties at 74° C found from chapter II are as follow ,

LiBr tables	water tables
$\Gamma f=1265$ kg/m^3	$\mu w=379 * 10^{-6}$ Pa .s
$\mu f=764 * 10^{-6}$ Pa.s	
kf=.544 W/m k	
Cp=2481 kj/kg k	

viscosity ratio $\mu=\mu_{LiBr} / \mu_{water} = 764/379=2.02$

mass flow rate $m= Q\ \Gamma_f= \dfrac{.9(3.7854)}{1000(60)} = .072$ kg/s

$$Re=\frac{4\ m}{\pi\ D\ \mu} = \frac{4\ (.072\ )}{\pi\ (\ .0376\ )(\ 764\ *10^{-6}\ )} = 3184$$

$$Pr = \frac{\mu\ Cp}{k} = \frac{764 * 10^{-6}\ (2481)}{.544} = 3.48$$

Convection heat transfer coefficient h_c is calculated using equation 6.5 as,

$$h = \frac{k}{D}\ (.02844)\ Re^{.8}\ Pr^{.4}\ \mu^{.327}$$

$$= (.544/.0376)(.02844)(3184)^{.8}(3.48)^{.4}$$
$$*(2.02)^{.327} = 541\ W/m^2k$$

Comparing this result with figure 6.21 , we find that at 74 °C , h≈550 W/m² k which agrees with the calculated one.

Example 8.2

Find the boiling heat transfer coefficient for 20% LiBr solution flowing at .45 GPM at temperature of 112 °C and vapor quality of .5 % .

Solution :

The properties found from chapter 2 are listed below.

LiBr solution	water vapor
$Cp=3538.8$ kj/kg k	$\mu g=12.48 *10^{-6}$
$\mu f=338 *10^{-6}$ Pa . s	$\Gamma g=.876$ kg/m^3
$\Gamma f= 1062$ kg/m^3	$\mu w=249 *10^{-6}$
$kf=.617$ W/m k	

Viscosity ratio $\mu = \mu_{LiBr}/\mu_{water}=338/249=1.357$

$$\text{mass velocity } G= Q\,\Gamma/\,A = \frac{.45\ (3.7854)(4)}{(60)(1000)\ \pi\ (.0376)^2} *(1062\ ) = 27.15 \text{ kg/m}^2 \text{ s}$$

$$Re = \frac{(1-x)\ G\ D_i}{\mu_f} = \frac{(1-.005)(27.15)(.0376)}{338*10^{-6}} = 3006$$

$$Pr = \frac{\mu_f\ Cp}{k_f} = \frac{338\ *10^{-6}\ (3539)}{.617} = 1.94$$

Convection heat transfer coefficient calculated from equation 6.5 assuming single phase flowing alone as ,

$$hc=\frac{k}{D}\ (.02844\ )Re^{.8}\ Pr^{.4}\ \mu^{.327}$$

$$=(.617/.0376)\ (.02844)(3006)^{.8}(1.94)^{.4}$$

$$*(1.357)^{.327}=407\ W/m^2k$$

Lockhart-Martinelli parameter Xtt is calculated as ,

$$Xtt=\left(\frac{1-x}{x}\right)^{.9}\left(\frac{\mu_f}{\mu_g}\right)^{.1}\left(\frac{\Gamma_g}{\Gamma_f}\right)^{.5}$$

$$=\left(\frac{1-.005}{.005}\right)^{.9}\left(\frac{338}{12.48}\right)^{.1}\left(\frac{.876}{1062}\right)^{.5}=4.75$$

Using equation 6.9 for 20% we get,

C1=28.37 and C2=.4173

Subtituting in equation 6.7 , the boiling heat transfer coiefficent h is ,

$$h=h_c\ C1(1/Xtt)^{C2} = 407(28.37)(1/4.75)^{.4173}$$

$$= 6027\ W/m^2\ k$$

From figure 6.42 , we find that at x=.5 %

$h \approx 5700\ W/m^2\ k$

The percentage error between the calculated and the

experimental is calculated as ,

$$\% \text{ error } = \frac{h_{exp} - h_{cal}}{h_{exp}} = \frac{5700 - 6027}{5700} = 5.7\ \%$$

NOMENCLATURE

A	Area cross section, m^2
Cp	Specific heat, J/kg k
CHF	Critical heat flux
D	Tube diameter, m
E	Voltage drop across the heater, V
F	Factor accounts for liquid velocity increase due to vapor
g	Acceleration due to gravity, m/s^2
G	Mass flux, $kg/s.m^2$
h	Heat transfer coefficient , W/m^2k
H	Enthalpy ,kJ/kg
I	Input Current, A
H_{FG}	Enthalpy of evaporization
k	Thermal conductivity , W/m.k
m	Mass flow rate, kg/s
M	Rotational frequency
ML	Mole fraction of liquid
MG	Mole fraction of vapor
NCB	Nucleate boiling
PB	Pool boiling
$\bar{P}$	Time averaged pressure
q	Heat added, W
q"	Heat flux, W/m^2
Q	Flow rate, m^3/s

S	Slip ratio
SCB	Subcooled boiling
$\bar{t}$	Time averaged temperature
t	tube thikness
T_m	Fluid mean temperature
T_{mi} , T_{mo}	Inlet and outlet Fluid mean temperature
$\triangle T_{SAT}$	Degree of super heat
$\triangle T_{SUB}$	Degree of subcooled
Ts	Surface temperature
T_{SAT}	Saturateds temperatrure
T_R	Refrigerant temperature
U	Enternal energy
$\bar{u}$	Time averaged velocity
v	Molecular viscosity
V	Velocity, m/s
x	Vapor quality
X	Concentration of LiBr by weight, %
Xtt	Lockhart- Martinlli Parameter
Y	Suppression factor
W	Work done
W_L,W_V	Area averaged velocity of liquid and vapor phase respectivily
α	Void fraction
ϵ_H	Eddy Diffusivity
ϵ_M	Eddy viscosity
μ	Dynamic Viscosity ,N/s.m^2

μ_S	Viscosity at the surface
μ^*	viscosity ratio $=\mu_{LiBr}/\mu_{water}$
∞	Molecular diffusivity
Γ	Density , kg/m^3
θ^2	Collier correlation
σ	Surface tension, N/m

Subscripts

A	absorbtion
AB	absorber
CO	condenser
C or CON	convection
CV	control volume
EV	evaporator
E	exit
GE	Generator
I	inlet
L	liquid
LO	assuming the total flow is liquid
m	mean
O	outlet
ONB	onset of subcooled boiling

S	surface
TP	two-phase

REFERENCES

1. *Source Book on Copper and Copper Alloys,* American Society for Metals, Metals Park ,Ohio , 1979.

2. Incropera, F. P., DeWitt D.P., *Fundamentals of Heat Transfer,* John Wiley & Sons , New York , 1981.

3 *Assembly Instruction for Thermocouple Kit N965,* OMEGA Engineering, Inc., Stamford , Connecticut, 1988.

4. Welding Handbook: *Welding ,cutting and Related Processes,* 6 ed, part B , American Welding Society , New York, 1971.

5. Welding Handbook: *Metals and Their Weldability,* 6 ed, American Welding Society, Miami, Florida, 1972.

6. Welding Handbook: *Fundamentals of Welding,* 6 ed, American Welding Society, Miami, Florida, 1972.

7. *OMEGA CC High Temperature Cement Operator's Manual,* OMEGA engineering, Inc. Stamford, Connecticut, 1989.

8. *OMNI-CAL Temperature Calibrator Operator's Manual,* OMIGA Engineering,Inc. Stamford, Connecticut, 1982 .

9. Hart, A.W and Beumel Jr.,O. F., *The Chemistry of Lithium,* Pergman Press , New York ,1973.

10. Collie, M.J., *Corrosion Inhibitors Developments Since 1980,* Noyes Data Corporation, New Jersey ,1983.

11. Berghmans, J., *Heat Pump Fundamentals* ,Martinus Nijhoff Publishers, Boston, 1983.

12. Van Wylen, Gordon J. and Sonntg, Richard, *Fundamentals of Classical Thermodynamics,* John Wiley & Sons, New York,1978.

13. *ASHRAE Handbook 1981 Fundamentals* , American Society of Heating, Refrigerating and Air-Conditioning Engineerings, Inc., Atlanta, GA ,1981.

14. Lowell A. McNeely, *Thermodynamic Properties of Aqueous solutions of Lithium Bromide* , ASHRAE Transaction , PH-79-3, No.3, American Society of Heating, Refrigerating and Air-Conditioning Engineerings, Inc., Atlanta, GA, pp. 413-434, 1979.

15. MARCH:*Instruction and Repair Parts For Model TE-5.5S-MD,* MARCH Manufacturing, Inc., Glenview, Illinois.

16. Roberson, John A. and Crowe, Clayton T., *Engineering Fluid Mechanics*, Houghton Mifflin Company, 2nd, Boston, pp. 360-396, 1980.

17. Bergles, A.E. and Others, *Two-Phase Flow and Heat Transfer in The Power and Process Industries*, Hemisphere Publishing Corporation , Washington, 1981.

18. Kays, W.M. and Crawford, M.E., *Convective Heat and Mass Transfer*, McGraw-Hill Book Company, 2nd, 1980.

19. Burmeister, Louis C., *Cnvective Heat Transfer*, John Wiley & Sons, New York, 1983.

20. Hartnett, James P. and Irvine, Thomas F., *Advances In Heat Transfer*, Academic Press, Inc., New York, vol 20, 1990.

21. Tong, L.S., *Boiling Heat Transfer and Two-Phase Flow*, John Wiley & Sons, Inc., New York, 1965.

22. Veziroglu, T.N. and Bergles, A.E., *Multi-Phase Flow and Heat Transfer III, Part A:Fundamentals*, Elsevier Scince Publishing Company Inc., New York, 1984.

23. Muratra, Keiji and Kenichi Hashizume, *An Investigation on Forced Convection Boiling of Nonazeotropic Refrigerant Mixtures,* J. Heat Transfer Japanese Research, Vol.19, Part 2, pp. 95-109, 1990.

24. Takamatsu, Horoshi and Others, *Forced Convective Boiling of Nonazeotropic Refrigerants Mixtures of R22 and R114 inside a Horizontal Tube,* J. Heat Transfer Japanese Research , Vol. 19 , part 3, pp.68-81, 1990.

25. Shock, R.A.W., *Nucleate Boiling in Binary Mixtures,* J. Heat Mass Transfer, Vol 20, pp. 701-709, Pergamon Press, Great Britain, 1977.

26. Yusufova, V.D. and Chernyakhovskiy, A.I., *Heat Transfer with Boiling Mixtures,* Heat Transfer-Sovet Research, Vol.8, no.4,pp. 57-62, July-August 1976.

27. Bergles, A.E. and Rohsenow, W.M., *The Determination of Forced-Convection Surface-Boiling Heat Transfer,* Journal of Heat Transfer, pp. 365-372, August 1964.

28. McAdams, W.H. and Others, *Heat Transfer at High Rates to Water with Surface Boiling,* Industrial and Engineering Chemistry, Vol.41 ,pp. 1945-1953, November 1949.

29. Gilmour, Charles, *Nucleate Boiling: a Correlation,* Chemical Engineering Progress, Vol.54, No.10, pp.78-79, October 1958.

30. Zyatnina, A.A. and Mitrofanova, T.V., Analytical *Determination of the Onset of Nucleate Boiling of Subcooled Water in Pipes,* Heat Transfer_Soviet Research, Vol. 21, No. 6, pp.742-749, Nov-Dec 1989.

31. Katto, Y., *A Physical Approach to Critical Heat Flux of Subcooled Flow Boiling in Round Tubes,* Int. J. Heat Mass Transfer, Vol. 33, No. 4, pp.611-620, 1990.

32. Bogart, Marcel J., *Lithium Bromide Absorption Refrigeration- A Calculator Program,* ASHRAE Journal, pp.23-28, August 1982.

33. Kawae, Nobuji and Others, *Water Vapor Evaporation into Laminar Film Flow of a Lithium Bromide-Water Solution,* J. Heat Transfer Research , Vol.18, Part 3, pp. 58-69, 1989.

34. Esteso, Miguel A. and Others, *Transference Number Measurements in Agueous Solutions at 25°C, Part 3 :Lithium Bromide,* J. Chemical Engineering Data, pp.474-476, 1987.

35. Zimmermann,A. and Keller J.U., *VLE in the System Water-Ammonia-Lithium Bromide,* Fluid Phase Equilibria, Vol. 53, pp.229-234, 1989.

36. Patial, K.R. and Others , *Experimental Evaluation of Aqueous Lithium Halides as Single-and Double-Salt Systems in Absorption Heat-Pumps,* Applied Energy , Vol.34, pp.99-111, 1989.

37. Durst,F. and Others, *Two-Phase Momentum, Heat and Mass Transfer in Chemical, Process, and Energy Engineering Systems,* Hemisphere Publishing Corporation, Vol.1, New York, 1979.

38. C.V. Sternling and L.J. Tichacek, *Heat Transfer Coefficients for Boiling Mixtures,* Chem. Engng. Sci. Vol. 16, No.3 and 4, pp.2 -337, Dec. 1961.

39. N. Irving Sax, *Dangerous Properties of Industrial Materials,* Litton Educational Publishing, Inc., 5th ed, New York, 1979.

40. *Carrier Corporation Specific gravity chart.*

41. Threlkeld, James L., *Thermal Environmental Engineering,* Prentice-Hall, Inc.New Jersey, 2nd ed, 1970.

42. Abu-Naji, Sami. *Designing and Manufacturing Heat Transfer Apparatus,* Senior Project, ME, KFUPM, 1990.

43. Uemura,Tadashi and Shigeo Hasaba , *Studies on the Lithium Bromide-Water Absorption Refrigerating Machine,* Technology Reports of Kansai University,Osaka, Japan, No.6, pp. 31-54, Dec. 1964.

44. Bogatykh,S.A. and I.D. Evnovich , *A Study of the Viscosities of Aqueous Solutions of LiCl, LiBr and $CaCl_2$ Applicable to the Normal Drying of Gases,* J. Appl. Chem., USSR, vol.36 , No. 8 , pp.1808-9, 1943.

45. *The Non-Invasive Ultrasonic Velocity Monitor: Installation and Operation Manual,* OMEGA Engineering, Inc., Stamford, CT, 1989.

46. Iyoki, S. and T. Uemura , *Vapor Pressure of the Water-Lithium Bromide System and the Water-Lithium Bromide-Zinc Bromide-Lithium Chloride System at High Temperatures,* Int. J. Refrigeration, Vol. 12,pp.278-282, Sep. 1989.

47. Lazzarin, R.M., *Commercially Available Absorption Heat Pumps:Some Experimental Tests,* Int. J. Refrigeration, Vol.11, pp.96-99, March 1988.

48. Uhlig, Herbert H. and R.W. Revie, *Corrosion and Corrosion Control,* John Wiley & Sons, New York, 3ed ed, 1985.

49. *Data Acquisition and control Unit 3497 A Operation and Service Manual*, Hewlett Packard Co., Colorado , 1981.

50. Schlichting, Hermann, *Boundary-Layer Theory* , McGraw-Hill Book Company, New York ,7th Ed., 1987.

51. M. Necati Qzisik, *Heat Conduction*, John Wiley & Sons, New York, 1980.

52. J.P.Holman, *Experimental Methods for Engineers*, McGraw-Hill Kogakusha, Ltd, Tokyo , 2nd Ed., 1971.

53. Douglas C.Montgomery, *Design and Analysis of Experiments*, John Wiley & Sons , New York, 2nd ed., 1984.

VITA

HUSSAIN ABDULLA AL-BAZROON

Candidate for the degree of

Master of Science in Mechanical Engineering

Thesis : **EXPERIMENTAL DETERMINATION OF HEAT TRANSFER COEFFICIENT FOR WATER-LITHIUM BROMIDE MIXTURE.**

Poigraphical:

Personal Data : Born in Qatif, Saudi Arabia, August 3, 1959.

Education : Graduated from Qatif High School in 1979 ; received the Bachelor of Science degree from King Fahd University of Petroleum and Minerals, with a major of Mechanical Engineering in 1986.

Professional Experience : Engineer IV in Saudi Aramco ,1986-1988.